Biophysical Studies of Conformational Changes of the Dcp1:Dcp2 mRNA decapping complex

Dissertation zur Erlangung des

Doktorgrades der Naturwissenschaften (Dr. rer. nat.)

der Fakultät für Biologie und Vorklinische Medizin

der Universität Regensburg

vorgelegt von

Christina Krempl

aus

Altötting

im Jahr

2023

Biophysical Studies of Conformational Changes of the Dcp1:Dcp2 mRNA decapping complex

Dissertation zur Erlangung des

Doktorgrades der Naturwissenschaften (Dr. rer. nat.)

der Fakultät für Biologie und Vorklinische Medizin

der Universität Regensburg

vorgelegt von

Christina Krempl

aus

Altötting

im Jahr

2023

Der Promotionsgesuch wurde eingereicht am:

18.09.2023

Die Arbeit wurde angeleitet von:

Prof. Dr. Remco Sprangers

Unterschrift:

Christina Krempl

Acknowledgements

Many people have contributed to the successful completion of this thesis. For this reason I want to express my gratitude by thanking

Prof. Dr. Remco Sprangers, for giving me the opportunity to do my PhD in your group and for your excellent supervision and mentorship. In particular, I want to thank you for sharing your excitement for NMR, for your unlimited support and your constructive advice, as well as for your open and encouraging attitude which created a very enjoyable atmosphere to work in.

Prof. Dr. Werner Kremer, for sparking my interest in structural biology.

Johanna Stöfl and **Nadine Stefan**, for your constant and excellent support in the lab and in the office. **Patricia Albrecht**, for caring for us in all organizational and personal matters. **Simon Grunert**, for taking care of the magnets with Werner.

Dr. Jan-Philip Wurm, for teaching me everything in the lab, for patiently answering all my questions and for proofreading parts of my dissertation. **Dr. Jan Overbeck**, **Dr. Daniela Lazzaretti**, **Dr. Jobst Liebau**, for your writing tips and for proofreading parts of my thesis. **Katarzyna Glowacz**, for all the preliminary work on finding optimal fluorophore labeling positions on Dcp1:Dcp2. **Julian Hübner**, **David Stelzig**, **Alexander Schmalix** and all other current and former members of the Sprangers and Wiesner labs, for being great colleagues.

Kinga Ay and **Carolin Apfel**, for great support in the RIGeL programme and **Prof. Dr. Christine Ziegler** and **Prof. Dr. Janosch Hennig** (University of Bayreuth) for RIGeL mentoring. **Prof. Dr. Christine Ziegler**, **Prof. Dr. Wolfram Gronwald**, **Prof. Dr. Dina Grohmann** and **Prof. Dr. Frank Sprenger**, for being on my thesis committee.

Dr. Markus Beck-Erlach, for teaching us how to put pressure on proteins. **Dr. Kevin Kramm** and **Prof. Dr. Dina Grohmann**, for collaboration on the smFRET project. **Agnes Adler** and **Prof. Dr. Marc Baldus** (Utrecht University), for collaboration on the LLPS project by performing all the solid state NMR measurements.

Martin Tollinger (University of Innsbruck), for sharing the plasmid of the KIX domain with us.

My **family** and **Alex**, for your constant and unconditional support.

Summary

Controlled degradation of messenger RNA (mRNA) is essential for the regulation of gene expression. The removal of the protective 5' cap structure of eukaryotic mRNA is a central step in this process and it is catalyzed by the Dcp1:Dcp2 decapping complex. During catalysis, Dcp1:Dcp2 undergoes large conformational changes which are regulated by interactions with several activator proteins including Edc1 and Edc3. The exact details of these structural rearrangements and their functional role in the decapping process are not fully understood yet. Nuclear magnetic resonance (NMR) spectroscopy is a well suited method to study dynamic processes and conformational changes of enzymes. In my dissertation I therefore made use of different NMR experiments and complementary techniques to study the mRNA decapping machinery from *S. pombe* in detail.

In Part III, I used $^{13}CH_3$ methyl group labeling of Dcp2 and conducted methyl Carr–Purcell–Meiboom–Gill (CPMG) NMR relaxation dispersion (RD) experiments on the Dcp1:Dcp2 decapping complex at high hydrostatic pressures. From these experiments I extracted information about the molecular volumes of the different conformations of the complex during the opening-closing pathway and about the effect of ATP on these volumes. This information could not be reliably obtained from known crystal structures, which underlines the potential of pressure-dependent NMR methods to provide insights into structural features of invisible protein conformations, even for high molecular weight complexes.

In Part IV, I examined the applicability of 5-fluorotryptophan labeling for studying protein dynamics with ^{19}F NMR experiments in three different biomolecular systems, namely the Dcp1:Dcp2 mRNA decapping complex, the KIX domain of the transcriptional coactivator CREB binding protein and the DcpS scavenger decapping enzyme. I found that the ^{19}F label on the 5-tryptophan has no measureable effect on the backbone dynamics of the examined proteins and slow protein motions could reliably be extracted from ^{19}F NMR experiments that are insensitive to tryptophan side chain motions. In contrast, I found that NMR relaxation experiments on the ^{19}F nucleus in this position do not always allow for the reliable extraction of kinetic and thermodynamic properties, so these data should always be supported by data from complementary techniques.

In Part V, I performed single molecule Förster resonance energy transfer (smFRET) experiments on the decapping complex. We first optimized the labeling positions of the fluorophores by testing several different combinations of labeling sites and cross-validated them with NMR experiments of fluorophore labeled Dcp1:Dcp2 complexes. In subsequent smFRET measurements I confirmed previously obtained NMR data and I examined the influence of different cofactors and substrates that are not suited for NMR experiments. Importantly, as the fluorophore labeling can influence the conformational equilibrium of the decapping complex,

cross-validation of smFRET data is crucial for a correct interpretation of the FRET efficiencies.

In the presence of Edc3, the Dcp1:Dcp2 mRNA decapping complex undergoes liquid-liquid phase separation (LLPS) and maturation into a gel-like state, about which little is still known. To examine changes in conformation and dynamics of Edc3 and Dcp2 in the transition to the mature state, we performed solid state NMR (ssNMR) experiments on mature Edc3 and Dcp1:Dcp2 (Part VI). We construct a model in which, after LLPS, the factors of the mRNA decapping machinery mature into a structurally inhomogeneous, gel-like state in which the molecular motions and intermolecular contacts that are averaged in solution are frozen out and no longer averaged. Our findings demonstrate the great capacity of ssNMR to study large molecular machines in the condensed, phase separated state.

Taken together, these results contribute to our knowledge of how conformational changes regulate mRNA decapping and, ultimately, add to a better understanding of how large molecular machines function.

Zusammenfassung

Der kontrollierte Abbau von Boten-RNA (mRNA) ist essentiell für die Regulation der Genexpression. Ein zentraler Schritt in diesem Prozess ist die Entfernung der schützenden 5'-Cap-Struktur der eukaryotischen mRNA und dieser wird durch den Dcp1:Dcp2-Decapping-Komplex katalysiert. Während der Katalyse durchläuft Dcp1:Dcp2 große Konformationsänderungen, die durch Wechselwirkungen mit verschiedenen Aktivatorproteinen, darunter Edc1 und Edc3, reguliert werden. Die genauen Details dieser strukturellen Änderungen und ihre funktionelle Rolle im Decapping-Prozess sind noch nicht vollständig verstanden. Die Kernspinresonanzspektroskopie (NMR) ist eine gut geeignete Methode, um dynamische Prozesse und Konformationsänderungen von Enzymen zu untersuchen. In meiner Dissertation habe ich daher verschiedene NMR-Experimente und ergänzende Techniken verwendet, um die mRNA-Abbaumaschinerie von *S. pombe* im Detail zu untersuchen.

In Part III verwendete ich die $^{13}CH_3$-Methylgruppenmarkierung von Dcp2 und führte Methyl-Carr-Purcell Meiboom-Gill (CPMG) NMR Relaxationsdispersionsexperimente (RD-Experimente) am Dcp1:Dcp2-Komplex bei hohem hydrostatischen Druck durch. Aus diesen Experimenten erhielt ich Informationen über die molekularen Volumina der verschiedenen Konformationen des Komplexes während seines Öffnungs- und Schließvorgangs und über die Wirkung von ATP auf diese Volumina. Diese Informationen konnten nicht zuverlässig aus bekannten Kristallstrukturen gewonnen werden, was das Potenzial druckabhängiger NMR-Methoden unterstreicht, Einblicke in strukturelle Eigenschaften unsichtbarer Proteinkonformationen, selbst von Komplexen mit hohem Molekulargewicht, zu erhalten.

In Part IV untersuchte ich die Anwendbarkeit der 5-Fluortryptophan-Markierung zur Messung von Proteindynamik mit ^{19}F-NMR-Experimenten und verwendete dazu drei verschiedene Systeme, nämlich den Dcp1:Dcp2-Komplex, die KIX-Domäne des transkriptionellen Koaktivators CREB-Bindungsprotein und das Scavenger-Decapping-Enzym DcpS. Ich fand heraus, dass die Markierung mit ^{19}F auf dem 5-Tryptophan keinen messbaren Einfluss auf die Dynamik des Rückgrats der untersuchten Proteine hat und dass langsame Proteinbewegungen zuverlässig aus ^{19}F-NMR-Experimenten extrahiert werden konnten, die unempfindlich gegenüber Tryptophan-Seitenkettenbewegungen sind. Im Gegensatz dazu habe ich festgestellt, dass NMR-Relaxationsexperimente am ^{19}F-Kern an dieser Position nicht immer eine zuverlässige Extraktion kinetischer und thermodynamischer Eigenschaften zulassen, sodass diese Daten immer durch Daten aus komplementären Techniken gestützt werden sollten.

In Part V führte ich Einzelmolekül-Förster-Resonanzenergietransfer-Experimente (smFRET-Experimente) am Dcp1:Dcp2-Komplex durch. Wir optimierten zunächst die Markierungspositionen der Fluorophore, indem wir verschiedene Kombina-

tionen von Markierungspositionen testeten und diese mit NMR-Experimenten an Fluorophor-markierten Dcp1:Dcp2-Komplexen überprüften. In anschließenden smFRET-Messungen bestätigte ich die zuvor erhaltenen NMR-Daten und untersuchte den Einfluss verschiedener Kofaktoren und Substrate, die für NMR-Experimente nicht geeignet sind. Da die Fluorophor-Markierung das Konformationsgleichgewicht des Dcp1:Dcp2-Komplexes beeinflussen kann, ist eine Kreuzvalidierung der smFRET-Daten für die korrekte Interpretation der FRET-Effizienzen von entscheidender Bedeutung.

In Gegenwart von Edc3 durchläuft der Dcp1:Dcp2-Komplex eine Flüssig-Flüssig-Phasentrennung (LLPS) und nimmt einen gelartigen Zustand an, über den bisher wenig bekannt ist. Um die Konformationsänderungen und die Dynamik von Edc3 und Dcp2 nach dem Übergang in den gelartigen Zustand zu untersuchen, führten wir Festkörper-NMR-Experimente (ssNMR-Experimente) an Edc3 und Dcp1:Dcp2 im Gelzustand durch (Part VI). Wir entwerfen ein Modell, in dem die Faktoren der mRNA-Decapping-Maschinerie nach LLPS in einen strukturell inhomogenen, gelartigen Zustand übergehen, in dem die in Lösung gemittelten Molekularbewegungen und intermolekularen Kontakte eingefroren sind und nicht mehr gemittelt werden. Unsere Ergebnisse zeigen die gute Eignung der ssNMR zur Untersuchung großer molekularer Maschinen im kondensierten, phasengetrennten Zustand.

Zusammengefasst tragen diese Ergebnisse zu unserem Verständnis bei, wie Konformationsänderungen den Abbau der mRNA-Cap-Struktur regulieren, wodurch letztlich ein tieferes Verständnis der Funktionsweise großer molekularer Maschinen gewonnen wird.

Publications

Published

Krempl, Christina and Remco Sprangers (2023). "Assessing the applicability of ^{19}F labeled tryptophan residues to quantify protein dynamics." In: *Journal of Biomolecular NMR* 77.1, pp. 55–67. issn: 1573-5001. doi: 10.1007/s10858-022-00411-2. url: https://doi.org/10.1007/s10858-022-00411-2

Author contributions: C.K.: Formal analysis, Investigation, Methodology, Software, Visualization, Writing, R.S.: Conceptualization, Formal analysis, Funding acquisition, Methodology, Project administration, Supervision, Validation, Writing.

Krempl, Christina, Jan-Philip Wurm, Markus Beck-Erlach, Werner Kremer and Remco Sprangers (2023). "Insights into the Structure of Invisible Conformations of Large Methyl Group Labeled Molecular Machines from High Pressure NMR." In: *Journal of Molecular Biology* 435.11, pp. 195-247. issn: 00222836. doi: 10.1016/j.jmb.2022.167922. url: https://linkinghub.elsevier.com/retrieve/pii/S0022283622005496

Author contributions: C.K.: Formal analysis, Investigation, Methodology, Software, Visualization, Writing. J.P.W.: Conceptualization, Investigation, Methodology, Supervision, Writing (review & editing). M.B.E.: Methodology, Writing (review & editing). W.K.: Conceptualization, Methodology, Resources, Supervision, Writing (review & editing). R.S.: Conceptualization, Formal analysis, Funding acquisition, Methodology, Project administration, Supervision, Validation, Writing.

In preparation

Krempl, Christina, Daniela Lazzaretti and Remco Sprangers (2023). "A structural biology view on the enzymes involved in eukaryotic mRNA turnover." In: *Biological Chemistry*. doi: 0.1515/hsz-2023-0182. url: https://doi.org/10.1515/hsz-2023-0182. Accepted for publication.

Author contributions: All the authors have accepted responsibility for the entire content of this submitted manuscript.

Contents

Acknowledgements v

Summary vii

Zusammenfassung ix

Publications xi

Abbreviations xvi

I. Introduction 1

1. mRNA decapping 3
- 1.1. Eukaryotic mRNAs . . . 3
- 1.2. The mRNA decapping complex Dcp1:Dcp2 . . . 6
- 1.3. The scavenger decapping enzyme DcpS . . . 9

2. Structural biology methods to study enzymes 13
- 2.1. Structural biology . . . 13
- 2.2. NMR spectroscopy . . . 15
- 2.3. Single molecule FRET experiments . . . 29

II. Materials and Methods 35

1. Molecular biology 37
- 1.1. Mutagenesis and Gibson Assembly . . . 37

2. Protein expression, isotope labeling and purification 37
- 2.1. Transformation and recombinant expression . . . 37
- 2.2. Isotope labeling . . . 38
- 2.3. Purification . . . 40

3. Protein fluorophore labeling 41
- 3.1. Cysteine-Maleimide coupling . . . 41
- 3.2. Staudinger Ligation . . . 42

4. RNA preparation 43
- 4.1. RNA transcription and purification . . . 43
- 4.2. 5' OH RNA production . . . 44
- 4.3. RNA 5' m^7G capping . . . 44

5. Liquid-liquid phase separation **45**
5.1. LLPS and maturation 45

6. NMR spectroscopy **45**
6.1. High pressure NMR 45
6.2. ^{19}F NMR experiments 47
6.3. NMR on fluorophore labeled complexes 48
6.4. Solid-state NMR experiments 48

7. smFRET experiments **49**
7.1. smFRET measurements 50
7.2. smFRET data analysis 50

8. Visualization **52**
8.1. Visualization 52

III. High Pressure NMR of Dcp1:Dcp2 53

1. Introduction **55**

2. Results **59**
2.1. Dcp1:Dcp2 mRNA decapping complex 59
2.2. Dcp1:Dcp2 mRNA decapping complex with ATP 65

3. Discussion **69**

IV. The Applicability of ^{19}F NMR 71

1. Introduction **73**

2. Results **77**
2.1. KIX domain of the CREB-binding protein 77
2.2. Dcp1:Dcp2 mRNA decapping complex 83
2.3. DcpS scavenger decapping complex 94

3. Discussion **99**

V. Single Molecule FRET experiments of the Dcp1:Dcp2 mRNA decapping complex 101

1. Introduction **103**

2. Results **107**
2.1. Validation of smFRET labeling positions 107
2.2. NMR experiments with fluorophore labeled Dcp1:Dcp2 111
2.3. smFRET measurements of the Dcp1:Dcp2 decapping complex . . 113

3. Discussion **121**

VI. Solid state NMR of mRNA decapping enzymes 125

1. Introduction **127**

2. Results **131**
2.1. LLPS of Edc3 131
2.2. LLPS of Dcp2 134

3. Discussion **139**

VII. Conclusion and Outlook 141

1. Conclusion and Outlook **143**

Bibliography **xviii**

Abbreviations

1D, 2D, 3D	one-, two-, threedimensional
AI	artificial intelligence
APBS	all photon burst search
ATP/ADP	adenosine tri-/diphosphate
AzF	4-Azido-L-Phenylalanine
BSA	bovine serum albumin
BTFA	3-bromo-1,1,1-trifluoroacetone
CEST	chemical exchange saturation transfer
CPMG	Carr-Purcell Meiboom-Gill
Cryo-EM	cryoelectron microscopy
Cryo-ET	cryoelectron tomography
CSA	chemical shift anisotropy
CSP	chemical shift perturbation
CD/CTD	C-terminal domain
ct	cross talk
Dcp(S)	(scavenger) decapping protein
DD	Dipole-dipole
de	direct excitation
Dhh	DEAD-box helicase homolog
DNA	deoxyribonucleic acid
DTT	Dithiothreitol
E. Coli	*Escherichia coli*
Edc	enhancer of decapping
eIF	eukaryotic Initiation Factor
EPR	electron paramagnetic resonance
EVH	enabled/vasodilator-stimulated phosphoprotein homology
EXSY	exchange spectroscopy
FID	free induction decay
FL	full length
GPCR	G protein-coupled receptor
GDP/GMP	guanosine di-/monophosphate
H. sapiens	*Homo sapiens*
HEPES	2-(4-(2-Hydroxyethyl)-1-piperazinyl)- ethanesulfonic acid
His	histidine
HIT	histidine triade
HIV	human immunodeficiency virus
HLM	helical leucine-rich motif
HMCQ	heteronuclear multiple quantum coherence
HP	high pressure
HSQC	heteronuclear single quantum coherence
IDR	intrinsically disordered region
INEPT	insensitive nuclei enhanced by polarization transfer
IPTG	isopropyl beta D-1 thiogalactopyranoside
K. lactis	*Kluyveromyces lactis*
LB	lysogeny broth
LLPS	Liquid-liquid phase separation
LSm	Like Smith
m^7G	N7-methyl guanosine
MAS	magic angle spinning
MBP	maltose binding protein
MD	molecular dynamics
mi-RNA	micro- ribonucleic acid
mRNA	messenger ribonucleic acid
NiNTA	Nickel-nitrilotriacetic acid
NMR	Nuclear magnetic resonance
NOE(SY)	Nuclear Overhauser effect (spectroscopy)
nt	nucleotide
NTD	N-terminal domain
(N)RD	(N-terminal) regulatory domain
NSR	nuclear spin relaxation
NUDIX	nucleoside diphosphates linked to a moiety X
OD_{600}	optical density at λ = 600 nm
P-body	Processing body
Pab	PolyA binding
PAGE	polyacrylamide gel electrophoresis
Pat	protein associated with topoisomerase II
PCR	polymerase chain reaction
PDB	protein data bank

PIE	pulsed interleaved excitation	**SDS**	Sodium dodecylsulfate
PRE	paramagnetic relaxation enhancement	**(sm)FRET**	(single molecule) Förster resonance energy transfer
RD	relaxation dispersion	**ssNMR**	solid state NMR
RDC	residual dipolar coupling	**SOFAST**	Band-selective optimized flip-angle short-transient
rf	radio frequency	**SPAD**	Single-photon avalanche diode
RF RD	rotating frame relaxation dispersion	**SQ**	single quantum
RNA	ribonucleic acid	**TEV**	tobaccho etch virus
RNP	Ribonucleoprotein	**TIRF**	total internal reflection fluorescence
S. cerevisiae	*Saccharomyces cerevisiae*	**TROSY**	transverse relaxation-optimized spectroscopy
S. pombe	*Schizosaccharomyces pombe*	**Xrn**	exoribonuclease
SARS-CoV	severe acute respiratory syndrome coronavirus	**UTR**	untranslated region
SEC	size exclusion chromatography	**WT**	wild type

Amino acids are abbreviated by their one- or three-letter code. Nucleobases are abbreviated by their one-letter code.

Part I.

Introduction

1. mRNA decapping

This chapter contains parts written for a review that I co-authored which was submitted to "Biological Chemistry".

1.1. Eukaryotic mRNAs

During gene expression in a cell, all steps from transcription and translation to RNA degradation are tightly regulated (Schoenberg and Maquat 2012). In that process, genetic information that is encoded in the DNA is transcribed into messenger RNA (mRNA). This transcript is then exported from the nucleus to the cytoplasm and translated into proteins by the ribosome. To maintain cellular homeostasis, the targeted degradation of mRNA is crucial, as it ensures that protein expression levels are regulated and an accumulation of excessive amounts of mRNA is prevented. Thus, no longer needed transcripts and aberrant transcripts which could potentially be translated into toxic proteins are degraded and the stability of specific mRNAs is modulated, so gene expression can rapidly be adapted to changing conditions in the cell.

In eukaryotes, mRNA possesses an m^7G cap structure at its 5' end and a polyA tail at its 3' end (Shatkin 1976). The 5' cap structure blocks access for the exoribonuclease Xrn1 and thereby protects the mRNA from rapid and uncontrolled degradation (Garneau, Wilusz, and Wilusz 2007). In addition, the cap is important for efficient translation as it interacts with the initiation factor eIF4F which in turn recruits the small ribosomal subunit as well as the polyA binding protein (Pab1) (Borman 2000; Sonenberg and Hinnebusch 2009; Topisirovic et al. 2011).

The simplest 5' mRNA cap structure is the cap0, which consists of an N7-methylated guanosine which is connected to the 5‘ end of the mRNA by a 5‘-5‘ triphosphate bridge (Shatkin 1976). When the ribose 2‘ OH group of the first 5‘ RNA base is additionally methylated, the structure is called cap1, and subsequent ribose 2‘ O- methylations result in the formation of cap2 to cap4 structures. These modifications result in differences in mRNA stability, but the exact mechanisms behind that are not fully understood yet (Boo and Kim 2020; Despic and Jaffrey 2023). Generally, methylation of multiple bases occurs more frequently in higher eukaryotes, whereas in simpler organisms like yeast, usually only the first base is methylated (Banerjee 1980).

The 3' polyA tail of the mRNA prevents premature degradation of the transcript from the 3' end by associating with Pab1, thereby connecting the 5' and 3' ends of the mRNA (Eckmann, Rammelt, and Wahle 2011; Mangus, Evans, and Jacobson 2003; Sonenberg and Hinnebusch 2009). Furthermore, it is involved in nuclear export and regulation of translation (Zhao, Hyman, and Moore 1999). The length of the polyA tail can vary significantly, and so it contains 70-80 nucleotides (nt) in yeast and over 250 nt in mammals. Moreover, its length influences cellular function

and consequently it varies for different transcripts and cellular functions (Jalkanen, Coleman, and Wilusz 2014).

Aside from polyA tail length, also other factors such as specific sequence elements (e. g. AU-rich elements in the 3' untranslated region (UTR)) or aberrations in the transcript affect the decay rates of mRNAs (Kurosaki, Popp, and Maquat 2019; Xu, Chen, and Shyu 1997). Thus, mRNA lifetimes have been shown to range from three to 90 minutes in yeast (Wang and Kiledjian 2001) and they can be even longer in humans (Yang, Nimwegen, et al. 2003).

Degradation of the mRNA transcript follows one of two main degradation pathways and proceeds either from the 5' or from the 3' end (Łabno, Tomecki, and Dziembowski 2016) (Figure 1.1). Both pathways are present in eukaryotes but different organisms preferably employ one or the other. 5' → 3' mRNA degradation is the major degradation pathway in yeast whereas 3' → 5' mRNA degradation is more abundant in mammals (Muhlrad, Decker, and Parker 1995; Wang and Kiledjian 2001).

In both pathways, mRNA degradation is initiated with the deadenylation of the 3' polyA tail, which occurs in two steps and is often rate limiting in mRNA decay. First, the deadenylase complex Pan2:Pan3 shortens the length of the polyA tail until it can only interact with one or two copies of Pab1 (Schäfer et al. 2019). This generally occurs at a length of less than 10 to 12 nt. Pab1 then dissociates from the mRNA and is replaced by the multi-subunit Ccr4:Not complex, which contains the catalytically active exonuclease CNOT7/Caf1/Pop2 and the deadenylase CNOT6/Ccr4, which further deadenylates the transcript (Parker 2012; Parker and Song 2004; Tucker et al. 2002; Wilusz, Wormington, and Peltz 2001). After deadenylation, highly specialized enzymes can then rapidly and irreversibly degrade the mRNA transcript, and this occurs either from the 5' end, via decapping by the Dcp2 enzyme and subsequent hydrolysis of the mRNA body by the exoribonuclease Xrn1, or from the 3' end, via processing by the cytoplasmic exosome and subsequent decapping by the scavenger decapping enzyme DcpS.

In 5' → 3' degradation, the heteroheptameric, doughnut-shaped LSm1-7 complex interacts with the deadenylated 3' end of the mRNA at its pore while its subunits LSm2 and LSm3 bind to the helical C-terminal region of the scaffolding protein Pat1 (Montemayor et al. 2020; Sharif and Conti 2013; Wu et al. 2014). The C-terminal region of Pat1 in turn recruits the mRNA decapping enzyme Dcp2 by binding one of multiple helical motifs in the intrinsically disordered C-terminus of Dcp2, thereby linking 3' deadenylated transcript recognition to 5' mRNA cap hydrolysis (Charenton, Gaudon-Plesse, et al. 2017; Deshmukh et al. 2008; Dijk 2002; Mugridge, Coller, and Gross 2018; Sharif and Conti 2013; Tharun and Parker 2001; Wang, Jiao, et al. 2002). Interestingly, human Dcp2 lacks that C-terminal intrinsically disordered region (IDR), and instead, the human Dcp1 protein contains a long, intrinsically disordered C-terminus (Charenton, Gaudon-Plesse, et al. 2017). Dcp2 then hydrolyzes the m^7G cap structure of the mRNA and generates the decapping products m^7GDP and 5' monophosphorylated mRNA (Steiger et al. 2003), which then gets further degraded by the exoribonuclease Xrn1 (Łabno, Tomecki, and Dziembowski 2016). 5' mRNA degradation however does not only involve Dcp2 but a much larger network of decapping factors, including the main activator of decapping Dcp1 as well as Edc1, Edc3 and Dhh1, which all contribute to an

enhanced decapping efficiency (Deshmukh et al. 2008; Sharif, Ozgur, et al. 2013; She, Decker, Chen, et al. 2006; Wurm, Holdermann, et al. 2017).

In 3' → 5' mRNA decay, the mRNA is first hydrolyzed by the cytoplasmic exosome complex. This multi-protein complex forms a catalytically inactive, barrel-like hexameric ring structure, called Exo-9, which the mRNA can enter via a narrow pore at the top (Liu, Greimann, and Lima 2006). The mRNA is then passed through the central channel and reaches the catalytically active Dis3/Rrp44 protein at the opposite side of the pore, where the mRNA is hydrolyzed in a highly processive way. The catalytically active complex of Dis3/Rrp44 and Exo-9 is termed Exo-10 (Januszyk and Lima 2014; Makino, Baumgärtner, and Conti 2013; Makino and Conti 2013; Schneider and Tollervey 2013). Degradation products of the exosome are single nucleotides and a small capped RNA fragment of two to five nucleotides (Fuchs et al. 2020; Mitchell et al. 1997). The 5' cap of this short fragment is then further degraded by the scavenger decapping enzyme DcpS (Dcs1p in yeast) which releases m^7GMP and a 5' diphosphorylated mRNA fragment (Nuss and Furuichi 1977).

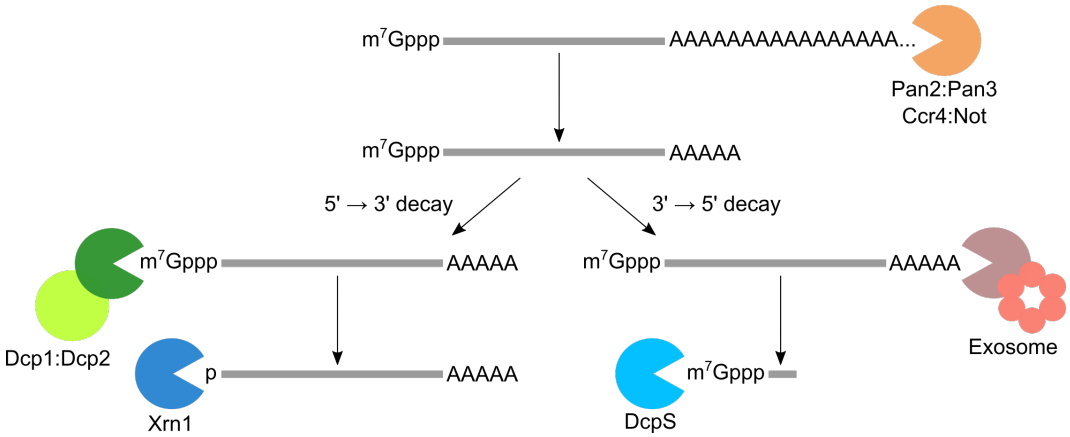

Figure 1.1.: mRNA degradation pathways. Degradation of eukaryotic mRNA is initiated by deadenylation by the Pan2:Pan3 and the Ccr4:Not complexes before it is subjected to one of two degradation pathways. In 5‘ → 3‘ decay, the 5‘ cap is hydrolyzed by the Dcp1:Dcp2 complex and then the mRNA body is further degraded by the exoribonuclease Xrn1. In 3‘ → 5‘ decay, the RNA is degraded from the 3‘ end by the exosome and then the DcpS enzyme removes the cap from the remaining short capped mRNA fragments.

Altogether, these hereby described pathways form the basis for the firm regulation of mRNA degradation. Certainly, a number of variations in these pathways exist in a cell which differ in their recruitment of the different factors and they include nonsense-mediated decay, non-stop decay and no-go decay (Lykke-Andersen and Jensen 2015; Schoenberg and Maquat 2012). Cellular mRNA levels are thus strongly regulated by tightly controlled mRNA degradation mechanisms. A detailed structural and mechanistic examination of these processes is however difficult due to the highly dynamic and flexible properties of the involved enzymes. Nonetheless, understanding the conformational changes and motions of these enzymes is indispensable as they drive the cellular processes like mRNA decay (Neu et al. 2015; Wurm, Holdermann, et al. 2017).

1.2. The mRNA decapping complex Dcp1:Dcp2

Dcp2 is the main mRNA decapping enzyme in the 5' → 3' mRNA decapping pathway (Garneau, Wilusz, and Wilusz 2007). It is composed of an N-terminal regulatory domain (RD; residues 1-95 in *S. pombe*) and a catalytic domain (CD; residues 96-243 in *S. pombe*), which are connected by a flexible, 4 amino acid long linker, and it contains an additional, intrinsically disordered C-terminus. The C-terminus is about 100 amino acids long in plants and humans and more than five hundred amino acids long in yeast, where it contains multiple helical leucine-rich motifs (HLMs) (Dijk 2002; McLennan 2006; Wang, Jiao, et al. 2002). The CD contains a loop-helix-loop NUDIX motif and therefore belongs to the NUDIX family of hydrolases. Generally, members of that family catalyze the hydrolysis of diphosphates which are linked to nucleosides and they often display a broad substrate specificity (Bessman, Frick, and O'Handley 1996). Dcp2, in particular, binds and hydrolyzes m^7G capped RNA (McLennan 2013). Cap hydrolysis occurs at the NUDIX motif through the coordination of catalytic Mg^{2+} ions via three conserved glutamates (Wurm, Holdermann, et al. 2017). The intrinsically disordered C-terminus of Dcp2 is reported to possess an autoinhibition mechanism for decapping, which could provide an intrinsic mechanism for the regulation of decapping activity (Paquette et al. 2018).

So far, most studies on the structure and function of decapping enzymes have been performed on *S. pombe* and *K. lactis* enzymes, but it is very likely that most of their features are conserved in higher eukaryotes (Jonas and Izaurralde 2013; Song, Bail, and Kiledjian 2013).

In *S. pombe* it was found that the isolated CD of Dcp2 displays limited decapping activity, but this activity is increased about 65-fold in the presence of the RD, and even more upon binding to different interaction partners (Wurm, Holdermann, et al. 2017). The central interaction partner of Dcp2 is the main activator of decapping Dcp1 and together they form the mRNA decapping complex Dcp1:Dcp2. Dcp1 binds tightly to the RD of Dcp2 whereby it stabilizes the N-terminal domain and consequently further increases the decapping activity of Dcp2 (Beelman et al. 1996; Steiger et al. 2003). Dcp1 possesses an enabled/vasodilator-stimulated phosphoprotein homology 1 (EVH1) protein domain and it can recruit other decapping factors with proline-rich motifs via a dynamic, hydrophobic β-sheet surface, which leads to an even further increase in decapping activity (Borja et al. 2011; Steiger et al. 2003; Wurm, Overbeck, and Sprangers 2016).

The Dcp1:Dcp2 decapping complex has been shown to be very dynamic and so the CD of Dcp2 can adopt different orientations relative to the rigid conformation that is formed between the RD of Dcp2 and Dcp1 (Charenton, Taverniti, et al. 2016; Floor, Borja, and Gross 2012; She, Decker, Sundramurthy, et al. 2004; She, Decker, Svergun, et al. 2008; Wurm, Holdermann, et al. 2017). Several crystal structures of Dcp2 alone and in complex with other decapping factors were solved and in these structures the domain orientations with respect to the catalytic site differ substantially. Three of the conformations observed in crystal structures, which are distinguished by the orientation of the CD relative to the rigid RD:Dcp1 structure, could be detected in solution. These three conformations comprise a catalytically inactive closed state, an open state which is also catalytically inactive but has a

high affinity for the mRNA body, and an active state in which mRNA decapping can occur (Figure 1.2). In addition, the dynamics between these conformations were examined and quantified in detail using NMR spectroscopy (Floor, Borja, and Gross 2012; Wurm, Holdermann, et al. 2017). These results demonstrate that a combination of multiple, complementary methods is invaluable to obtain a profound understanding of structures and dynamics of enzymes and, consequently, of their functions (Hennig and Sattler 2014).

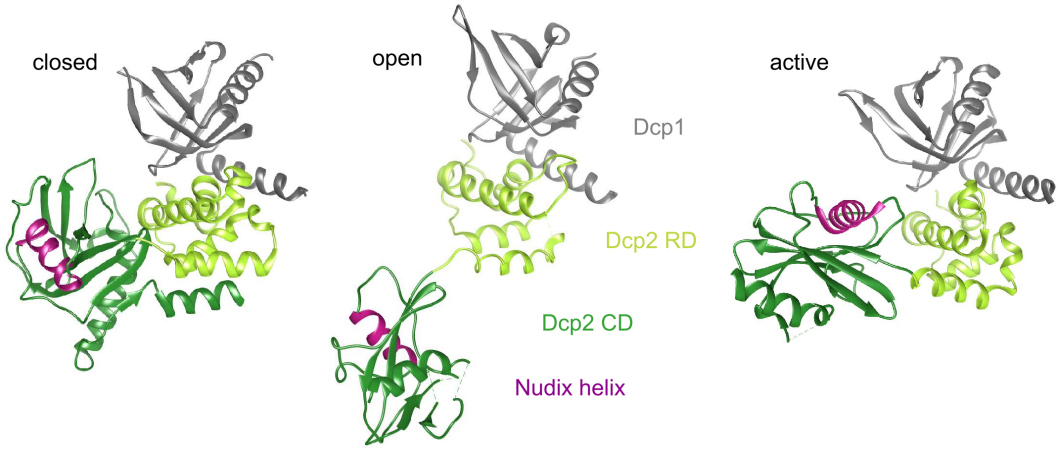

Figure 1.2.: Crystal structures of the Dcp1:Dcp2 mRNA decapping complex from *S. pombe*. Dcp1 here is colored in grey, the RD of Dcp2 in light green and the CD of Dcp2 in dark green. The Nudix helix, which is important for catalysis, is colored in magenta. In the absence of substrate, the Dcp1:Dcp2 mRNA decapping complex exchanges between a catalytically inactive closed (PDBiD 2qkm chains A, B) and an open conformation (PDBiD 2qkm chains C, D). In the presence of substrate and Edc1, its CD rearranges and the complex fully adopts the active conformation in which the Nudix helix is directed towards the catalytic center (PDBiD 5n2v).

Dcp2 exchanges between an open and a closed conformation with a rate of 1600 s^{-1} and both states are populated to 50 %. In complex with Dcp1, the same conformations are present and their exchange rate increases only slightly, but the conformational equilibrium of the complex shifts strongly towards the closed state (94 %) (Wurm, Holdermann, et al. 2017). The transition from the closed to the open state starts with a local rearrangement of interface residues of Dcp2, and in the next step, the two Dcp2 domains separate and adopt the open conformation.

The open and the closed state are, however, catalytically inactive. The two structured domains of Dcp2 share a split active site, but in the presence of Dcp1, access to the RNA binding site is blocked by the RD, and so mRNA binding is prevented and mRNA binding affinity is compromised. The presence of only substrate mRNA leads to a competition between mRNA binding and formation of the closed state in the decapping complex and results in the adoption of mainly open conformations and only a transient formation of the active state (Wurm, Holdermann, et al. 2017; Wurm and Sprangers 2019). A stable active conformation is only adopted in the joint presence of Edc1 and substrate. Edc1 is an approximately 200 aa long intrinsically disordered protein that binds to the β-sheet surface of Dcp1 and thereby stabilizes the active state of Dcp2 when substrate is present. In contrast, binding of Edc1 alone does not influence the open-closed equilibrium of the Dcp1:Dcp2 complex. Decapping activation by Edc1, in the presence of substrate, is achieved through a YAGxxF activation motif in the 25 aa short fragment that follows the proline rich region that binds to Dcp1 (Borja et al. 2011; Valkov et

al. 2016; Wurm, Overbeck, and Sprangers 2016). The YAGxxF motif is placed between the RD and the CD of Dcp2 and makes several stacking and hydrogen bonding interactions with both domains and thus gives rise to a stabilization of the catalytically active state of Dcp2. This stabilization is further secured by the m^7G cap structure, which binds at the active site between the RD (residue W43 in *S. pombe*) and a conserved loop in the CD of Dcp2 (residues R190 and K191), while at the same time the phosphate groups between the m^7G cap and the mRNA body bind to the NUDIX motif in the CD in the presence of three Mg^{2+} ions (Wurm and Sprangers 2019).

A different activity enhancement mechanism, in which no domain reorientations take place in solution, is observed upon binding of the enhancer of decapping Edc3 (Fromm, Truffault, et al. 2012). Edc3 is a scaffolding protein which consists of an N-terminal LSm domain, a C-terminal YjeF_N dimerization domain and an intrinsically disordered linker region (Sharif, Ozgur, et al. 2013; Tritschler et al. 2009). The N-terminal LSm domain of Edc3 binds to the HLMs in the disordered C-terminus of Dcp2 which leads to an extension of the C-terminal α-helix of the CD and thus an enlargement of the mRNA binding site in Dcp2, thereby enhancing Dcp2 activity (Charenton, Taverniti, et al. 2016; Mugridge, Tibble, et al. 2018).

The network of proteins interacting with Dcp2 is, however, much larger and includes many additional factors such as Dhh1, Xrn1, Upf1 and Pat1. The latter two, like Edc3, interact with short linear motifs in the intrinsically disordered C-terminus of Dcp2 and compete for binding to HLMs, which facilitates rapid rearrangement and adaptation of the protein conformation to changing conditions (He and Jacobson 2015; Jonas and Izaurralde 2013). Apart from harboring multiple HLMs for ligand binding, the intrinsically disordered C-terminus of Dcp2 also contains two autoinhibitory motifs which can interact with the structured core of Dcp2 (Paquette et al. 2018). This inhibits the formation of the catalytically active conformation by stabilizing the closed, inactive conformation. The autoinhibitory mechanism is alleviated in the presence of Edc3 and Pat1 as they bind in close proximity to the autoinhibitory motifs and thus prevent the formation of the autoinhibited state.

Taken together, Dcp1 as well as the intrinsically disordered C-terminus of Dcp2 are the driving forces in the regulation of mRNA decay as they both recruit different mRNA decay factors needed for the efficient decapping of mRNA.

Aside from controlling mRNA degradation through the recruitment of different decapping factors to the decapping complex and its subsequent activation, Dcp1:Dcp2 is additionally able to undergo liquid-liquid phase separation (LLPS), which is thought to be a further mechanism of regulation in the cell (Li, Banjade, et al. 2012). Together with mRNA and the other proteins of the mRNA decapping machinery, Dcp1:Dcp2 can be recruited into processing bodies (P-bodies) (Dijk 2002; Sheth and Parker 2003; Teixeira and Parker 2007). P-bodies are membrane-less, self-organized ribonucleoprotein foci in the cytoplasm of a cell that form via LLPS e. g. in response to stress situations like an excessive accumulation of mRNAs, and thus they serve to regulate and maintain the cellular equilibrium (Luo, Na, and Slavoff 2018; Stoecklin and Kedersha 2013). P-body formation is driven by protein-protein and protein-RNA interactions as well as by low-complexity protein sequences as can be found in the intrinsically disordered C-terminus of Dcp2 (Banani et al. 2017;

Fromm, Kamenz, et al. 2014). The exact mechanism of LLPS and its function is not completely understood yet. Thus, it is not clear whether P-bodies are sites of active mRNA degradation or sites for storage of translationally repressed mRNAs (Luo, Na, and Slavoff 2018). It was however found that the catalytic activity of Dcp2 in P-bodies *in vitro* is reduced compared to the disperse, non-phase separated state (Schütz, Nöldeke, and Sprangers 2017; Tibble et al. 2021). In the mRNA decapping machinery, the scaffolding protein Edc3 is central for LLPS. While Edc3 can undergo LLPS on its own, its IDR can interact with mRNA and mRNA decapping enzymes and thereby drive the formation of LLPS droplets (Fromm, Kamenz, et al. 2014; Schütz, Nöldeke, and Sprangers 2017). Edc3 is responsible for the recruitment of Dcp2 into P-bodies, by binding to HLMs in the intrinsically disordered C-terminus of Dcp2 at its LSm domain. Interestingly, the *in vitro* reconstituted LLPS droplets containing purified mRNA decapping enzymes and mRNA quickly mature into a gel-like aggregate of proteins and mRNAs from which they cannot be recovered, which, in consequence, is detrimental to the cell (Damman et al. 2019). Despite the insights gained, our understanding of LLPS and the maturation process of the decapping machinery is still limited. For example, it is not clear if the conformation of Dcp2 changes upon LLPS in favor of an enhancement or an inhibition of mRNA decapping.

1.3. The scavenger decapping enzyme DcpS

The scavenger decapping enzyme DcpS is involved in mRNA degradation from the 3' end (Nuss and Furuichi 1977). After deadenylation of the 3' polyA tail, the exosome degrades the mRNA body, producing single nucleotides as well as a short, 5' capped mRNA fragment of two to at most five nucleotides. (Fuchs et al. 2020; Januszyk and Lima 2014; Mitchell et al. 1997; Zinder, Wasmuth, and Lima 2016). These short, capped mRNAs are then further processed by DcpS. DcpS hydrolyses the 5' cap structure and subsequently releases m^7GMP and dephosphorylated RNA (Liu 2002; Nuss and Furuichi 1977; Wang and Kiledjian 2001).

In its apo state, the 80 kDa DcpS enzyme forms a symmetric homodimer (Liu 2002; Wang and Kiledjian 2001) with a domain-swapped fold. Both N- and C-terminal domains are well structured and connected by a flexible linker (Chen, Walsh, et al. 2005; Gu et al. 2004), but the domains show only little to no interaction with each other (Neu et al. 2015). At the active site of its C-terminal domain, DcpS possesses a histidine triade (H-X-H-X-H), which makes it a member of the Histidine Triad (HIT) protein family of pyrophosphatases (Séraphin 1992). Catalytic activity is only achieved when both N- and C- terminal domains come together as they form the catalytically competent active site together, between the N- and C-terminal lobes (Gu et al. 2004; Lima, Klein, and Hendrickson 1997; Liu 2002; Liu, Jiao, et al. 2004; Séraphin 1992).

To date, different crystal structures of DcpS in its apo state, as well as in complex with different cap analogues, m^7GDP and medicinal inhibitors have been solved for the human and the mouse enzyme (Chen, Walsh, et al. 2005; Gu et al. 2004; Han et al. 2005; Singh et al. 2008; Wojtczak et al. 2018). In yeast, the crystal structure was solved for the catalytically inactive form DcpS H268N in complex with the inhibitor m^7GDP (Neu et al. 2015) as well as in complex with the capped RNA dinucleotide

m^7GpppGU. In *C. thermophilum*, only the structure of the apo protein is available (Fuchs et al. 2020).

In all organisms, the structural symmetry of the apo DcpS enzyme is lifted upon ligand binding and a distinct, asymmetrical conformation is adopted in which a closed, catalytically active site and an open, inactive site are formed (Figure 1.3). In this asymmetric state, the side chain residues of the open site experience nearly no structural changes compared to the apo state, but at the closed site, substantial reorientations of a number of side chain residues take place when the N-terminal domain flips onto the C-terminal domain to form the catalytically competent active site around the ligand (Chen, Walsh, et al. 2005). Simultaneously, at the second binding site at the opposite side of the enzyme the N-terminal domain rotates around its central axis by 37° which corresponds to a 30 Å movement, opening up into the inactive conformation (Chen, Walsh, et al. 2005; Gu et al. 2004). In this inactive, open conformation, a second substrate can be recruited, and, while the first substrate is hydrolyzed at the first active site, the N-terminal domain of the second binding site flips over and encloses the new substrate at its now newly formed, second active site, which results in the release of the decapping products at the first active site. In this way, DcpS performs an allosterically regulated flipping motion to efficiently decap short, 5' capped mRNA fragments (Neu et al. 2015).

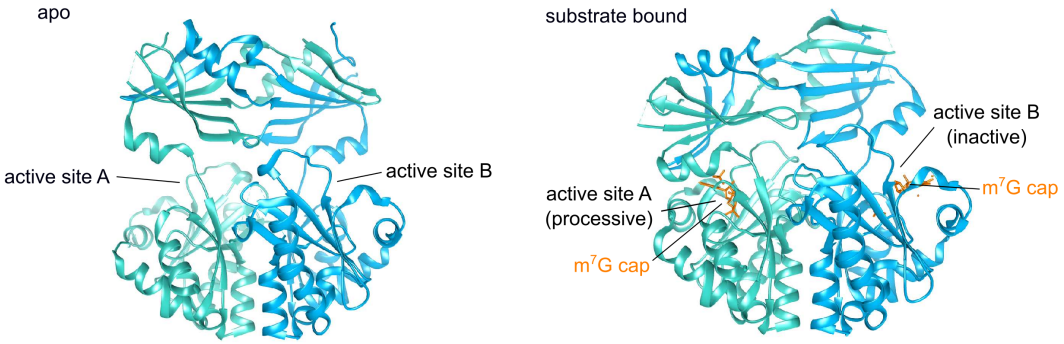

Figure 1.3.: Crystal strucutres of human DcpS. In the absence of substrate, the scavenger decapping enzyme DcpS is symmetric (PDBiD 2xml). In the presence of substrate, its domains rearrange and it adopts an asymmetric conformation (PDBiD 2xmm).

The decapping process itself is a hydrolysis reaction in which the central histidine of the HIT histidine triade serves as a nucleophile that attacks the α-phosphate of the triphosphate linkage at the cap of the short mRNA fragment. This results in the release of the decapping products m^7GMP and dephosphorylated mRNA (Chen, Walsh, et al. 2005; Lima, Klein, and Hendrickson 1997). At equimolar concentrations of mRNA substrate and DcpS enzyme, one binding site per dimer is occupied and at an excess of substrate, subsequent binding of substrate to the second binding site takes place (Gu et al. 2004; Liu, Rajagopal, et al. 2008; Neu et al. 2015). Interestingly, the first binding site has a much higher affinity to the mRNA cap (analogue) compared to the second binding site. This can be explained by the fact that the second substrate interacts only with residues of the C-terminal domain. The decapping products however have a very low affinity to the open binding site, which facilitates an efficient product release and subsequent binding of new substrate (Neu et al. 2015).

The rate of the decapping reaction depends on the concentration of available

substrate. Thus, under single turnover conditions, cap binding limits the decapping rate while under multiple turnover conditions, the reorientation of the side chain to form the catalytically competent state is the limiting factor for cap removal (Liu, Rajagopal, et al. 2008). Additionally, with increasing substrate concentration the enzyme's flipping motions to remove the mRNA cap increase. Too large of an excess of substrate and the resulting increase in speed of the domain motions was however found to strongly decrease catalytic turnover rates. The reason for this is that catalysis cannot be performed any more because the lifetime of the closed, catalytically competent conformation is too short to perform catalysis (Liu, Rajagopal, et al. 2008; Neu et al. 2015).

In addition, it was found that the catalytic activity of DcpS depends heavily on substrate length. It is most active on short substrates of one to two nucleotides and its activity decreases with increasing substrate length. At an excess of enzyme, a strongly reduced, residual activity was observed for substrates longer than 15 nucleotides (Liu 2002) while at an excess of substrate, the activity drops significantly from a one nucleotide capped RNA to a two nucleotide capped RNA and it reaches its basal activity for three nucleotides. Interestingly though, some basal activity still remains for substrates longer than three nucleotides. This dependence of catalytic activity on substrate length is due to the steric hindrance caused by the third mRNA nucleotide which prevents the formation of a stable asymmetric conformation and, with that, the catalytically competent closed site (Fuchs et al. 2020). Thus, DcpS processes only very short mRNAs which are intended for degradation instead of longer mRNAs that might still be actively translated, and, in line with that, DcpS has a much higher affinity for short substrates compared to long substrates (Neu et al. 2015). Furthermore, DcpS specifically recognizes the m^7G cap structure which it binds by specific side-chain interactions. Despite slight differences in molecular interactions, it is, however, irrelevant if the first base of the RNA body is G or A (Gu et al. 2004; Liu 2002; Nuss and Furuichi 1977).

Even though DcpS is active on its own, it can interact and form complexes with other proteins of the mRNA decapping machinery, e. g. components of the exosome or Xrn1 (Sinturel et al. 2012; Wang and Kiledjian 2001). Since Xrn1 is involved in the degradation of decapped mRNA in the 5' $\rightarrow$ 3' decay pathway, DcpS can in this way have an indirect influence on the regulation of mRNA decay from the 5' end as well as on mRNA stability, which is generally mediated by protein-protein interactions (Liu and Kiledjian 2005; Zhou et al. 2015). Furthermore, DcpS participates in miRNA processing (Bossé et al. 2013; Meziane et al. 2015) and pre-mRNA splicing (Shen et al. 2008), and it gets phosphorylated in response to cellular stress conditions such as changes in nutrient availability (Malys 2004). A special mechanism that is unique to DcpS in *S. cerevisiae* is the existence of an inactive homologue (Dcs2p) that can form heterodimers with active DcpS, thereby downregulating catalytic activity (Malys 2004; Malys and McCarthy 2006). However, the core protein fold is highly conserved among all species used here and therefore the mechanisms of substrate recognition and mRNA length sensing are the same for all species studied here, too (Fuchs et al. 2020).

2. Structural biology methods to study enzymes

2.1. Structural biology

The functions of proteins are determined by their structures and by the structural changes they undergo. The structural characterization of proteins thereby contributes to understanding the mechanisms underlying all biological processes, so knowledge about protein structures and about effects resulting from changes in their structures, as well as about their actions and interaction networks provides valuable information about their functions. This information contributes to a better understanding of diseases and provides the basis for advances in drug development and treatment of disease (Ng et al. 2015; Singh et al. 2008). In recent years, immense progress has been made in understanding protein aggregation into amyloid fibrils, which is strongly linked to severe illnesses like Alzheimer's disease, Parkinson's disease and type II diabetes (Fitzpatrick et al. 2017; Iadanza et al. 2018). Other examples for which an understanding of molecular mechanisms provided crucial insight for drug development include the recent rapid development of vaccines against severe acute respiratory syndrome coronavirus type 2 (SARS-CoV-2) (Lett et al. 2023; Yang and Rao 2021), but also the development of drug targets for cancer (Bridge et al. 2023; Scott, Wolchok, and Old 2012) and Human immunodeficiency virus (HIV) (Li, Mori, et al. 2023; Puhl et al. 2019).

To study the three-dimensional (3D) structures, motions and interactions of biological molecules, a wide variety of experimental techniques and instruments have been developed and advances in software and computational techniques have led to even further progress. Some key methods in structural biology to date are X-ray crystallography (Bernal and Crowfoot 1934; Kendrew et al. 1958), (cryo-) electron microscopy (cryo-EM) (Fischer et al. 2015; Ye, Liu, and Li 2022) and nuclear magnetic resonance (NMR) spectroscopy (Williamson, Havel, and Wüthrich 1985). While x-ray crystallography, which emerged in the 1920s and was first employed in structural biology to prove that DNA adopts a double helical structure (Bragg 1915; Bragg 1929; Watson and Crick 1953), allows to obtain atomistic 3D structures of bio-molecules, cryo-EM was developed in the 1970s but only recent advances in detector technology and software have led to its success today. Modern cryo-EM allows to obtain the conformations of proteins and protein complexes at Ångström resolution without the need for crystallization (Cheng et al. 2015; She, Decker, Svergun, et al. 2008). The foundations of NMR spectroscopy were laid in the 1940s when magnetic resonance signals of atomic nuclei were first observed (Bloch, Hansen, and Packard 1946; Purcell, Torrey, and Pound 1946). Since then advances in instrumentation, sample preparation and software have made NMR an equally powerful

method to study biomolecules. Thus, while X-ray crystallography and cryo-EM are mostly used to record static images of large biomolecules, the strength of NMR spectroscopy lies in the unique possibility to detect and quantify dynamic processes in biomolecules at atomic resolution. This information is crucial as most enzymes have to undergo structural rearrangements to fulfill their specific biological function in the cell. In this way, NMR spectroscopy complements structural data obtained from cryo-EM or X-ray crystallography with high-resolution data of enzyme dynamics (Hennig and Sattler 2014). In addition, despite constant improvements, obtaining high-resolution cryo-EM structures of proteins below 100 kDa remains challenging, so cryo-EM is more suitable for large, heterogeneous protein complexes (Wentinck, Gogou, and Meijer 2022), while studying large biomolecular complexes of hundreds of kDa or more is still a challenge for NMR spectroscopy, which is better suited to examine smaller proteins. This again highlights the importance of combining different techniques to characterize protein complexes as ultimately, the goal of structural biology is to profoundly understand how bio-molecular structures and motions are linked to biological function.

The motions of proteins take place on a wide range of timescales (Frauenfelder, Sligar, and Wolynes 1991; Henzler-Wildman and Kern 2007) (Figure 2.1). Fluctuations such as bond vibrations occur on the femtosecond timescale, methyl group rotations on the pico- to nanosecond timescale and rotameric jumps in side chains on the pico- to even the microsecond timescale. Larger collective motions, in which the involved proteins or protein complexes exchange between a ground state and one or more excited states, take place on the microseconds to seconds timescale (Alderson and Kay 2020; Baldwin and Kay 2009). These dynamics affect processes such as protein folding and unfolding (Dyson and Wright 2005; Korzhnev, Salvatella, et al. 2004; Neudecker, Lundström, and Kay 2009), catalytic turnover of enzymes (Boehr, Dyson, and Wright 2006; Fraser et al. 2009; Neu et al. 2015), protein aggregation (Ceccon, Tugarinov, and Clore 2021; Tycko 2006), ligand binding (Boehr, Nussinov, and Wright 2009; Boehr and Wright 2008) and allostery (Laskowski, Gerick, and Thornton 2009; Wurm, Sung, et al. 2021; Xie et al. 2020), for which both the exchange dynamics (kinetics) and the conformational equilibria of the interchanging states (thermodynamics) determine the function of the proteins.

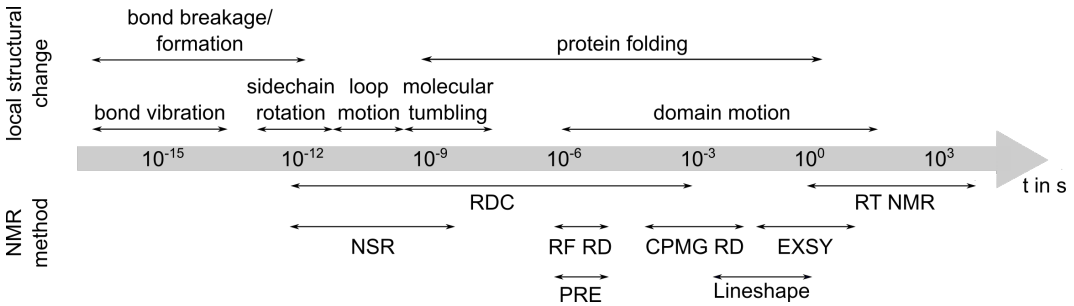

Figure 2.1.: Timescales of protein motions and corresponding NMR experiments. Protein dynamics take place on a wide range of timescales. A variety of NMR methods exists with which these functionally relevant motions can be studied. Here, the following abbreviations are used: Residual Dipolar Coupling (RDC), Real Time NMR (RT NMR), Nuclear Spin Relaxation (NSR), Rotating Frame Relaxation Dispersion (RF RD), Carr-Purcell Meiboom-Gill Relaxation Dispersion (CPMG RD), Exchange Spectroscopy (EXSY; also known as zz-exchange), Paramagnetic Relaxation Enhancement (PRE), Lineshape analysis. (Adapted from (Kleckner and Foster 2011).)

Apart from X-ray crystallography, cryo-EM and NMR, the field of structural biology includes a plethora of additional methods to study the structures, dynamics and interactions of bio-molecules. These include fluorescence-based methods such as single-molecule Förster resonance energy transfer (smFRET) (Mazal and Haran 2019), electron paramagnetic resonance (EPR) (Polyhach, Bordignon, and Jeschke 2011), various biochemical assays, mass spectrometry (Lento and Wilson 2022), cryo- electron tomography (cryo-ET) (Trinkaus et al. 2021) as well as computational techniques such as molecular dynamics (MD) simulations (Hollingsworth and Dror 2018) and artificial intelligence (AI) based structure prediction tools (Jumper et al. 2021; Tunyasuvunakool et al. 2021).

In the following sections, NMR spectroscopy and smFRET measurements will be described in more detail, as these techniques were used to obtain the results presented in this thesis.

2.2. NMR spectroscopy

NMR spectroscopy is an important method in structural biology with the unique advantage that motions of bio-molecules can be detected and quantified in solution. To investigate dynamics, a large number of experiments have been developed to probe molecular motions ranging from pico- and nanoseconds up to seconds and these motions can be mapped onto the structures of the bio-molecules, often with atomic or residue resolution. Furthermore, a specific feature of NMR is that it is very sensitive in monitoring interactions with atomic and temporal resolution such that it can be used to determine even weak/transient interactions which are often quite elusive for other methods (Bhabha et al. 2011; Overbeck, Stelzig, et al. 2022; Oyen et al. 2017; Stafford et al. 2015; Wurm, Sung, et al. 2021).

In the past, NMR experiments were limited to proteins and protein complexes with a molecular weight below ~ 40 kDa. For larger molecules, NMR spectral quality was strongly impaired due to fast transverse spin relaxation rates of observable nuclei. However, advances in sample preparation and isotope labeling methods as well as in pulse sequence design have facilitated the examination of bio-molecules with molecular weights of hundreds of kDa. Thus, even larger proteins and protein complexes such as the decameric exosome (400 kDa) or the large protein complex of the mRNA decapping machinery (> 125 kDa) can now be studied with NMR (Audin et al. 2013; Cvetkovic et al. 2017; Jiang and Kalodimos 2017; Schütz and Sprangers 2020; Sprangers and Kay 2007).

2.2.1. The basics of an NMR experiment

NMR spectroscopy is an experimental technique that exploits the principle that when atomic nuclei with a nonzero spin are placed in an external magnetic field B_0, they lose the degeneracy of their spin eigenstates and the spins precess around the direction of B_0 in a parallel or an antiparallel fashion (Keeler 2013). In accordance with Boltzmann's law, for nuclei with a positive gyromagnetic ratio, which quantifies the proportionality between angular momentum and magnetic dipole moment,

the probability for a parallel alignment of the spin along the external magnetic field, which corresponds to the lower energy eigenstate, is slightly larger, and averaging over all individual magnetic moments in a sample results in a net magnetization along the axis of B_0.

Even though there exist various approaches to describe an NMR experiment, in the following the magnetization vector approach (Bloch 1946), which describes the NMR experiment in terms of this bulk magnetization, will be used as it provides a simple and phenomenological understanding of the processes taking place in a basic NMR experiment.

In NMR spectroscopy, the bulk magnetization is perturbed by the application of a suitable oscillating magnetic field B_1, called a radio frequency (rf) pulse, which is applied perpendicular to the external magnetic field and which matches the precession frequency, called Larmor frequency, of the nuclei. This leads to the magnetization being tipped away from the direction of B_0 (by definition the z-direction) and the magnetization acquires components in x- and y-direction, the directions perpendicular to z.

After the rf pulse, the magnetization returns back to equilibrium along B_0 via two different relaxation processes, called longitudinal and transverse relaxation. While longitudinal relaxation describes the realignment of the perturbed spins along the direction of B_0, transverse relaxation describes the process by which the individual spins lose the coherence obtained from the rf pulse and thus the consequent decay of bulk magnetization in the xy-plane.

The precession and the decay of magnetization is detected as a time-dependent signal which is termed the free induction decay (FID). In order to obtain the frequency components that make up the FID signal, a Fourier transformation is applied to the FID which results in the characteristic intensity-frequency NMR spectrum (Figure 2.2).

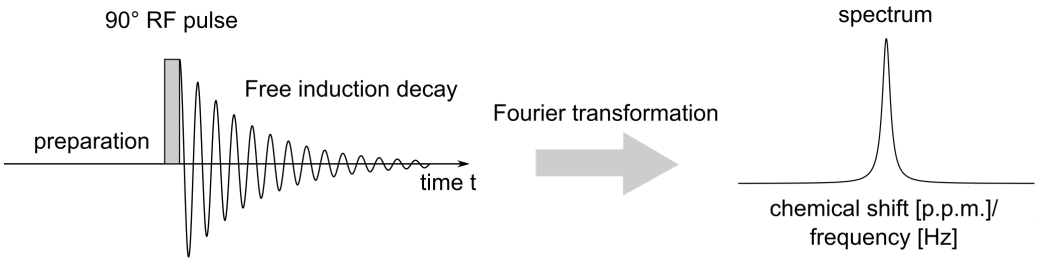

Figure 2.2.: A simple pulse-acquire NMR experiment. A 90° pulse is applied to the sample and its FID is recorded. Fourier transformation of the FID results in the characteristic frequency spectrum of the sample.

Since each nucleus in an NMR sample is located in a slightly different chemical environment due to e.g. its surrounding atoms in a protein, each nucleus experiences a slightly modulated external field B_0*, and therefore each nucleus resonates at a slightly different frequency. This is detected in the FID and therefore, after Fourier transformation, the resonances of the single nuclei appear as individual resonances at different positions in the NMR spectrum and their peak linewidths are proportional to the transverse relaxation rates.

In each NMR experiment, specific combinations of rf pulses and pulse sequences are applied, depending on the nuclei to be examined and on the goal of the experi-

ment. Most biological NMR experiments exploit the spin $\frac{1}{2}$ nuclei of isotopes of hydrogen, carbon and nitrogen, since H, C and N are the atomic building blocks of most biomolecules.

2.2.2. Methyl group and (backbone) nitrogen labeling

In the past, biomolecules with molecular weights above 40 kDa were not suited for NMR measurements due to the fast spin relaxation rates of nuclei in large biomolecules. This limit has however been substantially shifted upwards and now biomolecules and biomolecular complexes of hundreds of kDa can now be measured using NMR. This progress is partly due to the development of advanced pulse sequences that exploit the transverse relaxation optimized spectroscopy (TROSY) effect, which results in strong gains in sensitivity in the NMR spectra (Gueron, Leroy, and Griffey 1983; Pervushin et al. 1997; Salzmann et al. 1998; Yang and Kay 1999). Improvements in sample preparation, and in particular in isotope labeling combined with sample deuteration have substantially contributed to the extension of the applicability of NMR to large molecular machines. Especially isotope labeling of methyl groups has proven to be a very successful and powerful strategy to study large biomolecules (Goto and Kay 2000; Grzesiek et al. 1993; Kerfah et al. 2015; LeMaster 1987; Venters, Farmer II, et al. 1996; Venters, Huang, et al. 1995).

Methyl groups (CH_3) are abundant in organic molecules and about one third of amino acids contains methyl groups (alanine, threonine, valine, leucine, isoleucine and methionine). Since the three protons are equivalent, rotate fast around the central axis of the methyl group and they have favorable relaxation properties that can be exploited in NMR experiments, they are ideal probes for NMR spectroscopy to study large proteins up to hundreds of kDa (Gardner and Kay 1997; Schütz and Sprangers 2020; Tugarinov, Hwang, et al. 2003). Most of these experiments are conducted on fully protonated and ^{13}C-labeled methyl groups ($^{13}CH_3$) in an otherwise fully deuterated background. Here, deuteration is required to suppress dipolar interactions with non-methyl protons which would lead to additional relaxation effects and subsequent peak broadening in the resulting NMR spectra (Markus et al. 1994; Sattler and Fesik 1996).

Furthermore, enrichment with ^{13}C atoms in the methyl groups is necessary because the NMR-active ^{13}C nucleus has a low natural abundance (1.1 %). For this reason, labeling schemes have been developed in which appropriate ^{13}C-$^{1}H_3$ methyl groups are incorporated into proteins during expression or in which the proteins are post-translationally modified with isotope-labeled tags (Religa, Ruschak, et al. 2011; Theillet et al. 2012). In the case of cell-based expression in *Escherichia coli* (*E. coli*), isotopically labeled amino acids or amino acid precursors are added to the cells' growth medium, which is commonly D_2O-based, and the labeled compounds are metabolized by the expression host (Kerfah et al. 2015; Tugarinov, Kanelis, and Kay 2006). Often, a combination of labeled methyl groups is desirable to increase the amount of information contained in an NMR spectrum, yet, in order to avoid spectral overlap, modular isotope labeling is often required for a multi-subunit protein or a protein complex. To achieve this, the different subunits are expressed, labeled and purified separately and then reconstituted *in vitro* to form the full protein or protein complex. In this way, only the part of the protein that

contains NMR active nuclei will generate peaks in the NMR spectra. This approach also allows for differentially labeling distinct parts of a protein (Audin et al. 2013; Cvetkovic et al. 2017; Gelis et al. 2007; Ogunjimi et al. 2010).

Methyl group labeling and NMR experiments of methyl groups are particularly important for the study of large proteins, and therefore NMR experiments have been specifically designed, or adapted to the spin systems of ^{13}C-labeled methyl groups and include for example ^{13}C-methyl TROSY experiments (Schütz and Sprangers 2020; Tugarinov, Hwang, et al. 2003). Initially, however, these experiments were introduced for ^{1}H-^{15}N labeled proteins, for which uniform ^{15}N labeling can be achieved straightforwardly through the addition of $^{15}NH_4Cl$ and/or $^{15}(NH_4)_2SO_4$ to the cellular growth medium as the only source of nitrogen during expression (Ohki and Kainosho 2008).

For this reason, in the following, the heteronuclear single quantum correlation (HSQC) and TROSY experiments will first be explained for the ^{1}H-^{15}N spin system, before their adaptation and application for ^{13}C-$^{1}H_3$ methyl groups will be described.

2.2.3. The ^{1}H-^{15}N HSQC and the TROSY experiment

In an amide ^{1}H-^{15}N spin system, the combination of the ^{1}H and ^{15}N spins results in four different energy levels (Atkins and Friedman 2011). These energy levels, which are described as magnetization terms or coherences, have different relaxation rates and can be manipulated by the pulse sequence of an NMR experiment. The main contributions for transverse relaxation in this system arise from dipole-dipole coupling (DD) and chemical shift anisotropy (CSA). These relaxation mechanisms interfere destructively for some of the magnetization terms which results in extended transverse relaxation times, and therefore these magnetization terms are called slowly relaxing coherences (Pervushin et al. 1997).

One of the simplest NMR experiments to obtain information about correlations between two J-coupled nuclei in a biomolecule is the heteronuclear single quantum correlation (HSQC) experiment (Bodenhausen and Ruben 1980).

In a ^{1}H-^{15}N HSQC experiment, specifically, the 1H magnetization is excited, then transferred to the J-coupled ^{15}N nucleus where the magnetization evolves in order to record the ^{15}N chemical shift and then it is transferred back to ^{1}H and the FID is detected. In such an HSQC experiment, magnetization transfer is realized by the combination of multiple insensitive nuclei enhanced by polarization transfer (INEPT) pulse sequences, during which the fast and the slowly relaxing coherences in the sample are mixed before magnetization is detected. Each peak in the resulting NMR spectrum then shows the correlation between the ^{1}H and ^{15}N nuclei in the sample. ^{1}H-^{15}N HSQC experiments are convenient for experiments on the protein backbone, as each amino acid has one amide that results in one resonance. However, as all four coherences are mixed in this experiment, an average relaxation rate is obtained and thus the resonances in the spectrum can become relatively broad and weak. For small proteins with slow relaxation rates, however, this experiment still yields high quality spectra.

For larger proteins, the development of the transverse relaxation optimized spectroscopy (TROSY) experiment has led to significant improvements in spectral quality. In ^{1}H-^{15}N spin systems the destructive interference of DD interactions

and CSA for one of the four coherences results in the slow relaxation of this magnetization term. The TROSY experiment exploits this effect by selecting the slowly relaxing coherence and keeping it separate from the fast relaxing coherences throughout the experiment, so that no averaging of relaxation rates occurs. As a result, the slowly relaxing magnetization can be recorded and it yields a narrow and intense peak in the NMR spectrum (Pervushin et al. 1997). It has to be noted, though, that only one half of the initial magnetization is recorded to obtain the spectrum, so that TROSY experiments are mainly suited for larger proteins and complexes whose fast relaxation rates prevent the recording of high quality HSQC spectra.

Since the CSA for ^{1}H and ^{15}N in amide groups depends on the strength of the external magnetic field, an optimal cancellation of DD and CSA is reached at field strengths of around 21 T, which corresponds to a proton Larmor frequency of 900 MHz (Pervushin et al. 1997; Takeuchi, Arthanari, and Wagner 2016). Of note, the TROSY effect is also observed for aromatic CH groups but due to a different CSA of ^{13}C and ^{15}N, an optimal cancellation of DD interactions and CSA is here reached at around 14 T, or 600 MHz proton Larmor frequency (Pervushin et al. 1998).

2.2.4. The ^{1}H-^{13}C HMQC and the methyl-TROSY experiment

In the spin system of a ^{13}C-labeled methyl group, the combination of the carbon and the three proton spins yields 16 different energy levels (Ollerenshaw, Tugarinov, and Kay 2003; Tugarinov, Hwang, et al. 2003) which are connected by 28 fast or slowly relaxing single-quantum proton and single-quantum carbon as well as heteronuclear double-/zero-quantum transitions (Schütz and Sprangers 2020). In contrast to ^{1}H-^{15}N spin systems (and aromatic ^{13}C systems), the methyl-^{13}C CSA is very small, so transverse relaxation in methyl groups is dominated only by dipolar interactions and no (external magnetic field dependent) cancellation of DD interactions and CSA takes place to obtain a slowly relaxing coherence. However, in the methyl groups of high molecular weight proteins, the proton-proton and proton-carbon dipolar interactions interfere destructively, which also leads to slowly relaxing coherences (Tugarinov, Hwang, et al. 2003).

Analogous to the ^{1}H-^{15}N HSQC experiment, interconverting the fast and slowly relaxing methyl coherences multiple times in a ^{1}H-^{13}C HSQC experiment also leads to broad and weak signals, especially for large proteins. However, applying only a single 90° pulse on ^{1}H (in the heteronuclear multiple quantum (HMQC) experiment) instead prevents the mixing of the differently relaxing methyl coherences, so that large gains in sensitivity (up to three-fold higher) and thus relatively sharp and intense ^{1}H-^{13}C resonances can be obtained (Bax, Griffey, and Hawkins 1983; Mueller 1979; Tugarinov, Hwang, et al. 2003). This so-called methyl-TROSY effect can therefore be achieved with the HMQC experiment, in which the fast and the slowly relaxing coherences are not mixed and yield sharp and intense peaks in the spectrum, especially also for large proteins (Sprangers and Kay 2007). In addition, further improvements in spectral quality are achieved by deuteration because it attenuates relaxation due to dipolar interactions with H_2O protons or nearby protons in the protein since the dipolar interaction with deuterium is 50-fold weaker (Sattler and Fesik 1996).

2.2.5. Molecular dynamics and exchange processes

The strength of NMR spectroscopy compared to other structural biology methods is its ability to detect and measure biomolecular motions. These motions involve conformational changes and may be directly linked to enzymatic function. Thus, it is particularly interesting to study dynamics that take place on the same timescale as biological catalysis. Most enzymatic turnover rates range between approximately one to 10^5 s^{-1} and motions on such timescales can be quantified using a range of different NMR experiments, depending on which conformational states are involved. Dynamics experiments can then provide information about the thermodynamic (populations) and kinetic (exchange rates) properties of the underlying exchange process in the examined biomolecule. Experiments that allow to determine dynamics include Carr-Purcell Meiboom-Gill relaxation dispersion (CPMG RD) (Carr and Purcell 1954; Farber and Mittermaier 2015; Hansen, Vallurupalli, and Kay 2008; Meiboom and Gill 1958) and rotating-frame ($R_{1\rho}$) RD experiments (Palmer and Massi 2006) as well as exchange spectroscopy (EXSY) (Farrow et al. 1994; Jeener et al. 1979; Kloiber et al. 2011) and chemical exchange saturation transfer (CEST) experiments (Vallurupalli, Sekhar, et al. 2017).

For an exchange process to be detectable with NMR spectroscopy, the states between which the exchange occurs have to be magnetically distinguishable, e.g. by being in a distinct chemical environment each, or by having different relaxation properties. In the simplest case of a two-state exchange, a biomolecule interconverts between two states A and B with populations p_A and p_B, respectively, and an exchange rate $k_{ex} = k_A + k_B$, with $p_{A/B} = k_{A/B}/k_{ex}$. Importantly, since each state is in a different chemical environment, they resonate at frequencies ω_A and ω_B and the chemical shift difference is $\Delta\omega = |\omega_A - \omega_B|$ (Allerhand and Thiele 1966; Palmer and Koss 2019). The relationship between $\Delta\omega$ and k_{ex} defines the NMR timescale and three different exchange regimes can be distinguished. An exchange is classified as slow when $k_{ex} \ll |\Delta\omega|$, as intermediate when $k_{ex} \approx |\Delta\omega|$ and as fast when $k_{ex} \gg |\Delta\omega|$ and these exchange regimes have a direct influence on the appearance of the NMR spectrum (Figure 2.3). Note that the exchange regime may vary with the external magnetic field B_0 because $\Delta\omega$ scales linearly with the B_0 field strength (Kleckner and Foster 2011; Mittermaier and Kay 2009).

In the slow exchange regime, interconversion between the two states is slow compared to the frequency detection of the NMR experiment, which results in two separate resonances in the NMR spectrum, each with a distinct chemical shift, intensity and linewidth corresponding to the respective state. Suitable NMR experiments to measure slow exchange are CEST experiments as well as longitudinal exchange or EXSY experiments and they rely on the transfer of polarization from one state to the other (Furukawa et al. 2016; Religa, Sprangers, and Kay 2010).

In the intermediate exchange regime, resonances are significantly broadened. This exchange broadening is the result of conformational exchange during the detection period and in consequence the relaxation rate R_2 obtains an additional term R_{ex} from the exchange, resulting in $R_2^{obs} = R_2^0 + R_{ex}$ with R_2^0 being the relaxation rate in the absence of exchange. CPMG or $R_{1\rho}$ experiments can be used to quantify this exchange broadening by modulating R_{ex} either through the application of transverse rf pulses (CPMG) or constant spin-lock fields ($R_{1\rho}$).

In the limit of fast exchange, interconversion between the two states is very fast,

which results in signal averaging during detection and consequently one population-weighted average peak and relaxation rate $R_2^{obs} = p_A R_{2A} + p_B R_{2B}$. Both CPMG and $R_{1\rho}$ experiments can be used to quantify exchange in this regime, however with increasing exchange rates the population of the lowly populated excited state p_B and the chemical shift difference $\Delta\omega$ cannot be separated any more (Bothe, Stein, and Al-Hashimi 2014; Ishima and Torchia 1999; Korzhnev, Orekhov, et al. 2003). In the following, the zz-exchange and the CPMG experiment will be explained in more detail as these were part of the work performed for this thesis.

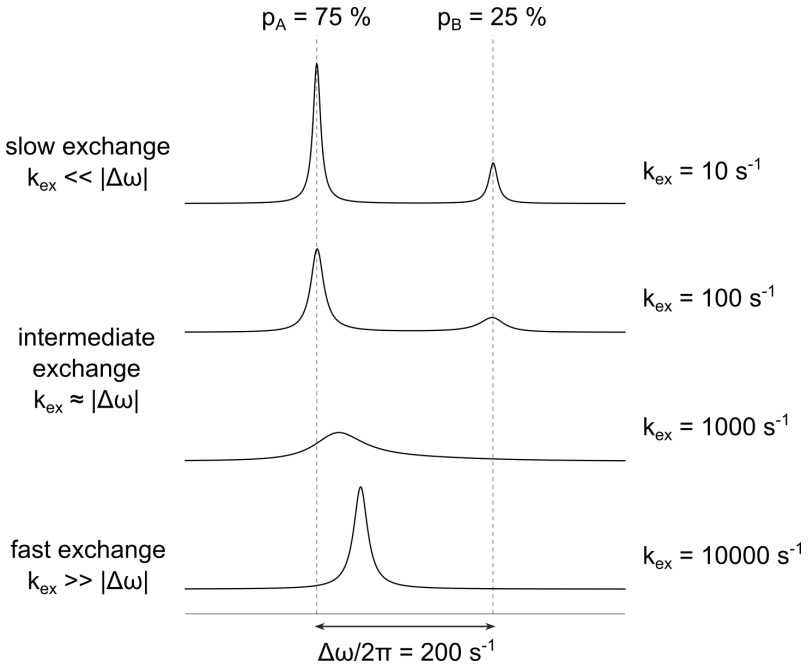

Figure 2.3.: NMR lineshape modulation through chemical exchange. The exchange regime in which chemical exchange between states A and B occurs determines the appearance of the resulting NMR spectra and it is defined by the relative magnitudes of k_{ex} and $|\Delta\omega|$.

2.2.6. The zz-exchange experiment

Biomolecular dynamics in the slow exchange regime can be detected and quantified using longitudinal, or, zz-exchange NMR experiments (Palmer, Kroenke, and Patrick Loria 2001). Motions in this time regime include changes in protein conformation such as rearrangement of protein domains (Key et al. 2009; Religa, Sprangers, and Kay 2010), binding and release of ligands (Doucleff and Clore 2008; Sahu, Clore, and Iwahara 2007; Sprangers, Gribun, et al. 2005), changes in secondary structure (Kuloğlu et al. 2002; Nikolaev and Pervushin 2007) and isomerization processes (Sarkar et al. 2007), all of which can be involved in biomolecular catalysis (Falzone, Wright, and Benkovic 1994; Sprangers, Gribun, et al. 2005). Exchange spectroscopy (EXSY), and, in particular, longitudinal zz-exchange experiments are based on transferring longitudinal magnetization between different states by chemical exchange (Farrow et al. 1994; Jeener et al. 1979; Montelione and Wagner 1989). Zz-exchange experiments require that the interchanging states are sufficiently populated and have a clearly distinguishable chemical shift. During the experiment, each probe is first labeled by its chemical shift to identify its initial state, magnetization is then

allowed to evolve during a mixing time τ_{mix}, in which exchange between state A and B can occur, before the final chemical shift of each probe is again detected to identify its final state. In the case of chemical exchange in the slow exchange regime, this results in two diagonal auto peaks (one for each state A and B) and in two cross peaks (for exchange from A to B and vice versa). Thus, cross peaks between the two states in a zz-exchange experiment indicate the presence of slow exchange (Figure 2.4). Variation of τ_{mix} for a series of spectra and evaluation of the auto and cross peak intensities can then be used to extract exchange rates and longitudinal decay rates of the exchange. In practice, between five and 20 spectra are usually recorded with mixing times depending on the exchange rate, and for each spectrum the intensity of each of the set of peaks is extracted and plotted. For an optimal choice of experimental parameters and in the presence of exchange, intensities decay for the auto peaks while for the cross peaks, a build-up of intensities and subsequent decay can be observed. From fits of these curves k_{ex}, p_A and R_1 rates can then be extracted. In the case of two-state exchange, the intensities of the respective auto and cross peaks are described by

$$I_{AA/BB}(\tau_{mix}) = p_{A/B}(p_{A/B} + p_{B/A}\exp(-k_{ex}\tau_{mix}))\exp(-R_1\tau_{mix}) \tag{2.1}$$

and

$$I_{AB}(\tau_{mix}) = p_A p_B(1 - \exp(-k_{ex}\tau_{mix}))\exp(-R_1\tau_{mix}) \tag{2.2}$$

assuming $R_{1A} = R_{1B}$. The longitudinal zz-exchange experiment is therefore a valuable method to record biomolecular motions on the slow exchange timescale, when the exchanging conformations are sufficiently populated, and it is limited mostly by spectral crowding and by poor sensitivity, as the experiment generates an additional set of peaks which can be difficult to detect and quantify (Kleckner and Foster 2011).

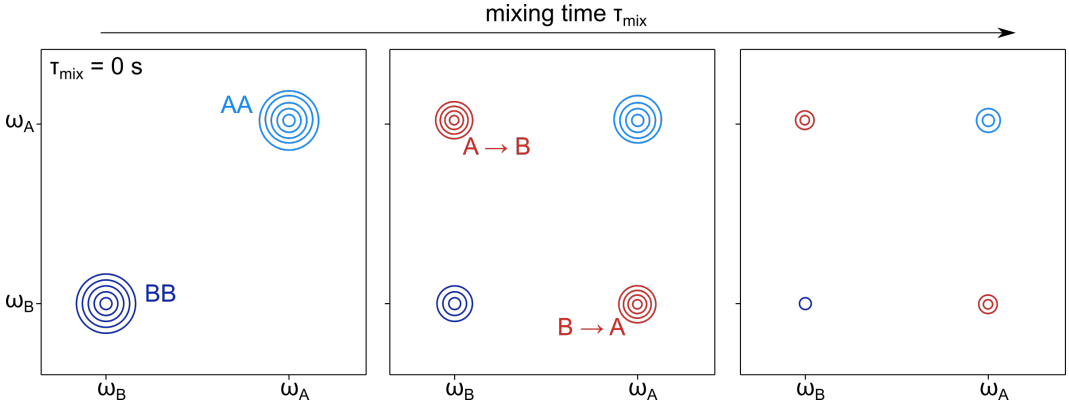

Figure 2.4.: The zz-exchange experiment. In the case of slow exchange between states A and B, longitudinal zz-exchange experiments here result in two distinct diagonal auto peaks (AA and BB) and in two cross peaks (A → B and B → A), which indicate the transfer of magnetization between states A and B during the mixing time t_{mix}.

2.2.7. The CPMG experiment

Carr-Purcell Meiboom-Gill relaxation dispersion (CPMG RD) experiments can be used to quantify the dynamics of intermediate ($k_{ex} \sim |\Delta\omega|$) and fast ($k_{ex} > |\Delta\omega|$) exchange processes in biomolecules in the time range of 0.3 – 10 ms (Kempf and Loria 2002; Loria, Berlow, and Watt 2008; Palmer, Kroenke, and Patrick Loria

2001). Dynamics on this timescale include motions of loops, side chains or entire domains as well as changes in the secondary structure of biomolecules (Beach et al. 2005; Fraser et al. 2009; Kovrigin and Loria 2006; Vallurupalli and Kay 2006), which influence processes such as ligand binding and release (Boehr, McElheny, et al. 2006, 2010; Brüschweiler, Schanda, et al. 2009; Doucet, Watt, and Loria 2009; Sprangers, Gribun, et al. 2005), folding and unfolding processes (Korzhnev and Kay 2008; Korzhnev, Neudecker, et al. 2005; Neudecker, Lundström, and Kay 2009; Schanda, Brutscher, et al. 2008; Sugase, Dyson, and Wright 2007), or catalytic turnover (Eisenmesser, Millet, et al. 2005; Eisenmesser, Bosco, et al. 2002). CPMG RD experiments can be used to extract kinetic (via exchange rates k_{ex}), thermodynamic (via populations p_A, p_B) and structural (via chemical shift differences $\Delta\omega$) parameters of the respective processes.

As the dynamics measured with CPMG RD experiments occur in the intermediate to fast exchange regime, for a two-state exchange, usually only one exchange broadened resonance can be observed in the NMR spectrum which shows an enhanced relaxation rate $R_2^{obs} = R_2^0 + R_{ex}$ (Palmer, Kroenke, and Patrick Loria 2001). In the CPMG experiment, this signal broadening due to chemical exchange is studied as it reflects the underlying protein dynamics (Carr and Purcell 1954; Meiboom and Gill 1958). In practice, a series of evenly spaced spin-echo pulse sequences, τ-180-τ, is applied to transverse magnetization within a fixed time delay, called the relaxation delay T_{CPMG}. τ is a delay time and the 180° rf pulse is applied in either ± x or ± y direction. The spin-echo pulse elements serve to refocus transverse magnetization, as is shown in Figure 2.5.

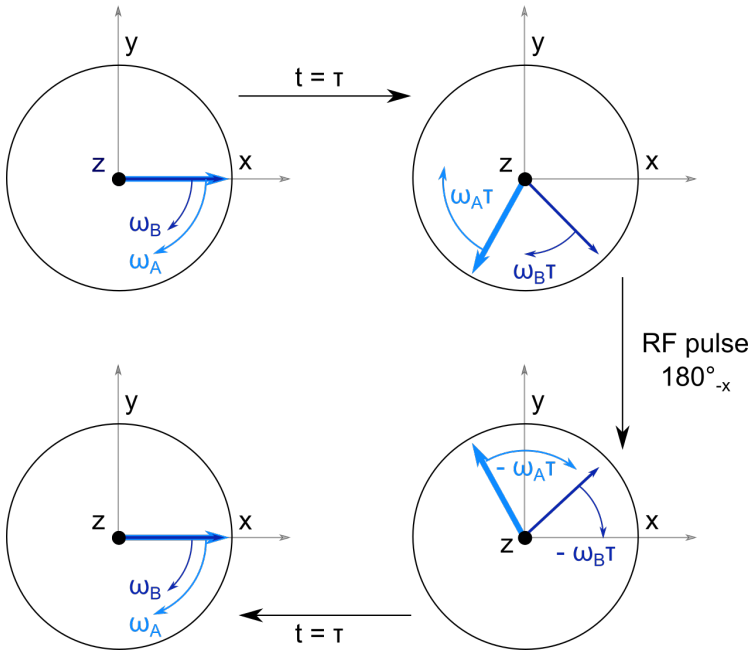

Figure 2.5.: Spin-echo pulse element with two spins. First, magnetizations A and B are coherent in x-direction. During the time τ, A gets ahead of B. The 180°$_{-x}$ RF pulse flips the magnetizations on the x-axis but not their phases, so after the time τ they return to the x-axis where they are refocused. If the average chemical shift of one of the spins differs between the first and the second τ period due to exchange processes, it will not return to the x-axis after the time $t = 2\tau$, so the magnetization vectors will not be fully refocused.

This is however only possible when each individual magnetization vector that contributes to the bulk magnetization exhibits the same average chemical shift

during the first and the second τ period. If this is not the case, and the individual spins experience different chemical shifts during the first and second τ period due to exchange processes in the protein, the magnetization is not completely refocused after the spin echo delay time t = 2τ, which results in signal broadening. The refocusing efficiency depends on the difference of the average chemical shift in the first and second delay period and a larger difference corresponds to faster dynamics and, consequently, broader peaks. In the CPMG RD experiment, a series of spectra is recorded in which T_{CPMG} is fixed but for each spectrum the number of spin-echo elements, and thus the delay time τ, is varied. Commonly, the number of pulses is given as the CPMG frequency $\nu_{CPMG} = \frac{1}{4\tau}$. Typical values for ν_{CPMG} are 50-2000 Hz and usually between ten and 20 spectra are recorded for one CPMG RD experiment. In a system that undergoes intermediate to fast conformational exchange the relaxation rate depends on ν_{CPMG}, and this dependence can be used to extract information about the exchange process. The remaining signal intensity after $t = T_{CPMG}$ can be expressed as

$$I(\nu_{CPMG}) = I_0 \exp\Big(-R_2^{obs}(\nu_{CPMG})\Big)T_{CPMG}, \tag{2.3}$$

where I_0 is the signal intensity at $T_{CPMG} = 0$. In the case of exchange, plotting $R_2{}^{obs}(\nu_{CPMG})$ results in the characteristic dispersion curve and for fast exchange processes this data can be fitted to a fast exchange equation for two-state exchange,

$$R_2^{obs} = R_2^0 + \frac{p_A p_B \Delta\omega^2}{k_{ex}}[1 - \frac{2\tanh(k_{ex}\tau)}{2k_{ex}\tau}]. \tag{2.4}$$

In the fast exchange equation,the parameters p_A and Δω are convoluted and cannot be extracted separately, so that an independent interpretation of populations and chemical shift differences is not possible (Baldwin 2014; Kempf and Loria 2002; Luz and Meiboom 1963; Millet et al. 2000). Nonetheless, k_{ex}, $R_2{}^0$ and R_{ex} can still be obtained from dispersion curves in the fast exchange regime. For other exchange regimes, the dispersion curves can be fitted to an exact equation for two-site exchange from which the parameters p_A, k_{ex}, R_{ex} and Δω can be rapidly extracted (Baldwin 2014).

2.2.8. The potential of ^{19}F NMR

Most commonly, biomolecular NMR experiments are based on spin systems containing ^{1}H, ^{13}C and/or ^{15}N. However, these experiments often require a significant amount of experimental time and sample preparation is often elaborate and expensive. A number of alternative approaches have been developed to circumvent these issues and include the use of the NMR-active nuclei ^{3}H, ^{19}F, or ^{31}P (Ahmmed et al. 2021; Kalinowski 1986; Krivdin 2023; "Modern Aspects of ^{31} P NMR Spectroscopy" 2019; Overbeck, Kremer, and Sprangers 2020). Particularly NMR on the ^{19}F nucleus has gained popularity as ^{19}F nuclei are almost completely absent from biological samples and can be artificially incorporated into proteins at specific sites of interest, where they can be used as sensitives probes for structure, dynamics and interactions. One way to incorporate a ^{19}F label into a protein is to employ fluorinated amino acids that replace the natural amino acid in the protein, e.g. fluor-tryptophan

instead of tryptophan (Crowley, Kyne, and Monteith 2012; Lu et al. 2019). Moreover, fluorinated methyl groups can be attached to cysteine side chains (Ye, Larda, et al. 2015) and nucleotides can be labeled with ^{19}F by introducing selectively fluorinated nucleotides (Chrominski et al. 2020; Hennig, Scott, et al. 2007). Due to the limited number of fluorine nuclei in the NMR sample, NMR spectra show only few resonances, so it is often sufficient to record simple one-dimensional (1D) spectra to obtain site-specific information very rapidly. In addition, ^{19}F is well suited for measuring relaxation dispersion (RD) experiments because its large chemical shift dispersion (Lau and Gerig 2000) can lead to large chemical shift differences between the ground and the excited states of the proteins and thus to large amplitudes in RD curves. Furthermore, the costs for ^{19}F labeling are low and deuteration, especially of larger enzymes, is usually not required because the ^{19}F nucleus is often remote from protons in the sample. Finally, the high gyromagnetic ratio of fluorine, $\gamma_{\text{fluorine}} = 0.9413 * \gamma_{\text{proton}} = 25.181 * 10\ \text{Ts}^{-1}$, allows for the matching and tuning of the ^{1}H channel in the spectrometer probehead to the ^{19}F resonance frequency.

^{19}F NMR is therefore a very well suited complementary approach to detect and quantify biomolecular motions (Gronenborn 2022; Kitevski-LeBlanc and Prosser 2012; Overbeck, Kremer, and Sprangers 2020) and a large number of examples exist in the literature in which NMR on ^{19}F is used to study structural and dynamic features of biomolecules. These examples include studies of G-protein coupled receptors (GPCRs) (Frei et al. 2020; Kim, Chung, et al. 2013; Liu, Horst, et al. 2012; Pan et al. 2022), the activation of a fold-switch glycosyltransferase PimA in mycobacteria (Liebau et al. 2020), the unfolding transition of a cold-shock protein (Overbeck, Kremer, and Sprangers 2020), dynamics in the catalytic cycle of the exoribonuclease Xrn2 (Overbeck, Stelzig, et al. 2022), and functional conformational changes of calmodulin (Hoang and Prosser 2014). It is however possible that the incorporation of ^{19}F alters the structure and stability of the proteins (Acchione et al. 2012; Minks et al. 1999; Xiao, Parsons, et al. 1998), so this possibility must be considered before interpreting data obtained on ^{19}F.

2.2.9. High pressure NMR

Most proteins are highly dynamic and sample multiple conformations which are often essential for function. However, it is not always possible to directly observe all conformations a protein can adopt, as these might not necessarily be highly occupied in solution (Oyen et al. 2017; Wurm, Sung, et al. 2021). Information about these states is nonetheless important as they can be involved in catalytic processes as well as in (un-) folding and misfolding or aggregation, which ultimately strongly affect the cellular equilibrium. NMR spectroscopy is an excellent method to study these conformations and changes thereof, and a number of NMR experiments have been developed to examine the thermodynamic and kinetic properties of the respective conformations by extracting information about the invisible minor states from visible major state resonances (Alderson and Kay 2020; Baldwin and Kay 2009; Bouvignies et al. 2011).

To obtain even deeper insights into the thermodynamic and kinetic properties of proteins, the conformations of a protein can be modulated in a number of ways including changes in sample conditions (salt concentration, pH, or addition of

denaturants) or other experimental parameters (temperature, hydrostatic pressure) (Privalov and Gill 1988). The application of hydrostatic pressure, in particular, has proven to be an elegant and powerful way of such modulation and it is well suited to examine the fundamental processes taking place in proteins for a number of reasons (Akasaka 2006; Kitahara and Akasaka 2003). Increasing the hydrostatic pressure can only slightly influence the difference in free energy of interchanging states but this is sufficient to shift the populations of those states. In addition, pressure can modify the energy of transition states, which results in changes in exchange rates. These pressure-induced changes can then be used to extract volumetric information about the examined molecule (Akasaka 2003, 2006; Gross and Jaenicke 1994). In addition, it is beneficial that pressure perturbations are generally completely reversible, and thus it is not surprising that, despite the high technical demands of applying high pressure to an NMR sample, high pressure NMR has gained much popularity (Sprangers 2021). Examples of high pressure NMR include studies of allostery in the RAS protein (Kalbitzer et al. 2013), folding processes in apomyoglobin (Kitahara, Yamada, et al. 2002) and conformations of the β1-adrenergic receptor (Abiko, Grahl, and Grzesiek 2019). Moreover, pressure jump methods and devices have been developed to examine structural and dynamic features of biomolecules (Alderson, Charlier, et al. 2017; Charlier, Courtney, Alderson, et al. 2018; Charlier, Courtney, Anfinrud, et al. 2018; Kremer et al. 2011; Roche et al. 2013).

For a protein that exchanges between two states A and B (with populations p_A and p_B = 1 - p_A and forward and backward rates k_A and k_B with $k_{ex} = k_A + k_B$) at ambient pressure, the difference in (Gibbs) free energy between these states is

$$\Delta G_{AB} = G_B - G_A = -RT \ln(K_{eq}), \tag{2.5}$$

with R being the gas constant, T the absolute temperature and K_{eq} the equilibrium constant, which is given by $K_{eq} = p_B/p_A$. At constant temperature but variable pressure p, Taylor expansion of ΔG_{AB} around p_0 yields

$$\Delta G_{AB} = \Delta G_0 + \Delta V(p - p_0) - \frac{1}{2}\Delta\kappa_T(p - p_0)^2, \tag{2.6}$$

with ΔG_0 and ΔV_0 being the differences in free energy and volume between states A and B at ambient pressure p_0 = 10 bar and $\Delta\varkappa_T$ is the difference in isothermal compressibility between the two states (Akasaka 2003, 2006; Akasaka and Matsuki 2015). Assuming equal isothermal compressibility for both states, the last term can be neglected and the equilibrium constant can be expressed as

$$K_{eq} = \exp\left(\frac{-\Delta G_0 - \Delta V_0(p - p_0)}{RT}\right). \tag{2.7}$$

Experimental determination of K_{eq} at different pressures p therefore yields direct information on the changes in molecular volume ΔV_0 between states A and B.

Usually, a folded protein contains cavities which can significantly contribute to its molecular volume. In its unfolded state, in contrast, these cavities are absent and therefore the volume of the unfolded protein is usually smaller. Thus, the change in molecular volume upon protein folding, $\Delta V_0 = V_B - V_A$, has a positive value and, consequentially, negative volume changes indicate the loss of secondary or

tertiary structure. In line with that, the application of high pressure to biomolecules eventually leads to their unfolding or denaturation.

Aside from providing information about volumetric changes between two interchanging states A and B, the application of pressure can also be used to obtain insights into the free energy of activation. From transition state theory it is known that

$$k = \frac{\kappa k_B T}{h} \exp\left(\frac{-\Delta G'}{RT}\right) \tag{2.8}$$

(Eyring equation), where k is either the forward (k_A) or the reverse (k_B) rate constant, $\varkappa$ the transmission coefficient, k_B Boltzmann's constant, h Planck's constant and ΔG' the free energy of activation of the forward (ΔG_{AB}') or the reverse (ΔG_{BA}') rate (Laidler and King 1983). Using the Taylor expansion of ΔG_{AB} from above, this leads to

$$k = \frac{\kappa k_B T}{h} \exp\left(\frac{-\Delta G_0' - \Delta V_0'(p - p_0)}{RT}\right) = \exp\left(\ln(k_0) - \frac{\Delta V_0'(p - p_0)}{RT}\right). \tag{2.9}$$

Here, k_0 is the forward ($k_{0,AB}$) or reverse ($k_{0,BA}$) rate at standard pressure p_0. From experimental determination of k_{AB} and k_{BA} at different pressures p, volume differences between state A, or state B, and the transition state can be extracted.

Both K_{eq} and k_A and k_B can be extracted from CPMG relaxation dispersion measurements (Korzhnev and Kay 2008; Palmer 2015), and therefore, recording these experiments at different pressures allows for the extraction of volume differences between conformational states of a protein which thus provides important insights into structural changes that take place in biomolecules. In the past, a number of studies of exchange processes of biomolecules under pressure were conducted using NMR measurements. These include the characterization of the three-state folding process of a Fyn SH3 domain mutant (Tugarinov, Libich, et al. 2015), studies of the dynamic folding pathways of SH3 domains (Bezsonova et al. 2006), the determination of the transition state ensembles of the enzyme adenylate kinase (Stiller et al. 2019) and of a mutant of the apocytochrome b562 (Korzhnev, Bezsonova, et al. 2006). Most of these high pressure NMR studies focus on ^{15}N based experiments of relatively small proteins with molecular weights up to 30 kDa. In these cases, the application of pressure generally results in chemical shift perturbations (CSPs) of the ^{1}H-^{15}N resonances, and non-linear pressure-dependent CSPs are associated with the presence of internal cavities in the examined biomolecules, which get compressed when pressure is applied (Akasaka and Li 2001; Akasaka, Li, et al. 1999; Beck Erlach et al. 2017; Gagné et al. 2020; Xu, Gagné, et al. 2021). In addition, the disappearance of resonances at elevated pressures is often observed and can also be attributed to conformational fluctuations around cavities under high pressure (Maeno et al. 2015). In summary, high pressure NMR methods can be extremely useful to obtain valuable insights into biomolecular processes and structural details of proteins that are not directly observable under ambient conditions.

2.2.10. Solid state NMR

Solution-state NMR is an extremely powerful method to examine dynamic and heterogeneous biomolecular systems at atomic resolution. However, it is limited to

non-solid samples in which the fast molecular tumbling rate of its components averages the orientation dependence of nuclear spin interactions and thereby leads to high-resolution NMR spectra. For solid and semi-solid structures, these anisotropic interactions are not averaged, which results in strong line broadening of the NMR spectra. Thus, it is not possible to record high quality solution state NMR spectra of proteins after these have undergone LLPS and matured into a gel-like state, so solution state NMR is not suited to examine if and how these condensates could have an impact on the regulation of protein function. To regain spectral resolution, solid state NMR (ssNMR) methods, and in particular magic angle spinning (MAS) techniques, have been developed which allow for the determination of the chemical structure and the dynamics of non-liquid systems, and consequently also for obtaining information about proteins in their LLPS or mature state (Ackermann and Debelouchina 2019; Ader, Frey, et al. 2010; Murray et al. 2017; Reif et al. 2021; Schanda and Ernst 2016; Tycko 2011). ssNMR spectra are recorded in an external magnetic field by placing the sample into a rotor which is rotated with high spinning frequencies at the specific angle ϑ_{MAS} = 54.74° (Figure 2.6).

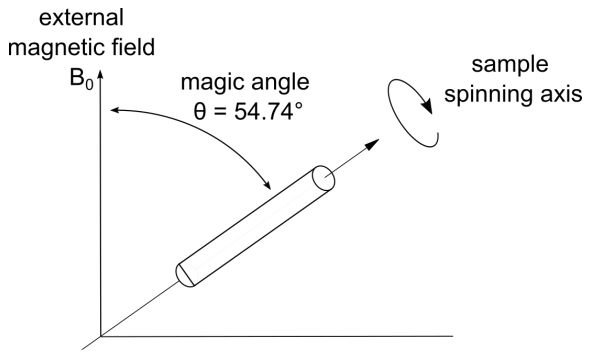

Figure 2.6.: Magic angle spinning (MAS). The solid NMR sample is placed into a small rotor which is tilted by the magic angle angle ϑ_{MAS} = 54.74° and rotated at frequencies up to > 100 kHz around its axis.

Magic-angle spinning (Andrew, Bradbury, and Eades 1958) averages the orientation dependent spin interactions in the NMR sample. This effect arises because the dipolar coupling D between the individual nuclei in a strong external magnetic field depends on the angle ϑ between the external magnetic field and the connection vector of the nuclei. It is expressed as $D \sim 3\cos^2\vartheta - 1$ and it vanishes for angle ϑ_{MAS} = 54.74°. It follows that the dipolar interaction between the nuclei vanishes when being rotated at that angle. The averaging of anisotropic interactions via MAS differs fundamentally from the molecular tumbling process in solution as it is not the result of a rapid stochastic process, but is controlled in a time-dependent, periodic manner via fast sample rotation. As a result, the anisotropic spin interactions are not always fully averaged and this leads to residual line broadening. However, at the same time the amount of averaging can be manipulated and measured which provides insights into the dynamics of the examined sample. Thus, an advantage of ssNMR compared to solution NMR is the ability to measure both rigid parts and flexible parts of a sample (Baldus 2022; Schanda and Ernst 2016). In order to extract structural and dynamical data from the sample, the radio frequency pulse sequences used in solution state NMR to manipulate the magnetization of the sample must be adapted accordingly. Scalar-based correlation experiments utilize ^{1}H-^{15}N INEPT transfer to measure spectra of the flexible parts in a sample while dipolar-based correlation experiments make use of cross-polarization to probe the rigid parts in the sample. Flexible components in a sample have shorter spin-lattice relaxation times, so that pulse sequences for probing these mobile parts have shorter delay

cycles and dipolar dephasing filters are coupled to fast pulsing such that the resulting NMR spectra contain signals from only the flexible elements in the sample. Additionally, similar to solution NMR, INEPT or HMQC sequences serve to enhance the signal intensity of the flexible regions (Ahlawat et al. 2022; Cavanagh et al. 2007). Cross-polarization, in contrast, is used to probe the rigid parts of a solid or semi-solid sample (Hartmann and Hahn 1962; Pines, Gibby, and Waugh 1972). This technique is used to enhance the signal from spins with lower gyromagnetic ratios, such as ^{15}N, by transferring magnetization from high gyromagnetic ratio spins such as ^{1}H via dipolar interactions during a period of constant irradiation, also called the spin locking period (Andronesi et al. 2005). Subsequently, the FID of the lower gyromagnetic ratio spin is detected and yields spectra of the rigid parts in the ssNMR sample.

Due to its ability to obtain not only information about the rigid parts of a sample but also about a wide range of dynamic processes, ssNMR has become a very important method for studying the molecular structures and dynamics of complex biological systems and it has been used in a wide number of applications, ranging from the study of amyloid fibrils and protein aggregates (Chen and Tycko 2010; Heise et al. 2005; Paravastu et al. 2009) to membrane proteins (Ader, Pongs, et al. 2010; Xiao, Bolton, et al. 2019), entire cells and cellular components (Ghassemi et al. 2022; Wang, Phyo, and Hong 2016), biological materials and even human tissues (Ghosh et al. 2021; Kaplan et al. 2016). In addition, improvements in sample preparation and isotope labeling, as well as advances in spectrometer hardware have increased the importance of ssNMR for studying challenging biological systems. To date, magnets can reach fields of 28.2 T (1.2 GHz), and rotors with diameters of 1.3 mm and spinning frequencies of > 100 kHz are commercially available. In laboratory settings, even frequencies of up to 200 kHz with 0.4 mm rotor diameters have already been reached (Marchanka and Carlomagno 2019; Nishiyama et al. 2023; Samoson 2019; Ye, Malon, et al. 2014). The field of ssNMR is thus continually improving and may provide exciting future findings about the connection of enzyme dynamics with function.

2.3. Single molecule FRET experiments

The advantage of NMR experiments compared to most other biophysical and biochemical methods is its ability to detect and characterize conformational changes of biomolecules even when the excited states of the molecules are only very lowly populated (Oyen et al. 2017; Wurm, Sung, et al. 2021). For this, however, high sample concentrations and long data acquisition times are usually required, which presents a limit to the extent and quality of data that can be recorded with NMR experiments. Many proteins may not be stable during the experimental times required for NMR, which may be days to weeks, or, in extreme cases, NMR concentrations can exceed the proteins' threshold concentration for phase separation, which leads to a loss of peak intensity in the spectra (Damman et al. 2019). Furthermore, peaks in NMR spectra can be severely broadened, even beyond detection, when highly dynamic processes are present in proteins, that sample a multitude of conformations (Wurm, Holdermann, et al. 2017). An alternative and complementary approach to examine the conformations of proteins in solution are single molecule Förster resonance

energy transfer (smFRET) experiments (Algar et al. 2019; Lerner, Barth, et al. 2021; Lerner, Cordes, et al. 2018). In contrast to NMR experiments, smFRET experiments only require short data acquisition times and low protein concentrations, so that they are well suited for examining biomolecular systems that cannot be studied well with NMR.

The principle of FRET experiments is based on the non-radiative dipole-dipole energy transfer between two light-sensitive molecules like fluorophores (Gust et al. 2014; Medintz and Hildebrandt 2013). Since the efficiency of this energy transfer is inversely proportional to the sixth power of the distance between the fluorophores, it is very sensitive to changes in distance, which makes FRET an ideal tool to measure distances, and with that also conformational changes in biomolecules that have been tagged with a fluorophore (Hellenkamp et al. 2018; Schuler and Eaton 2008).

In a smFRET experiment, a donor fluorophore is excited by a laser beam whose wavelength matches the absorption frequency of the donor and the energy is transferred to a suitable acceptor fluorophore via dipole-dipole interaction if the acceptor is in close spatial proximity (Gust et al. 2014; Medintz and Hildebrandt 2013). The excited acceptor then returns back to its ground state by emitting the absorbed energy in the form of a photon which is then detected. In this way, the FRET signal of individual molecules can be resolved and thereby provides insights into kinetic and conformational processes on a single molecule level. The rate of energy transfer k_T between fluorophores is described by

$$k_T = K\frac{Q_D\kappa^2 J}{\tau_D N_A n^4}\frac{1}{R^6}, \tag{2.10}$$

whereby Q_D denotes the fluorescence quantum yield of the donor in the absence of the acceptor, which is equivalent to the ratio of emitted to absorbed photons, $\varkappa^2$ is the dipole orientation factor, J is the spectral overlap integral, τ_D is the average lifetime of the donor in its excited state, N_A is Avogadro's constant, K is a constant with value $K = \frac{9\ln(10)}{128\pi^5}$, n is the refraction index of the medium and R the distance between the fluorophores. From this equation, the efficiency of the FRET energy transfer, E, can be computed as

$$E = \frac{E_{D\rightarrow A}}{E_{D,abs}} = \frac{k_T}{\tau_D^{-1} + k_T}, \tag{2.11}$$

where $E_{D\rightarrow A}$ is the energy transferred from donor to acceptor molecule and $E_{D,abs}$ is the energy absorbed by the donor. The Förster Radius R_0 is defined as the distance between the fluorophores at which half of all donor excitations are transferred to the acceptor (E = 0.5; Figure 2.7) (Forster 1946), so Equation 2.10 and Equation 2.11 simplify to

$$k_T = \frac{1}{\tau_D}\left(\frac{R_0}{R}\right)^6 \tag{2.12}$$

and

$$E = \frac{1}{1 + \left(\frac{R}{R_0}\right)^6}. \tag{2.13}$$

It must be noted that some conditions have to be fulfilled for an energy transfer to

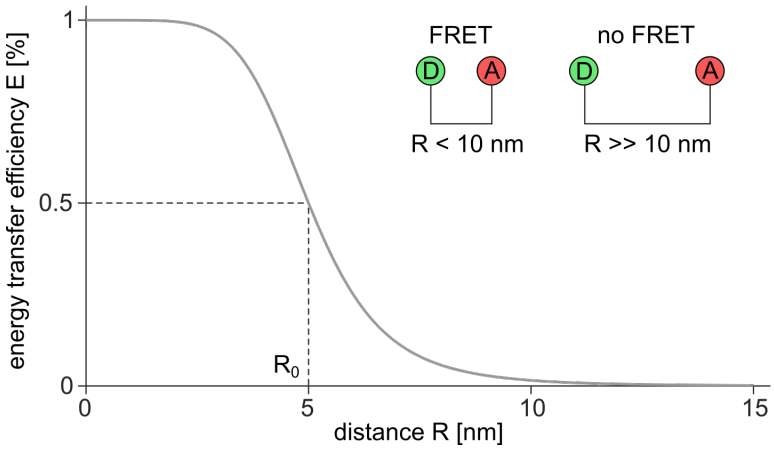

Figure 2.7.: FRET efficiency. The efficiency of energy transfer between two fluorophores depends on the distance R between the fluorophores. The highest sensitivity for changes in distance is at the Förster Radius R_0.

occur (Schuler 2006). First, the dipole moments of the respective fluorophores must not be orthogonally oriented towards each other while their maximum transfer efficiency is achieved when their relative orientation is collinear (Dale, Eisinger, and Blumberg 1979). This geometric relationship is expressed in the dipole orientation factor $\varkappa^2$, as $\varkappa^2 = (\cos\vartheta_T - 3\cos\vartheta_D\cos\vartheta_A)^2$, with ϑ_D and ϑ_A being the angles between the connection vector of the fluorophores and the dipole moment of donor or acceptor, respectively, and ϑ_T the angle between the two dipole moments. Thus, a parallel alignment of fluorophores results in $\varkappa^2 = 1$, while a collinear arrangement results in $\varkappa^2 = 4$ and an orthogonal orientation in $\varkappa^2 = 0$, which completely inhibits the energy transfer between the fluorophores. For freely diffusing molecules and assuming freely and isotropically rotating fluorophores with rotation rates significantly exceeding the energy transfer rates, statistical distribution of all possible orientations of dipole moments results in an average $\varkappa^2$ value of $\frac{2}{3}$ (Dale, Eisinger, and Blumberg 1979).

Second, the spectral overlap integral J must not be zero. Thus, for optimal energy transfer, the emission spectrum of the donor and the absorption spectrum of the acceptor must have the largest possible overlap while at the same time the spectra must still be well separable to keep the accidental detection of donor fluorescence during the detection of the acceptor emission, called crosstalk, to a minimum.

Lastly, the distance between the fluorophores should be between 2 nm and 10 nm. For distances larger than 10 nm, energy transfer efficiency is strongly reduced and for distances below 2 nm, fluorescence can be quenched due to collisions (dynamic quenching) or complex formation (static quenching) of the fluorophores (Förster and Forster 1960).

The advantage of single molecule FRET compared to methods probing an ensemble of molecules is that measurements are not averaged, which implies that the heterogeneity within a sample, which can arise from different conformations of the examined molecules, as well as important kinetic information about the molecules can be determined (Berg et al. 2018; Voith von Voithenberg and Lamb 2018). smFRET experiments have for example been used to characterize the conformations and dynamics of the enzyme staphylococcal nuclease (Ha et al. 1999), the functional role of the conformational flexibility of the human Argonaute 2 protein (Willkomm

et al. 2022) and the conformational dynamics of the μ-opioid receptor (Zhao, Elgeti, et al. 2023).

The detection of photon emission from single molecules has become possible through improvements in sample labeling and measurement techniques as well as through advances in instrumentation, including the development of very sensitive fluorescence microscopes. Typically, smFRET experiments are performed either on freely diffusing fluorescently labeled molecules or on molecules that are immobilized on a surface (Gust et al. 2014; Mazal and Haran 2019; Voith von Voithenberg and Lamb 2018). For surface immobilized molecules, a total internal reflection fluorescence (TIRF) (Axelrod 2001; Moerner and Fromm 2003) microscope is used in which only molecules that are fixed to the surface of a measurement chamber are excited while noise from the bulk of the sample is rejected. This technique allows for the parallel observation of many molecules for an extended period of time, which is an advantage when studying dynamic biomolecular processes at slow timescales. As a consequence, acquisition times for smFRET experiments on surface-immobilized molecules can range between one to 30 seconds, which is the time until photobleaching of the fluorophores occurs.

Freely diffusing molecules are usually studied using a confocal microscope (Deniz, Dahan, et al. 1999; Moerner and Fromm 2003; Nie, Chiu, and Zare 1994). Here, laser beams are focused onto a small confocal volume within a sample chamber and when a fluorescently labeled molecule diffuses through the excitation volume, its donor fluorophore gets excited by the laser which leads to the emission of a photon. This emitted light is then focused onto a pinhole to reduce background noise by rejecting light that is out of focus and it is detected with a single-photon avalanche diode (SPAD) detector (Michalet et al. 2013). From this signal, the FRET efficiency can be calculated. The accumulation of FRET efficiencies from many single pairs of fluorescently labeled molecules then yields a FRET histogram which contains information about the distribution of the different conformations present in the examined molecule. The low sample concentrations (picomolar) and the small confocal volume (~ one femtoliter) ensure that only one molecule diffuses through the confocal volume at a time, and, depending on the speed of diffusion, it remains inside the confocal volume between 0.5 and 5 ms. During that time, it is alternatingly irradiated with two different lasers whose wavelengths correspond to either the maximum absorption wavelength of the donor or of the acceptor fluorophore. Photon emissions resulting from these excitations are then separated by wavelength, and consequently by donor or acceptor signal, and recorded by two separate detectors. Acquisition times for smFRET experiments on freely diffusing molecules vary strongly and can range from a few minutes up to several hours, depending on the complexity of the conformational distribution within the examined sample (Gust et al. 2014; Voith von Voithenberg and Lamb 2018).

For smFRET to take place, each molecule needs to be labeled with both a donor and an acceptor fluorophore. Since this cannot always be guaranteed, it is not always clear if a low FRET efficiency value is the result of a large distance between the fluorophores or if the molecule was not labeled with an acceptor fluorophore (Deniz, Dahan, et al. 1999). A solution to this problem is the pulsed interleaved excitation (PIE) method (Hendrix and Lamb 2013; Müller et al. 2005) (Figure 2.8).

This method allows to distinguish between molecules whose acceptor fluorophore

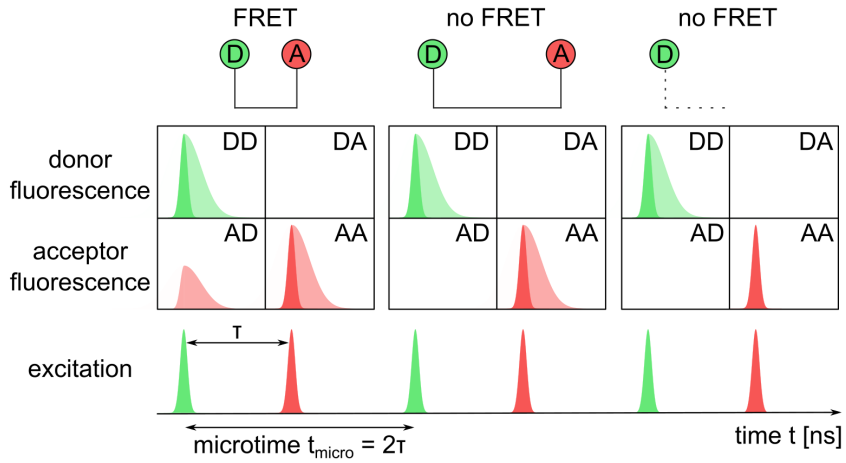

Figure 2.8.: The PIE method. The PIE method allows to distinguish between molecules whose acceptor fluorophore is missing and molecules for which both fluorophores are present but too far apart for FRET to take place. Therefore, the fluorophore labeled sample is excited by two different lasers (here red and green) in an alternating fashion. In the left image, the molecule is labeled with both fluorophores and they are at a suitable distance for FRET to take place. Thus, a signal is detected for both the donor and the acceptor after donor excitation (donor emission after donor excitation (DD) and acceptor emission after donor excitation (AD)) but only an acceptor signal is recorded after acceptor excitation (AA). Here, photon emission is depicted by the lighter colored shade after the pulse. In the middle, donor emission is detected only after donor excitation and acceptor emission only after acceptor excitation, which indicates that the distance between the fluorophores is too large for FRET to occur. In the image on the right, the molecule was not labeled with an acceptor fluorophore, so only a donor signal can be detected after donor excitation.

is missing and molecules for which both fluorophores are present but too far apart for an efficient FRET to take place. Two different lasers, one at the excitation wavelength of the donor and one at the excitation wavelength of the acceptor, are used and they irradiate the sample in an alternating fashion. After each pulse, both donor and acceptor fluorescence are recorded in their respective detection channels. The time difference τ between each pulse is chosen such that excitation, emission and detection from the preceding pulse are completed before the next laser beam is emitted. The time it takes to complete one donor and acceptor excitation cycle is called the microtime $t_{micro} = 2\tau$ and it often ranges between 10 and 30 ns. The emitted photons are counted using time-correlated single-photon counting (TCSPC) (O'Connor and Phillips 1984), which is a method to count and detect photons while simultaneously recording the timepoint of photon emission with respect to the laser pulses within the respective microtime. As a consequence, for each individual photon it can be determined whether it was emitted due to donor or due to acceptor excitation. In this way, if no signal is detected for both fluorophores after acceptor excitation, the acceptor is missing but if only donor signal is detected after donor excitation and only acceptor signal after acceptor excitation, both fluorophores are present but too far apart for an energy transfer to occur. Only when both donor and acceptor signal are recorded after donor excitation and only acceptor signal after acceptor excitation, FRET has taken place.

From this information, correction factors can be calculated and they include crosstalk and direct excitation as well as the so-called β- and the γ- factor (Dahan et al. 1999; Deniz, Laurence, Dahan, et al. 2001; Gust et al. 2014; Lee, Kapanidis, et al. 2005). Crosstalk quantifies the number of photons emitted from the donor which are detected in the acceptor channel, direct excitation is the number of photons emitted with donor wavelength after direct excitation of the acceptor, the β- factor describes the correlation between the theoretical fluorophore extinction coefficient

and the intensity of the laser at the extinction wavelength, and the γ- factor specifies differences in quantum yields and detection efficiencies between donor and acceptor. These factors are used to correct the measured FRET efficiencies and thus eliminate experimental inaccuracies. From Gaussian fits of the corrected FRET efficiency histograms, the distribution of conformations present in the examined sample can then be extracted (Schrimpf et al. 2018).

In this way, smFRET provides rapidly accessible data on short intra- and intermolecular distances and on changes thereof which therefore makes it a powerful research tool to study biomolecular processes in their native environment in detail. Especially in combination with complementary biophysical and biochemical methods, a profound understanding of the structures and dynamics of biomolecules can be obtained whose interplay ultimately determines the molecules' functions.

Part II.

Materials and Methods

1. Molecular biology

1.1. Mutagenesis and Gibson Assembly

The genes encoding for *S. pombe* Dcp1, Dcp2 constructs and Edc3 constructs were cloned into a modified pET-M11 vector containing an N-terminal, TEV cleavable hexahistidine tag (N-His_6-TEV). The gene encoding for Dcp2 1-270 was generated by fusion at its N-terminus with the maltose binding protein (MBP) via Gibson assembly to enhance the solubility of the protein and it was cloned into a modified pET-M40 vector containing a TEV cleavage site at its N-terminus and a non-cleavable His_6 tag at its C-terminus.

The genes encoding for DcpS from *C. thermophilum* with the inactivating mutation N258A were cloned into a pRSFM-11 vector containing an N-terminal, TEV cleavable hexahistidine tag (N-His_6-TEV). The genes encoding for DcpS from *H. sapiens* and *S. cerevisiae* (Dcs1p) were cloned into a pET-M1060 vector containing an N-terminal, TEV cleavable His_6-NusA-His_6 tag.

All point mutations in Dcp1 (N110C, N112C, N119C), Dcp2 (M202amber, S154amber, W43A) and DcpS (N258A, W77Y, W188Y, W220Y, W208Y) were introduced using standard quick-change methods.

The plasmid of the KIX domain of the human CBP protein was kindly provided by M. Tollinger (University of Innsbruck) and it was cloned into a pET-15b vector containing an N-terminal His_6 tag followed by a thrombin cleavage site.

2. Protein expression, isotope labeling and purification

2.1. Transformation and recombinant expression

All proteins in this study were over-expressed in and isolated from *E. coli* BL21(DE3) CodonPlus-RIL cells (Stratagene). For Dcp2 proteins carrying a stop codon mutation, E. coli BL21 (DE3) Codon PlusRIL cells (Addgene) contained an additional pEvol plasmid which allowed for over-expression using the amber-suppression system. To that end, plasmids were transformed into the cells that were subsequently grown overnight at 37°C on LB agar plates in the presence of chloramphenicol and kanamycin or ampicillin (KIX). Colonies were resuspended in a 25 ml LB pre-culture supplemented with 1 mM kanamycin or ampicillin and 1 mM chloramphenicol and grown to an optical density OD_{600} of 0.8 - 1.0 at 37°C for subsequent inoculation of the respective pre-cultures or main cultures.

Expression in LB cultures occured via addition of the LB pre-culture to the final expression volume of LB medium, which was supplemented with 1 mM chloramphenicol and 1 mM kanamycin. Cells were grown to an OD_{600} of 0.8 at 37°C, then the temperature was reduced to 20°C and protein expression was induced with 1 mM IPTG.

Proteins carrying a stop codon mutation were grown in LB cultures using the amber-suppression system. The LB pre-cultures were added to the final expression volume of LB medium and the cells were grown at 37°C. At an OD_{600} of 0.2, 200 mg/l of the unnatural amino acid AzF (SantaCruz Bioscience) was added. To induce the expression of the AzF-tRNA-synthetase, which is encoded in the pEvol vector and whose expression is controlled by the araBAD promotor, 0.02 % (w/v) L-Arabinose (Roth) was added at an OD_{600} of 0.4. Subsequently, the temperature was lowered to 20°C and at an OD_{600} of 0.8, protein expression overnight was induced by addition of 0.5 mM IPTG.

Expression in H_2O M9 minimal medium was achieved by using 1 ml of LB pre-culture to inoculate a 100 ml H_2O-based M9 minimal medium pre-culture, that was incubated overnight at 37°C. The overnight culture was diluted with 900 ml H_2O M9 medium and grown to an OD_{600} of 0.8 at 37°C, then the temperature was changed to 20 °C and protein expression was induced by addition of 1 mM IPTG.

Expression in partially (~ 80-90 %) or fully (100 %) deuterated M9 minimal medium was achieved by using 1 ml of LB pre-culture to inoculate a 50 ml H_2O-based M9 minimal medium pre-culture. H_2O M9 pre-cultures were grown at 37°C and centrifuged for 10 minutes at 3500 g. Pellets were resuspended in 100 ml ^{14}N or ^{15}N recycled D_2O M9 pre-culture (~ 80-90 % D_2O) using 4 g/l protonated glucose, or in 100 ml D_2O M9 medium using 2 g/l $^{2}H^{12}C$ glucose, at an OD_{600} of 0.15 and grown overnight at 37°C. Next, 900 ml of the respective D_2O, or recycled D_2O, M9 medium were added to the overnight pre-culture, cells were grown to an OD_{600} of 0.8 at 37°C and then protein expression over night was induced by addition of 1 mM IPTG and a temperature reduction to 20°C.

Cells were harvested 12-18 h after induction by centrifugation at 5000 rpm for 20 min and cell pellets were stored at -20°C.

2.2. Isotope labeling

Deuteration of the proteins was achieved by making use of an M9 medium that contained 100 % D_2O and ^{2}H, ^{12}C-glucose (2 g/l) and partial deuteration was achieved by using an M9 minimal medium that was based on 90 - 95 % D_2O and protonated glucose.

NMR active ($^{13}CH_3$) methyl groups were introduced into the proteins at the isoleucine-δ1, leucine-δ, valine-γ, methionine-ε and alanine-β positions. To that end, 60 mg/l 2-ketobutyric acid-4-^{13}C,3,3-$^{2}H_2$, 100 mg/l 2-Keto-(3-methyl- ^{13}C)-butyric acid-4-^{13}C,3- ^{2}H and 100 mg/l L-Methionine-(methyl- ^{13}C) were added to the cells which were grown in D_2O-based M9 minimal medium at an OD_{600} of 0.6 - 0.8. 40 minutes later, 100 mg/l L-Alanine-3- ^{13}C,2- ^{2}H was added. 20 minutes later protein expression was induced.

Methionine-ε only labeling in LB medium was achieved by adding 500 mg/l L-Methionine-(methyl- ^{13}C) 1 h before induction.

^{1}N labeling of proteins was achieved by adding $^{15}NH_4Cl$ used as the sole nitrogen source in the H_2O- or D_2O-based expression medium.

Incorporation of 5-fluorotryptophan into the proteins was achieved by using 5-fluoroindole as a precursor. To that end, 50 mg/l 5-fluoroindole (Crowley, Kyne, and Monteith 2012) that was dissolved in DMSO at a 100 mg/ml stock concentration was added to the expression medium 1 hour prior to induction.

Table 2.1 shows which protein constructs were expressed in which medium and with which label. Mutants of proteins were prepared in the same way as the respective wild type protein.

Experiment	Construct *	Label	Expression medium
High pressure NMR	Dcp1	none	recycled D_2O
	Dcp2 96-243	ILMVA	100 % D_2O
	Dcp2 1-243	ILMVA	100 % D_2O
^{19}F NMR	KIX domain of the human CBP protein (res. 321-407)	^{19}F ^{15}N ^{19}F and ^{15}N	H_2O H_2O H_2O
	DcpS (from *H. sapiens*, *S. cerevisiae*, *C. thermophilum*)	^{19}F	H_2O
	Dcp1	^{19}F ^{15}N ^{19}F and ^{15}N none	H_2O H_2O H_2O LB
	Dcp2 1-95	^{19}F ^{15}N ^{19}F and ^{15}N none	H_2O H_2O H_2O LB
	Dcp2 1-243	^{19}F ^{19}F, IM ILMVA	H_2O recycled D_2O 100 % D_2O
smFRET	Dcp1	fluorophore fluorophore, Methionine	LB LB
	Dcp2 1-270	fluorophore fluorophore, Methionine	LB + amber suppr. LB + amber suppr.
ssNMR	Dcp1	none	recycled D_2O
	Dcp2 1-270	none ^{15}N, Methionine	recycled D_2O recycled D_2O
	Edc3 FL	^{15}N none	recycled D_2O recycled D_2O
	Edc3 YjeF_N	^{15}N	recycled D_2O

* from *S. pombe* unless indicated otherwise.

Table 2.1.: Summary of all experiments, protein constructs, labels and expression media used in this thesis.

2.3. Purification

Cell pellets were solubilized in lysis buffer, supplemented with 0.1 % (v/v) Triton X-100, 1 µg/ml DNase I and 200 µg/ml lysozyme. To proteins used for phase separation experiments, 5 mM MgCl were added and for ^{19}F labeled proteins, 1 mM EDTA, and, after lysis, 2 mM $MgSO_4$ were added. Cells were lysed by sonication on ice and the lysate was cleared by centrifugation (18000 rpm, 30 min, 4°C) and filtered. The filtered supernatant was applied to a NiNTA-column which was equilibrated in lysis buffer. Purification occurred via a wash step with 5 -10 column volumes of lysis buffer and the subsequent elution of the target protein from the column using elution buffer. For Dcp2 constructs used for high pressure NMR experiments, the wash step additionally included 5 column volumes of wash buffer A and 10 column volumes of wash buffer B. The His_6-tag and the MBP-tag were removed either by TEV cleavage during dialysis overnight against dialysis buffer at 4 °C or by incubation with thrombin during dialysis overnight against dialysis buffer A at 4 °C (KIX domain). The His_6-tag and the TEV protease were removed from the target protein by applying the dialysed solution to a NiNTA column that was equilibrated in dialysis buffer and the MBP tag was removed from Dcp2 1-270 by a reverse NiNTA column that was equilibrated in lysis buffer and washed with one column volume of 75 % diluted lysis buffer. The Dcp2 1-270 protein was then eluted using elution buffer. Proteins used for fluorophore labeling were concentrated and frozen at -80°C. Dcp1:Dcp2 decapping complexes without fluorophores were formed by combining both proteins in a 2:1 ratio and excess of Dcp1 was removed, and all other protein constructs were further purified, by size exclusion chromatography (16/600 Superdex S75/ 16/600 Superdex S200; GE Healthcare) in size exclusion buffer. Fractions containing the purified protein or protein complex were combined and concentrated using a spin concentrator. For KIX, the buffer was exchanged to NMR buffer B. For high pressure NMR experiments, the buffer was exchanged to NMR buffer A. For NMR measurements, 5 % D_2O and 0.03 % NaN_3 were added to the sample. Protein concentrations were determined by absorption measurements at 280 nm using the NanoDrop 2000/2000c (Thermo Scientific). Final protein concentrations varied between 170 and 300 µM for high pressure CPMG experiments in a final volume of 250 µl, between 50 and 80 µM for methyl TROSY (HMQC) experiments and between 100 and 500 µM for ^{19}F NMR measurements, both in a volume of 500 µl, between 20 and 100 µM for NMR measurements on fluorophore labeled proteins in a volume of 250 µl and between 500 and 800 µM in a volume of 200-300 µl for subsequent induction of LLPS. For high pressure NMR meausrements of the Dcp1:Dcp2:ATP complex an ATP concentration of 10 mM was used. This high ATP concentration was used to ensure saturation of the ATP binding site such that ligand exchange will not result in CPMG relaxation dispersions. All buffers used are listed in Table 2.2.

Buffer name	Contents	Used for proteins for
lysis A	400 mM NaCl, 50 mM sodium phosphate, pH 7.4, 10 mM imidazole	hp-NMR, smFRET
lysis B	250 mM NaCl, 25 mM sodium phosphate, pH 7.4, 10 mM imidazole	LLPS
lysis C	150 mM NaCl, 50 mM sodium phosphate, pH 7.4, 5 mM imidazole	^{19}F
wash A	1 M NaCl, 50 mM sodium phosphate, pH 7.4	Dcp2 hp-NMR
wash B	400 mM NaCl, 50 mM sodium phosphate, pH 7.4, 30 mM imidazole	Dcp2 hp-NMR
elution A	150 mM NaCl, 50 mM sodium phosphate, pH 7.4, 300 mM imidazole	hp-NMR, smFRET, ^{19}F NMR
elution B	250 mM NaCl, 25 mM sodium phosphate, pH 7.4, 300 mM imidazole	LLPS
dialysis A	150 mM NaCl, 25 mM sodium phosphate, pH 7.4 and 1 mM DTT	hp-NMR, smFRET, ^{19}F NMR KIX
dialysis B	125 mM NaCl, 25 mM HEPES, pH 7.3, 0.5 mM EDTA, 1 mM DTT	LLPS
dialysis C	25 mM Tris, pH 8.0, 75 mM NaCl, 1 mM DTT	^{19}F NMR
size exclusion A	125 mM NaCl, 25 mM HEPES, pH 7.3 and 1 mM DTT	hp-NMR, smFRET, ^{19}F NMR, LLPS
size exclusion B	25 mM NaCl, 25 mM HEPES pH 8.0, 1 mM DTT	^{19}F NMR DcpS
NMR A	125 mM NaCl, 25 mM HEPES, pD 7.3, 1 mM DTT in 100 % D_2O	hp-NMR
NMR B	25 mM NaCl, 50 mM potassium phosphate, pH 5.8	^{19}F NMR KIX
FRET	125 mM NaCl, 25 mM HEPES, pH 7.3	smFRET
no salt ssNMR	25 mM HEPES, pH 7.3	LLPS

Table 2.2.: Summary of all buffers for protein purification and for experiments performed in this thesis.

3. Protein fluorophore labeling

3.1. Cysteine-Maleimide coupling

Chemoselective labeling of proteins with fluorophores can be achieved by coupling of fluorophores to amino acid residues such as cysteines. Cysteines contain sulfhydryl (thiol) groups that can form covalent bonds with maleimide groups of

fluorophores (Tyagi and Lemke 2012). For this reaction, disulfide bridges in the cyteines that may potentially have formed via oxidation need to be reduced, as these do not react with maleimides. This method ist fast and efficient (Kim, Ho, et al. 2008), but for proteins that contain multiple cysteine residues, site-specific labeling cannot be achieved unless cysteines that should not be labeled are removed through mutation, which can have a destabilizing effect on the protein structure.

Dcp1 from *S. pombe* contains no cysteine residues, so for fluorophore labeling of the protein, cysteine point mutations were introduced at the specific labeling sites and maleimide-activated fluorophore dyes (Maleimido-DyLight 650; (ThermoFischer)) were coupled to the cysteines via cysteine-maleimide coupling. Before labeling, NiNTA-purified Dcp1 was applied to a size exclusion chromatography column (Superdex 75; GE Healthcare) in size exclusion buffer (125 mM NaCl, 25 mM HEPES, pH 7.3 and 1 mM DTT) and fractions containing Dcp1 were pooled and concentrated. To reduce the cysteine thiol group of Dcp1, the protein was incubated in 1 mM DTT for 1 h at room temperature and afterwards the DTT was removed using a PD-miniTrap G-10 desalting column (GE Healthcare) that was equilibrated in FRET buffer (125 mM NaCl, 25 mM HEPES, pH 7.3), according to the manufacturer's instructions. Dcp1 was eluted using FRET buffer. Afterwards, the protein was incubated in darkness at room temperature with the fluorophore at a 5-fold molar excess for more than 1 h for the fluorophore labeling reaction to take place. 5 mM DTT was added to the fluorescently labeled Dcp1 and then stored at -80°C until complex formation with fluorphore labeled Dcp2.

3.2. Staudinger Ligation

Dcp2 from *S. pombe* contains five cysteine residues, so cysteine-maleimide coupling was not suited for site-specific fluorophore labeling of the enzyme. Alternative to cysteine-maleimide coupling, an unnatural amino acid can be inserted into the protein of interest during expression (Noren et al. 1989) and these unnatural amino acids can be coupled to functional groups of the fluorophores. As unnatural amino acids do not occur naturally in any protein, this method ensures high labeling specificity. In addition, the used functional groups are highly reactive and compact in size, which is both very advantageous (Agrawal and Hackenberger 2013). Different non-proteinogenic amino acids containing bioorthogonal methoxy-, keto-nitro- or azide groups exist and they have been used for fluorophore labeling (Wang and Schultz 2005). For Dcp2, specifically, fluorophore labeling was achieved via Staudinger ligation (Saxon and Bertozzi 2000) between the azide group N_3 that was inserted into the protein via the unnatural amino acid AzF using the amber-suppression system (see section 2.1) and a conjugated phosphine group on the phosphine-activated fluorescent dye (Phosphine DyLight 550; Thermo Fischer). In this reaction, the azide group of AzF covalently binds to the phosphine group of the fluorophore (Köhn and Breinbauer 2004).

Prior to the reaction, the buffer of NiNTA purified Dcp2 was changed to FRET buffer and then it was incubated with the fluorophore at a 5-fold molar excess for 3 h in darkness at room temperature. The labeled Dcp2 was stored at -80°C until complex formation with fluorophore labeled Dcp1.

Dcp1:Dcp2 complexes of fluorescently labeled proteins were formed by combination of both proteins at a 2:1 molar ratio and subsequent incubation for 20 min in darkness. Excess Dcp1 and fluorophores were removed by size exclusion chromatography (Superdex 75 for NMR measurements, 10/300 Superdex S75 for FRET measurements; both GE Healthcare) in size exclusion buffer (125 mM NaCl, 25 mM HEPES, pH 7.3 and 1 mM DTT). Elution of the complex and of the fluorophores was monitored via UV absorption at 280 nm, 550 nm and 650 nm and fluorophore labeling was detected using a fluorescence image scanner (AmershamTM Imager 600, GE Healthcare). For NMR experiments, all fractions containing the fluorescently labeled Dcp1:Dcp2 complex were combined and concentrated to 500 µl, then 5 % D2O and 0.03 % NaN_3 were added and the sample was stored at -20°C. For all FRET experiments, the SEC fraction containing the highest absorption value for all three detected wavelengths was chosen and FRET experiments were immediately performed with the freshly prepared complexes.

4. RNA preparation

4.1. RNA transcription and purification

RNAs used for smFRET experiments and ssNMR measurements were produced using standard *in vitro* transcription with T7 RNA polymerase. RNA sequences identical to the first 7, 15, 80 or 380 nucleotides (nt) of the *S. cerevisiae* MFA2 mRNA were designed and modified such that the pyrimidines in the first 16 nt were changed to purines in order to facilitate testing for successful capping of the RNAs via RNAse A digestion. Anti-sense strand and sense strand primers containing the T7 promoter sequence and the (reverse complementary) target RNA sequence, respectively, were mixed at equimolar amounts to 1 µM concentration and added to 40 mM Tris pH 8.0, 5 mM DTT, 1 mM spermidine, 0.01 % Triton X-100, 4 mM nucleoside triphosphates, 20–60 mM $MgCl_2$, and 0.2 µM T7 RNA polymerase. The reaction was incubated for 4 h at 30°C, EDTA was added to solubilize the insoluble pyrophosphate and the RNA was precipitated at 20°C in 0.3 M NaOAc, pH 5.2 and 0.7 volumes of isopropanol or, for RNAs shorter that 10 nt, in 0.2 M NaCl and 3.5 volumes of EtOH. After centrifugation for 1 h at 9000 × g, the pellet was washed with cold EtOH (75 %), dried and resuspended in water.

Transcribed RNA was purified by denaturing anion exchange chromatography on a high-performance liquid chromatography (HPLC) system with a DNAPac PA100 column (22 × 250 mm; Dionex). The RNA was applied to the column which was heated to 60°C and equilibrated in 20 mM Tris, pH 8.0 and 5 M Urea. Elution occurred via a NaCl gradient, fractions containing RNA were collected, precipitated, desalted using a PD-10 column (GE Healthcare) and concentrated.

4.2. 5' OH RNA production

80 nt 5' OH- RNA was synthesized via fusion of previously transcribed and purified 80 nt RNA (section 4.1) to a 5' hammerhead ribozyme (HHR), which is 41 nt long and folds into three helices. The 5' end of the HHR contains a 10 nt long sequence which is complementary to the 5' end of the target RNA and with which it forms a stem structure. RNA with a hydroxylgroup at its 5' end is then obtained via HHR cleavage at the specific cleavage site located at the position following the region that is complementary to the RNA (Avis, Conn, and Walker 2012).

The template DNA for the *in vitro* transcription of the HHR was produced in a 500 µl reaction in H_2O using 10 µM each of two primers with an 18 nt long overlap, 100 µl 5 × Q5 buffer, 0.02 U/µl Q5 polymerase and 0.6 µM dNTPs each. After initial denaturation for 2 min at 95°C, 10 PCR cycles consisting of a 10 s denaturation step at 98°C, a 20 s primer-hybridisation step at 60°C, and a 5 min elongation step at 72°C were then performed before the final elongation step for 4 min at 72°C.

In vitro transcription of the HHR was achieved in 40 mM Tris, pH 8.0, 0.01 % (v/v) Triton-X 100, 1 mM spermidine, 5 mM DTT, 4 mM NTPs each, 30 mM $MgCl_2$, 40 µg/ml T7 polymerase and 500 µl template DNA obtained from the preceding PCR reaction. H_2O was added until a volume of 5 ml was reached and the reaction was incubated at 37°C for three hours. Next, 15 mM $MgCl_2$ were added for a total $MgCl_2$ concentration of 45 mM and the reaction was incubated at 95°C for 1 h to ensure the correct formation of the hammerhead structure. Cleavage of the HHR occured over night at 37°C and its success was confirmed with 10 % denaturing Urea-PAGE.

For separation of the 5' OH- RNA and the HHR, the mixture containing target RNA, HHR and uncleaved intermediate species was loaded onto a pre-warmed preparative denaturing polyacrylamide gel (10 %) and the gel was run until the RNA products were fully separated. Visualisation of the RNA was achieved via UV-shadowing and the part containing the target RNA was cut from the gel. For extraction of the target RNA, the gel fragment was cut into small pieces and incubated at room temperature over night in 20 ml 300 mM NaAcO. After subsequent centrifugation and filtration (0.8 nm filter pore size), 1 volume isopropanol was added to the supernatant for precipitation over night at - 20°C. The precipitate was pelleted, the pellet resuspended in H_2O, aliquotted and frozen at -20°C until usage.

4.3. RNA 5' m^7G capping

To add a N7-methylguanosine cap to the 5' end of the RNAs, purified RNA was dissolved at a concentration of 20 µM in 50 mM Tris, pH 8.0, 5 mM KCl, 1 mM $MgCl_2$, and 1 mM DTT before 0.5 mM GTP, 0.1 mM SAM and vaccinia capping enzyme were added and the reaction was incubated at 37°C. The capping reaction was stopped and the capping enzyme was removed by heating to 95°C for 10 min. After centrifugation for 10 min at 4500 × g, the capped RNA was precipitated and resuspended in H_2O or FRET buffer. Capping success was confirmed using denaturing Urea-PAGE for RNAs shorter than 20 nt or by RNAse A digestion followed by denaturing Urea-PAGE for 80 nt and 380 nt long RNAs.

5. Liquid-liquid phase separation

5.1. LLPS and maturation

Protein complexes for liquid-liquid phase separation and subsequent maturation were obtained from separately expressed and purified components. To that end, the labeled protein (Dcp1:Dcp2 or Edc3) was combined with a 1.3- to 1.5-fold molar excess of either the Edc1 peptide (sequence SILYAGPTFTHSPAASNLPIPTFLHS), and/or 2.5-3-fold molar excess mRNA or m^7GDP and a 1.3 to 1.5-fold molar excess of the unlabeled protein (Dcp1:Dcp2 or Edc3).

Phase separation was induced by adding four volumes of buffer containing no salt (25 mM HEPES pH 7.3, 1 mM DTT). The phase separated protein complex was kept at room temperature for > 1h for maturation and gel formation and then the sample was centrifuged for 20 minutes at 16000g to collect all gel droplets.

6. NMR spectroscopy

6.1. High pressure NMR

6.1.1. NMR measurements

All NMR measurements were performed on a Bruker NEO spectrometer that operated at a proton frequency of 500 (Dcp2 catalytic domain; nitrogen cooled TCI probehead) or 800 (Dcp1:Dcp2 complexes; helium cooled TCI probehead) MHz at 303 K. For measurements at standard pressure (1 bar) a 500 µl sample volume was used. Measurements at higher pressure levels were performed using a special high pressure system consisting of a ceramic cell (Daedalus Innovations LLC) that holds 250 µl sample, a pressure autoclave and a PBI Pressure Hub (Pressure BioSciences Inc, MA) which is synchronized with the spectrometer and allows for automatic pressure control and the recording of automatic pressure series. The NMR buffer contained 125 mM NaCl, 25 mM HEPES, pD 7.3 and 1 mM DTT in 100 % D_2O. In addition, 50 µM DSS was added for referencing. NMR samples had a protein concentration between 170 and 300 µM for high pressure relaxation dispersion experiments and between 50 and 80 µM for methyl TROSY (HMQC) experiments. Spectra were recorded at pressures ranging from 10 bar to 2750 bar and spectra processing was done with the NMRPipe/NMRDraw software (Delaglio et al. 1995).

6.1.2. Chemical shift assignments

The chemical shifts of the isolated Dcp2 catalytic domain were assigned based on assignments of Dcp2 in the Dcp1:Dcp2 complex, on a 3-dimensional (H)-C-C-H NOESY experiment (mixing time 400 ms) that was recorded on the Dcp2 CD and on the known structure of the CD (She, Decker, Svergun, et al. 2008). NOESY experiments were visualized and manually analyzed using CARA (cara.nmr.ch).

6.1.3. Relaxation dispersion measurements

^{13}C single quantum Carr–Purcell-Meiboom–Gill relaxation dispersion experiments (Lundström et al. 2007) were performed at 800 MHz proton frequency with CPMG frequencies of 77, 154, 231, 308, 462, 615, 846, 1077, 1308, 1538, 1769, 2000 Hz and a relaxation delay of 26 ms. Peaks were picked and integrated using the NMRPipe/NMRDraw software (Delaglio et al. 1995). Intensities were converted into relaxation rates and RD curves were fitted numerically using in-house Matlab scripts which are based on the exact analytic equations presented by Baldwin (Baldwin 2014). Fitting was performed simultaneously for the methyl groups of M221, M164, V222 (γ1 and γ2) and L226 (δ1), that could be analyzed at all pressures in the absence and presence of ATP. It was assumed that $|\Delta\omega_C|$ was independent of the applied pressure. The $|\Delta\omega_C|$ value was fixed for each methyl group based on the resonance frequency of the methyl group in the Dcp2 catalytic domain (fully open conformation) and the resonance frequency in the Dcp1:Dcp2 or Dcp1:Dcp2:ATP complex (94 % closed conformation). It is important to note that the extracted volume changes were indistinguishable when assuming that the Dcp1:Dcp2 or Dcp1:Dcp2:ATP complexes at ambient pressure were either 90 or 98 % closed. Errors in the individual relaxation rates were determined based on duplicate measurements and were assumed to have a standard deviation of at least 1 Hz. Errors in the extracted exchange parameters were obtained from refitting the data 250 times after randomly varying the experimentally determined relaxation rates based on the errors in these rates. In that process the starting parameters for the minimization were randomly varied by 10 %. The volume changes were obtained by simultaneously fitting the pressure dependence of the determined equilibrium constant as well as the forward and reverse rates using the Eyring relationship. It is worth noting that the CPMG data and the pressure dependence of the rates could also be well fitted at the same time, which yielded highly similar volume changes (i.e. enforcing the CPMG fitting parameters to obey the Eyring equation).

6.1.4. Protein cavities, volumes and images

Protein voids were located using the program HOLLOW (Ho and Gruswitz 2008), based on the Dcp2 protein in the closed conformation (PDB ID: 2QKM, chain B) that was energy minimized in Chimera (Pettersen et al. 2004) using the command "Minimize Structure". Internal cavities were separated from surface cavities by manual inspection in Pymol (The PyMOL Molecular Graphics System, Version 2.0 Schrödinger, LLC.). Protein volumes were calculated using the program ProteinVolume (Chen and Makhatadze 2015). To that end, the coordinates of the two open and two closed conformations of Dcp1:Dcp2 were extracted from the PDB (PDB ID:

2QKM, chains A/B, C/D, E/F and G/H), protons were added to the model using the Chimera (Pettersen et al. 2004) command "AddH", after which the structural models were minimized in Chimera using the command "Minimize Structure", based on the default settings. For the comparison of the volumes of the open and closed conformations of Dcp2 and Dcp1:Dcp2 (two crystallographically independent copies of each conformation are present in the crystal) only the atoms that are present in all models (PDB ID: 2QKM) were considered and all ligand atoms were removed. Protein images were prepared using Pymol.

6.2. ^{19}F NMR experiments

6.2.1. NMR measurements

NMR spectra were recorded at 298 K (KIX) or 303 K (Dcp1, Dcp2, DcpS) on Bruker NEO spectrometers that operate at 500, 600 or 800 MHz proton frequency and that are equipped with nitrogen (500 and 600) or helium (800) cooled TCI probe heads and NEO consoles. ^{19}F experiments were recorded at 500 or 600 MHz proton frequency by tuning the proton channel to the ^{19}F frequency. Acoustic ringing artifacts were suppressed using a three pulse "aring" sequence (Overbeck, Kremer, and Sprangers 2020). For ^{15}N CPMG experiments frequencies ($\omega_{CPMG}/2\pi$) between 0 and 1000 Hz and relaxation delays of 50 ms (KIX) or 60 ms (Dcp1, Dcp2) were used. For ^{19}F CPMG experiments frequencies ($\omega_{CPMG}/2\pi$) between 0 and 5000 Hz and a relaxation delay of 10 ms were used. Longitudinal exchange experiments were recorded using a series of 2 dimensional ^{19}F-^{19}F EXSY (NOESY) experiments on samples containing 0.4 mM DcpS (monomer concentration) in the presence of a 1:1, 1:2, 1:4, 1:6, 1:8, 1:10, 1:12 or 1:14 molar excess of m^{7}GpppG using 19 different mixing times ranging from 3 µs to 800 ms. Due to fast relaxation of the ^{19}F magnetization the acquisition time in the indirect dimension in the NOESY experiments was restricted to 2.8 ms. Errors in all experiments were extracted from two or three recorded sets of experiments. Methyl TROSY experiments were recorded using a SOFAST HMQC sequence (Schanda and Brutscher 2006), using a carbon acquisition time of 21 ms. NMR data were processed using the NMRPipe/NMRDraw software suite (Delaglio et al. 1995), figures displaying NMR spectra were produced using NMRView (onemoonscientific.com) and data were analyzed with in-house written Matlab scripts.

6.2.2. Chemical shift assignments

Tryptophan resonances were assigned by a mutational approach that we often use to assign methyl group resonances (Sprangers, Gribun, et al. 2005; Sprangers and Kay 2007), where spectra of the wild-type complex were compared with spectra of the complex that lacked individual tryptophan residues. The W43A assignment mutation in Dcp2 residues 1-95 and Dcp2 residues 1-243 as well as the N258A, W77Y, W188Y, W220Y and W208Y mutations in DcpS were introduced using standard quick-change methods.

6.2.3. Relaxation dispersion measurements

For the CPMG experiments the effective transverse relaxation rates were calculated as $R_2^{eff} = -\frac{1}{T_{CPMG}} * \ln(\frac{I}{I_0})$, where I is the intensity of the peak and I_0 the reference intensity recorded without the constant time CPMG relaxation delay. Relaxation dispersion curves were numerically fitted to a two-state exchange model (Baldwin 2014), in which the populations (p_a, $p_b = 1 - p_a$), the exchange rate (k_{ex}), the absolute value of the chemical shift difference between the two states ($|\Delta\omega|$) and the transverse relaxation rates (assumed to be identical for both states) were used as fitting parameters. Data from different residues and different magnetic fields were fitted simultaneously to a single exchange rate and a single population of the excited state.

6.2.4. Zz-exchange experiments

To extract the rates from the longitudinal exchange experiments the intensities of the cross- and autopeaks were fitted to one global two-state exchange process (Sprangers, Gribun, et al. 2005) in which $I_{cross} = Ap_ap_b\exp(-\rho\, t_{mix})*[1-\exp(k_{ex}t_{mix})]$ and $I_{auto} = B\exp(-\rho\, t_{mix})*[p_a^2 + p_ap_b\exp(-k_{ex}t_{mix})]$. Here, I_{cross} and I_{auto} are the intensity of the cross and auto peaks respectively, p_a and p_b are the populations for the open and the closed state of the enzyme that were fixed to 0.5 due to the symmetric nature of the dimer, ρ is the longitudinal relaxation rate, t_{mix} the mixing time, k_{ex} the exchange rate and A and B are scaling factors. To determine the goodness of the fits, Monte Carlo simulations with 100 fit iterations were used. In this process, the mean values of all data points were randomly varied according to a normal distribution with a width that corresponds to the respective standard deviation of the data point that was determined from multiple measurements.

6.3. NMR on fluorophore labeled complexes

NMR spectra were recorded at 303 K on a Bruker Avance III spectrometer that operates at 800 MHz proton frequency and that is equipped with a helium cooled TCI probe head and a NEO console. Fluorophore labeled proteins had concentrations between 20 and 60 µM in a sample volume of 250 µl and samples without fluorophore tags had concentrations between 150 and 220 µM in a volume of 500 µl. Methyl TROSY experiments were recorded using a SOFAST HMQC sequence (Schanda and Brutscher 2006). NMR data were processed using the NMRPipe/NMRDraw software suite (Delaglio et al. 1995).

6.4. Solid-state NMR experiments

Lyophilization of proteins for solid-state NMR experiments occured overnight and was followed by subsequent rehydration. Preparation of gel samples containing maturated proteins is described in section 5.1. Lyophilized and mature-phase proteins were placed into 1.3 mm ssNMR rotors and ssNMR experiments were conducted using a 1.3 mm triple-resonance ^{1}H/X/Y MAS probe with a proton resonance frequency of 800 MHz. Scalar-based correlation experiments made use of

^{1}H-^{15}N INEPT transfer. Samples were spun at MAS frequencies of 55, 58 and 60 kHz at an approximate real temperature of 310 K. Cross-polarization (CP) steps with amplitude ramps of 80–100 % and 15 kHz PISSARRO decoupling were employed and hNH and hCH spectra were recorded (Weingarth, Bodenhausen, and Tekely 2009). The Bruker TopSpin 3.6.2 software was utilized for spectra processing. Linear prediction in the indirect dimension was utilized. Chemical shift referencing was done by utilizing the water resonance. The spectra were analysed using POKY from NMRFAM-Sparky (Lee, Rahimi, et al. 2021; Lee, Tonelli, and Markley 2014). In Table 6.1, ssNMR parameters are summarized.

Sample	Expt. *	Scans	Acquisition time (ms) (dir./ind. dim.)	Window function	MAS (kHz)
Dcp1:Dcp2	NH dip.	320	22/9	Qsine (3)	58
	CH dip.	320	23/9	Qsine (2.5)	58
Dcp1:Dcp2 + 1.3 × Edc3 FL	NH dip.	640	22/9	Qsine (3)	60
	CH dip.	640	23/9	Qsine (2.5)	60
Dcp1:Dcp2 + 1.5 × Edc1 + 1.5 × Edc3	NH dip.	1280	22/9	Qsine (3)	58
	CH dip.	640	23/9	Qsine (2.5)	58
Dcp1:Dcp2 + 1.5 × Edc3 + 4 × m^7GDP	NH dip.	892	22/9	Qsine (3)	60
	CH dip.	1152	23/9	Qsine (2.5)	60
Dcp1:Dcp2 + 1.5 × Edc1 + 4 × m^7GDP + 1.2 × Edc3 FL	NH dip.	512	22/9	Qsine (3)	60
	CH dip.	1792	23/9	Qsine (2.5)	60
Edc3 FL	NH dip.	1984	20/7	Qsine (3)	60
	NH scal.	576	20/20	Qsine (3)	60
Edc3 YjeF_N	NH dip.	1792	20/7	Qsine (3)	60
	NH scal.	640	20/20	Qsine (3)	60
Edc3 FL + 1.1 × Dcp1:Dcp2	NH dip.	1984	20/7	Qsine (3)	55
	NH scal.	512	20/20	Qsine (3)	55
Edc3 FL + 2.5 × 30 nt RNA	NH dip.	6528	20/7	Qsine (3)	60
	NH scal.	1248	20/20	Qsine (3)	60
Edc3 FL + 1.1 × Dcp1:Dcp2 + 2.5 × 30 nt RNA	NH dip.	2688	20/7	Qsine (3)	60
	NH scal.	832	20/20	Qsine (3)	60

* dip. = dipolar, scal. = scalar

Table 6.1.: Summary of all ssNMR experiments and corresponding parameters used.

7. smFRET experiments

7.1. smFRET measurements

Single molecule FRET experiments were performed on a confocal MicroTime200 fluorescence microscope (PicoQuant) which operates with two pulsed laser diodes at 532 nm (LDH-P-FA-530B) and 636 nm (LDH-DC-640 with a ZET 635/10 coherent clean-up filter). Excitation laser beams were reflected on a dichroic multi-band mirror (ZT 532 / 640RPC) and focused in the sample chamber using a water-immersion objective (UplanSApo × 60/1.2 W). Fluorescence light was collected using the water-immersion objective, focused onto a 50 µm confocal aperture and spectrally separated into donor and acceptor detection channels by a dichroic mirror (T635LPX) and additional band-pass filters (donor: FF01-582/64, acceptor: H690/70). Detection channels were recorded simultaneously by an EMCCD camera, whereby single photons were detected using an avalanche photodetector (SPCM-AQRH-14-TR) and time-resolved detection of single photons was achieved using time-correlated single-photon counting (TCSPC; HydraHarp 400).

Prior to the measurements, the sample chambers were filled with 200 µl BSA buffer (2 mg/ml BSA, 125 mM NaCl, 25 mM HEPES, pH 7.3) to prevent adhesion of the decapping complex to the chamber walls and subsequently washed with FRET buffer. Dcp1:Dcp2 samples were diluted between 1:10 and 1:20 with FRET buffer to obtain picomolar sample concentrations. In this way it is guaranteed that only single protein complexes diffuse through the confocal volume at a time.

Substrates, substrate analogues and activator proteins were added to the Dcp1:Dcp2 complex in the following concentrations: 15 µM capped RNA (7 nt, 15 nt), 5 µM capped RNA (7 nt, 15 nt, 80 nt, 380 nt), 5 µM 5' OH RNA (80 nt), 50 µM Edc1, 10 µM Pat1, 5 µM Edc3 LSm, 5 µM Edc3 full-length, 2 mM ADP, 2 mM m^7GDP.

Measurements were performed two to three times for each complex under identical conditions in a sample volume of 50 µl and each measurement took between 30 and 60 minutes. Operation of the microscope and data collection was realised using the SymPhoTime 64 software package. We aimed for at least 10000 photon bursts per measurement and the fluorophores were alternatingly excited by the 532 nm and the 636 nm laser with a repetition rate of 40 MHz and a power of 80 mW and 20 mW, respectively. Thereby, the duration of each pulsed interleaved excitation (PIE) cycle was 25 ns.

7.2. smFRET data analysis

smFRET data were analyzed with the software PAM (PIE analysis in Matlab version 1.3; http://www.cup.uni-muenchen.de/pc/lamb/) and Matlab.

smFRET data collected by the SymPhoTime 64 software contain information about the timepoint of photon emission, as well as about the detection channel of the recorded photon emission signal. The PAM software uses this information to sort the recorded signals into three PIE channels: Donor detection after donor excitation (DD), acceptor detection after donor excitation (DA) and acceptor de-

tection after acceptor excitation (AA) (section 2.3). From the number of detected photons the uncorrected FRET efficiency, called proximity ratio E_{PR} and the raw stoichiometry S_{raw} for every photon burst were calculated via $E_{PR} = \frac{N_{DA}}{N_{DD}+N_{DA}}$ and $S_{raw} = \frac{N_{DD}+N_{DA}}{N_{DD}+N_{DA}+N_{AA}}$. Photon burst search was performed using the all photon burst search (APBS) algorithm, which detects photon bursts in all PIE channels, and one burst contained at least 50 photons of which at least 10 photons had to be detected at a time within a sliding time window of 500 µs. Complexes labeled with only a donor fluorophore or only an acceptor fluorophore have an S_{raw} value of ≈ 1 or ≈ 0, respectively, and were excluded from the analysis by restriction of S_{raw} to values between 0.2 and 0.8. S_{raw} and E_{PR} values were corrected from crosstalk (ct) and direct excitation (de),

$$ct = \frac{E_{PR}(DD)}{1 - E_{PR}(DD)}, \qquad (7.1)$$

$$de = \frac{S_{raw}(AA)}{1 - S_{raw}(AA)}, \qquad (7.2)$$

and the β- and the γ- factor,

$$\beta = \frac{\epsilon_A^{\lambda^A} I_A}{\epsilon_D^{\lambda^D} I_D}, \qquad (7.3)$$

$$\gamma = \frac{Q_A g_A}{Q_D g_D}, \qquad (7.4)$$

were included to yield the corrected FRET efficiencies,

$$E = \frac{N_{DA} - (ct * N_{DD} - de * N_{AA})}{\gamma * N_{DD} + N_{DA} - (ct + N_{DD} - de * N_{AA})}, \qquad (7.5)$$

and the corrected stoichiometry values,

$$S = \frac{\gamma * N_{DA} + N_{DA} - (ct * N_{DD} - de * N_{AA})}{\gamma * N_{DD} + N_{DA} + \beta * N_{AA} - (ct * N_{DD} - de * N_{AA})}. \qquad (7.6)$$

Correction factors were calculated for data recorded within one day.

Corrected and normalized FRET efficiency values were binned (50 bins, bin size = 0.02) and resulting FRET histograms were fitted to one to three Gaussian functions,

$$y = y_0 + \frac{A}{\omega\sqrt{\frac{\pi}{2}}} \exp\left(-2\frac{(x - x_c)^2}{\omega^2}\right), \qquad (7.7)$$

with A being the area under the curve, ω the full width half maximum, x_c the efficiency value of the peak maximum and y_0 any offset of the function.

The full width half maximum of each Gaussian function was restricted to $\omega^2 < 0.2$ and the approximate position of the peak maximum of each Gaussian function as well as the number of Gaussian functions to be used for the fit was included from prior knowledge about the examined protein complex and from test measurements. To that end, peak maxima between FRET efficiencies of 0.19 and 0.33 were assigned to the closed conformation of the Dcp1:Dcp2 decapping complex, maxima between 0.45 and 0.55 were assigned to the open conformation and maxima between 0.7 and 0.9 to the active conforamtion. Starting values for fits of the FRET efficiencies were set to 0.3, 0.5 and 0.8, respectively. Integration over each individual Gaussian curve

finally determined which conformation of the examined complex is populated to what extent.

8. Visualization

8.1. Visualization

All images of structures were prepared with Chimera (Pettersen et al. 2004), images of NMR spectra were prepared using NMRView (www.onemoonscientific.com) and in-house written scripts. Figures were prepared using Inkscape (https://inkscape.org/).

Part III.

High Pressure NMR of Dcp1:Dcp2

Results presented in this part were published in the JOURNAL OF MOLECULAR BIOLOGY (Krempl, Wurm, et al. 2023), the chapter is therefore largely identical to the publication in both text and figures. R. Sprangers, J.-P. Wurm and W. Kremer conceptualized the project, C. Krempl performed experiments with help from J.-P.W. and methodological input from W.K. and M. Beck-Erlach. C.K. and R.S. analyzed and interpreted data together with J.-P.W., and R.S. and C.K. wrote the paper. All authors commented on the manuscript.

1. Introduction

Proteins are highly dynamic biomolecules that can sample different structural states. Many of these conformations are functionally relevant, especially in enzymes that need to change conformation to interact with substrates, to form a catalytically competent state or to release the reaction products. For many proteins our current structural knowledge is, however, limited to a static image of one of the possible states that a biomolecule can adopt (Blundell and Wright 2022). This visualized state is, however, not necessarily occupied to the largest degree in solution, or catalytically important. Solution state NMR spectroscopy is especially suited to study conformational changes and to determine the associated thermodynamic and kinetic parameters. These data can then complement static structural information, such that a more complete picture of the protein energy landscape can be obtained (Bhabha et al. 2011; Overbeck, Stelzig, et al. 2022; Oyen et al. 2017; Stafford et al. 2015; Wurm, Sung, et al. 2021).

In the following, we consider a protein that dynamically exchanges between two structurally different states A and B (with the forward rate k_{AB} and the backward rate k_{BA}, where $k_{ex} = k_{AB} + k_{BA}$): $A \underset{k_{BA}}{\overset{k_{AB}}{\rightleftharpoons}} B$. The populations of A ($p_A$) and B ($p_B$ = 1-p_A) and the equilibrium constant $K_{eq} = \frac{p_B}{p_A}$ are determined by the (Gibbs) free energy difference ΔG_{AB} between the two states according to

$$\Delta G_{AB} = G_B - G_A = -RT \ln(K_{eq}), \tag{1.1}$$

where R is the gas constant and T is the absolute temperature. The free energy difference between A and B can be modulated by several means, including changes in the sample conditions (pH, salt or the addition of denaturants) or by changing other experimental parameters (temperature or hydrostatic pressure). Based on such experiments, it is possible to obtain insights into the thermodynamic differences (e.g. entropy, enthalpy and volume) between the two states. Increasing the hydrostatic pressure has been reported to be a very subtle way to shift populations of interchanging states as this minimally influences the free energy difference between the two states (thermodynamics) (Akasaka 2006; Kitahara and Akasaka 2003). At the same time, the applied pressure can alter the energy of transition states, which results in changes in the exchange rates between the states (kinetics). High pressure NMR applications are becoming increasingly popular, despite the

technical challenges that are associated with applying hydrostatic pressure to an NMR sample (Sprangers 2021). A small and far from complete list of impressive pressure NMR studies include the study of folding intermediates for apomyoglobin (Kitahara, Yamada, et al. 2002), the determination of the conformational equilibria for the β1-adrenergic GPCR (Abiko, Grahl, and Grzesiek 2019), the identification of allosteric mechanisms in the RAS protein (Kalbitzer et al. 2013) and the study of a β-strand register shift in the ARNT protein (Xu, Gagné, et al. 2021). In addition, highly advanced pressure jumps equipment has been designed and dedicated NMR experiments have been developed (Alderson, Charlier, et al. 2017; Charlier, Alderson, et al. 2018; Charlier, Courtney, Alderson, et al. 2018; Charlier, Courtney, Anfinrud, et al. 2018; Kremer et al. 2011; Roche et al. 2013). These examples highlight the power and potential of using elevated pressure to reveal molecular details.

The effect that pressure has on the free energy difference between states A and B (at constant temperature) can, based on a Taylor expansion, be written as (Akasaka 2006; Akasaka and Matsuki 2015)

$$\Delta G_{AB} = \Delta G_0 + \Delta V(p - p_0) - \frac{1}{2}\Delta\kappa_T(p - p_0)^2, \tag{1.2}$$

where ΔG_0 and ΔV_0 are, respectively, the free energy and the volume differences between states A and B at standard pressure (1 bar), p and p_0 are the pressure and the standard pressure and $\Delta\varkappa_T$ is the change in isothermal compressibility between states A and B. When the compressibility of states A and B is the same, the equilibrium constant changes with pressure according to

$$K_{eq} = \exp\left(\frac{-\Delta G_0 - \Delta V_0(p - p_0)}{RT}\right). \tag{1.3}$$

The determination of K_{eq} at different pressures p can thus provide direct insights into the difference of the molecular volume between states A and B (ΔV_0).

Upon protein folding the volume of a protein tends to increase due to the formation of molecular cavities. A negative volume change ($\Delta V_0 = V_B - V_A$) is thus usually associated with a loss of secondary or tertiary structure. In accordance with that, high hydrostatic pressures will eventually result in the (partial) unfolding or denaturation of proteins.

Based on transition state theory it is possible to obtain insights into the free energy of activation through the Eyring equation

$$k = \frac{\kappa k_B T}{h}\exp\left(\frac{-\Delta G'}{RT}\right), \tag{1.4}$$

where k is the forward (k_{AB}) or reverse (k_{BA}) rate constant, $\varkappa$ is the transmission coefficient, k_B is the Boltzmann constant, h is the Planck constant and ΔG' is the free energy of activation that is associated with the forward ($\Delta G'_{AB}$) or reverse ($\Delta G'_{BA}$) rate. Including the dependence of the free energy on the pressure this expression can be rewritten as:

$$k = \frac{\kappa k_B T}{h}\exp\left(\frac{-\Delta G'_0 - \Delta V'_0(p - p_0)}{RT}\right) = \exp\left(\ln(k_0) - \frac{\Delta V'_0(p - p_0)}{RT}\right), \tag{1.5}$$

where k_0 is the (forward $k_{0,AB}$ or reverse $k_{0,BA}$) rate at standard pressure. The pressure dependence of k_{AB} and k_{BA} thus provides insights into the volume differences between state A and the transition state or between state B and the transition state.

Carr–Purcell–Meiboom–Gill (CPMG) relaxation dispersion (RD) NMR experiments (Korzhnev and Kay 2008; Palmer 2015) can provide quantitative insights into k_{AB} and k_{BA} as well as K_{eq}. Even when the sparsely populated second state is not directly observable in NMR spectra, the exchange process between states A and B can be quantified based on the exchange broadening of the resonances of the majorly populated state A, e.g. by measuring the effective transverse relaxation rate as a function of CPMG frequency. Performing CPMG RD experiments at different pressures thus provides a means to obtain information on the volume differences between the ground state and an invisible protein conformation or the transition state. This information is highly valuable as it gives direct insights into the nature of the structural changes that occur in biomolecules. Indeed, previous work that quantified exchange processes using NMR methods has revealed unique insights into e.g. the enzymatic mechanisms from an adenylate kinase (Stiller et al. 2019), the two- and three-state folding pathways of the drnN, G48M Fyn (Bezsonova et al. 2006) and A39V, N53P, V55L Fyn SH3 domains (Tugarinov, Libich, et al. 2015), the structural properties of the transition-state ensemble of a mutant version of apocytochrome b562 that folds in a two state mechanism (Korzhnev, Bezsonova, et al. 2006), the destabilizing effect of cavities for the T4 lysozyme L99A protein (Xue et al. 2019), the folding (Dreydoppel, Becker, et al. 2018) and aromatic ring flipping (Dreydoppel, Dorn, et al. 2021) of GB1 and the folding of two domains of the ribosomal protein L9 (Zhang et al. 2016). These high pressure NMR studies mainly focused on ^{15}N based RD experiments, which are suited for proteins up to a molecular weight of approximately 30 kDa, but fail for larger complexes due to very fast transverse relaxation rates that prevent the recording of NMR spectra with sufficient signal to noise. In the current work, we focus on the use of $^{13}CH_3$ methyl groups in an otherwise fully deuterated background that provide high quality spectra even for molecular machines that are far over 100 kDa (Audin et al. 2013; Cvetkovic et al. 2017; Jiang and Kalodimos 2017; Rosenzweig et al. 2013; Schütz and Sprangers 2020; Sprangers and Kay 2007).

One of the complexes that is well studied using methyl TROSY (Tugarinov, Hwang, et al. 2003) methods is the 45 kDa Dcp1:Dcp2 mRNA decapping complex (Floor, Borja, and Gross 2012; Wurm, Holdermann, et al. 2017; Wurm and Sprangers 2019). This complex contains the Dcp1 decapping activator and the Dcp2 enzyme, that can be divided into a regulatory domain (RD, residues 1-95 in *S. pombe*), that is connected to the catalytic domain (CD, residues 96-243 in *S. pombe*) via a flexible linker, as well as a C-terminal intrinsically disordered extension. The Dcp2 regulatory and catalytic domains can adopt three different relative orientations. First, an auto-inhibited closed state, where the RD and CD interact in a non-productive manner and where the substrate RNA binding groove is inaccessible. Second, the open state, where the RD and CD do not interact and tumble independently. Third, the catalytically competent state, where the RD and CD interact such that the catalytic Nudix motif is in close spatial proximity to the mRNA cap structure and hydrolysis of the substrate can take place (Charenton, Taverniti, et al. 2016; Wurm, Holdermann, et al. 2017). This catalytically competent state of the enzyme is only

stably formed when mRNA substrate as well as the decapping activator Edc1 are recruited (Wurm, Overbeck, and Sprangers 2016). The Dcp2 enzyme is thus a highly dynamic protein that samples a complex energy landscape and in which the different states have different functions during catalysis. Based on CPMG RD experiments we established39 that the apo Dcp1:Dcp2 complex mainly adopts the closed conformation (p_{closed} = 0.94) (Mugridge, Ziemniak, et al. 2016; She, Decker, Svergun, et al. 2008) in solution, whereas a small fraction adopts the open conformation (p_{open} = 0.06) (She, Decker, Svergun, et al. 2008) (Figure 2.1). Previously we also determined that the closed and open conformation exchange at a rate (k_{ex} = $k_{closed - open}$ + $k_{open - closed}$) of around 2800 s^{-1} (Wurm, Holdermann, et al. 2017).

In this work, we exploit ^{13}C methyl group CPMG RD experiments on ILVMA labeled samples of the Dcp1:Dcp2 complex at different pressures. The pressure response of the Dcp1:Dcp2 dynamics was used to extract differences in the volume between the closed, the transition and the open state. Our work thereby reveals that high pressure NMR techniques can also be applied to molecular machines that are too large for ^{1}H-^{15}N based NMR spectroscopic approaches.

2. Results

2.1. Dcp1:Dcp2 mRNA decapping complex

The Dcp1:Dcp2 mRNA decapping complex that we study here has a molecular weight of 45 kDa and the low quality ^{1}H-^{15}N NMR spectra do not allow for the recording of ^{15}N based NMR relaxation data, even upon full deuteration of the complex. For that reason, we make use of methyl TROSY methods (Tugarinov, Hwang, et al. 2003) of spectroscopically isolated $^{1}H_3$-^{13}C labeled methyl groups of isoleucine, leucine, valine, alanine and methionine residues in a per-deuterated background. These samples can be prepared through the use of dedicated precursor molecules that are incorporated into the protein of interest during over-expression in *E. coli* (Goto and Kay 2000; Kerfah et al. 2015; Schütz and Sprangers 2020). The NMR active methyl groups are excellent probes to study the dynamics within the decapping complex (Wurm, Holdermann, et al. 2017). To simplify the NMR spectra we restricted the methyl group labeling to the Dcp2 enzyme, while the Dcp1 protein was present in an NMR invisible form.

Two copies of the closed and open conformations are present in a crystal structure of the Dcp1:Dcp2 complex that was determined in the presence of ATP (Figure 2.1) (She, Decker, Svergun, et al. 2008). To assess if pressure can potentially be used to modulate the equilibrium between the open and the closed conformation we calculated the molecular volumes (Chen and Makhatadze 2015) of both states (Figure 2.2).

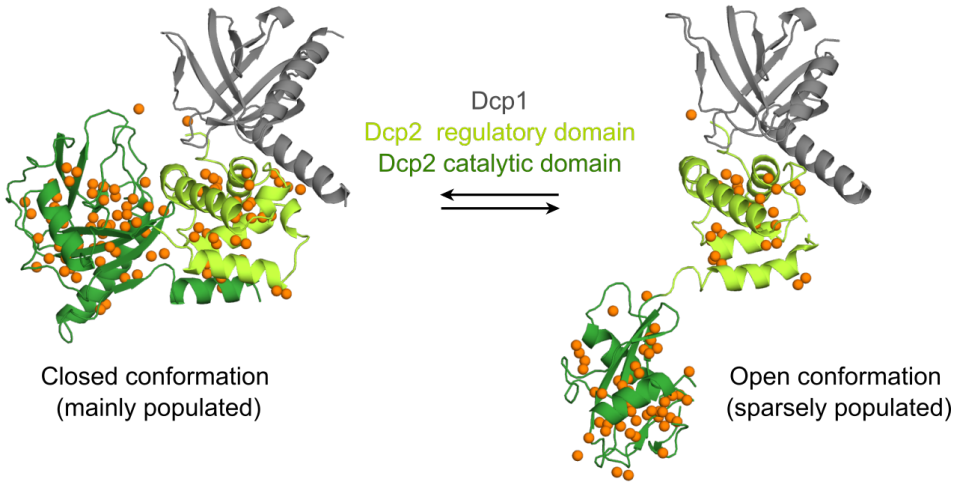

Figure 2.1.: Structure and dynamics in the Dcp1:Dcp2 mRNA decapping complex. Structure of the Dcp1:Dcp2 complex that can adopt a closed (left) and an open (right) conformation (She, Decker, Svergun, et al. 2008) (PDB ID: 2qkm). Dcp1 is colored grey, the Dcp2 regulatory domain in light green and the Dcp2 catalytic domain in dark green. The regulatory and catalytic domain of Dcp2 are in direct contact in the closed state. The NMR methyl probes of isoleucine, leucine, valine, alanine and methionine residues are shown as orange spheres.

This simple calculation suggests that the transition from the closed to the open conformation is not associated with a significant change in molecular volume ($p > 0.1$).

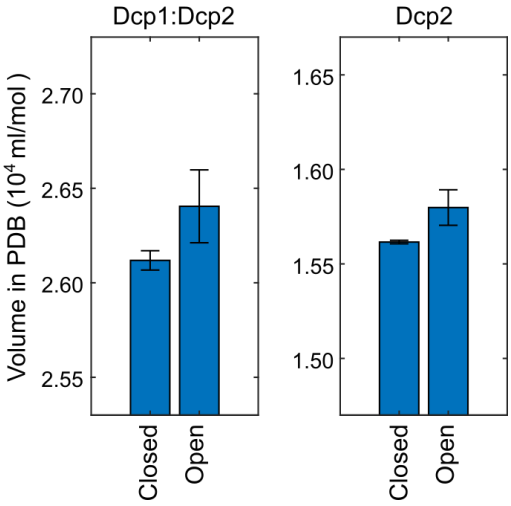

Figure 2.2.: Calculated volumes of the Dcp1:Dcp2 mRNA decapping complex. The calculated (Chen and Makhatadze 2015) volumes of the closed and open conformations of Dcp1:Dcp2 (left) and Dcp2 (right) based on the crystal structure of the complex (She, Decker, Svergun, et al. 2008) (PDB ID: 2qkm). The error bars indicate the standard deviations and are based on the structures of the two closed and two open conformations of the complex in the crystal structure, respectively.

To experimentally follow the pressure response of the Dcp1:Dcp2 complex with high spatial resolution we recorded methyl TROSY NMR spectra between 10 and 2750 bar (1 to 275 MPa) (Figure 2.3 A). Increasing the experimental pressure resulted in a global and gradual shift of the methyl group resonances, as is expected based on experiments with model peptides (Beck Erlach et al. 2017). The extent and direction of the chemical shift perturbations (CSPs), however, differed from residue to residue. Previously, the non-linearity of pressure induced CSPs has been linked to the presence of internal cavities in proteins (Akasaka and Li 2001; Akasaka, Li, et al. 1999; Gagné et al. 2020; Xu, Gagné, et al. 2021). In Dcp2, we observe this behavior for a number of resonances (Figure 2.3 B), indicating that the corresponding residues are close to

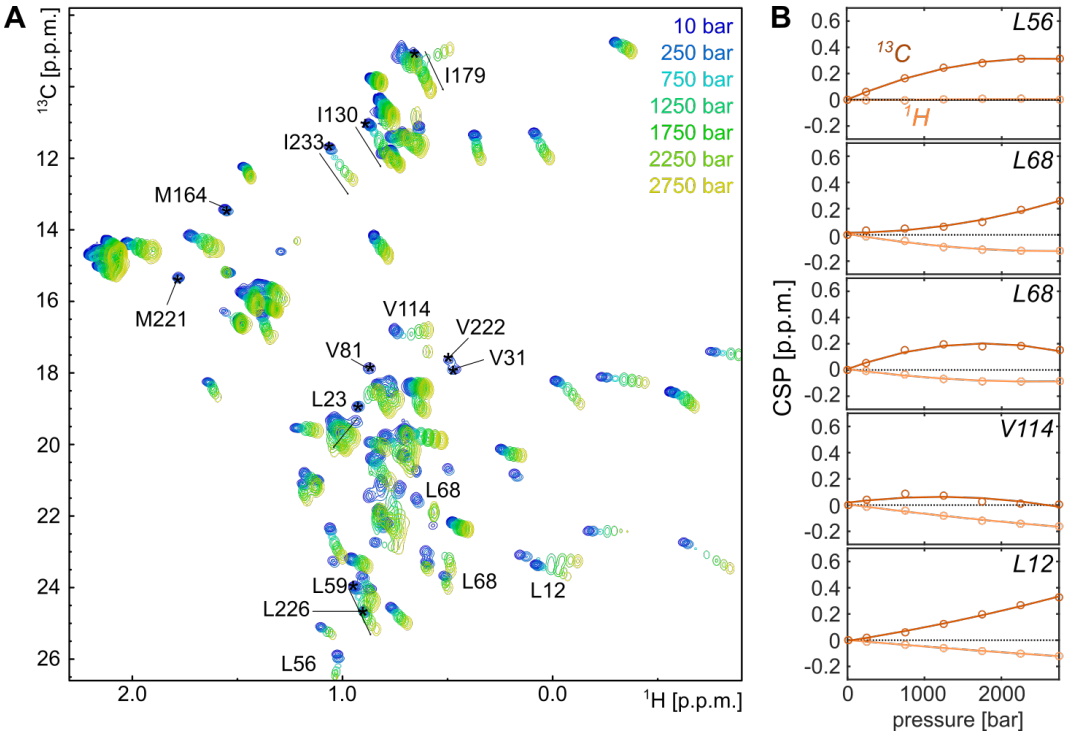

Figure 2.3.: Pressure induced chemical shift perturbation of the methyl groups in Dcp2. (A) ^{1}H-^{13}C methyl TROSY spectra of the Dcp1:Dcp2 decapping complex, where Dcp2 is NMR active in the ILVMA methyl groups, whereas Dcp1 is NMR invisible. (B) Examples for non-linear pressure dependent chemical shift changes. Dark and light orange lines and data points correspond to the ^{13}C and the ^{1}H direction, respectively.

internal voids that are compressed at elevated pressure. In addition, we observe that a number of resonances disappear when the pressure exceeds 750 bar.

Also this behavior has been linked to pressure induced conformational fluctuations around protein cavities (Maeno et al. 2015). Taken together, these data indicate that Dcp2 contains internal cavities and/or that Dcp2 undergoes conformational rearrangements that are pressure dependent. Next, we calculated the location of the cavities within Dcp2 based on the structure of the enzyme in the closed conformation. We found that the interface between the N-terminal regulatory and the C-terminal catalytic domain, that changes upon the closed to open transition, contains voids in the closed conformation (Figure 2.4). Interestingly, most of the resonances that either disappear or that shift non-linearly are from residues that are in close spatial proximity to this region (Figure 2.4).

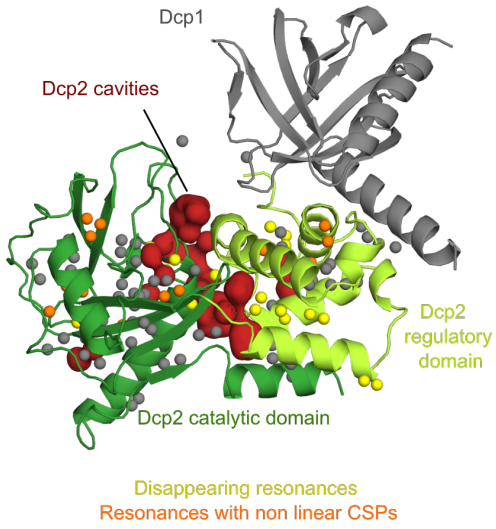

Figure 2.4.: Structure of the Dcp1:Dcp2 complex in the closed conformation, colored as in Figure 2.1. The residues for which the NMR resonances disappear or that experience non-linear chemical shift perturbations are marked in yellow and orange respectively. The calculated major cavities in Dcp2 are indicated with a red surface.

We noticed that Dcp1:Dcp2 is not stable for extended times at pressures that exceed 600 bar, likely due to partial destabilization of the complex that results in denaturation. For our subsequent experiments we thus limited our measurements to relatively low hydrostatic pressures between 10 and 600 bar. Interestingly, we noted that the signals of M164 and M221 shift with respect to the other resonances (Figure 2.5, top left panel) at elevated pressure. Previously, we have shown that these methyl groups directly report on the conformational equilibrium between the closed and the open conformation in Dcp2 (Wurm, Holdermann, et al. 2017). As the exchange between the closed and open positions is fast on the NMR timescale, the population of both states can be approximately extracted from the resonance positions. In our high pressure experiments, the resonance frequencies of M164 and M221 are, however, influenced by two effects: on the one hand directly by the applied hydrostatic pressure and on the other hand indirectly by a shift in the conformational equilibrium. To disentangle these effects, we also recorded methyl TROSY spectra of the Dcp2 C-terminal catalytic domain at the same elevated pressures. The resonances of this Dcp2 fragment correspond to the fully open conformation of Dcp1:Dcp2, as the Dcp2 N-terminal regulatory domain and Dcp1, that are needed for the formation of the closed Dcp2 conformation, are missing. For all pressures we then calculated the distance between the M164 and M221 open-state chemical shift (based on the Dcp2 C-terminal catalytic domain) and the chemical shift for those residues in the Dcp1:Dcp2 complex (closed to 94 %; $\ln(K_{eq})$ = -2.75)

(Figure 2.5). Based on the assumption that the chemical shift difference between the open and the closed state is independent of pressure in the limited pressure range that we use here, we derived the equilibrium constants at the elevated pressures and noticed that these increase ($\ln(K_{eq})$ increases).

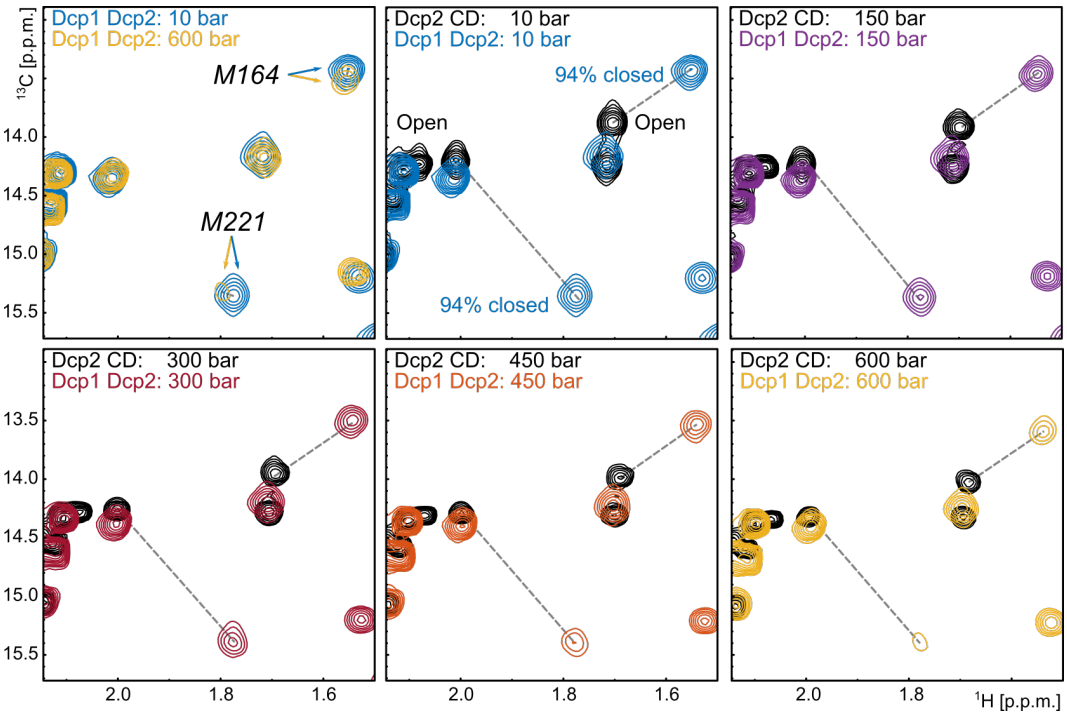

Figure 2.5.: High pressure results in a shift of the populations towards the open state. Methionine region of methyl TROSY spectra of the Dcp1:Dcp2 complex at different pressures between 10 and 600 bar (colored contours) and of the Dcp2 catalytic domain (black). The dashed lines indicate the shift of the methyl resonances of M164 and M221 between the open state (black contours) and the equilibrium of the states that are sampled by the Dcp1:Dcp2 complex. The spectra in the top left panel were shifted manually based on resonances that are remote from the Dcp2 RD CD interface, to compensate for the global pressure induced chemical shift perturbations. The arrows in the top left panel highlight the shift of the complex towards the open state.

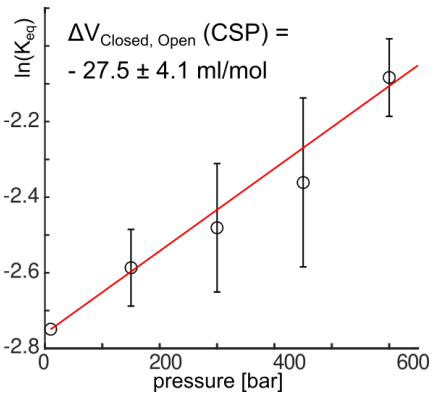

Figure 2.6.: Derivation of the volume difference between the open and closed state. Increasing the pressure results in a shift towards the open state, from which the volume difference between the closed and the open state was derived.

For increased pressures a shift of the conformational equilibrium towards the open conformation thus takes place, revealing that the open conformation has a smaller molecular volume than the closed conformation. Based on the dependency of Keq on pressure we derived a volume difference between the closed and the open conformation of -27.5 ± 4.1 ml/mol (-45.5 ± 6.8 Å^3) (Figure 2.6). This is in agreement with the void volumes that are secluded at the interface between the regulatory and catalytic domains in the closed conformation of the complex (Figure 2.4), but contradicts the simple overall volume calculations that we performed (Figure 2.2).

To independently confirm this result and to obtain insights into the volume differences between the transition state structure and the closed, respectively the open conformation, we turned to ^{13}C single quantum (SQ) CPMG RD experiments at the different

pressures. We found that five different methyl groups from 4 residues that are located at the interface between the Dcp2 regulatory and catalytic domain show clear RD profiles that can be analyzed at all pressures. To analyze these data we first determined the chemical shift difference between the closed and the open states based on the NMR resonances of the Dcp1:Dcp2 complex (94 % closed) and the Dcp2 catalytic domain (open) (Figure 2.7). At a pressure of 10 bar, we could then fit the CPMG RD data to one global two state exchange process and obtained a forward rate ($k_{closed \rightarrow open}$) of 155 ± 26 s^{-1} and a backward rate ($k_{open \rightarrow closed}$) of 3280 ± 200 s^{-1}, and thus a K_{eq} of 0.047 ± 0.005 (Figure 2.8, Table 2.1).

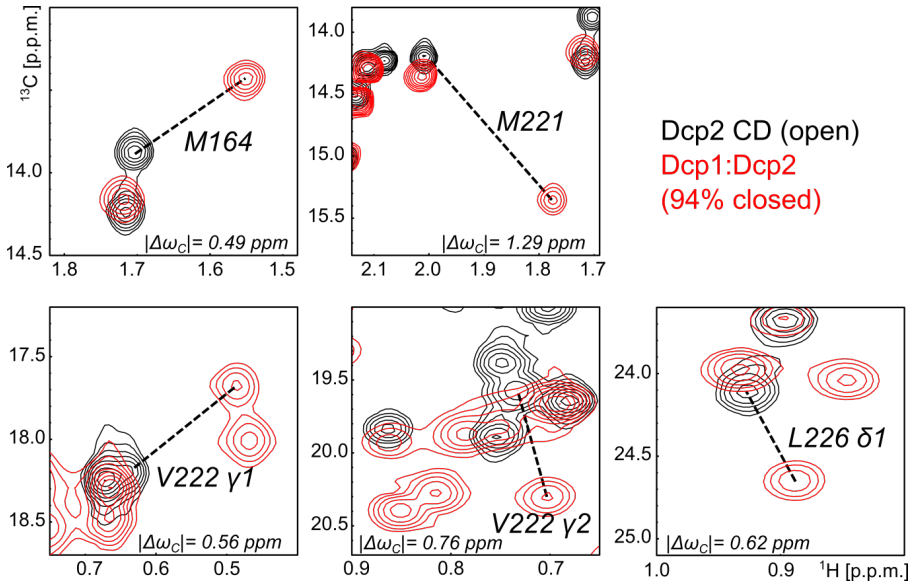

Figure 2.7.: Overlay of the NMR spectra of the Dcp1:Dcp2 complex (red; 94 % closed) and the Dcp2 catalytic domain (CD; black, 100% open). The derived chemical shift differences between the two states are indicated.

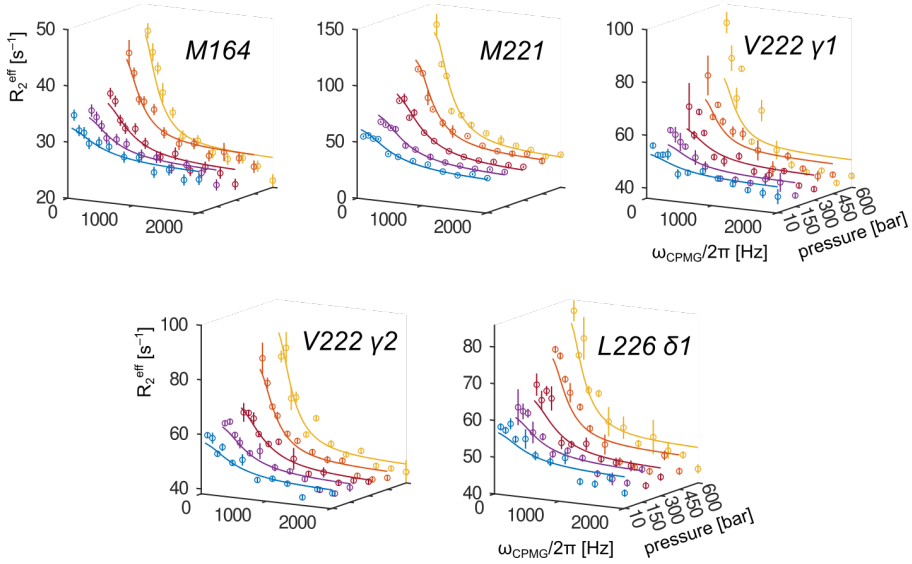

Figure 2.8.: ^{13}C SQ CPMG RD curves for 5 methyl groups at 5 different pressures. The data points are indicated with circles, vertical lines indicate error bars that represent the standard deviation derived from two independent measurements. The drawn lines are a global fit of the data to a two-site exchange model.

This is in reasonably good agreement with exchange parameters ($k_{closed \rightarrow open} \sim 170\ s^{-1}$ and $k_{open \rightarrow closed} \sim 2650\ s^{-1}$) that were previously extracted from data that was recorded at ambient pressure and on a sample where the methyl labeling was restricted to the isoleucine and methionine residues (Wurm, Holdermann, et al. 2017).

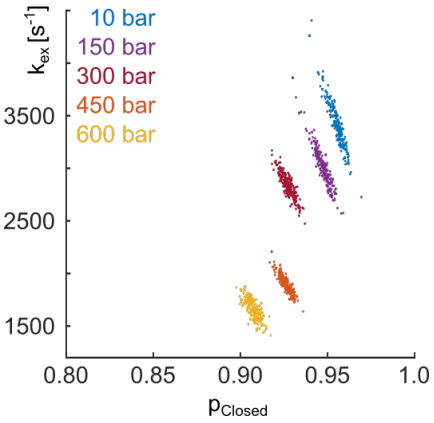

Figure 2.9.: Distribution of p_{closed} and k_{ex}, for the different pressures, derived from 250 fitting cycles where the experimental data was randomly varied according to the experimental error.

Next, we performed CPMG RD dispersion measurements at 150, 300, 450 and 600 bar. We analyzed the CPMG RD curves for five methyl groups at five different pressures simultaneously (Figure 2.8), assuming that the chemical shift difference between the two states was independent of the hydrostatic pressure. Our analysis revealed that elevated pressures resulted in a shift towards the open conformation (Figure 2.9, Table 2.1), from which we extracted that the volume difference between the closed and open conformation (V_{open} - V_{closed}) is - 30.4 ± 4.1 ml/mol (Figure 2.10 A, Table 2.1). This finding is in good agreement with the volume difference that was determined from the resonance position in the NMR spectra (Figure 2.6) and thus independently confirms that the open conformation has a smaller molecular volume than the closed state due to the loss of voids at the interface between the Dcp2 catalytic and regulatory domains. Based on the changes in $k_{closed \rightarrow open}$, and $k_{open \rightarrow closed}$ with pressure (Figure 2.10 B), we determined that the volume of the transition state is similar to the volume of the closed conformation (Figure 2.10 C).

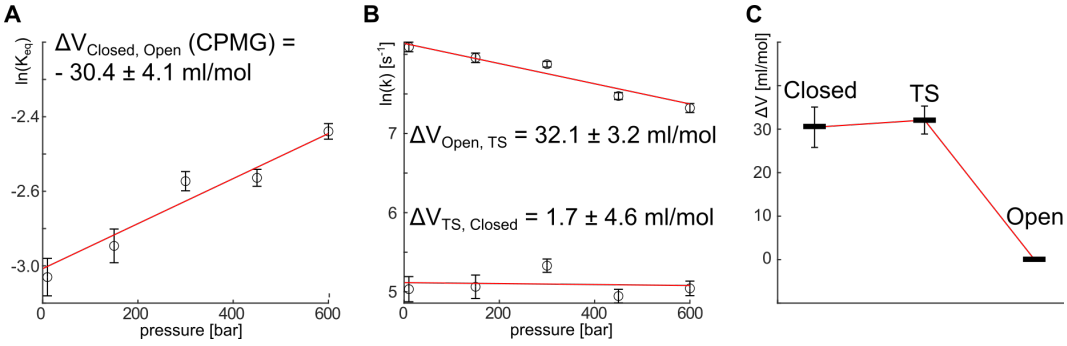

Figure 2.10.: Volumetric properties of the Dcp1:Dcp2 complex. (A) Pressure dependence of the equilibrium constant and the derived volume difference between the closed and the open state. (B) Pressure dependence of the forward (closed to open; bottom) and reverse (open to closed; top) rates that were used to determine the volume differences between the closed or the open conformation and the transition state. (C) Volume changes of Dcp1:Dcp2 during the transition from the closed to the open state. TS: transition state. The error bar shown for the closed state corresponds to the standard deviation of the volume difference between the closed and the open state (panel A), the error bar shown for the TS corresponds to the standard deviation of the volume difference between the open state and the TS (panel B).

It is tempting to speculate that also the structure of the transition state is similar to the structure of the closed state. In that case, the opening pathway of the complex could be initiated by a reshuffling of the interface contacts that subsequently results in the dissociation of the Dcp2 regulatory and catalytic domains. Tryptophan 43 might be a central residue in the initial steps of the opening of the Dcp2 enzyme.

	Dcp1:Dcp2		Dcp1:Dcp2:ATP	
pressure (bar)	p_{closed}	k_{ex} (s^{-1})	p_{closed}	k_{ex} (s^{-1})
10	0.955 (± 0.004)*	3434 (± 227)	0.951 (± 0.003)	2870 (± 104)
150	0.947 (± 0.005)	3018 (± 201)	0.940 (± 0.003)	2708 (± 109)
300	0.927 (± 0.004)	2841 (± 112)	0.920 (± 0.002)	2718 (± 67)
450	0.926 (± 0.003)	1903 (± 89)	0.878 (± 0.004)	2985 (± 113)
600	0.907 (± 0.004)	1671 (± 99)	0.880 (± 0.004)	2333 (± 71)

* The indicated errors are based on a bootstrap error analysis, where the data was resampled and refitted 250 times.

Table 2.1.: Exchange parameters for the Dcp1:Dcp2 and the Dcp1:Dcp2:ATP complexes at different pressures.

This residue is located in the middle of the RD-CD interface and has been shown to play an important role in stabilizing the closed conformation (Floor, Borja, and Gross 2012).

2.2. Dcp1:Dcp2 mRNA decapping complex with ATP

ATP binding has been suggested to stabilize the closed conformation of Dcp1:Dcp2 (She, Decker, Svergun, et al. 2008; Wurm, Holdermann, et al. 2017). We therefore added 10 mM of this nucleotide to the Dcp1:Dcp2 complex.

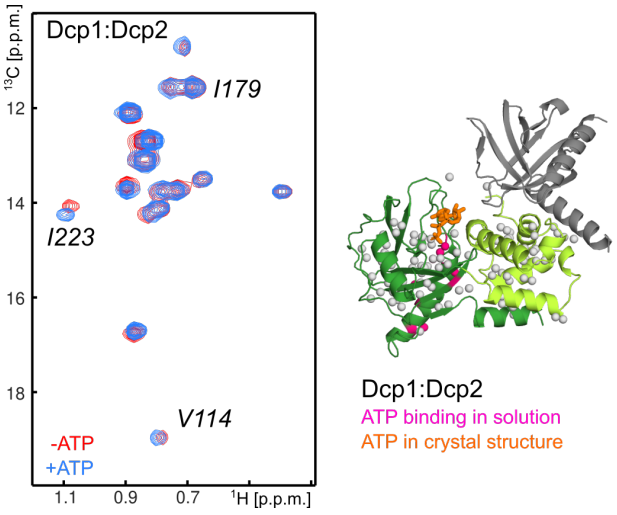

Figure 2.11.: Binding of ATP to the Dcp1:Dcp2 catalytic domain. Overlay of the methyl TROSY spectrum of Dcp1:Dcp2 in the absence (red) and presence (blue) of ATP. The residues that experience the strongest chemical shift perturbations upon addition of ATP are highlighted in pink on the structure of the closed conformation of the complex. The bound ATP in the crystal structure is shown in orange.

This resulted in CSPs for a number of methyl group resonances in the catalytic domain of Dcp2 that are located around the Box B region that interacts with the mRNA body of the substrate (Figure 2.11). We next performed the ATP titration with the isolated catalytic domain that mimics the open conformation (Figure 2.12). In this case we observed larger CSPs that localize to a region that includes the C-terminal end of the Nudix helix that is important for the recognition of the capped mRNA substrate. Interestingly, neither the ATP induced CSPs in the closed (Dcp1:Dcp2) state nor the CSPs in the open (CD) state agree very well with the site where ATP binding has been observed in the crystal structure of the complex (Figure 2.11). Based on these findings we conclude that ATP can interact with the mRNA de-

capping complex in multiple ways and that the interaction mode depends on the conformation of the complex.

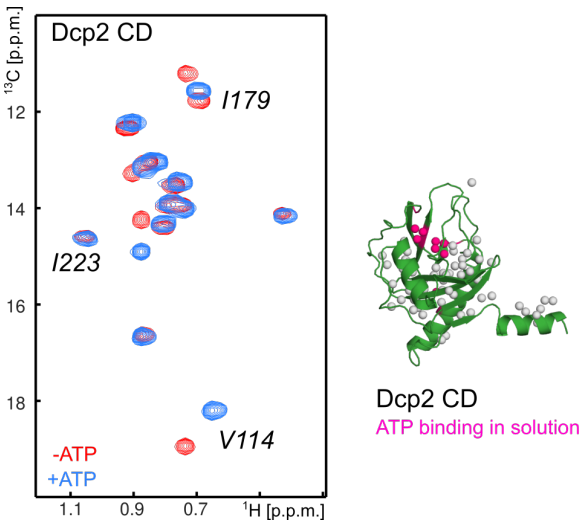

Figure 2.12.: Binding of ATP to the Dcp2 catalytic domain. Overlay of the methyl TROSY spectra of the Dcp2 catalytic domain (CD) in the absence (red) and presence (blue) of ATP. The residues that experience the strongest chemical shift perturbations upon addition of ATP are highlighted in pink on the structure of the domain.

An ATP induced shift in the closed-open equilibrium would be directly observable in RD CPMG experiments, where an increase in the population of the closed state from e.g. 94 to 97 % would result in a ~ 50 % reduction of the amplitude of the RD curves. We noticed, however, that the amplitudes of the CPMG RD curves are almost insensitive to the addition of ATP (Figure 2.13). This finding shows that ATP does not significantly shift the populations towards the closed (or open) conformation under the experimental conditions that we used here. To fit the CPMG RD curves in the presence of ATP we used the chemical shift differences between the Dcp1:Dcp2:ATP complex (94 % closed) and the Dcp2 catalytic domain:ATP complex (open) (Figure 2.14). Interestingly, the changes in $|\Delta\omega_c|$ due to ATP binding (Figure 2.7 and Figure 2.14) can to a large degree explain the changes in the CPMG RD curves (Figure 2.13) at ambient pressure.

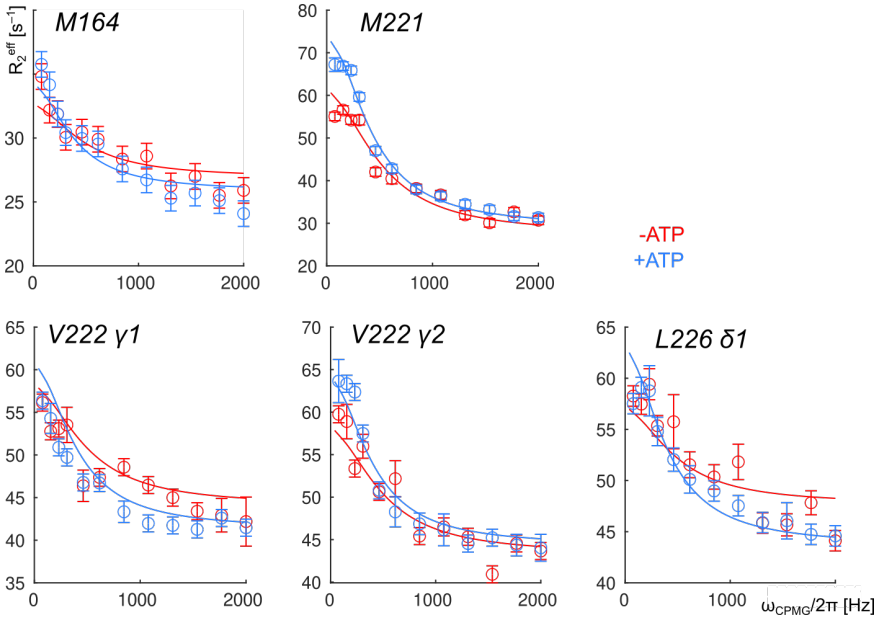

Figure 2.13.: ^{13}C SQ CPMG relaxation curves for five methyl groups at the interface between the Dcp2 regulatory and catalytic domains in the absence (red) and presence (blue) of ATP. The addition of ATP has a minor influence on the amplitude of the RD curves, indicating that the addition of ATP does not result in a shift of the equilibrium between the closed and open states. The data points are indicated with circles, vertical lines indicate error bars that represent the standard deviation derived from two independent measurements. The drawn lines are a global fit of the data to a two-site exchange model as described in Figure 2.8, Figure 2.15.

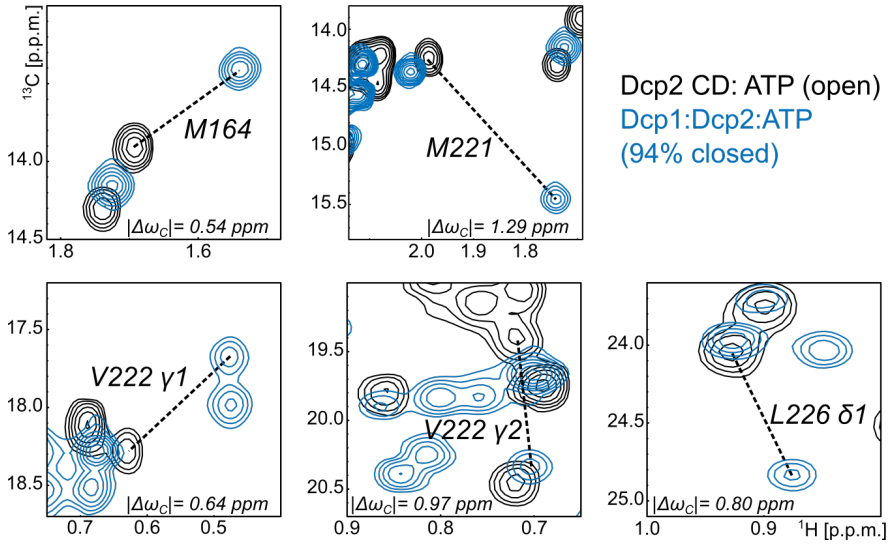

Figure 2.14.: Overlay of the NMR spectra of the Dcp1:Dcp2:ATP complex (blue; 94 % closed) and the Dcp2 catalytic domain in complex with ATP (CD; black, 100 % open). The derived chemical shift differences between the two states are indicated.

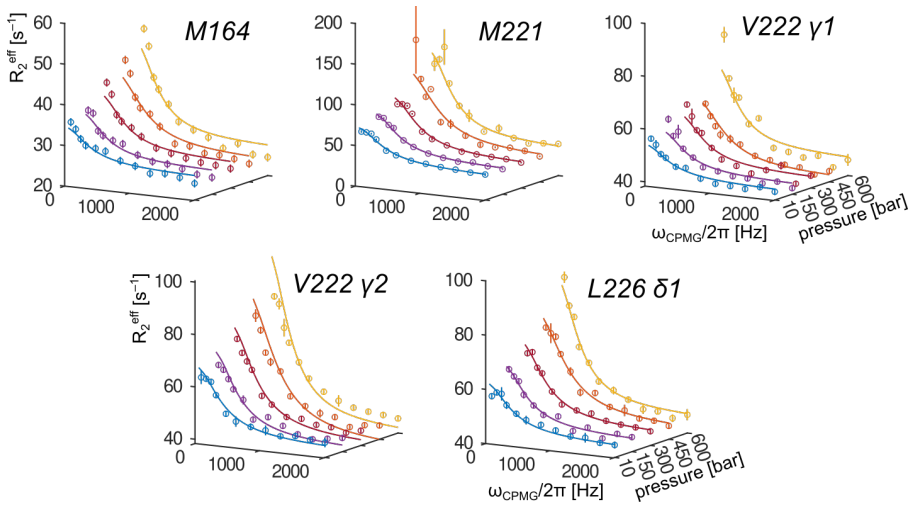

Figure 2.15.: ^{13}C SQ CPMG RD curves for five methyl groups at five different pressures. The data points are indicated with circles, the error bars represent the standard deviation derived from two independent measurements. The drawn lines are a global fit of the data to a two-site exchange model.

Subsequently we increased the pressure in a stepwise manner and recorded CPMG RD curves on the Dcp1:Dcp2:ATP complex. Like for the apo complex, we fitted the data of all pressures simultaneously, assuming that the chemical shift differences between the open and closed state are pressure independent between 10 and 600 bar (Figure 2.15, Table 2.1). With pressure, we observed a gradual shift of the populations towards the open state (Figure 2.16), from which we extracted a volume difference of -41.0 ± 2.3 ml/mol (Figure 2.17 A). Compared to the complex without ATP, the change in molecular volume is thus larger. The changes in the forward and reverse rates with pressure (Figure 2.17 B) reveal that the volume of the transition state now lies in-between the volumes of the closed and open state (Figure 2.17 C).

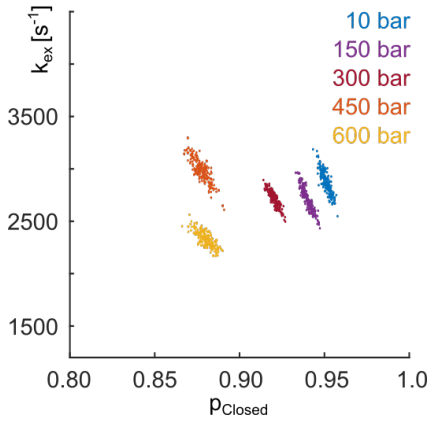

Figure 2.16.: Distribution of p_{closed} and k_{ex}, for the different pressures derived from 250 fitting cycles where the experimental data were randomly varied according to the experimental error.

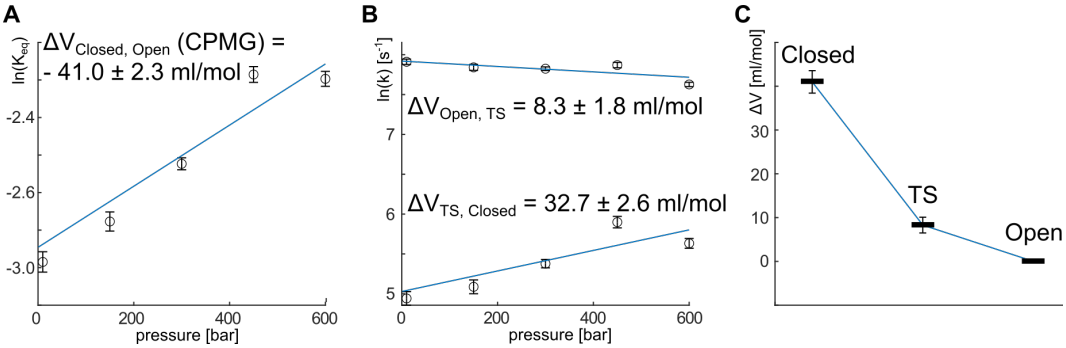

Figure 2.17.: Volumetric properties of the Dcp1:Dcp2:ATP complex. (A) Pressure dependence of the equilibrium constant and the derived volume difference between the closed and the open state. (B) Pressure dependence of the forward (closed to open; bottom) and reverse (open to closed; top) rates and the derived volume differences between the closed or the open state and the transition state. (C) Volume changes of Dcp1:Dcp2:ATP during the transition from the closed to the open state. The error bar shown for the closed state corresponds to the standard deviation of the volume difference between the closed and the open state (panel A), the error bar shown for the TS corresponds to the standard deviation of the volume difference between the open state and the TS (panel B).

3. Discussion

Many conformations that a protein can adopt are not directly detectable due to their low abundance. Knowledge about the nature of these states is, however, important as they can be catalytically important and as (local) unfolding may result in protein aggregation or mis-folding that can have a severe impact on cellular homeostasis. NMR methods are very well suited to obtain information about invisible minor states from resonances of the visible major state (Alderson and Kay 2020; Baldwin and Kay 2009; Bouvignies et al. 2011). Importantly, this information can be obtained with a very high spatial resolution.

In summary, we here studied how the Dcp1:Dcp2 complex exchanges between a closed and an open conformation. Based on ^{13}C SQ CPMG RD experiments at different pressures, we extracted information about the volume changes along the closing-opening pathway of the complex. Our data is in agreement with a model in which the opening of the apo complex first involves local rearrangements of the interface residues without changing the overall shape of the complex, before both domains then dissociate into the fully open conformation. In the presence of ATP, the volume of the complex changes in a stepwise manner. This is in agreement with a situation where the interactions between ATP and the Dcp2 CD change when the complex shifts into the open conformation. Interestingly, we observe such a change of the Dcp2:ATP interactions in our NMR titrations, where the Dcp1:Dcp2 complex binds ATP via the Box B region and where the Dcp2 CD interact with ATP via a region next to the Nudix domain (Figure 2.11 and Figure 2.12).

It is worth noting that the experimentally determined changes in the molecular volume between the closed and open state could not be reliably extracted from known static crystal structures (Figure 2.2), which highlights the importance of the methodology that we exploited here. Our combination of methyl labeling and high pressure NMR methods provides the means to obtain unique insights into the volumetric properties of large molecular machines.

Part IV.

The Applicability of ^{19}F NMR

Results presented in this part were published in the JOURNAL OF BIOMOLECULAR NMR (Krempl and Sprangers 2023), the chapter is therefore largely identical to the publication in both text and figures. R. Sprangers designed experiments, C. Krempl performed experiments and analyzed data, R.S. and C.K. wrote the manuscript.

1. Introduction

Most proteins fold into specific three dimensional structures to perform their functions. These structures are not static but undergo a multitude of conformational changes at timescales that range from picoseconds to hours (Henzler-Wildman and Kern 2007; Palmer 2004). Especially for enzymes these structural rearrangements are important for function, however, unfortunately, our knowledge regarding these dynamics is often insufficient.

NMR spectroscopy is unique in its ability to detect and quantify molecular motions in biomolecules (Alderson and Kay 2021; Audin et al. 2013; Palmer 2004; Wurm, Sung, et al. 2021). Especially biomolecular motions that occur on the same timescale as biological catalysis are of interest, as those conformational changes might be directly correlated with function. Turnover rates of enzymes range from roughly 1 to 10^5 per second and depending on the populations of the conformational states involved, these motions can be quantified with Carr-Purcell-Meiboom-Gill (CPMG) (Farber and Mittermaier 2015) and rotating-frame ($R_{1\rho}$) (Palmer and Massi 2006) relaxation dispersion (RD) experiments and/or exchange spectroscopy (EXSY) (Kloiber et al. 2011) and CEST approaches (Vallurupalli, Sekhar, et al. 2017). From these NMR experiments thermodynamic (populations) and kinetic (exchange rates) information that is associated with a given exchange process in a biomolecule can be extracted. The majority of these experiments is based on the recording of a set of ^{1}H-^{15}N or ^{1}H-^{13}C correlation spectra, which often requires a significant amount of spectrometer time.

An alternative to these approaches is the use of the fluorine (^{19}F) nucleus for NMR experiments. Fluorine is nearly completely absent from biological samples, but it can be artificially incorporated into proteins, e.g. through the use of fluor-tryptophan residues (Crowley, Kyne, and Monteith 2012; Lu et al. 2019), the incorporation of other fluorinated amino acids (Furter 1998; Jackson, Hammill, and Mehl 2007; Khan et al. 2006; Ycas et al. 2020) or through the attachment of fluorinated methyl groups (^{12}C-$^{19}F_3$) to cysteine side-chains (Ye, Larda, et al. 2015). In addition, ^{19}F can be incorporated into nucleic acids through the use of selectively fluorinated nucleotides (Chrominski et al. 2020; Hennig, Scott, et al. 2007; Puffer et al. 2009; Sochor et al. 2016). This targeted ^{19}F labeling of biomolecules presents several advantages compared to conventional ^{15}N or ^{13}C labeling strategies. First, the limited number of fluorine nuclei in the biomolecule results in simple NMR spectra with only one or a few resonances. 1D spectra, that can be recorded relatively rapidly, thus suffice to obtain site-specific information. Second, the large chemical shift dispersion of ^{19}F (Lau and Gerig 2000) can result in a large chemical shift

difference between the ground and excited states of a protein that leads to large amplitudes in RD curves. Third, the costs for ^{19}F labeling are low and deuteration of larger proteins is usually not required as the fluorine is often remote from protons in the complex. Finally, recent advances in NMR probe-head design allow for the tuning of the ^{1}H channel to ^{19}F, thereby bypassing the need for obtaining dedicated fluorine probe-heads. Taken together, ^{19}F NMR methods provide a complementary approach to detect and quantify dynamic processes in biomolecules (Gronenborn 2022; Kitevski-LeBlanc and Prosser 2012). To that end, we recently introduced a number of ^{19}F relaxation dispersion (RD) experiments that are able to quantify dynamic processes (Overbeck, Kremer, and Sprangers 2020; Overbeck, Stelzig, et al. 2022).

Here, we aim at addressing two questions that challenge the general applicability of ^{19}F NMR methods to obtain biologically relevant insights into protein dynamics. For a number of model systems, we probe if motions in these proteins are affected by the incorporation of 5-fluorotryptophan residues, as a replacement of a proton with a fluorine atom can potentially influence global protein dynamics due to differences in electronegativity and van der Waals radii. Subsequently, we assess if the introduced ^{19}F labels are reliable probes to report on global motions in these proteins and if ^{19}F and ^{15}N derived dynamic parameters are in agreement.

We focus on four model proteins: (i) the KIX domain of the transcriptional co-activator CREB binding protein (Wang, Marshall, et al. 2012), (ii) Dcp1 and (iii) Dcp2 that together form the Dcp1:Dcp2 mRNA decapping complex (Wurm and Sprangers 2019) and (iv) the DcpS scavenger decapping enzyme (Fuchs et al. 2020; Gu et al. 2004). These proteins have been shown to exhibit global dynamics on different timescales. Motions in the KIX domain take place in the medium fast millisecond time regime ($k_{ex} \sim 550\ s^{-1}$) (Brüschweiler, Schanda, et al. 2009). Dcp1 possesses an aromatic groove that exchanges between different states with an exchange rate around $1200\ s^{-1}$ (Wurm, Overbeck, and Sprangers 2016). In the absence of an mRNA substrate, the mRNA decapping complex Dcp1:Dcp2 furthermore exchanges between two distinct conformations in the fast millisecond time regime ($k_{ex} \sim 2800\ s^{-1}$) (Wurm, Holdermann, et al. 2017). The motion of the scavenger decapping enzyme DcpS takes place in the slow millisecond to seconds time regime, depending on the concentration of the substrate ($k_{ex} = 1 - 20\ s^{-1}$) (Neu et al. 2015). All these complexes contain at least a single tryptophan residue in a region that has been shown to be dynamic. Importantly, for the enzymes Dcp2 and DcpS the observed motions are important for the catalytic cycle.

Here, we show that the incorporation of 5-fluorotryptophan does not change the dynamics of the studied proteins as judged by ^{15}N and methyl-TROSY studies. However, for the KIX domain, for Dcp1 and for Dcp2, the exchange parameters that we obtain from ^{19}F RD measurements are not in agreement with those extracted from ^{15}N RD experiments. The cause of these inconsistencies likely arises from faster motions of the tryptophan side chains. These fast dynamics result in CPMG RD dispersion profiles that are simultaneously influenced by side chain and backbone motions and that thus cannot be interpreted with a simple two-state exchange model. For the DcpS decapping enzyme, we show that the dynamics that we extract from ^{19}F EXSY measurements are in excellent agreement with previous results that were based on methyl TROSY experiments (Neu et al. 2015; Schütz and Sprangers

2020; Tugarinov, Hwang, et al. 2003). Our findings thus highlight that it is possible, but potentially misleading, to draw conclusions on global protein dynamics based on ^{19}F data derived from a limited number of probes.

2. Results

2.1. KIX domain of the CREB-binding protein

Dynamics in the KIX domain of the CREB-binding protein are important for the allosteric communication between two ligand binding sites (Brüschweiler, Konrat, and Tollinger 2013). Extensive previous studies reveal that this domain exchanges between a folded and a partially unfolded high energy state with an exchange rate of ~ 550 s^{-1} (Brüschweiler, Schanda, et al. 2009). Here, we labeled the domain with ^{15}N (Figure 2.1) and recorded nitrogen relaxation dispersion (RD) profiles (Figure 2.2, Figure 2.3). Based on that data, we confirm that the domain undergoes a global two-site exchange process (p_a = 97.7 ± 1.2 %, k_{ex} = 1255 ± 221 s^{-1}). Those values deviate slightly from the previously reported exchange parameters, which we attribute to differences in the buffer composition.

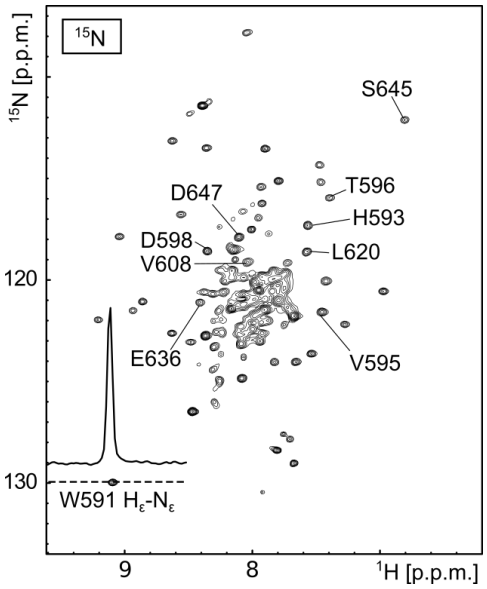

Figure 2.1.: ^{1}H-^{15}N spectrum of the ^{15}N labeled KIX domain. The 1D trace in the spectrum shows the H_ε-N_ε signal of the W591 side-chain at the N-terminal end of the domain.

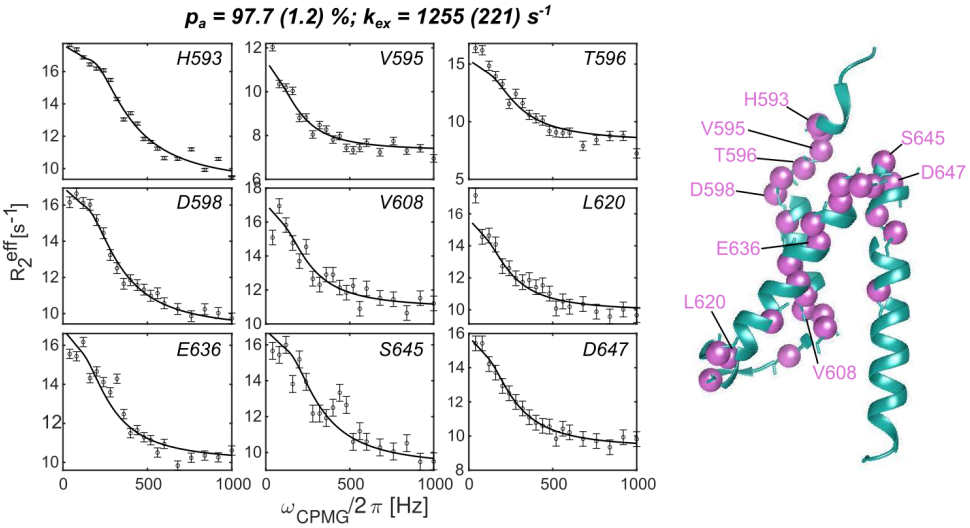

Figure 2.2.: ^{15}N CPMG relaxation dispersion (RD) profiles that report on the folding-unfolding of the ^{15}N labeled KIX domain. The residues that undergo chemical exchange are highlighted on the structure of the domain (Brüschweiler, Konrat, and Tollinger 2013) (PDBid: 2LXT)

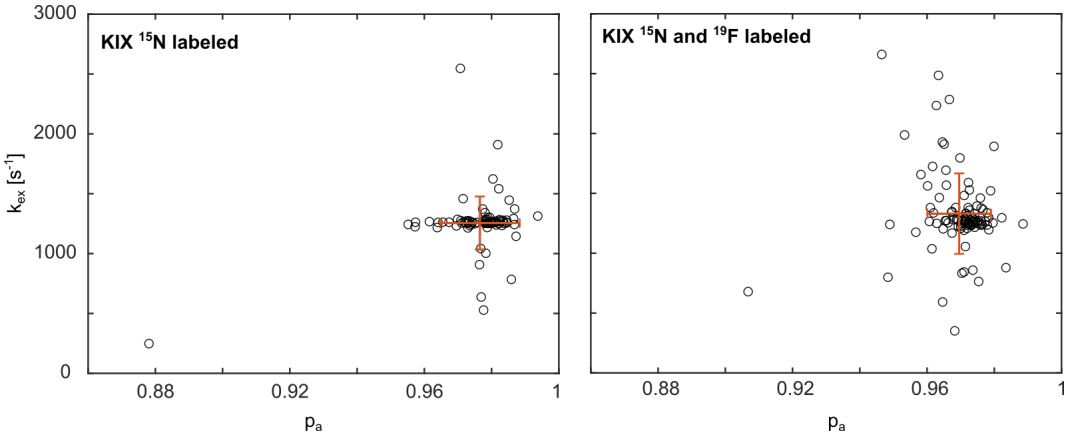

Figure 2.3.: Result of 100 Monte Carlo simulations used to extract exchange parameters for the ^{15}N CPMG RD data recorded on the ^{15}N labeled KIX domain (left; p_a = 97.7 ± 1.2 %, k_{ex} = 1255 ± 221 s^{-1}) and on the ^{15}N 5-fluorotryptophan labeled KIX domain (right; p_a = 97.0 ± 1.0 %, k_{ex} = 1331 ± 336 s^{-1}). The orange cross represents the average population of the ground state (p_a) and exchange rate (k_{ex}). The error bars indicate the standard deviations in both parameters.

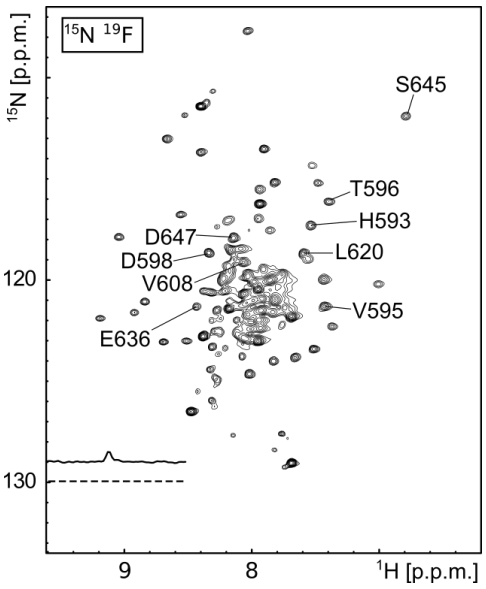

Figure 2.4.: ^{1}H-^{15}N spectrum of the ^{15}N, 5-fluorotryptophan labeled KIX domain. The strong reduction of the signal of the W591 H_ε-N_ε side-chain resonance reveals the efficient incorporation of the ^{19}F label.

The KIX domain contains a single tryptophan residue that stacks on the top of the exchanging helical bundle and we reasoned that a partial unfolding of the KIX domain should be sensed by the aromatic side-chain. To validate that, we simultaneously labeled the KIX domain with ^{15}N and 5-fluorotryptophan. The incorporation of the ^{19}F label was highly efficient as can be judged from the strong reduction in the H_ε-N_ε signal in the proton-nitrogen spectrum (Figure 2.4). Structurally, the impact of the ^{19}F incorporation was minimal, as judged from the small CSPs that are limited to resonances of residues in close spatial proximity to the tryptophan residue (Figure 2.5; Figure 2.6, Figure 2.7). Subsequently, we recorded ^{15}N CPMG RD experiments on the ^{15}N labeled KIX domain that contains the 5-fluorotryptophan (Figure 2.5, Figure 2.3, Figure 2.8).

A global fit of this data reveals that the exchange parameters (p_a = 97.0 ± 1.0 %, k_{ex} = 1331 ± 336 s^{-1}) were unaffected by the presence of the 5-fluorotryptophan. In line with these findings, it is possible to fit the ^{15}N RD profiles of the ^{15}N and the ^{15}N-^{19}F labeled samples simultaneously to one exchange process (p_a = 98.2 ± 0.4 %; k_{ex} = 924 ± 136 s^{-1}) (Figure 2.11, Figure 2.9). This demonstrates that the incorporation of the ^{19}F label does not interfere with the global dynamics of the protein, which is a prerequisite for the applicability of ^{19}F methods (Figure 2.10 A) to extract relevant information regarding protein motions. Next, we recorded ^{19}F CPMG RD experiments at two field strengths and fitted these to a two-site exchange process (Figure 2.10 B). This analysis revealed a tenfold faster exchange rate (p_a = 97.4 ± 0.9 %, k_{ex} = 11442 ± 1261 s^{-1}) compared to the ^{15}N derived parameters

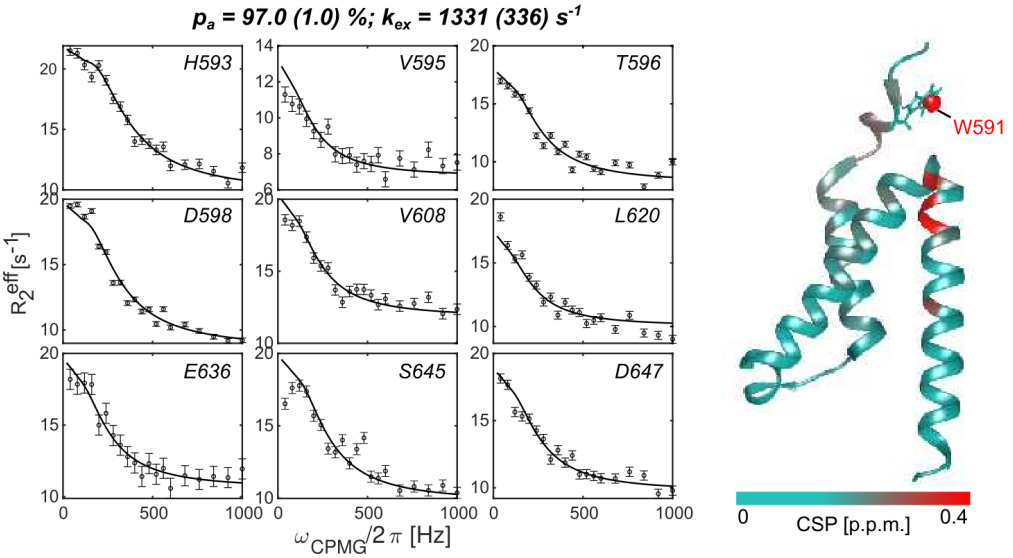

Figure 2.5.: The ^{15}N CPMG RD profiles are not influenced by the incorporation of the 5-fluorotryptophan. The chemical shift perturbations (CSPs) that are induced by the ^{19}F atom are limited to a region that is close to the tryptophan residue (Figure 2.6).

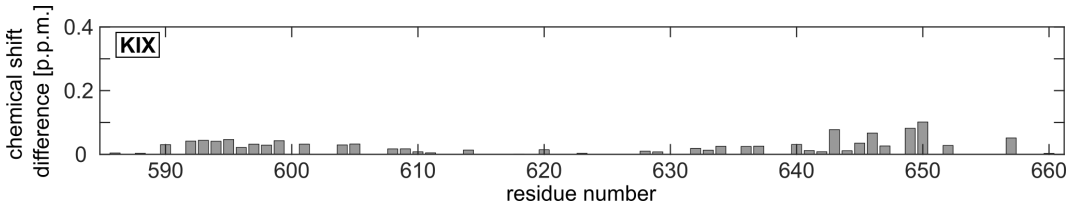

Figure 2.6.: Chemical shift perturbations in the KIX domain upon replacement of all tryptophan residues with 5-fluorotryptophan. CSPs are calculated in ppm as CSP = $\sqrt{(0.1 * \Delta\delta N)^2 + (\Delta\delta H)^2}$. Figure 2.5 shows the KIX structure that is colored according to the CSPs, where the replaced tryptophan residues are shown as sticks.

(Figure 2.5).

Attempts to simultaneously fit the ^{15}N and ^{19}F CPMG data to one exchange process were not successful (Figure 2.12), which confirms that the motions that the ^{19}F labeled tryptophan side chain experiences are different from the global backbone motions that we assessed using ^{15}N RD experiments. A higher flexibility of the tryptophan side chain compared to the protein backbone is not unexpected and in that case the recorded RD curves will be a superposition of the slower backbone and the faster side chain motions. This results in data that can no longer be analyzed with a single two-state exchange model. This notion highlights the challenges and potential pitfalls that are associated with drawing conclusions regarding global protein motions based on ^{19}F based measurements only.

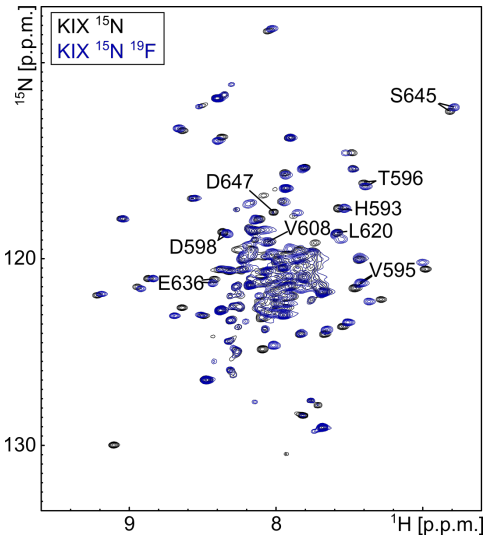

Figure 2.7.: Overlay of the ^{1}H-^{15}N spectra of the ^{15}N (black; Figure 2.1) and ^{15}N ^{19}F (blue; Figure 2.4) labeled KIX domain.

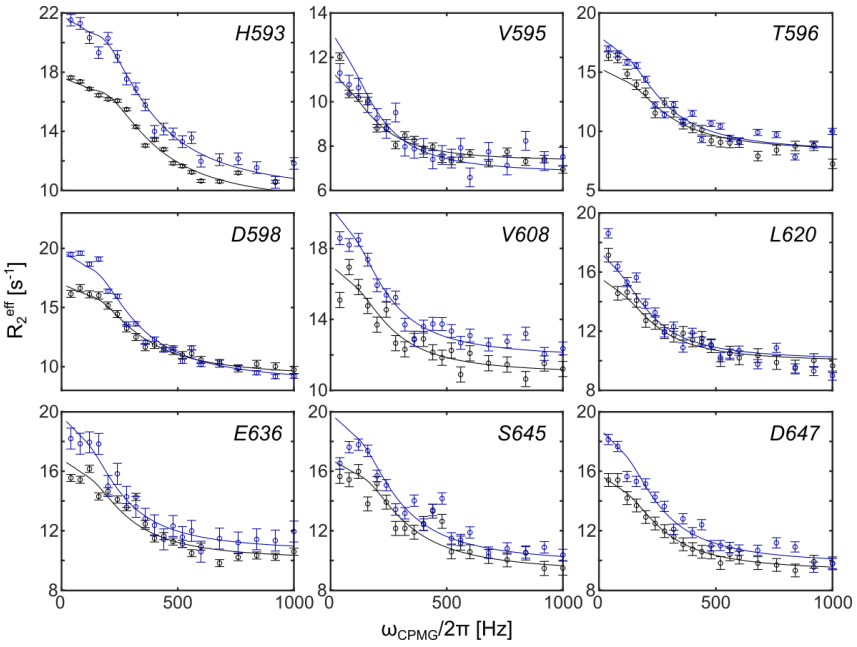

Figure 2.8.: Differences in the CPMG RD curves of the ^{15}N and ^{15}N ^{19}F labeled KIX domain: overlay of the ^{15}N CPMG RD curves recorded on the ^{15}N (black; Figure 2.2) and ^{15}N ^{19}F (blue; Figure 2.5) labeled KIX domain. The differences in the amplitude of the RD curves can be attributed to changes in the chemical shift differences ($|\Delta\omega_N|$) between the ground and excited state between the two labeling schemes and do not necessarily reflect differences in populations or exchange rates between the two samples.

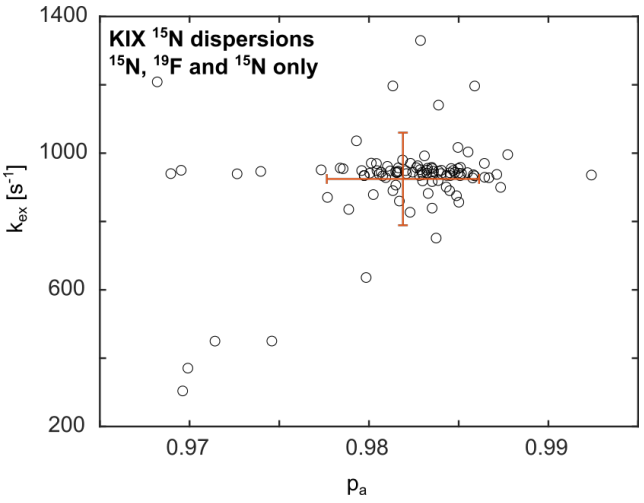

Figure 2.9.: Result of 100 Monte Carlo simulations to extract exchange parameters for a simultaneous fit of the ^{15}N CPMG RD data recorded on the ^{15}N labeled KIX domain and on the ^{15}N 5-fluorotryptophan labeled KIX domain (p_a = 98.2 ± 0.4 %; k_{ex} = 924 ± 136 s^{-1}). The orange cross represents the average population of the ground state (p_a) and exchange rate (k_{ex}). The error bars indicate the standard deviations in both parameters.

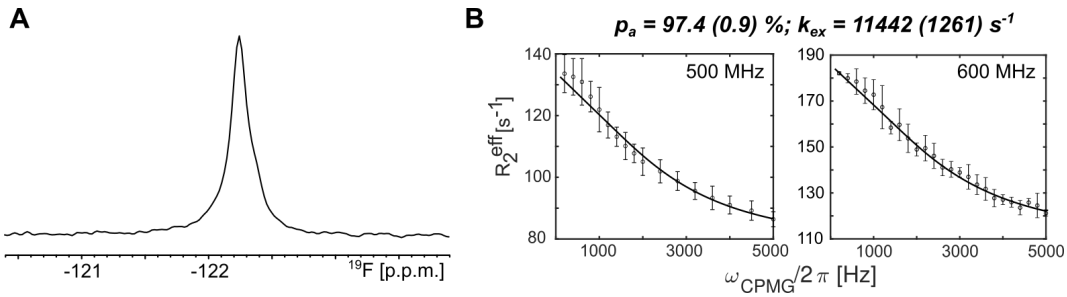

Figure 2.10.: Influence of 5-fluorotrypthphan incorporation on the dynamics in the KIX domain. (A) 1D ^{19}F NMR spectrum of the 5-fluorotryptophan labeled KIX domain. (B) ^{19}F CPMG RD profiles of the 5-fluorotryptophan labeled KIX domain, recorded at 500 and 600 MHz proton frequency.

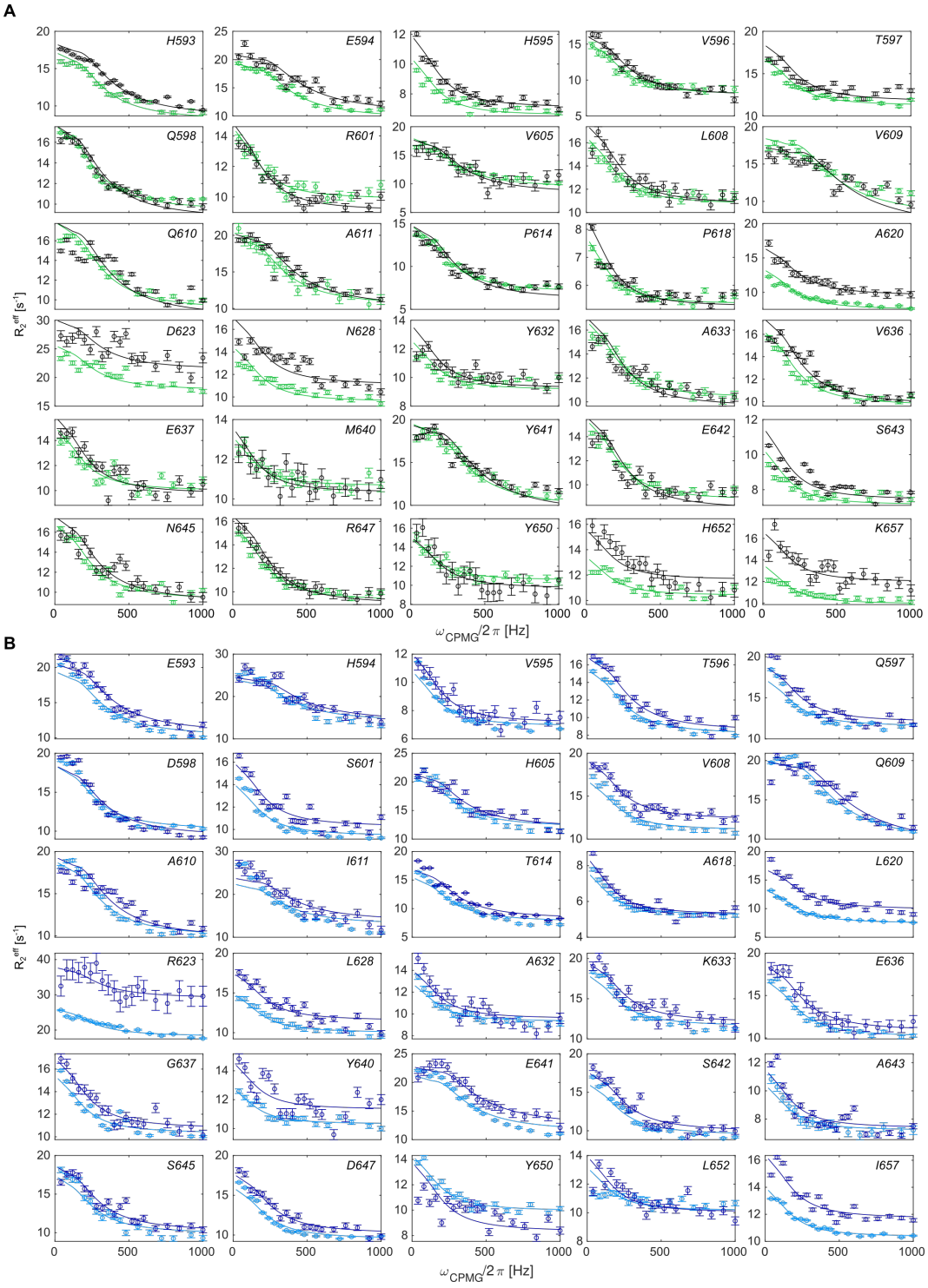

Figure 2.11.: ^{15}N relaxation dispersion profiles of the ^{15}N (A) and ^{15}N 5-fluorotryptophan labeled KIX domain (B) recorded at a 500 MHz proton frequency (green, light blue) and 600 MHz proton frequency (black, dark blue). The drawn lines are a simultaneous fit of all data from both proteins to a two-site exchange process (p_a = 98.2 ± 0.4 %; k_{ex} = 924 ± 136 s^{-1}).

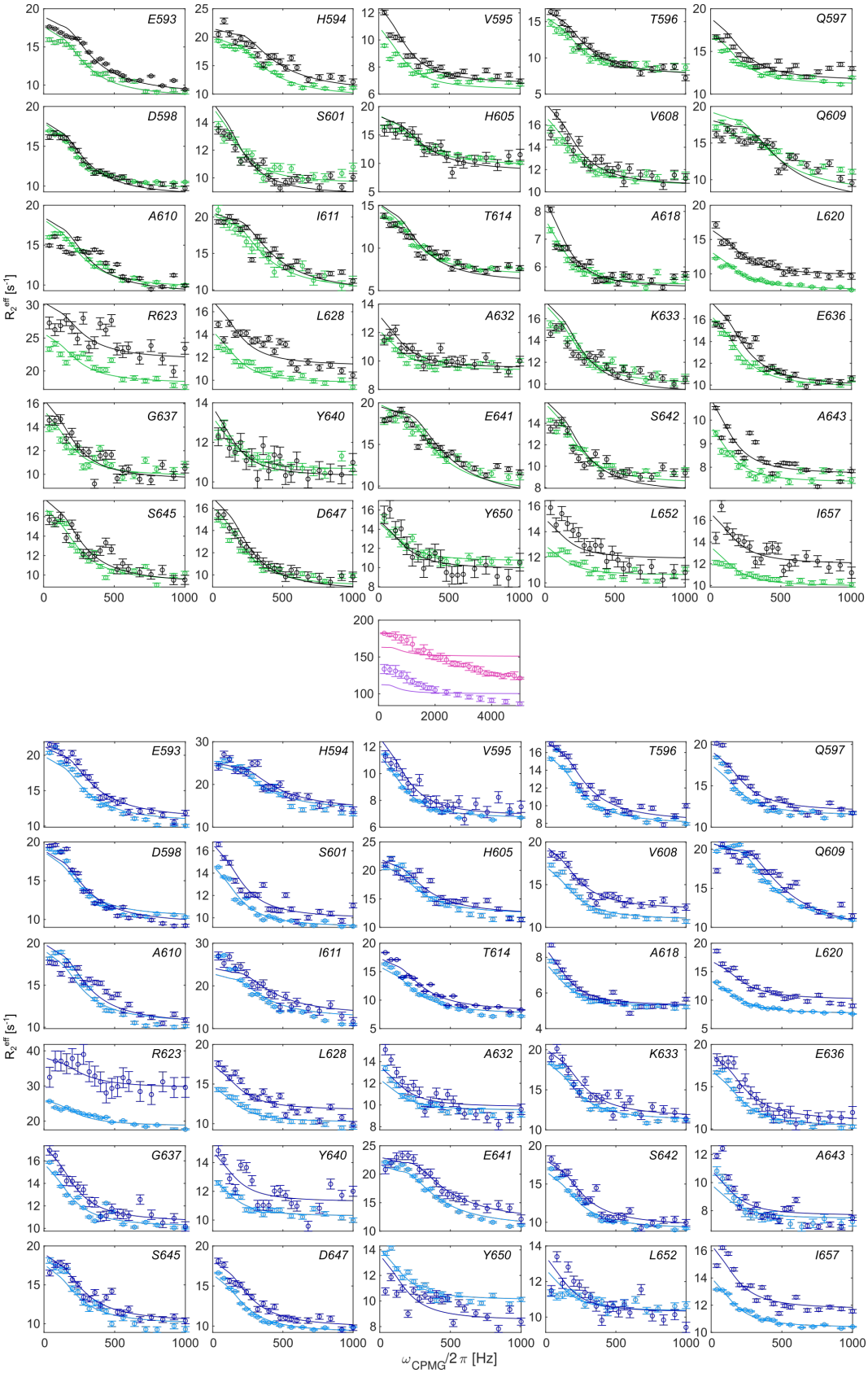

Figure 2.12.: Relaxation dispersion (RD) profiles of the ^{15}N labeled KIX domain (top; ^{15}N RD) and the ^{19}F and ^{15}N labeled KIX domain (middle; ^{19}F RD and bottom; ^{15}N RD). Data was recorded at a 500 MHz proton frequency (green, purple, light blue) and 600 MHz proton frequency (black, pink, dark blue). The drawn lines represent an effort to simultaneously fit all data from both proteins to a two-site exchange process. The ^{19}F and ^{15}N data are not compatible (see middle panel), indicating that the RD data of the 5-fluorotryptophan and the backbone are not the same.

2.2. Dcp1:Dcp2 mRNA decapping complex

We next extended our analysis to the Dcp1:Dcp2 mRNA decapping complex that is composed of the decapping enzyme Dcp2 and its main activator Dcp1. Dcp2 consists of an N-terminal regulatory domain (NRD; amino acids 1-95) that interacts with Dcp1, a C-terminal catalytic NUDIX domain (CTD; amino acids 96-243) and a long C-terminal intrinsically disordered region (IDR; amino acids 244-743).

Previous ^{15}N based CPMG relaxation dispersion experiments revealed that Dcp1 contains a flexible groove that exchanges between two states at a rate of ~ 1200 s^{-1} and that can recruit proline-rich elements (Wurm, Overbeck, and Sprangers 2016). In addition, methyl based single quantum CPMG RD experiments on the Dcp1:Dcp2 complex showed that the NRD and CTD of Dcp2 undergo inter-domain motions at a rate of 2800 s^{-1} (Wurm, Holdermann, et al. 2017). These large conformational changes are important for the regulation of the catalytic activity of the enzyme complex (Wurm and Sprangers 2019). Conveniently, it is possible to express Dcp1 and Dcp2 separately and fluorotryptophan labeling can thus be restricted to either Dcp1 or Dcp2.

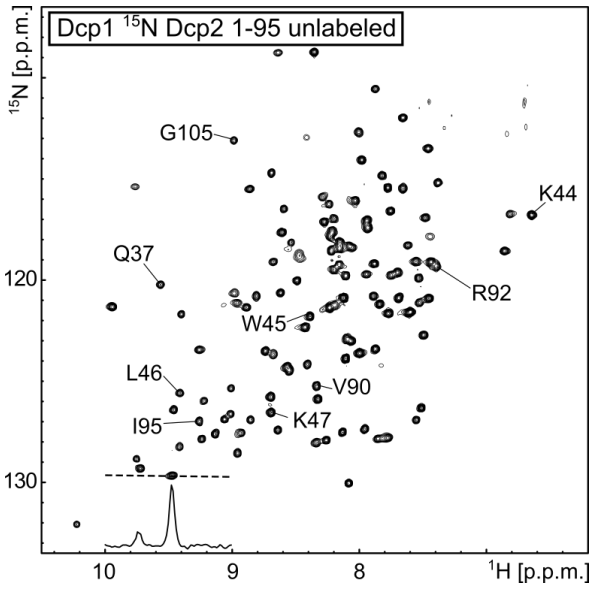

Figure 2.13.: ^{1}H-^{15}N spectrum of the ^{15}N labeled Dcp1 in a minimal Dcp1:Dcp2 complex (Dcp2 is NMR inactive). The 1D trace in the spectrum shows one of the tryptophan H_ε-N_ε signals.

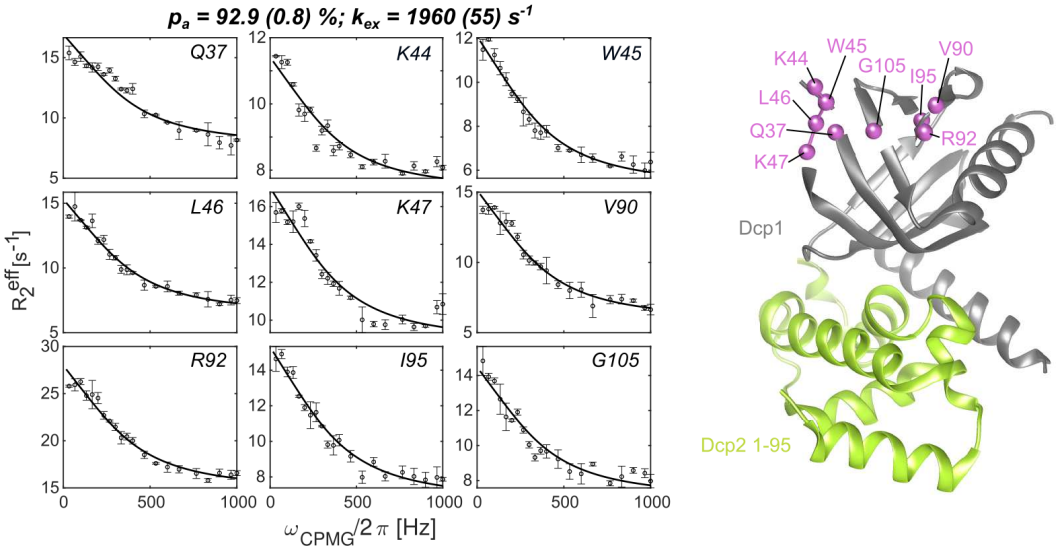

Figure 2.14.: Dynamics of Dcp1 in a minimal Dcp1:Dcp2 complex. ^{15}N CPMG relaxation dispersion (RD) profiles that report on the dynamics in the aromatic groove of the Dcp1 protein (Wurm, Overbeck, and Sprangers 2016). The residues that undergo chemical exchange are highlighted on the structure of the domain (She, Decker, Svergun, et al. 2008) (PDBid: 2QKL). Dcp1 is colored gray, the Dcp2 regulator domain is NMR invisible and colored light green.

We first prepared a minimal Dcp1:Dcp2 complex that contains ^{15}N labeled Dcp1 and the unlabeled NRD of Dcp2 (Figure 2.13). ^{15}N based relaxation dispersion experiments showed clear dynamics in the aromatic groove of Dcp1 (Figure 2.14, Figure 2.15).

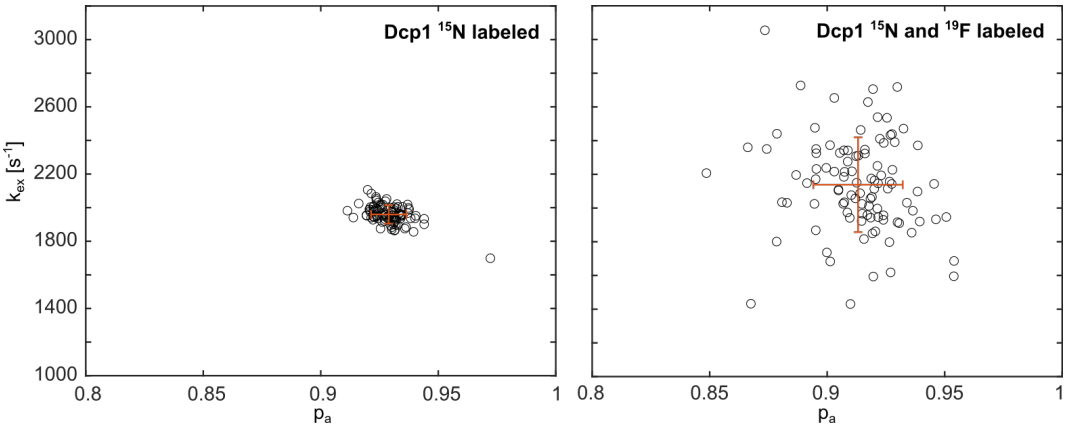

Figure 2.15.: Result of Monte Carlo to extract exchange parameters for the ^{15}N CPMG RD data recorded on the ^{15}N labeled Dcp1 protein (left) and on the ^{15}N 5-fluorotryptophan labeled Dcp1 protein (right). The orange cross represents the average population of the ground state (p_a) and exchange rate (k_{ex}). The error bars indicate the standard deviations in both parameters.

Fitting these data to a global exchange process revealed a ground state population p_a of 92.9 ± 0.8 % and an exchange rate k_{ex} of 1960 ± 55 s^{-1}. These data agree with previous measurements, where small deviations in the exchange parameters are due to differences in the used buffer system.

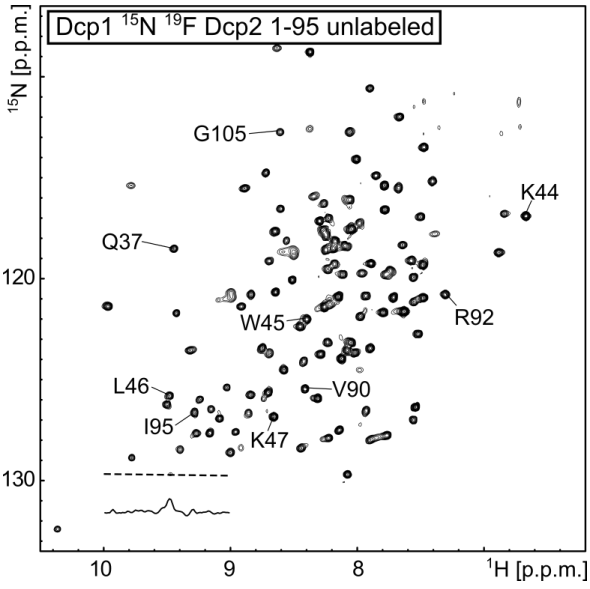

Figure 2.16.: Influence of 5-fluorotrypthphan incorporation on spectra of Dcp1 in a minimal Dcp1:Dcp2 complex. ^{1}H-^{15}N spectrum of the ^{15}N, 5-fluorotryptophan labeled Dcp1:Dcp2 complex. The strong reduction of the H_ε-N_ε side-chain signal reveals the efficient incorporation of the ^{19}F label.

Subsequently, we prepared the Dcp1:Dcp2 complex but this time by labeling Dcp1 with ^{15}N and 5-fluorotryptophan. The 5-fluorotryptophan labeling was efficient as judged by the strong reduction of the H_ε-N_ε resonances in the 2D NMR spectrum (Figure 2.16). Replacement of the natural tryptophan residues with 5-fluoro- tryptophan resulted in minor chemical shift perturbations in the ^{1}H-^{15}N correlation map, revealing that the introduced fluorine atoms have no global effect on the structure of the complex (Figure 2.17, Figure 2.19).

The absence of large differences in dynamics between the ^{15}N and the ^{15}N/^{19}F labeled proteins can be further corroborated by the fact that it is possible to fit the nitrogen RD profiles from both datasets (without and with ^{19}F labeling) simultaneously (Figure 2.22, Figure 2.23), which results in a ground state population of 91.8 ± 1.1 % and an exchange rate k_{ex} of 2220 ± 121 s^{-1} (Figure 2.21).

We subsequently recorded ^{15}N CPMG RD curves on this sample from which we extracted a ground state population of 91.3 ± 1.9 % and an exchange rate k_{ex} of 2138 ± 281 s^{-1} (Figure 2.15). Based on that, we conclude that the introduction of 5-fluorotryptophan had no measurable effect on the backbone dynamics of Dcp1.

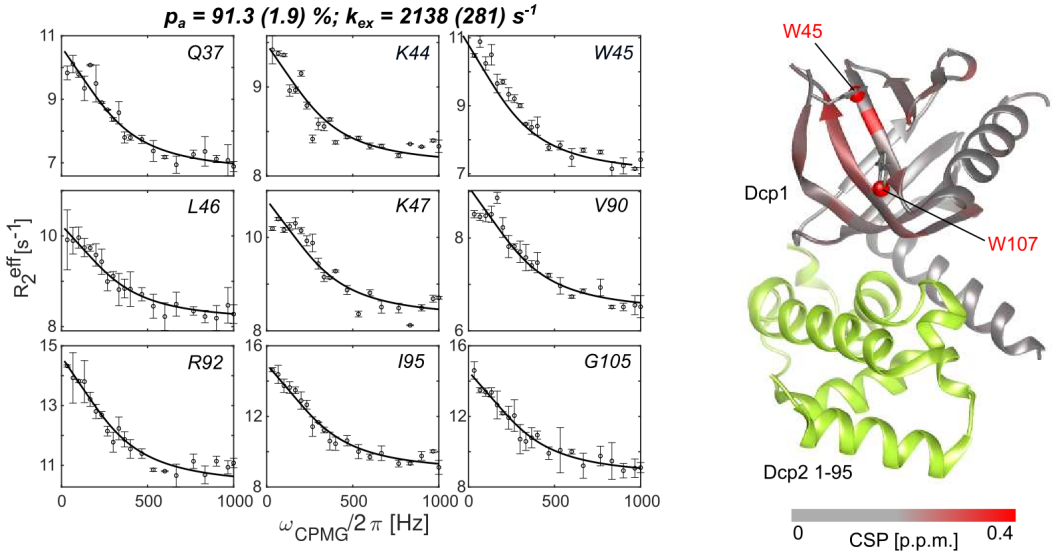

Figure 2.17.: Influence of 5-fluorotrypthphan incorporation on the dynamics of Dcp1 in a minimal Dcp1:Dcp2 complex. The ^{15}N CPMG RD profiles are not influenced by the incorporation of the 5-fluorotryptophan. The chemical shift perturbations (CSPs) that are induced by the two 5-fluorotryptophan residues are limited to the region that is close to the tryptophan residue (see also Figure 2.18).

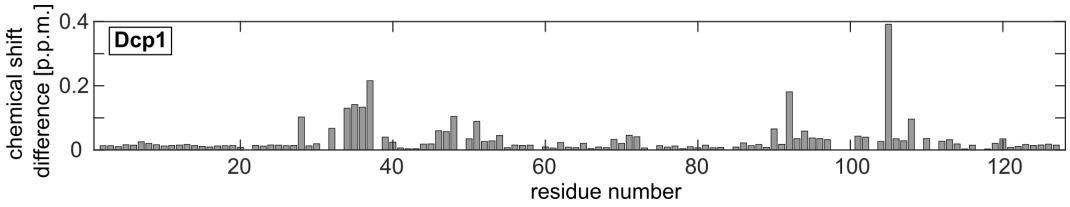

Figure 2.18.: Chemical shift perturbations in Dcp1 upon replacement of all tryptophan residues with 5- fluorotryptophan. CSPs are calculated in ppm as CSP = $\sqrt{(0.1 * \Delta\delta N)^2 + (\Delta\delta H)^2}$. The structures displayed in Figure 2.17 are colored according to the CSPs, where the replaced tryptophan residues are shown as sticks.

The ^{19}F NMR spectrum of the Dcp1 labeled complex shows two distinct resonances (Figure 2.24 A) that result from Trp 45 and 107 in Dcp1. We next recorded ^{19}F CPMG RD experiments and extracted exchange parameters by jointly fitting the data of the two residues in the aromatic groove to a two-site exchange model. We obtained a population p_a of the ground state of 98.9 ± 1.1 % and an exchange rate k_{ex} of 6840 ± 1109 s^{-1} (Figure 2.24 B). As observed for the KIX domain, this exchange rate is significantly faster than the rates obtained from ^{15}N CPMG experiments, indicating that the ^{19}F data does not report on the global exchange process that we quantified based on the ^{15}N data. In agreement with that, it is not possible to fit the ^{19}F and the ^{15}N relaxation dispersion data simultaneously to one exchange process (Figure 2.25). The faster timescale of the ^{19}F data suggests that the fluorotryptophan side-chains are more flexible than the backbone of the protein and that the ^{19}F tryptophan indole ring does not solely report on the global exchange process in the Dcp1 aromatic groove, although Trp 45 is centrally located in this groove.

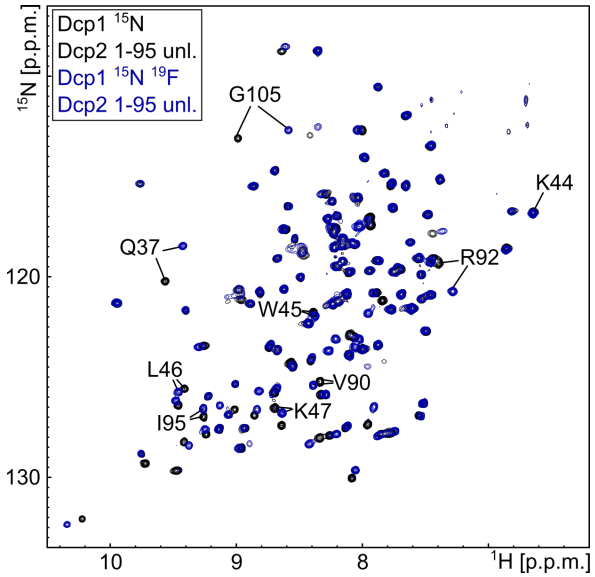

Figure 2.19.: Differences in the NMR spectra of ^{15}N and ^{15}N ^{19}F labeled Dcp1 in the Dcp1:Dcp2 complex is shown in the overlay of the ^{1}H-^{15}N spectra of ^{15}N (black; Figure 2.13) and ^{15}N ^{19}F (dark blue; Figure 2.16) labeled Dcp1.

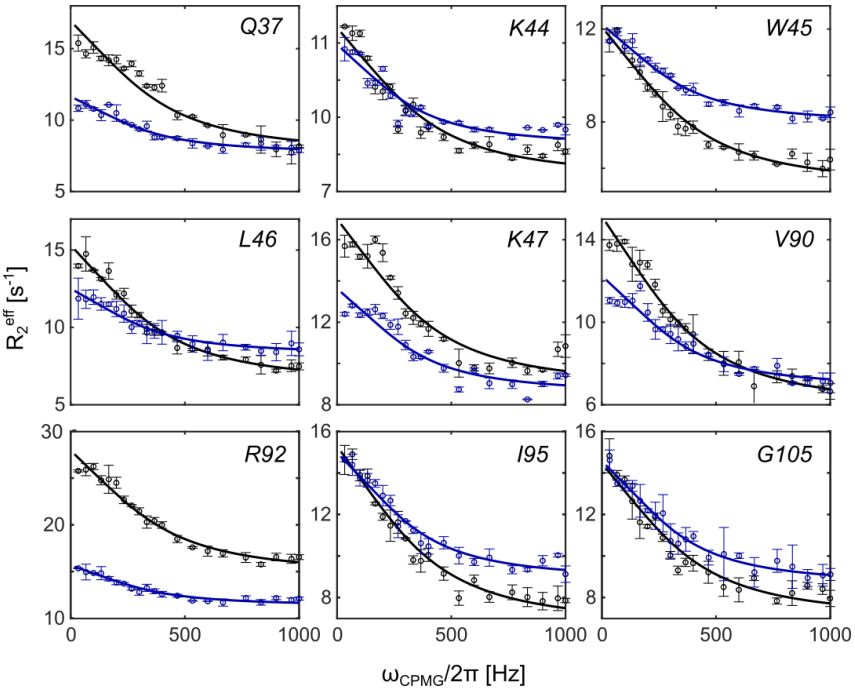

Figure 2.20.: Differences in the CPMG RD curves of ^{15}N and ^{15}N ^{19}F labeled Dcp1 in the Dcp1:Dcp2 complex is shown in the overlay of the ^{15}N CPMG RD curves recorded on ^{15}N (black; Figure 2.14) and ^{15}N ^{19}F (dark blue; Figure 2.17) labeled Dcp1. The differences in the amplitude of the RD curves can be attributed to changes in the chemical shift differences ($|\Delta\omega_N|$) between the ground and excited state between the two labeling schemes and do not necessarily reflect differences in populations or exchange rates between the two samples.

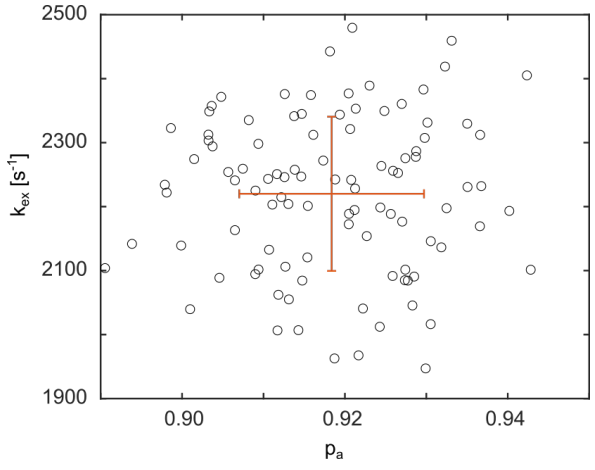

Figure 2.21.: Result of 100 Monte Carlo simulations to extract exchange parameters for a simultaneous fit of the ^{15}N CPMG RD data recorded on the ^{15}N labeled Dcp1 protein and on the ^{15}N 5- fluorotryptophan labeled Dcp1 protein. The orange cross represents the average population of the ground state (p_a) and the exchange rate (k_{ex}). The error bars indicate the standard deviations in both parameters.

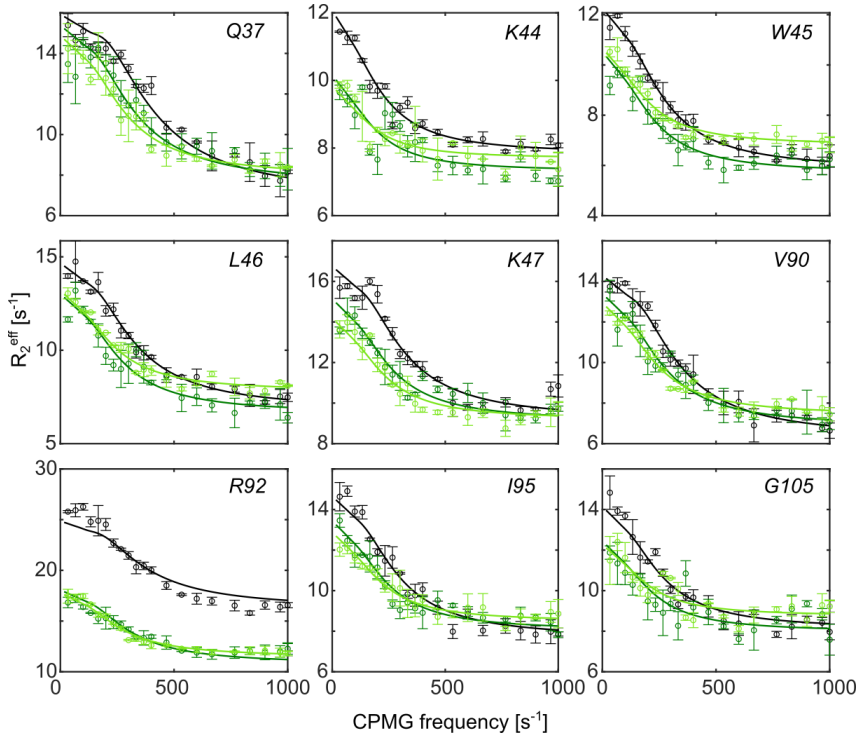

Figure 2.22.: ^{15}N relaxation dispersion profiles of the ^{15}N labeled Dcp1 protein recorded at a 500 MHz (light green), 600 MHz (dark green) and 800 (black) MHz proton frequency. The drawn lines are a simultaneous fit of all data from both proteins in Figure 2.22 and Figure 2.23 to a two-site exchange process (p_a = 91.8 ± 1.1 %; k_{ex} = 2220 ± 121 s^{-1}).

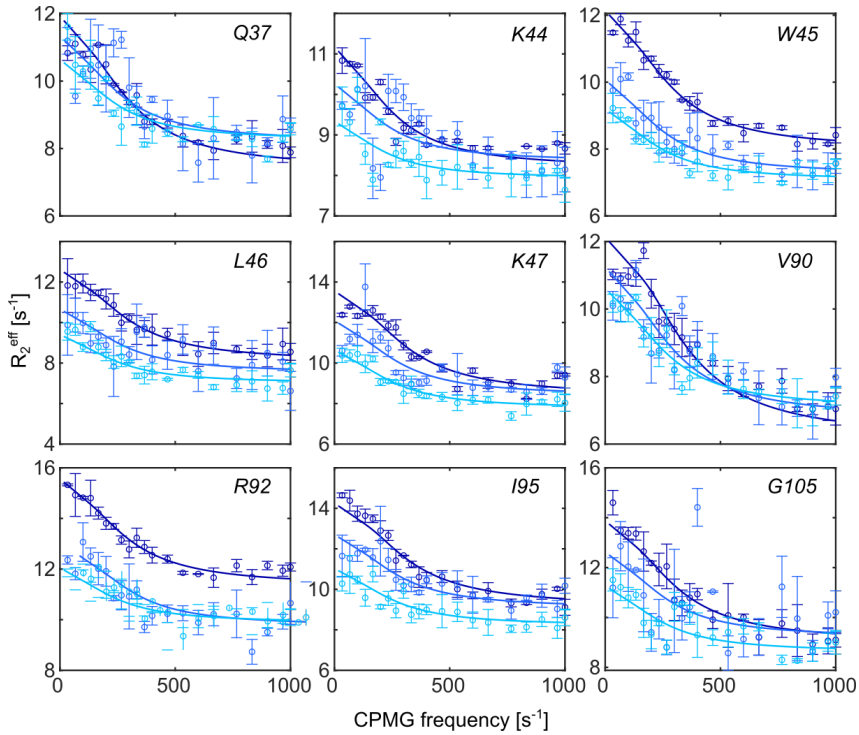

Figure 2.23.: ^{15}N relaxation dispersion profiles of the ^{15}N-fluorotryptophan labeled Dcp1 protein recorded at a 500 MHz (light blue), 600 MHz (medium blue) and 800 (dark blue) MHz proton frequency. The drawn lines are a simultaneous fit of all data from both proteins in Figure 2.22 and Figure 2.23 to a two-site exchange process (p_a = 91.8 ± 1.1 %; k_{ex} = 2220 ± 121 s^{-1}).

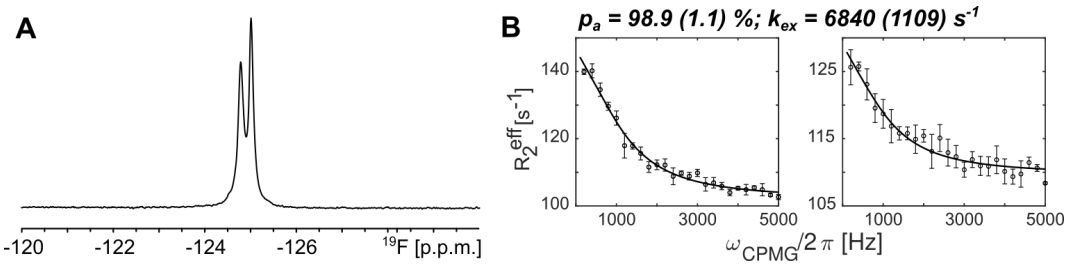

Figure 2.24.: Influence of 5-fluorotrypthphan incorporation on the dynamics of Dcp1 in a minimal Dcp1:Dcp2 complex. (A) 1D ^{19}F NMR spectrum of the 5-fluorotryptophan Dcp1:Dcp2 complex. (B) ^{19}F CPMG RD profiles of the upfield- and downfield ^{19}F signals, recorded at 500 MHz proton frequency.

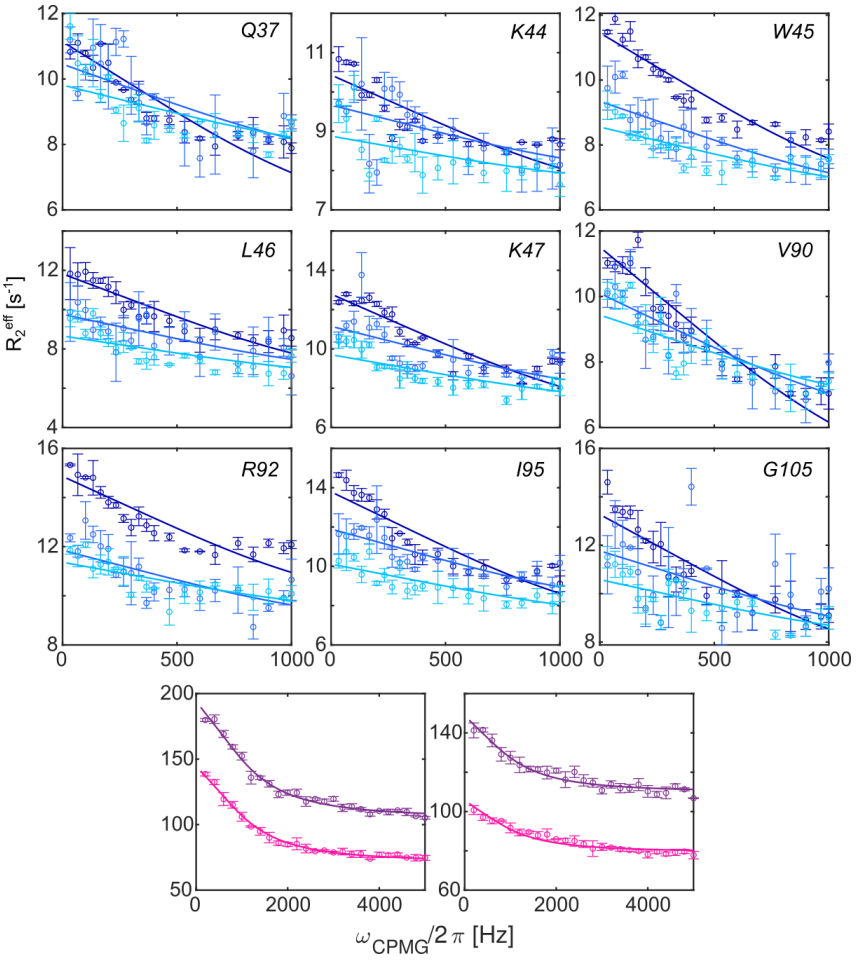

Figure 2.25.: ^{15}N (top) and ^{19}F (bottom) relaxation dispersion profiles recorded on the ^{15}N, 5- fluorotryptophan labeled Dcp1 protein. ^{15}N data was recorded at a 500 MHz (light blue), 600 MHz (medium blue) and 800 (dark blue) MHz proton frequency, ^{19}F data was recorded at 500 (pink) and 600 (purple) MHz protein frequency. The drawn lines represent an effort to simultaneously fit the ^{15}N and ^{19}F RD data to a two-site exchange process. The ^{19}F and ^{15}N data are not compatible, indicating that the nitrogen and fluorine RD profiles do not report on the same process.

In a next set of experiments, we assessed the motions in the Dcp2 NRD. To that end, we measured nitrogen RD experiments on a complex of unlabeled Dcp1 and ^{15}N labeled NRD from Dcp2. The results indicate the presence of an exchange process in the Dcp2 NRD with a ground-state population of 97.9 ± 3.1 % and an exchange rate k_{ex} of 1712 ± 1098 s^{-1} (Figure 2.26, Figure 2.29). The three Dcp2 tryptophan residues are in close spatial proximity to this flexible region and thus potentially sense these global motions (Figure 2.26). To assess that, we labeled the Dcp2 NRD with 5-fluorotryptophan and obtained a fluorine spectrum with three distinct resonances (Figure 2.27 A). These three residues showed clear RD dispersions, however, the extracted exchange parameters (p_a = 52.1 ± 7.0 %, k_{ex} = 17795 ± 2967 s^{-1}) reveal an exchange rate that was, as above, faster than the exchange rate that was extracted from the ^{15}N data. As for KIX and Dcp1, it was hence not possible to fit the ^{15}N and ^{19}F RD data simultaneously (Figure 2.30). Of note, the ^{15}N-^{19}F labeled Dcp2 protein expressed with yields that were sufficient for the recording of 1D ^{19}F RD curves, but that were too low to allow for the recording of ^{15}N relaxation data with sufficient signal to noise. We can thus not directly probe for potential changes in the backbone motions that could be caused by the ^{19}F labeling. However, we anticipate that these changes are very small as the CSPs caused by the ^{19}F introduction (Figure 2.31) are comparable to those that we observed upon introduction of ^{19}F labels in the KIX domain and the Dcp1 protein.

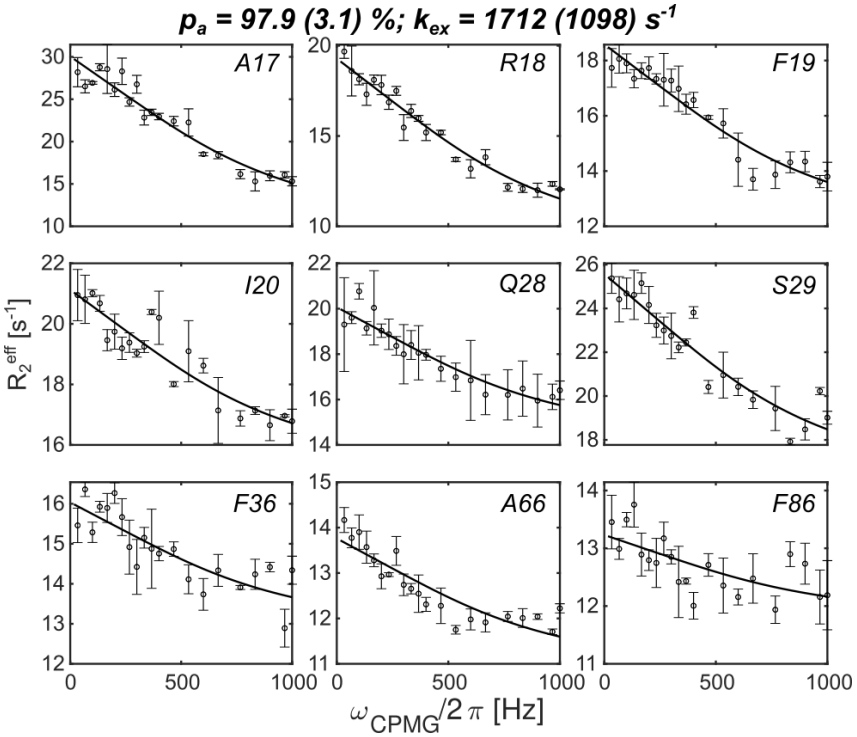

Figure 2.26.: Measurement of dynamics in the Dcp2 N-terminal regulatory domain (NRD), in complex with Dcp1. ^{15}N CPMG relaxation dispersion (RD) profiles for a set of residues in the Dcp2 NRD. The data is recorded on a ^{15}N, 5-fluorotryptophan labeled Dcp2 sample.

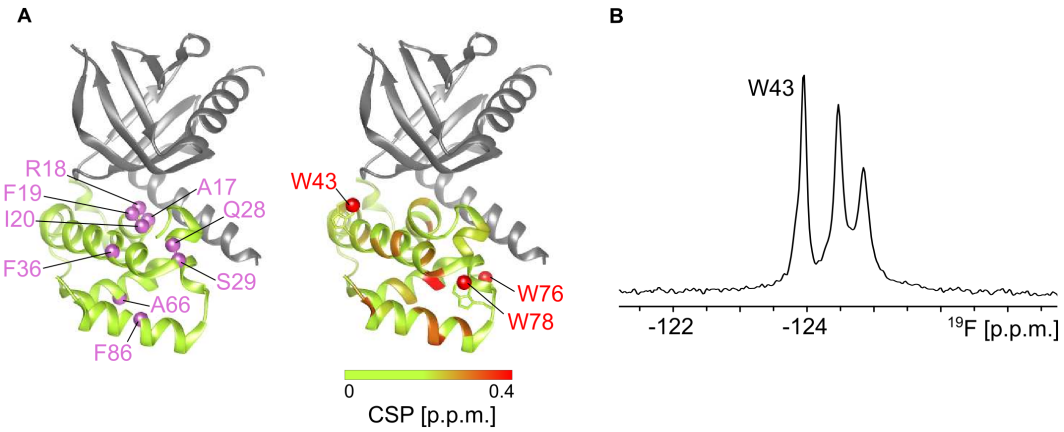

Figure 2.27.: Measurement of dynamics in the Dcp2 N-terminal regulatory domain (NRD), in complex with Dcp1. (A) The observed dynamics cluster in the core of the Dcp2 NRD. Three tryptophan residues surround the mobile region. Dcp1 is NMR invisible and colored gray, the Dcp2 regulatory domain is colored light green. The chemical shift perturbations (CSPs) that are induced by the three 5-fluorotryptophan residues in the Dcp2 domain are limited to the region that is close to the tryptophan residue (Figure 2.31). (B) ^{19}F NMR spectrum of the ^{15}N, 5-fluorotryptophan labeled Dcp2 sample. The W43 resonance is assigned by mutagenesis.

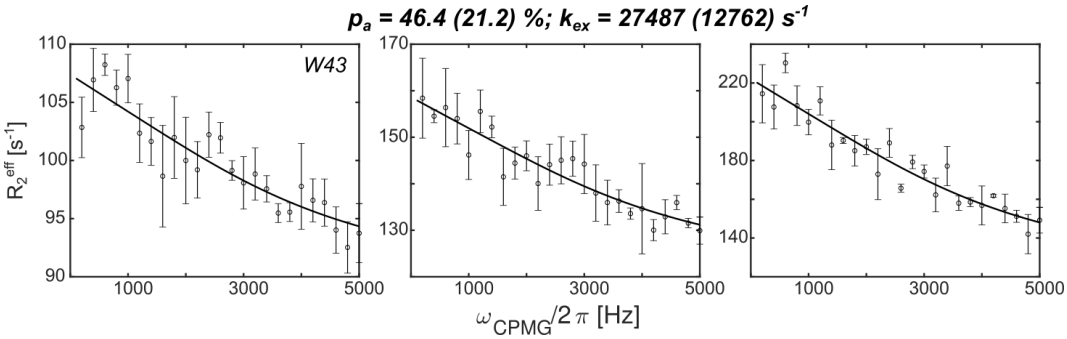

Figure 2.28.: Measurement of dynamics in the Dcp2 N-terminal regulatory domain (NRD), in complex with Dcp1. Here, ^{19}F CPMG relaxation dispersion profiles of the three ^{19}F resonances, recorded at 600 MHz proton frequency, are shown.

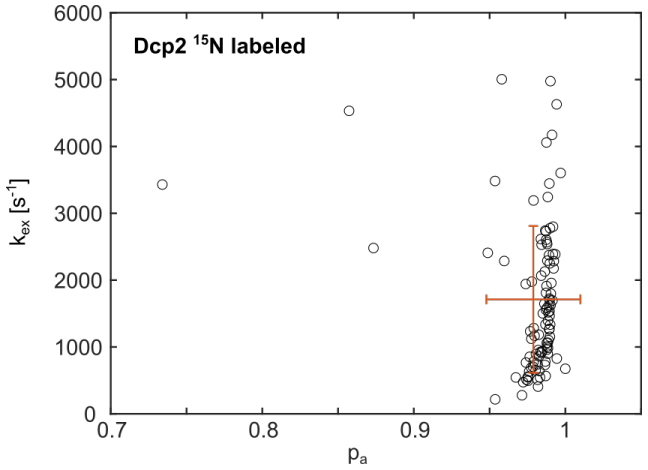

Figure 2.29.: Result of Monte Carlo to extract exchange parameters for the ^{15}N CPMG RD data recorded on the ^{15}N 5-fluorotryptophan labeled Dcp2 protein in the Dcp1:Dcp2 NTD complex. The red cross represents the average population of the ground state (p_a) and exchange rate (k_{ex}). The error bars indicate the standard deviations in both parameters. p_a = 97.9 ± 3.1 %; k_{ex} = 1712 ± 1098 s^{-1}.

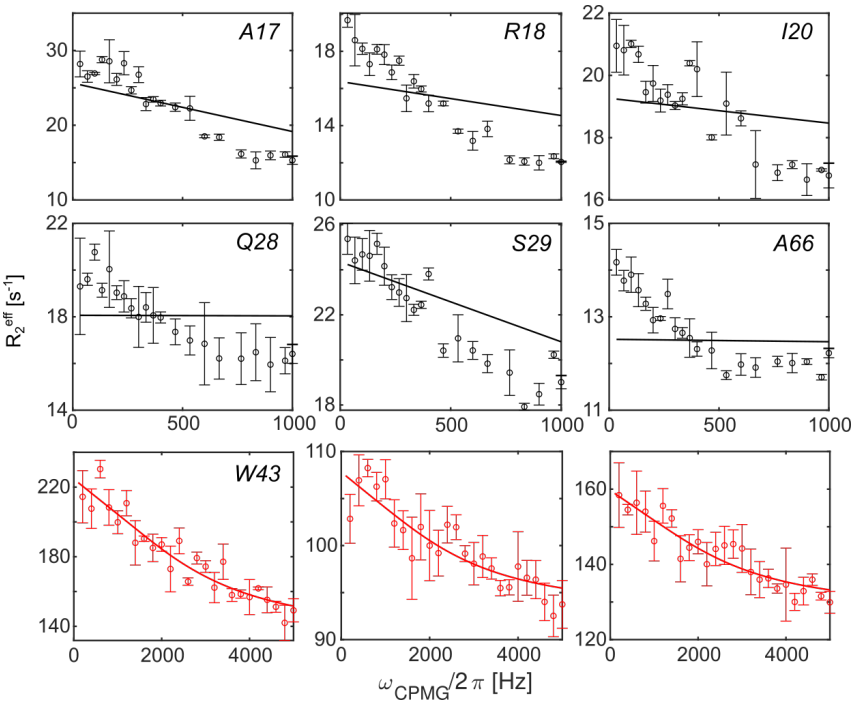

Figure 2.30.: ^{15}N (black) and ^{19}F (red) relaxation dispersion profiles recorded on the ^{15}N, 5- fluorotryptophan labeled Dcp2 protein. ^{15}N data was recorded at 800 (black) MHz proton frequency, ^{19}F data was recorded at 600 (red) MHz protein frequency. The drawn lines represent an effort to simultaneously fit the ^{15}N and ^{19}F RD data to a two-site exchange process. The ^{19}F and ^{15}N data are not compatible, indicating that the motions of the 5-fluorotryptophan and the motions of the backbone are not the same.

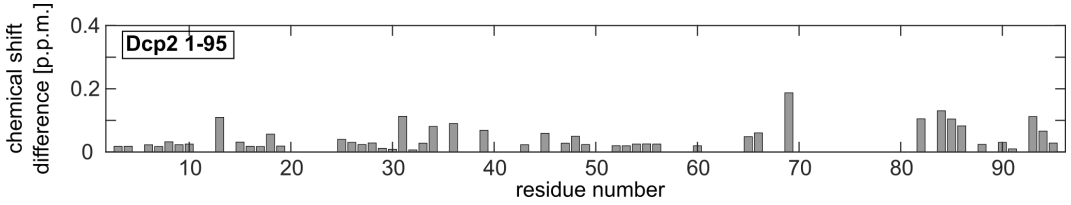

Figure 2.31.: Chemical shift perturbations in Dcp2 upon replacement of all tryptophan residues with 5- fluorotryptophan. CSPs are calculated in ppm as CSP = $\sqrt{(0.1 * \Delta\delta N)^2 + (\Delta\delta H)^2}$. The structures in Figure 2.27 A are colored according to the CSPs, where the replaced tryptophan residues are shown as sticks.

In the three examples above, we focused on relatively small assemblies, with molecular weights of 10 kDa (KIX domain) and 26 kDa (Dcp1:Dcp2-NRD). We next aimed at recapitulating the exchange between the open and closed state in the 46 kDa Dcp1:Dcp2-NRD-CTD complex (k_{ex} = 2800 s^{-1}). In this process the CTD of Dcp2 can either dock onto the NRD of Dcp2 (closed conformation; 94 %), or it can be detached from the NRD (open conformation; 6 %) (Wurm, Holdermann, et al. 2017). The Dcp2 NRD contains a catalytically important gatekeeper tryptophan residue (W43) (Floor, Borja, and Gross 2012) that is solvent exposed in the open conformation and tightly packed onto the Dcp2-CTD interface in the closed state (She, Decker, Svergun, et al. 2008). The exchange between these open and closed conformations of Dcp2 have been shown to be important for the regulation of the mRNA decapping activity (Wurm, Holdermann, et al. 2017). To determine the ^{19}F chemical shift of the "open" state of the gatekeeper 5-fluorotryptophan we first assigned W43 through mutagenesis in the Dcp1:Dcp2-NRD construct (Figure 2.27 A, Figure 2.33), where the gatekeeper tryptophan is solvent exposed due to the lack of the CTD. Next, we prepared a Dcp1:Dcp2-NRD-CTD complex in which the seven Dcp2 tryptophan residues are replaced with 5-fluorotryptophan. The resulting ^{19}F spectrum shows five separated resonances of which we assigned the most upfield signal to W43 through mutagenesis (Figure 2.34, Figure 2.36). The ^{19}F resonance of

W43 in the NRD thus shifted significantly downfield due to the interaction with the CTD. This confirms that Dcp2 is mostly present in the closed conformation.

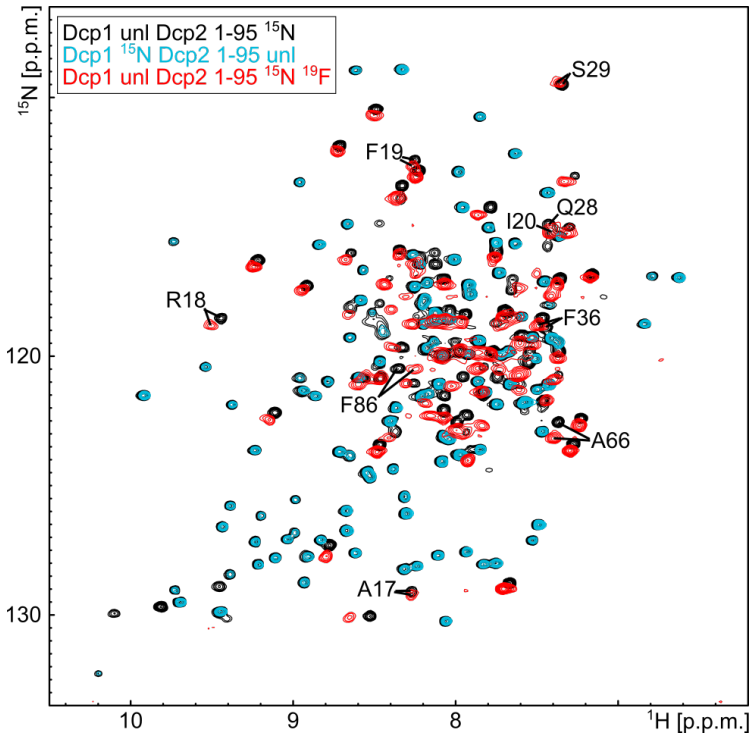

Figure 2.32.: Differences in the NMR spectra of ^{15}N and ^{15}N ^{19}F labeled Dcp2 in the Dcp1:Dcp2 complex.shown in the overlay of the ^{1}H-^{15}N spectra of the ^{15}N labeled Dcp1:Dcp2 complex (black; both Dcp1 and Dcp2 are ^{15}N labeled), the Dcp1:Dcp2 complex where Dcp2 is ^{15}N ^{19}F labeled (red) and the Dcp1:Dcp2 complex in which Dcp1 is ^{15}N labeled (blue).

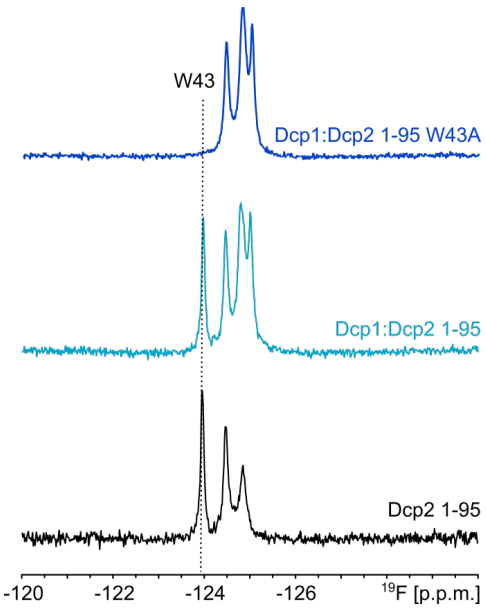

Figure 2.33.: Assignment of the W43 ^{19}F 5-fluorotryptophan resonance in Dcp2 (residues 1-95). The lower (black) spectrum shows the resonances of the three Dcp2 Trp residues in the Dcp1:Dcp2 (residues 1-95) complex (Dcp1 is not ^{19}F labeled). The middle (light blue) spectrum shows the resonances of the five Trp resonances in the Dcp1:Dcp2 (residue 1-95) complex. The top spectrum shows the resonances of the four Trp resonances in the Dcp1:Dcp2 (residue 1-95; W43A) complex. The most upfield shifted signal disappears, allowing a straightforward assignment of this resonance to W43.

To assess this finding independently, we prepared a sample that contains ^{19}F labeled tryptophan residues as well as methyl ^{13}C labeled isoleucine and methionine residues. Previously, we showed that the resonance frequencies of M164 and M221 in methyl TROSY spectra directly report on the open-closed equilibrium in Dcp2 (Wurm, Holdermann, et al. 2017). Importantly, the incorporation of ^{19}F tryptophan only had a very small effect on the position of those resonances (Figure 2.35) that corresponds to a less than 5 % shift of the Dcp2 conformational equilibrium

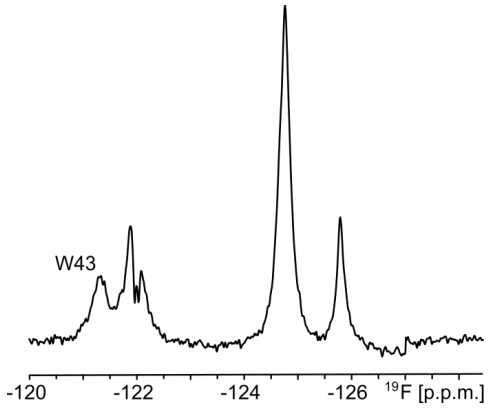

Figure 2.34.: The Dcp2 regulatory (NRD) and catalytic domains (CTD), in complex with Dcp1. The 1D ^{19}F spectrum of the complex with 5-fluorotryptophan labeled Dcp2 reveals 5 resonances for the 7 tryptophan residues. The resonance of the gatekeeper tryptophan (W43) is assigned through mutagenesis. Note the shift of the W43 frequency between the complex with and without (Figure 2.27 B) the Dcp2 CTD.

towards the closed state. This finding corroborates that the introduction of 5-fluorotryptophan has, if at all, a limited impact on the structure and dynamics of protein complexes (Figure 2.35).

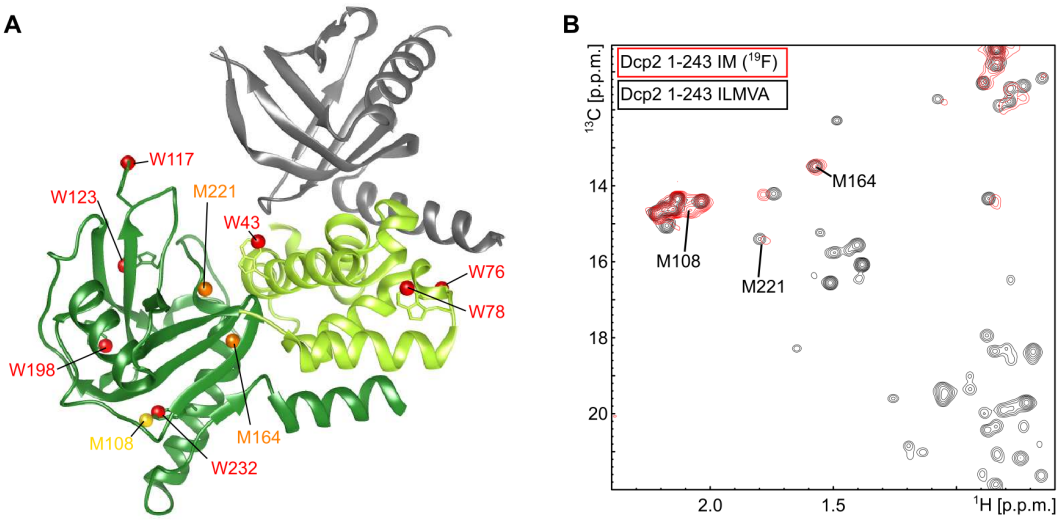

Figure 2.35.: (A) Structure of the Dcp1-Dcp2 NRD-CTD complex. Dcp1 is NMR invisible and colored gray, the Dcp2 NRD is colored light green and the Dcp2 CTD is colored dark green. The seven tryptophan residues are colored red. Methionine 221 and 164, that report on the open-closed transitions in the complex, are colored orange. Methionine 108, that experiences a CSP in the methyl TROSY spectrum due to the incorporation of 5-fluorotryptophan, is colored yellow. (B) Overlay of the methionine region of methyl TROSY spectra of the Dcp1 (NMR inactive): Dcp2 (ILMVA methyl labeled) complex (grey) and the Dcp1 (NMR inactive): Dcp2 (IM methyl and 5-fluorotryptophan labeled) complex (red). The methionine resonances of M221 and M164, that report on the conformation of the complex, are labeled.

Based on the ^{19}F 1D spectra of the 46 kDa Dcp1:Dcp2 complex we subsequently attempted to record ^{19}F based CPMG experiments. We realized, however, that the ^{19}F R_2 relaxation rates were around 200 s^{-1}, which prevents the use of sufficiently long CPMG relaxation delays that are required for the recording of CPMG frequencies lower than a couple of 100 Hz. In that light, the Dcp1:Dcp2-NRD-CTD complex is beyond the limit of where 5-fluorotryptophan based ^{19}F spectroscopy can be employed to extract detailed information regarding protein dynamics. It should be noted that the molecular weight of the Dcp1:Dcp2-NRD-CTD enzyme complex also prevented us from assessing dynamics through ^{15}N based RD experiments. We have, however, shown that high quality ^{19}F RD CPMG curves can be recorded for the 100 kDa Xrn2 enzyme after labeling the protein with BTFA (Overbeck, Stelzig, et al. 2022). This shows that the fluorine relaxation properties of 5-fluorotryptophan

residues are less advantageous than those of CF_3 groups on cysteine side-chains.

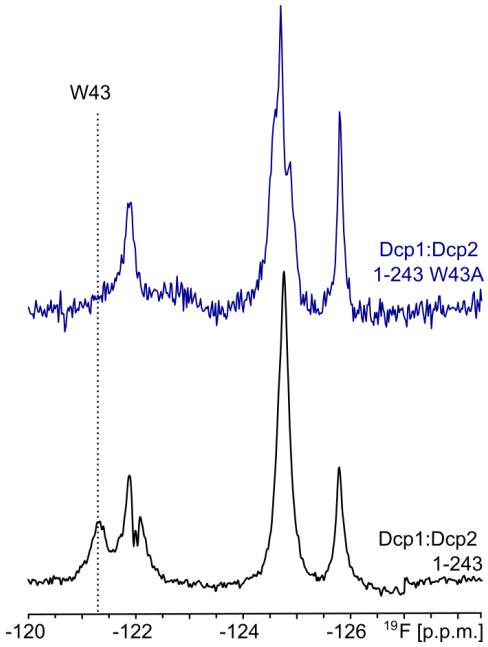

Figure 2.36.: Assignment of the W43 ^{19}F 5-fluorotryptophan resonance in Dcp2 (residues 1-243). The lower (black) spectrum shows the resonances of the seven Dcp2 Trp residues in the Dcp1:Dcp2 (residues 1-243) complex (Dcp1 is not ^{19}F labeled). The top (blue) spectrum shows resonances of the six Trp resonances in the complex where tryptophan 43 is replaced with an alanine. The most upfield signal disappears, allowing the assignment of this resonance to W43. Note that the frequency of W43 shifts from -123.95 (Figure 2.29) to -121.31 ppm when the Dcp2 catalytic domain is included in the Dcp1:Dcp2 complex.

2.3. DcpS scavenger decapping complex

Finally, we assessed if ^{19}F NMR methods can accurately address motions in the 80 kDa scavenger decapping enzyme DcpS. DcpS is a homo-dimer that contains two active sites at the interface between the N- and C-terminal lobes of the enzyme (Figure 2.37 A) (Gu et al. 2004). Upon recruitment of a short mRNA substrate, the N- and C-terminal lobes close around one of the two active sites, which simultaneously opens the other active site. As a result, the complex transits from a symmetric apo conformation to an asymmetric substrate bound conformation. Binding of a second substrate to the open binding site of the asymmetric DcpS:substrate complex results in seesaw-like flipping motions, where the two active sites on both sides of the enzyme alternatingly close and open. Previously, we have shown that the rate of these flipping motions increases with increasing substrate concentration (Fuchs et al. 2020; Neu et al. 2015). For our studies here, we used the DcpS enzyme from *C. thermophilum* that contains six tryptophan residues and that yields high quality ^{19}F NMR spectra (Figure 2.37 B). Of note, the ^{19}F NMR spectra of the human and the *S. cerevisiae* DcpS enzymes yielded ^{19}F spectra of inferior quality, rendering those unsuitable for detailed ^{19}F NMR experiments (Figure 2.38). Previously, we reported that the seesaw motions in DcpS take place at rates that are too slow to be accurately captured by CPMG and/or $R_{1\rho}$ experiments. Here, we thus turned to longitudinal EXSY experiments, where we determine the intensity of cross peaks in a series of 2D NOESY spectra that were recorded with different mixing times. This is possible in the current case as all ^{19}F-^{19}F distances in the enzyme are over 15 Å (Figure 2.37 A) and all cross peaks in the spectrum must thus result from exchange and not from NOEs. Upon addition of an equimolar amount of the short m^7GpppG mRNA cap substrate (1 substrate per DcpS monomer), a number of the

resonances split, as a result of the formation of the asymmetric conformation in DcpS (Figure 2.37 B).

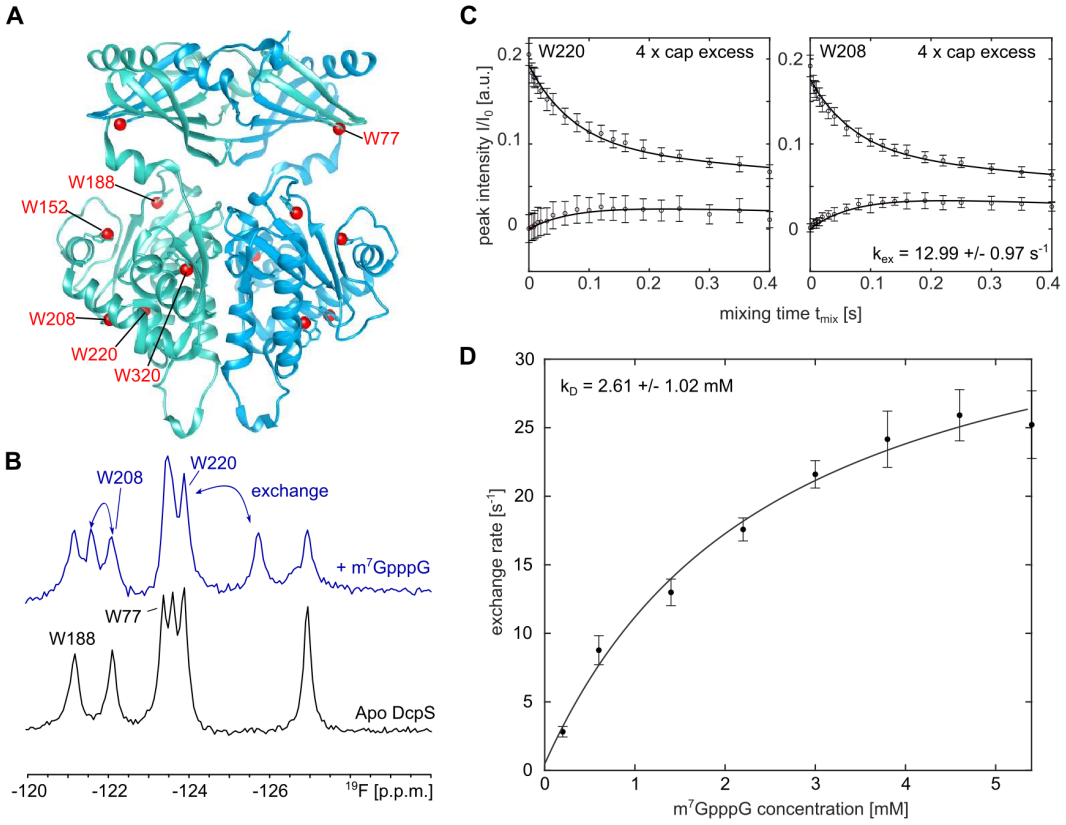

Figure 2.37.: The 80 kDa DcpS scavenger decapping enzyme. (A) Structure of the homodimeric enzyme, with the two different protomers colored in green and blue. The seven tryptophan residues are highlighted as red spheres. (B) ^{19}F NMR spectra of the apo enzyme (bottom) and the enzyme in complex with m^{7}GpppG (1 substrate per dimer). Assignments for the fluorine resonances are indicated. (C) Longitudinal exchange experiment to quantify the flipping motion in the enzyme in the presence of a fourfold molar excess of the m^{7}GpppG substrate. The two panels visualize the exchange that is sensed by W208 and W220, the drawn line corresponds to a global fit of the data to a two-site exchange mechanism, where the populations of state A and B are fixed to 0.5. (D) The flipping rate increases with increasing substrate concentration. The drawn line corresponds to a fit of the data to a two state binding model of the DcpS enzyme and the m^{7}GpppG ligand.

Based on the decay of the auto peaks and the buildup of exchange peaks in the EXSY spectra (Figure 2.37 C) we extracted an exchange rate of 2.8 ± 0.4 s^{-1} for the seesaw like motion in DcpS. We subsequently added 2-, 4-, 6-, 8-, 10-, 12- and 14-fold molar excesses of the mRNA cap substrate and observed a step-wise increase in the exchange rate to 25.2 ± 2.5 s^{-1} (Figure 2.37 D, Figure 2.39). This dependency of the rate of the seesaw motion on the substrate concentration agrees with previous studies that we performed on the *S. cerevisiae* DcpS enzyme (Neu et al. 2015), where we made use of methyl TROSY spectroscopy on deuterated and isoleucine labeled samples (Schütz and Sprangers 2020). Based on that, we conclude that ^{19}F NMR is, in this case, a suitable alternative to methyl TROSY NMR spectroscopy for the quantification of conformational exchange in the presence of varying amounts of substrate. Mechanistically, the addition of increasing amounts of ligand results in the increased occupation of the open binding site. This notion is affirmed by the observation that the exchange rates at the different ligand concentrations can be fitted to a simple binding model (Figure 2.37 D).

Based on that, an affinity of m^{7}GpppG for the open binding site of 2.6 ± 1.0 mM

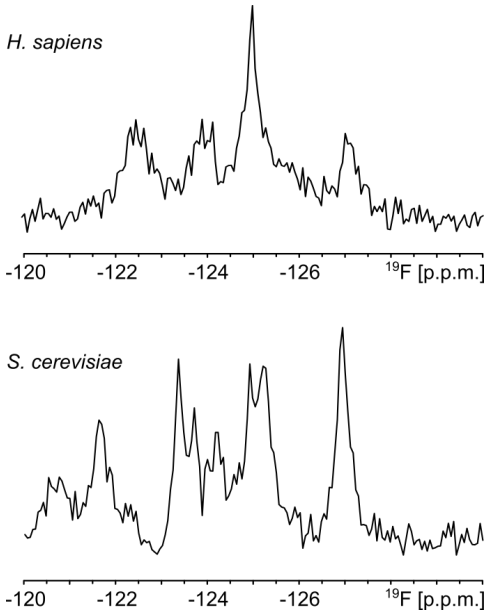

Figure 2.38.: ^{19}F NMR spectra (500 MHz proton frequency) of the 80 kDa DcpS complexes from *H. sapiens* (245 µM; top) and from *S. cerevisiae* (165 µM; bottom). The spectral quality is low, preventing accurate extraction of protein dynamics.

can be extracted. This affinity agrees well with the affinity that is extracted from the shift of the fluorine resonance in the open binding site upon substrate addition (2.48 ± 0.85 mM) (Figure 2.40). Binding of the m^{7}GpppG ligand and the rate of the DcpS flipping motions are thus directly correlated.

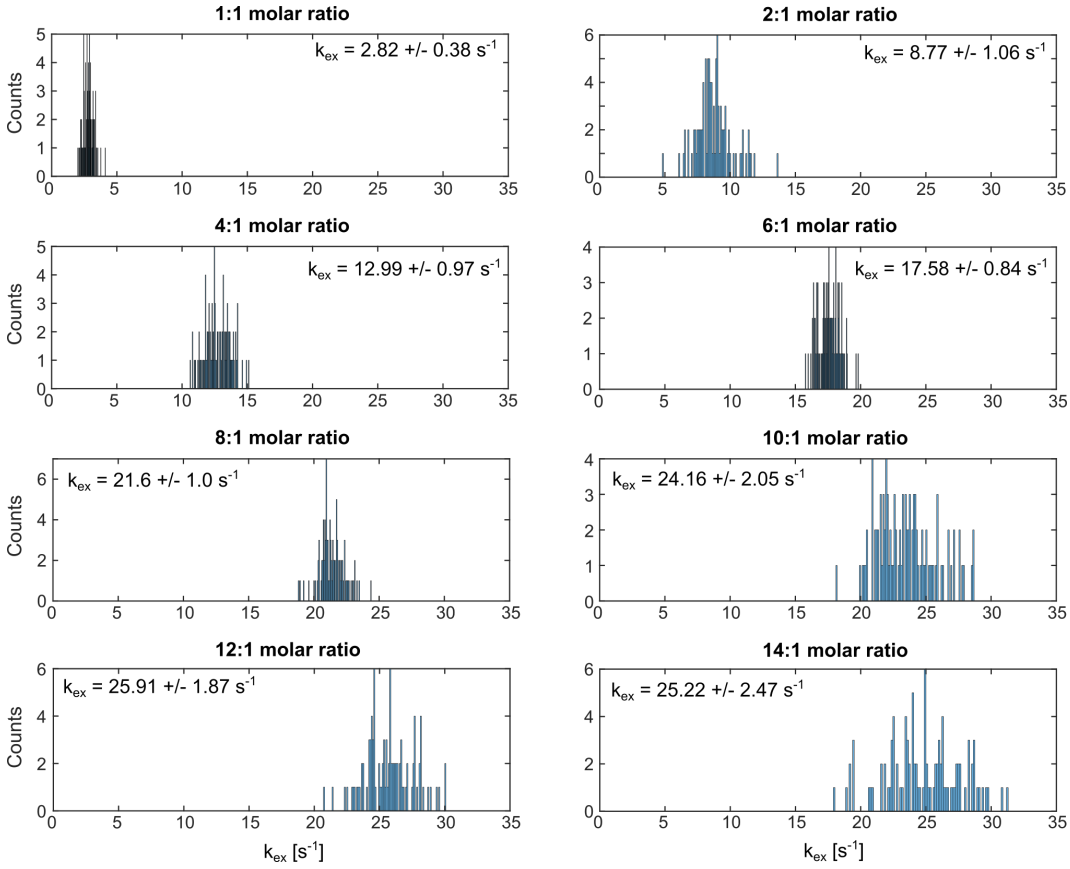

Figure 2.39.: DcpS flipping rates extracted from 100 Monte Carlo simulations at different substrate: enzyme ratios.

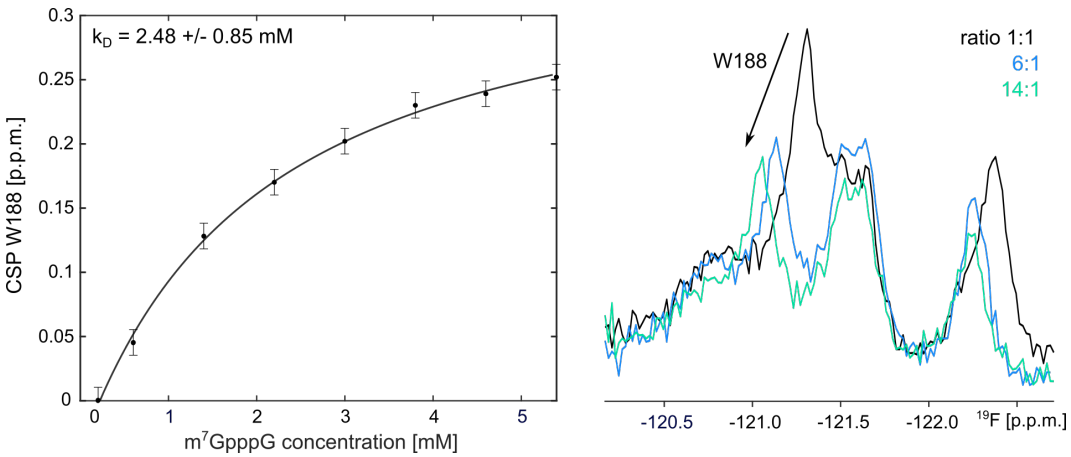

Figure 2.40.: Determination of the DcpS:m^{7}GpppG affinity based on the shift of one of the Trp resonances with increasing amounts of the ligand.

3. Discussion

Protein dynamics are essential for function. It is thus important to have access to methods that can determine the thermodynamic and kinetic parameters that are associated with protein motions. Solution state NMR spectroscopy has proven to be a highly successful method in that regard. Most NMR methods rely on labeling strategies that visualize the protein backbone through ^{1}H-^{15}N based spectra or on the use of methyl containing side chains in combination with ^{1}H-^{13}C methyl TROSY based experiments. These methods provide information with a high spatial resolution and relaxation data is normally recorded as a set of 2D experiments. In that regard, ^{19}F NMR methods can have an advantage as these can often be recorded rapidly in a 1D manner due to the limited number of well resolved resonances.

Numerous impressive examples are available in the literature where ^{19}F NMR methods have been exploited to extract information regarding protein motions (Kitevski-LeBlanc and Prosser 2012). These include studies of a fold-switch in the mycobacterial glycosyltransferase PimA (Liebau et al. 2020), calmodulin (Hoang and Prosser 2014), the nonstructural protein 1 of influenza A virus (Aramini et al. 2014), GPCRs (Didenko et al. 2013; Frei et al. 2020; Kim, Chung, et al. 2013; Liu, Horst, et al. 2012; Manglik et al. 2015; Pan et al. 2022), the periplasmic glucose/galactose receptor (Luck et al. 1996), diacyl-glycerol kinase (Shi et al. 2011), a cold shock protein (Overbeck, Kremer, and Sprangers 2020), alkaline phosphatase (Hull and Sykes 1974), the chaperone PapD (Bann et al. 2002), spider silk (Sarker et al. 2016), the protease trypsin (Ruben et al. 2020) and the Xrn2 exoribonuclease (Overbeck, Stelzig, et al. 2022). However, to our knowledge, it has never been systematically evaluated whether the incorporation of ^{19}F labels has an effect on the native protein dynamics, despite reports that show that ^{19}F labeling can have an effect on protein structure and stability (Acchione et al. 2012; Dalvit and Vulpetti 2016; Minks et al. 1999; Xiao, Parsons, et al. 1998).

Here, we show that the incorporation of 5-fluorotryptophan residues has, if at all, a minor effect on the native dynamics in a number of globular proteins (the KIX domain, Dcp1 or Dcp2). This result is encouraging and a prerequisite for the use of ^{19}F NMR methods. This finding is also in agreement with previous reports that showed that the overall structure of the GB1 protein is not influenced by the incorporation of 5- fluorotryptophan (Campos-Olivas et al. 2002) and that the stability of the cold shock protein B from *B. subtilis* is unaffected by fluorine labeling (Welte et al. 2020).

Proteins are dynamic at multiple timescales at the same time. The lifetimes of the states correlate with the energy barrier between the states, which is normally small for local motions of loops and side-chains (faster timescale motions) and significantly higher for global concerted motions (slower timescale motions). Slower timescale motions in enzymes have been directly linked with function and studying these motions is thus of a high biological interest. Fast side-chain motions are also

functionally important and have been correlated with the conformational entropy of proteins, which plays a role in e.g. protein stability and ligand interactions (Hoffmann, Mulder, and Schäfer 2022; Kasinath, Sharp, and Wand 2013; Wand and Sharp 2018). The CPMG RD experiments that we record here reveal dynamics of the incorporated 5-fluorotryptophan residues with exchange rates that are on the order of 10,000 s^{-1}. These fast motions could originate from rotameric jumps of the aromatic side-chains. Interestingly, these fast side-chain motions are readily detected in ^{19}F based experiments, but were not visible in nitrogen based CPMG RD experiments on the H_ϵ-N_ϵ groups of the indole rings. This difference between the fluorine and nitrogen based RD experiments results from the lower gyromagnetic ratio ($\gamma_{^{15}N} \sim 0.11^* \gamma_{^{19}F}$) and the smaller chemical shift range of nitrogen. As a result the $|\Delta\omega_N|$ values are considerably smaller than the corresponding $|\Delta\omega_F|$ values. When the local side chain motions are relatively fast, as we observe here, the amplitude of the RD curves depends on $|\Delta\omega|^2$. Consequently, the amplitude of the nitrogen based RD curves will be significantly smaller and cannot be detected reliably anymore. Slower motions can, however, be well detected using nitrogen based RD experiments (Figure 2.2, Figure 2.14, Figure 2.26). ^{19}F based RD experiments are also highly sensitive to the motions that we detected in the backbones of the KIX domain, Dcp1 and Dcp2. The highly sensitive ^{19}F experiments will thus simultaneously detect faster (side chain) and slower (backbone) motions of the 5-fluorotryptophan residues. Depending on the rates, population and chemical shift differences the RD curves can be strongly biased towards the faster of the slower of the two processes and the resulting RD curves cannot be analyzed using a two-state model anymore. As it is a-priory not possible to conclude if multiple exchange processes are superimposed or not, we suggest to support kinetic and thermodynamic properties that are derived from ^{19}F measurements with complementary data. This is especially relevant when the ^{19}F RD curves indicate the presence of faster motions that most likely result from side chain dynamics and not from global motions. In that light it is worth mentioning that we previously validated ^{19}F derived parameters for the Xrn2 enzyme with data that was recorded on methyl groups (Overbeck, Stelzig, et al. 2022). Likewise, we here show that EXSY experiments, that are insensitive to potential tryptophan side chain motions that are fast on the NMR chemical shift timescale, are very well suited to extract slow processes like the domain flipping motions in DcpS. Based on that, we anticipate that a careful interpretation of fluorine relaxation data will result in ample insights into biological function.

Part V.

Single Molecule FRET experiments of the Dcp1:Dcp2 mRNA decapping complex

In preliminary experiments, different fluorophore labeling positions were tested by K. A. Glowacz (Glowacz 2021) and corresponding data is presented in Table 2.1, Figure 2.1 and Figure 2.3. Further results were obtained and analyzed by C. Krempl with assistance from Johannes Schmoll and methodological input from Kevin Kramm.

1. Introduction

Most proteins fold into one or more specific three dimensional structures which, together with their motions and interactions, determine their specific functions in a cell. Structural rearrangements are therefore tightly connected to cellular function. Nuclear magnetic resonance (NMR) spectroscopy is a powerful method to detect and characterize these conformational changes as it can be used to detect conformations which are populated only to a very low degree (~ 0.5 %) (Korzhnev and Kay 2008; Oyen et al. 2017; Wurm, Sung, et al. 2021). The high protein concentrations of ~ 50 - 500 µM and often times long data acquisition times, which can take several hours to days, that are required for NMR measurements can however limit the extent of data that can be recorded. The protein concentrations necessary for NMR measurements can for example exceed the proteins' threshold concentration for phase separation which leads to a loss of peak intensity in the NMR spectra (Damman et al. 2019). Furthermore, highly dynamic processes in proteins that sample a multitude of conformations can also lead to severe peak broadening, even beyond detection, in the NMR spectra (Wurm, Holdermann, et al. 2017). An alternative and complementary approach to examine the conformations of proteins in solution are Förster resonance energy transfer (FRET) experiments (Algar et al. 2019; Lerner, Barth, et al. 2021; Lerner, Cordes, et al. 2018). Compared to NMR experiments, FRET experiments only require short data acquisition times (ranging from a few minutes to hours) and low protein concentrations (picomolar concentrations) and are therefore well suited for examining biomolecular systems that are difficult to access with NMR studies. For instance, FRET experiments were used to study the conformations and dynamics of the enzyme staphylococcal nuclease (Ha et al. 1999), the folding process of the chymotrypsin inhibitor 2 (Deniz, Laurence, Beligere, et al. 2000; Schuler and Eaton 2008), the link between conformational dynamics and molecular recognition of the maltose-binding protein (MBP) (Kim, Lee, et al. 2013) and the functional role of the conformational flexibility of the human Argonaute 2 protein (Willkomm et al. 2022). We here combine single molecule FRET (smFRET) and solution state NMR experiments to study the conformations of the 45 kDa Dcp1:Dcp2 mRNA decapping complex from *S. pombe* and we are particularly interested in the influence of different substrates and activator proteins on the conformational equilibrium of Dcp1:Dcp2. The decapping complex plays a central role in the degradation of mRNA as it catalyzes the removal of the 5' cap structure from the mRNA body which is then further degraded by exoribonucleases (Li and Kiledjian 2010; Mugridge, Coller, and Gross 2018; Schoenberg and Maquat 2012). The decapping enzyme Dcp2 is composed of an N-terminal regulatory domain (RD,

residues 1-95 in *S. pombe*) which is flexibly connected to a catalytic domain (CD, residues 96-243 in *S. pombe*) and an intrinsically disordered C-terminal extension. The decapping activator Dcp1 interacts tightly with Dcp2 by binding to its RD and it increases the decapping activity of Dcp2. During the catalytic cycle, Dcp1:Dcp2 undergoes large structural rearrangements that have previously been characterized using methyl- transverse relaxation-optimized spectroscopy (TROSY) NMR methods (Tugarinov, Hwang, et al. 2003) and it was found that three distinct conformations of the complex exist in solution (Wurm, Holdermann, et al. 2017). The apo complex exchanges between an open (with population p_{open} = 0.06) (She, Decker, Svergun, et al. 2008) and a closed conformation (with population p_{closed} = 0.94) (Mugridge, Ziemniak, et al. 2016; She, Decker, Svergun, et al. 2008) which are both catalytically inactive. Only in the presence of both the decapping activator Edc1 and mRNA substrate, the complex fully adopts a catalytically active conformation (Charenton, Taverniti, et al. 2016; Wurm, Holdermann, et al. 2017; Wurm, Overbeck, and Sprangers 2016). The stabilization of the catalytically active conformation is achieved in the presence of both Edc1 and the m^7G RNA cap structure, as both factors connect the the two structured domains of Dcp2 in their catalytically competent orientation. Specifically, the m^7G RNA cap structure is recognized by residues in both the CD and the RD of Dcp2 that form the split active site of the complex (Mugridge, Tibble, et al. 2018; Wurm, Holdermann, et al. 2017) and Edc1 contains a ~ 25 amino acid short fragment that consists of a YAGxxF activation motif that interacts with both the CD and the RD of Dcp2, and a proline rich region that binds to Dcp1 (Borja et al. 2011; Valkov et al. 2016; Wurm, Overbeck, and Sprangers 2016). The presence of capped mRNA, however, leads to strong peak broadening in the NMR spectra of the decapping complex, which likely results from a shift in the exchange timescale and/or in the populations of the equilibrium between the three states the complex can adopt. However, it might also be possible that the complex adopts another, yet uncharacterized state when substrate is available (Wurm, Holdermann, et al. 2017). Furthermore, the presence of the enhancer of decapping Edc3, another protein in the mRNA decapping network, leads to phase separation of the complex at NMR concentrations and, in consequence, a strong signal reduction in the NMR spectra (Damman et al. 2019; Fromm, Kamenz, et al. 2014; Schütz, Nöldeke, and Sprangers 2017). In both cases, the quality of the NMR spectra is not sufficient for a quantitative analysis of the recorded NMR data.

To assess how different mRNA substrates as well as the decapping activators Edc3 and Pat1 (Sharif, Ozgur, et al. 2013) influence the conformations of the decapping complex, we used smFRET experiments to complement our NMR data. To that end, we first tested different combinations of fluorophore labeling positions (one fluorophore in Dcp1 and one in Dcp2) that are expected to result in markedly different FRET efficiencies for the three different states by calculating the FRET efficiencies for each combination of fluorophore labeling positions in Dcp1 and Dcp2 and performing smFRET test measurements. Surprisingly, not all test measurements agreed with the calculated FRET efficiency values for the different pairs of labeling positions. Consequently, we performed NMR measurements of Dcp1:Dcp2 complexes with fluorophore labels attached at different labeling sites and found that for one pair of labeling positions, the closed and the active state of the protein are formed as expected. For all other labeling positions we tested, the

NMR spectra revealed that in the presence of the fluorophores, the conformational equilibrium of the complex is shifted and the active state is not formed any more, which we attribute to interactions between the large fluorescent labels and the protein surface. Consequently, we want to highlight that cross-validating smFRET data when studying dynamic complexes is important as the choice of labeling positions is crucial for a correct interpretation of the FRET efficiencies. For the fluorophore labeling positions we used in our FRET experiments, cross-validation with NMR experiments confirmed that they reliably report on the conformations of the complex. Thus, smFRET measurements of the Dcp1:Dcp2 complex resulted in the same conformational equilibria as were previously found with NMR measurements and the FRET efficiencies for the three different conformations that the complex can adopt could clearly be distinguished and evaluated. Furthermore, we were able to examine the influence of different mRNA substrates and activator proteins on the conformational equilibrium of Dcp1:Dcp2 and we could extend the smFRET measurements to studying how capped RNAs of different lengths and the full length Edc3 protein in combination with RNA substrate affect the conformations of the decapping complex, which so far has not been possible with NMR methods.

2. Results

2.1. Validation of smFRET labeling positions

To efficiently use smFRET experiments to measure conformational changes within the Dcp1:Dcp2 decapping complex, fluorophores had to be attached at specific positions in Dcp1 and Dcp2 such that the distance between the two fluorophores was different for the three possible states the complex can adopt. The efficiency of energy transfer E strongly depends on the distance R between the fluorophores,

$$E = \frac{1}{1 + (\frac{R}{R_0})^6}, \tag{2.1}$$

and the highest sensitivity for distance changes is achieved at fluorophore distances between 0.5 R_0 and 1.5 R_0, with the Förster radius R_0 being defined as the distance at which E = 0.5, meaning half of all photons absorbed by the donor fluorophore are transferred to and absorbed by the acceptor fluorophore. Therefore, for the fluorophores Maleimido DyLight 650 and Phosphine DyLight 550 that we used for our experiments and for which R_0 = 52 Å, their distances could not be below 26 Å or above 78 Å (Schulz et al. 2016). Fluorophore labeling of Dcp1 was achieved via the introduction of a cysteine mutation at the desired labeling site and subsequent cysteine-maleimide coupling with the Maleimido DyLight 650 fluorophore (see section 3.1). Due to the presence of multiple cysteine residues in the wild type Dcp2 protein, we introduced an amber stop codon (UAG) mutation at the desired labeling site in Dcp2 to incorporate the unnatural amino acid AzF into the protein sequence to which the Phosphine DyLight 550 fluorophore could in a later step be ligated via Staudinger Ligation (see section 3.2). To select suitable pairs of labeling positions, we determined the distances between the C_β atoms of the respective mutated amino acids from the known crystal structures of the different conformations of Dcp1:Dcp2 and used these values to calculate the corresponding FRET efficiencies via Equation 2.1. It must be noted that the calcualted FRET efficiencies are only rough estimates as the fluorophores are flexible and an exact modeling of the fluorophores was not possible due to missing information about the fluorophore structures from the manufacturer's side. Labeling sites were then chosen based on a significant difference between the FRET efficiency values for the closed and the active conformation, as the open conformation of the complex is highly dynamic, due to only few contacts between the two Dcp2 domains, and therefore the known crystal structure (PDBiD 2QKM, chains C and D) represents only one out of many different possible domain orientations (She, Decker, Chen, et al. 2006). The FRET efficiency value for the open conformation was later determined from measurements of the Dcp1:Dcp2 complex carrying a point mutation through which the open conformation is stabilized. In addition, amino acids used

Labeled amino acid pair	Active (PDBiD 5n2v)		Closed (PDBiD 2qkm)	
	Distance [Å]	FRET efficiency	Distance [Å]	FRET efficiency
22:215 (*)	57	0.37	26	0.98
42:215 (*)	49	0.59	29	0.97
100:119	47	0.65	23	0.99
112:202	57	0.37	51	0.53
100:202	62	0.26	42	0.78
22:202	65	0.21	40	0.83
119:215 (*)	61	0.28	41	0.81
61:215 (*)	63	0.24	32	0.95
119:135	36	0.90	57	0.37
119:154	42	0.78	67	0.18

Table 2.1.: Test positions for fluorophore labeling of Dcp1 and Dcp2 (denoted as 22:215 Dcp1 being labeled at residue 22 and Dcp2 at residue 215). The distance between the fluorophore labeling positions had to be substantially different between the closed and in the active conformation and they were determined from distance measurements between the C_β atoms of the respective amino acids in the crystal structures of the closed and the active conformation of the decapping complex (PDBiD 2qkm, chains A and B and PDBiD 5n2v). Residues 207-218 of Dcp2 in the active conformation are not resolved in the crystal structure and so the distances were determined between the C_β atom of the respective amino acid in Dcp1 and Asn217 in Dcp2 (labeled with a (*)). Furthermore, residues 40-43 of Dcp1 in the closed conformation are not resolved, so the distances were determined between the C_β atom of amino acid Asp39 in Dcp1 and M215 in Dcp2. FRET efficiency values were calculated using Equation 2.1.

for fluorophore labeling could not be conserved or involved in interactions with substrate or activator proteins or in interactions between the RD and CD of Dcp2. Only pairs of labeling positions fulfilling these criteria were used for subsequent validation and test measurements. Test measurements were performed for different fluorophore positions on i) the free complex, as from solution NMR it is known that it adopts the closed conformation to 94 % and the open conformation to 6 %, and on ii) the Dcp1:Dcp2 complex after addition of Edc1, m^7GDP and Mg^{2+}, as this leads to the formation of the active conformation (Wurm, Holdermann, et al. 2017).

Table 2.1 shows all tested pairs of labeling positions, their respective distances obtained from the crystal structures, and the corresponding calculated FRET efficiencies for the closed and for the active conformation. FRET histograms from the corresponding test measurements are shown in Figure 2.1.

For fluorophore labels at amino acid 119 in Dcp1 and at amino acid 154 in Dcp2 (denoted as 119:154; Figure 2.2), the measured FRET efficiencies are well separated and agree with the calculated, expected values from the preceding theoretical considerations (Figure 2.1 J). For labeling positions 22:215, 42:215 and 100:119 (Figure 2.1 A-C), measurement results also agree with the calculated values and their populations are well separated in the FRET histogram. Due to very high FRET values close to 1 for the free complex, however, fitting the data to Gaussian distributions is not viable and so these positions were excluded from further measurements. For labeling positions 112:202 and 100:202 (Figure 2.1 D, E), the measured FRET efficiency values differ from the calculated values and they are nearly identical for both the closed and the active conformation. The reason for this might be that the attachment of fluorophores to the proteins changes the conformational equilibrium of the complex or the fluorophores might block the formation of the active or the closed state. Slight deviations between the calculated and the measured

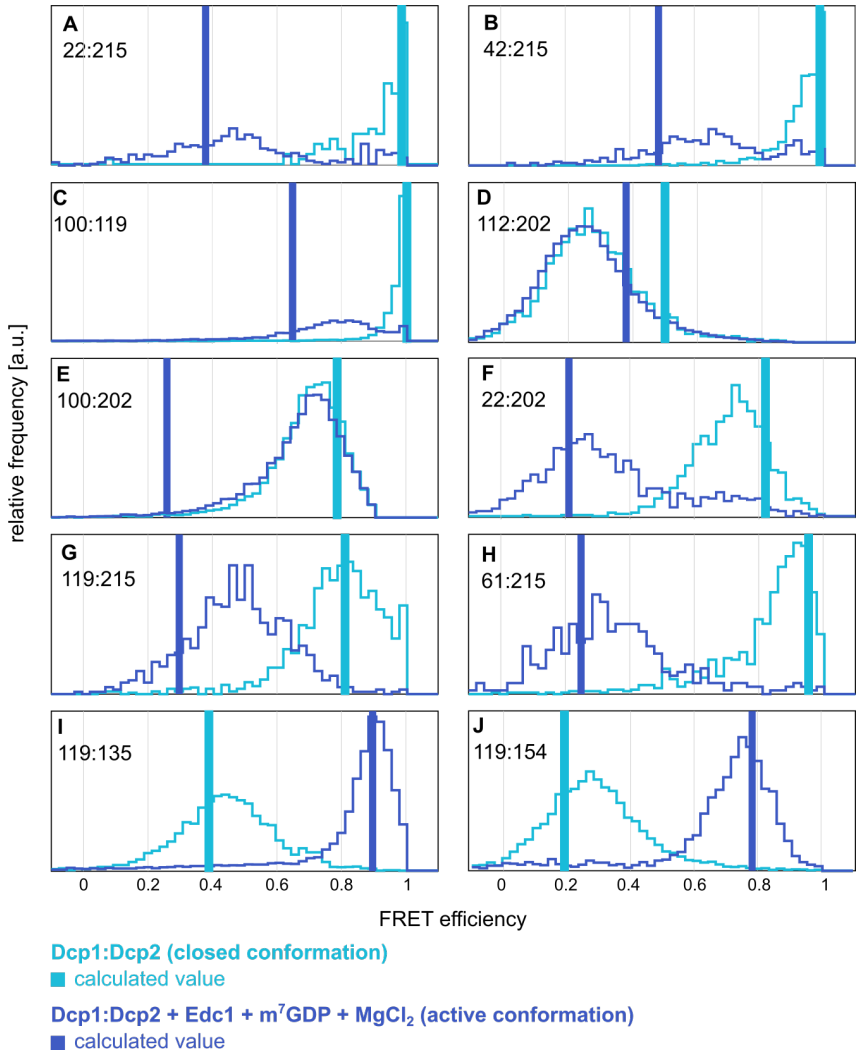

Figure 2.1.: Calculated and measured FRET efficiencies for different fluorophore labeling positions of the closed and the active state. The FRET efficiency values for the closed and the active conformation must be distinguishable in order to accurately report on the population of each conformation. The light blue curves show the results of smFRET measurements of the apo complex in its closed conformation and the dark blue curves show smFRET measurement results after addition of Edc1, m^7GDP and $MgCl_2$, which induces the active conformation of the complex ((Wurm, Holdermann, et al. 2017)). The calculated values for each conformation is shown as light blue (closed conformation) or as dark blue (active conformation) bars.

efficiency values are however expected and tolerated as the size and flexibility of the fluorophores were not taken into account when determining the distances between the fluorophores from the crystal structures. Of all tested labeling positions, pairs 22:202, 119:215, 61:215, 119:135 and 119:154 (Figure 2.1 F-J) show good agreement between the calculated and the measured FRET efficiency values and the closed and the active conformation are clearly distinguishable in the FRET histograms.

These pairs were next used to test if also the open conformation of the complex is formed and can be distinguished from the closed and the active conformation in the FRET histogram. To that end, we introduced the mutations W43A and Y220G in Dcp2 as both mutations are known to destabilize the closed state and thereby shift the equilibrium of the complex towards the open state. In comparison, the stronger destabilizing effect on the closed conformation is reported for the W43A mutation (Paquette et al. 2018; Tibble et al. 2020; Wurm, Holdermann, et al. 2017). In smFRET

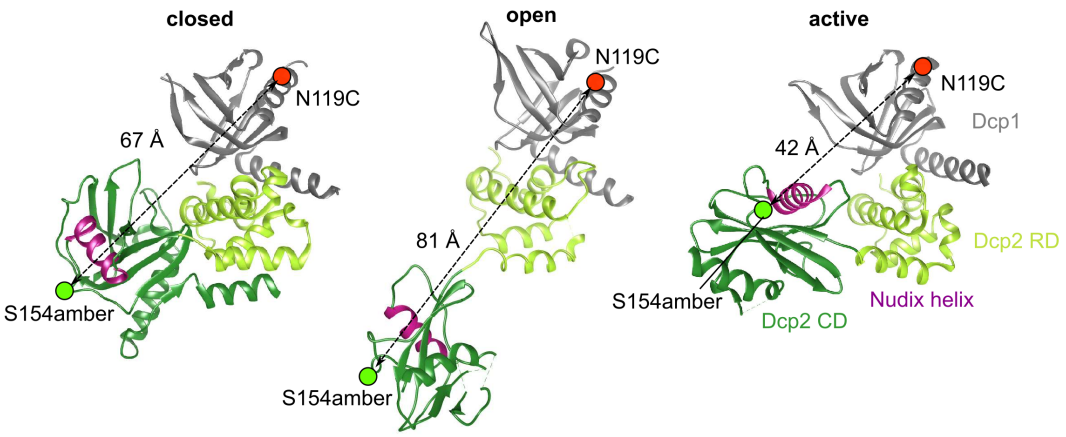

Figure 2.2.: Distances between fluorophore labeling positions in the open, closed and active conformations of Dcp1:Dcp2. For fluorophores at positions 119 in Dcp1 (green circle) and 154 in Dcp2 (red circle), their distances differ significantly between the closed (PDBiD 2qkm, chains A,B), open (PDBiD 2qkm, chains C,D) and active conformation (PDBiD 5n2v).

experiments of the mutated complex in the open conformation we found that the presence of fluorophores either prevents the formation of the open conformation or the FRET efficiency value for the open state overlaps with the value for the closed conformation for labeling pairs 119:215, 22:202 and 119:135 (Figure 2.3 A).

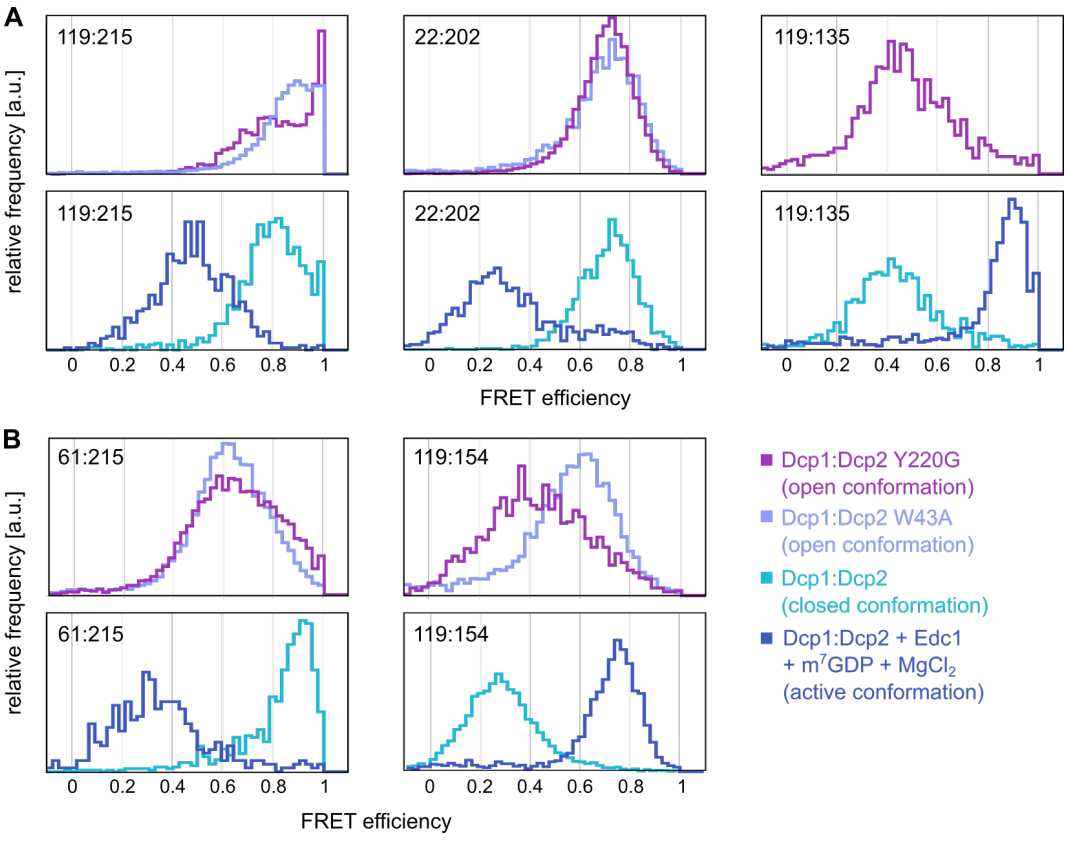

Figure 2.3.: FRET efficiencies for different fluorophore labeling positions of the open state. To be able to distinguish and quantify all three conformations of the mRNA decapping complex, the corresponding peaks in the smFRET histograms must be distinguishable. For labeling positions 119:215, 22:202 and 119:135, the peak for the open state, which is formed through the mutations W43A (purple lines) or Y220G (pink lines) in Dcp2, either overlaps with the peak for the closed state (light blue lines) or the open state was not formed correctly. For labeling positions 61:215 and 119:154, the open conformation is formed and results in a peak that can be distinguished from the peaks for the closed and for the active (dark blue lines) conformation.

As for these pairs no three distinct FRET populations could be distinguished for the open, closed and active conformation, they were also excluded from further measurements. For labeling positions 61:215 and 119:154, in contrast, smFRET measurements of the complex carrying the W43A or the Y220G mutation show a clearly distinguishable peak that corresponds to the open state (Figure 2.3 B). Moreover, a stronger destabilization of the closed state by the W43A mutation is observed for labeling positions 119:154, so fluorophore labeling at residue 119 in Dcp1 and residue 154 in Dcp2 results in the best agreement with the known behaviour of the complex.

2.2. NMR experiments with fluorophore labeled Dcp1:Dcp2

In the preparation and test measurement phase, fluorophore labeling positions for the Dcp1:Dcp2 mRNA decapping complex were chosen such that there is a large difference in FRET efficiencies between the three different conformations the complex can adopt. To that end, we calculated theoretically expected FRET efficiency values for different pairs of fluorophore labeling positions and compared these values to subsequent smFRET measurements of the labeled complexes. For labeling positions 119:154, the calculated and the measured FRET efficiency values were in good agreement (Figure 2.1 J). Against our expectations however, the calculated and the measured FRET efficiency values for labeling positions 112:202 and 100:202 did not agree and in addition, the values for the closed and the active conformation showed strong overlap for these labeling sites. We therefore assumed that attaching fluorophores to the complex can shift the equilibrium of its conformations and that the fluorophores could block the formation of the active (pair 100:202; Figure 2.1 E) or of the closed state (pair 112:202; Figure 2.1 D). To validate this assumption, we performed NMR experiments on the Dcp1:Dcp2 complex in its closed and in its active state with and without fluorophores attached at the different labeling sites. To exclude that the mutations introduced for site-specific fluorophore labeling have an influence on the conformations of Dcp1:Dcp2, we labeled the methionine methyl groups of Dcp2 with $^{13}CH_3$ and recorded methyl ^{1}H-^{13}C correlation NMR spectra of the free Dcp1:Dcp2 complex, which adopts the closed conformation in solution, and of the complex after addition of Edc1 and m^7GDP, which adopts the active conformation, all carrying the respective mutations including amber suppression with AzF (N119C:S154amber, N100C:M202amber, N112C:M202amber) and compared the resulting spectra to NMR spectra of the wild type protein.

From previous studies it is known that the ^{1}H-^{13}C resonances of methionines 221 and 164 of Dcp2 directly report on the conformation of the Dcp1:Dcp2 complex. Both methionines are located at the interface between the CD and the RD of Dcp2 (Figure 2.4 A, B) and they are very sensitive to changes in domain orientation of the Dcp1:Dcp2 complex. The corresponding methionine resonances appear at very distinct positions in the ^{1}H-^{13}C methyl-TROSY spectrum for the protein in its closed or in its active conformation (Figure 2.4 C) (Wurm, Holdermann, et al. 2017). An overlay of the spectra of the complexes carrying the point mutations with spectra of the Dcp1:Dcp2 wild type shows no chemical shift differences for resonances

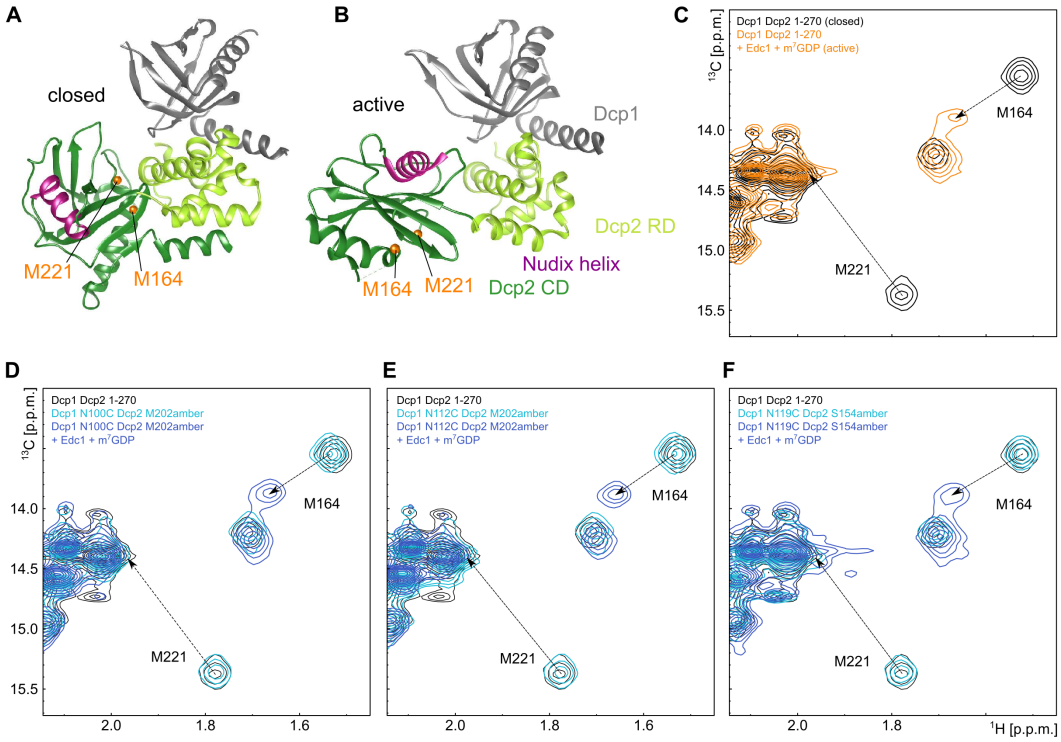

Figure 2.4.: NMR spectra of Dcp1:Dcp2 with cysteine and amber stop codon point mutations. Crystal structures of Dcp1:Dcp2 in (A) the closed conformation (PDBiD 2qkm, chains A,B) and (B) in the active conformation (PDBiD 5n2v). NMR active residues M164 and M221 are colored in orange. (C) NMR spectra of wild type Dcp1:Dcp2 1-270 in the closed conformation (black) and in the active conformation after addition of Edc1 and m^7GDP (orange). (D-F) Comparison of the spectra of the Dcp1:Dcp2 1-270 wild type in the closed conformation (black) and the complex with point mutations in Dcp1 (N100C, N112C, N119C) and Dcp2 (M202amber, M154amber). The spectra show that the mutations do not change the conformational equilibrium (light blue). The active state of the complex carrying the mutations is formed after addition of Edc1 and m^7GDP, which can be monitored by the shift of peaks M164 and M221 to the position of the active state (dark blue).

M221 and M164 neither in the free form nor after induction of the active state through adding Edc1 and m^7GDP (Figure 2.4 D-F). We conclude that the mutations do not largely alter the conformational equilibrium of the complex.

NMR measurements of the complexes which were additionally labeled with fluorophores, however, differed depending on the fluorophore position. For pair 100:202, the presence of fluorophores influences the closed conformation of the complex by stabilizing the closed state more strongly and after addition of Edc1 and m^7GDP, this stabilization of the closed state increases even more, while the formation of the active state is prevented (Figure 2.5 A).

For pair 112:202, the attachment of fluorophores does not influence the formation of the closed state of the complex as can be seen by a good overlap of resonances M221 and M164 with the NMR spectra of the wild type proteins (Figure 2.5 B). However, the active conformation is not clearly formed any more upon addition of Edc1 and m^7GDP and the reporter resonances either disappear from the spectrum, or, more likely, are broadened beyond detection which hints at an equilibrium between different conformations of the complex that are in intermediate exchange. In either case, a full formation of the active state as for the wild type cannot be observed for labeling positions 112:202. For labeling pair 119:154, the spectra in the free form of the complex and after formation of the active state do not differ from the wild type spectra and so for these positions, the closed and the active

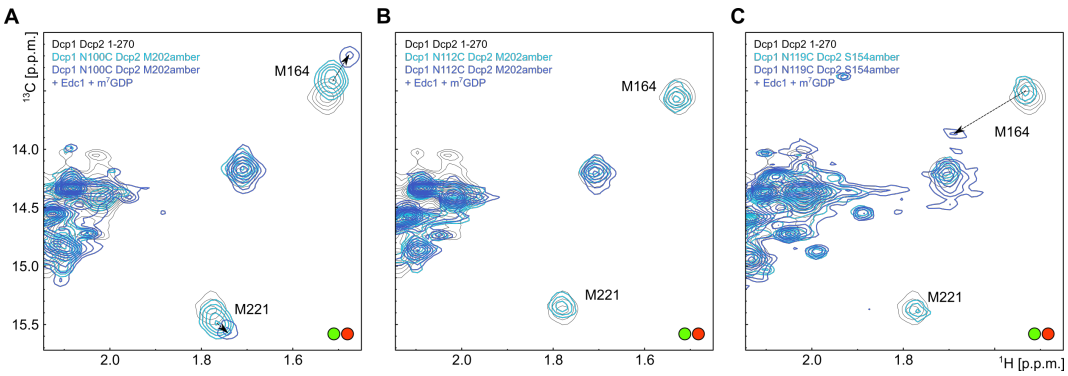

Figure 2.5.: NMR spectra of Dcp1:Dcp2 with fluorophore labels. (A) The position of fluorophore labels on the Dcp1:Dcp2 mRNA decapping complex has a significant impact on the conformation of the complex. For fluorophores at labeling positions 100:202, the closed conformation is more populated than in the wild type complex and the addition of Edc1 and m^7GDP leads to an even stronger stabilization of the closed conformation instead of inducing the active conformation. (B) For fluorophores at labeling positions 112:202, the closed conformation is formed as for the wild type, but upon addition of Edc1 and m^7GDP, peaks M221 and M164 disappear. (C) For fluorophores at positions 119:154, both the open and the active conformation are formed.

conformations form as expected (Figure 2.5 C).

We conclude that the positions of the fluorophores in the Dcp1:Dcp2 complex have a strong influence on the conformational equilibrium of the complex and the fluorophores can, depending on their position, block the formation of the active state. As a consequence, results from smFRET measurements can be completely distorted by an inappropriate choice of labeling positions, which in turn makes a good choice of labeling positions crucial for a correct interpretation of FRET efficiencies. In our case, the labeling positions 119:154 were shown to be well suited for studying the conformations of the Dcp1:Dcp2 mRNA decapping complex with smFRET measurements and they were therefore used for further studies.

2.3. smFRET measurements of the Dcp1:Dcp2 decapping complex

Preliminary smFRET experiments and NMR measurements of the Dcp1:Dcp2 mRNA decapping complex confirmed that the complex adopts its closed conformation in the absence of substrate. Subsequent smFRET measurements using fluorophore labeling positions 119:154 revealed one large and one small peak in the FRET histogram which we assigned to the closed, inactive, and to the open conformation, respectively (Figure 2.6). The closed conformation was detected at a FRET efficiency of 0.20 ± 0.04 and the open conformation at a FRET efficiency of 0.47 ± 0.03. The open conformation was identified based on the position of the peak maximum in previous test measurements

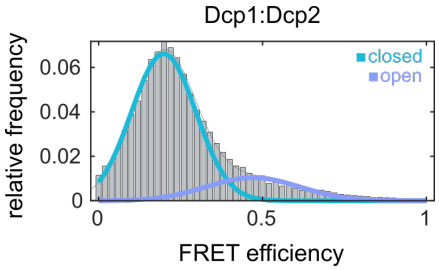

Figure 2.6.: smFRET measurements of the apo Dcp1:Dcp2 1-270 mRNA decapping complex using fluorophore labeling positions 119:154. smFRET experiments of the Dcp1:Dcp2 1-270 complex reveal one large (light blue) and one small peak (violet) in the FRET histogram, corresponding to the closed, inactive, and to the open conformation, respectively. These results agree with data from previous NMR measurements ((Wurm, Holdermann, et al. 2017)).

of the W43A mutant of Dcp2, which fully adopts the open conformation of the decapping complex (Figure 2.7). From Gaussian fits of the histogram, populations of 81 % and 19 % could be extracted for the closed and the open state, respectively. These values agree reasonably well with existing data from NMR experiments, in which it was found that the complex exchanges between the closed and the open conformation and that the closed conformation is adopted to 94 % in the absence of substrate (Wurm, Holdermann, et al. 2017).

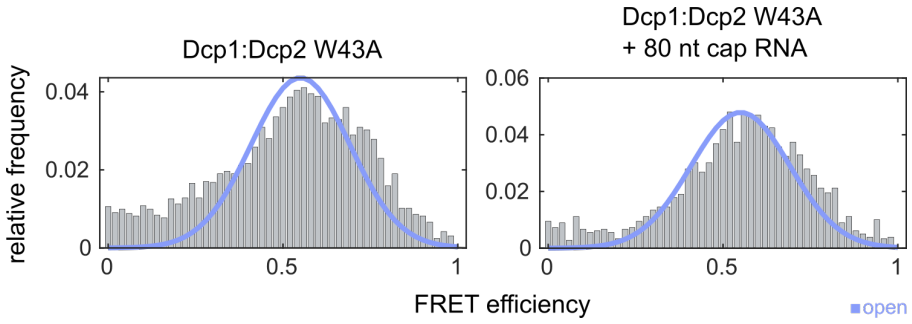

Figure 2.7.: smFRET measurements of Dcp1:Dcp2 1-270 W43A (fluorophores at positions 119:154) without and with an 80 nt capped mRNA. The mutation W43A in Dcp2 leads to the stabilization of the open conformation of the complex both in the presence and in the absence of capped RNA. smFRET measurements of the complex carrying the W43A mutation were used to determine the position of the open conformation in the FRET histogram.

A clear shift of FRET efficiencies to a higher value (0.73 ± 0.00), and thus a shift to the active conformation, is observed upon addition of Edc1 and a 15 nt or a 80 nt capped mRNA to the Dcp1:Dcp2 complex (Figure 2.8, middle and right panel). Edc1 together with capped RNA stabilizes the complex fully in its active state, which is reflected by the single strong peak in the FRET histogram. This finding is in agreement with previously obtained NMR data (Wurm, Holdermann, et al. 2017). We conclude that, by comparing our results to NMR data, the pair of labeling positions 119:154 that we chose for our smFRET experiments, cannot only be used to detect the different conformations of the decapping complex but it can also be used to correctly quantify their populations. It has to be noted that the activator protein Edc1 alone does not have a strong influence on the conformations of Dcp1:Dcp2 and it only slightly increases the population of the active state (Figure 2.8, left panel). A complete shift to the active conformation could only be detected when capped RNA was present at the same time.

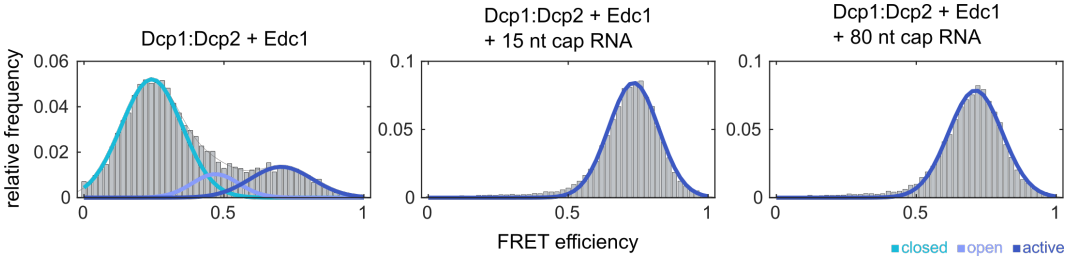

Figure 2.8.: smFRET measurements of Dcp1:Dcp2 1-270 (fluorophores at positions 119:154) with Edc1 and without (left panel) or with capped RNA (middle and right panel). The activator protein Edc1 alone only slightly increases the population of the active conformation of Dcp1:Dcp2, and a complete shift to the active conformation can be detected when capped RNA is present at the same time.

The addition of capped RNA only to Dcp1:Dcp2 results in NMR spectra with severely broadened peaks, which indicates that the open-closed equilibrium of

the apo complex is lifted and the complex adopts multiple conformations (Wurm, Holdermann, et al. 2017). The low quality of the NMR spectra however prevents a quantitative evaluation of the distribution of populations.

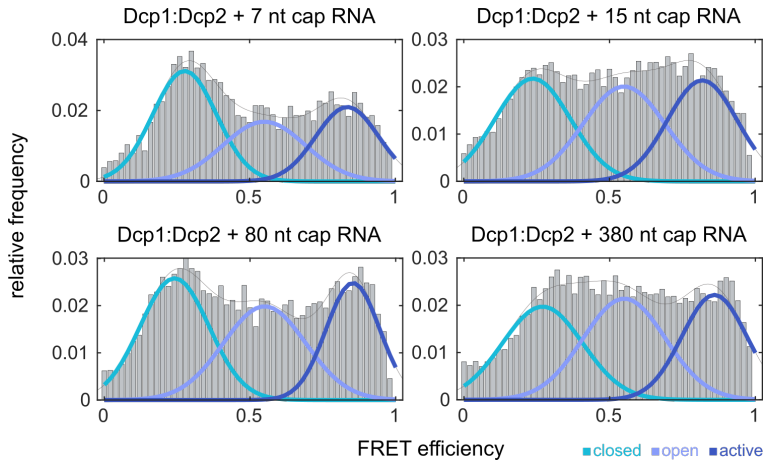

Figure 2.9.: smFRET measurements of Dcp1:Dcp2 1-270 (fluorophores at positions 119:154) with capped RNAs of different lengths. Addition of capped RNA increases the population of the open and of the active conformation of the Dcp1:Dcp2 complex.

smFRET experiments reveal that indeed, the conformational equilibrium of the decapping complex shifts upon addition of capped RNA and an increase of the open and of the active state can be observed. The distribution of populations is however very broad and no clearly separable peaks are visible in the FRET histograms. For quantification, the binned FRET efficiency values were fitted to three Gaussian functions, each with width < 0.2 and using the FRET efficiencies for the three different states obtained from previous measurements as initial fit parameters (see section 7.2). Results from the fits reveal that the closed, open and active conformation of the complex are populated to nearly equal amounts in the presence of capped RNA and this result is independent of the length of the added RNA, as the distribution of populations remains similar after the addition of a 7 nt, 15 nt, 80 nt or a 380 nt capped RNA (Figure 2.9). Interestingly, the FRET efficiency for the active state is shifted to a considerably higher value in the presence of capped RNA compared to the FRET efficiency of the active conformation in the presence of both capped RNA and Edc1 (see Figure 2.8). This result is also independent of RNA length. We assume that in both cases the active conformation is formed and no new conformation is detected. The difference in FRET efficiencies for the active state might instead be explained by the presence of Edc1, which could influence the rotation of the fluorophores or their orientation towards each other, or, alternatively, Edc1 binding at a position between the fluorophores could increase the distance between the fluorophores. All these explanations would result in a lower FRET efficiency value in the presence of Edc1, as is observed in our experiments. A more detailed dicussion will be presented in chapter 3.

In previously published literature it is reported that the Pat1 and Edc3 proteins increase the activity of Dcp1:Dcp2 (Lobel, Tibble, and Gross 2019; Paquette et al. 2018). However, in our smFRET measurements both the addition of Pat1 or the LSm domain of Edc3 do not influence the conformation of the decapping complex in the absence of RNA, as no significant change in the corresponding FRET histograms can be seen, but the complex remains mainly in the closed state (Figure 2.10, left panels). Furthermore, also the additional presence of capped RNA does not induce a major conformational change (Figure 2.10 middle and right panels) compared

to when only capped RNA is present with the decapping complex but no Pat1 or Edc3 (see Figure 2.9). In the case of adding the Edc3 LSm domain and capped RNA to the decapping complex, all three conformations are present to similar amounts. When instead Pat1 and capped RNA are added, again all three conformations are present, but the closed conformation is populated to a slightly larger degree than the open and the active conformation. A stabilization of the active conformation through the activator proteins Pat1 or the LSm domain of Edc3 could therefore, both in presence and in the absence of capped RNA, not be observed.

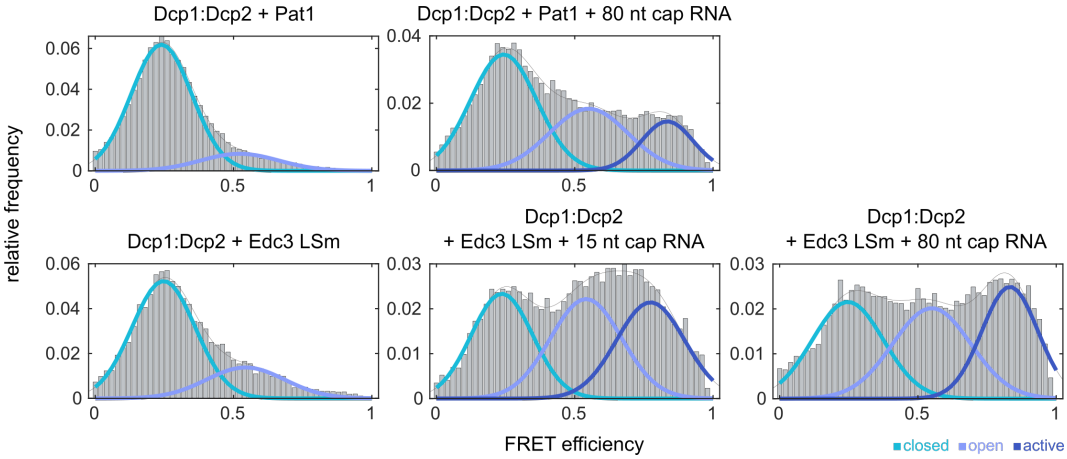

Figure 2.10.: smFRET measurements of Dcp1:Dcp2 1-270 (fluorophores at positions 119:154) with Pat1 or Edc3. Pat1 as well as the Edc3 LSm domain do not have an influence on the conformation of Dcp2 and do not stabilize the active state with RNA. This is surprising, as Edc3 and Pat1 are both reported to increase the activity of the enzyme (Lobel, Tibble, and Gross 2019; Paquette et al. 2018).

At micromolar concentrations, the decapping complex undergoes liquid-liquid phase separation in the presence of full length Edc3 and RNA, so their influence on the conformations of Dcp1:Dcp2 cannot be studied using NMR (Schütz, Nöldeke, and Sprangers 2017; Tibble et al. 2021). For smFRET experiments, however, much lower protein concentrations in the picomolar range are sufficient and there the complex remains soluble. We were thus able to perform smFRET measurements of the complex with full length Edc3 together with a 7 nt capped RNA.

Longer RNAs, especially RNAs longer than 30 nucleotides, strongly shift the liquid-liquid phase separation boundaries to lower Edc3 and Dcp1:Dcp2 concentrations (Schütz, Nöldeke, and Sprangers 2017), so we used an only 7 nt short capped RNA for our smFRET experiments to prevent liquid-liquid phase separation of Edc3 and capped RNA, while still being able to keep the RNA concentration at 15 µM to ensure saturation of Dcp2. In addition, it was found previously that the first five nucleotides of capped RNA interact with the Dcp2 catalytic domain at a position between the m^7G binding site and a Box B region that follows the NUDIX domain and that is involved in methyl-cap-specific hydrolysis activity (Piccirillo, Khanna, and Kiledjian 2003; Wang, Jiao, et al. 2002; Wurm, Holdermann, et al. 2017). For this

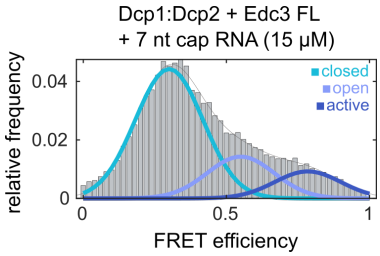

Figure 2.11.: smFRET measurements of Dcp1:Dcp2 1-270 (fluorophores at positions 119:154) with Edc3 FL and capped RNA. Dcp2 in complex with full length Edc3 and RNA substrate phase separates at NMR concentrations but remains disperse at the low concentrations needed for FRET measurements. However, also here, no stabilization of the active state can be observed.

reason we kept the length of the capped RNA above five nucleotides. Subsequently, we performed smFRET measurements of Dcp1:Dcp2 with full length Edc3 together with a 7 nt capped RNA. However, also for this complex, no stabilization of the active state is observed, as is shown in Figure 2.11.

Finally, ADP, the decapping product m^7GDP and an uncapped 80 nt 5'OH RNA were added individually (Figure 2.12). For ADP and m^7GDP, a clear shift towards the active or the open conformation could not be observed compared to the samples with only capped RNA. This might indicate that the complex will return to the apo conformation after the decapping reaction. For the uncapped RNA, however, the active state is populated to some degree, so the active state can already be formed through interactions with only the RNA body and does not strictly require the RNA cap. An overview over all Dcp1:Dcp2 populations obtained by smFRET measurements is given in Figure 2.13 and corresponding values are listed in Table 2.2.

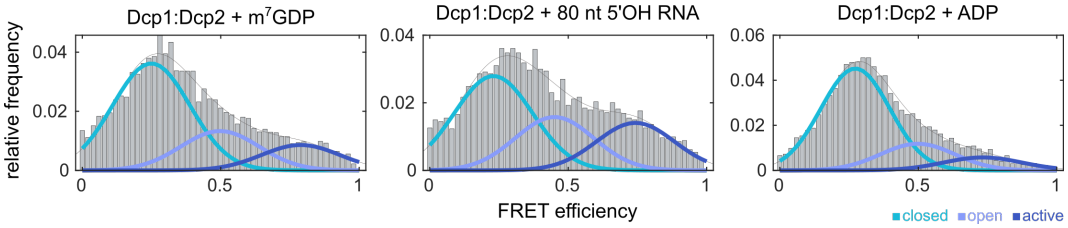

Figure 2.12.: smFRET measurements of Dcp1:Dcp2 1-270 with ADP, m^7GDP and 5'OH RNA. For ADP and the decapping product m^7GDP, no clear shift towards the active or the open conformation can be detected. This might reveal that the complex will return to the apo conformation after mRNA decapping. Adding 5'OH RNA leads to some remaining signal for the active state, indicating that the formation of the active state can still occur through interactions with the mRNA body and does not necessarily need the mRNA cap.

Construct	closed	open	active
Dcp1:Dcp2	0.81	0.19	0.00
Dcp1:Dcp2 + Edc1	0.70	0.11	0.19
Dcp1:Dcp2 + Edc3 LSm	0.75	0.25	0.00
Dcp1:Dcp2 + 5' OH RNA (80 nt)	0.48	0.28	0.24
Dcp1:Dcp2 + 15 nt capped RNA	0.34	0.36	0.30
Dcp1:Dcp2 + Edc1 + 15 nt capped RNA	0.00	0.00	1.00
Dcp1:Dcp2 + Edc3 LSm + 15 nt capped RNA	0.32	0.36	0.32
Dcp1:Dcp2 + m^7GDP	0.62	0.24	0.14
Dcp1:Dcp2 + 80 nt capped RNA	0.38	0.35	0.27
Dcp1:Dcp2 + Edc1 + 80 nt capped RNA	0.00	0.00	1.00
Dcp1:Dcp2 + Edc3 LSm + 80 nt capped RNA	0.34	0.36	0.30

Dcp1:Dcp2 + ADP	0.70	0.20	0.10
Dcp1:Dcp2 + Pat1	0.85	0.15	0.00
Dcp1:Dcp2 + Pat1 + 80 nt capped RNA	0.51	0.33	0.16
Dcp1:Dcp2 W43A	0.00	1.00	0.00
Dcp1:Dcp2 W43A + 80 nt capped RNA	0.00	1.00	0.00
Dcp1:Dcp2 + 380 nt capped RNA	0.34	0.38	0.28
Dcp1:Dcp2 + 7 nt capped RNA (5 μM)	0.65	0.22	0.13
Dcp1:Dcp2 + 7 nt capped RNA (15 μM)	0.55	0.21	0.24
Dcp1:Dcp2 + 7 nt capped RNA (20 μM)	0.43	0.30	0.27
Dcp1:Dcp2 + 7 nt capped RNA + Edc3 FL	0.66	0.21	0.13

Table 2.2.: Overview over Dcp1:Dcp2 populations obtained with smFRET measurements using fluorophore labeling positions 119:154.

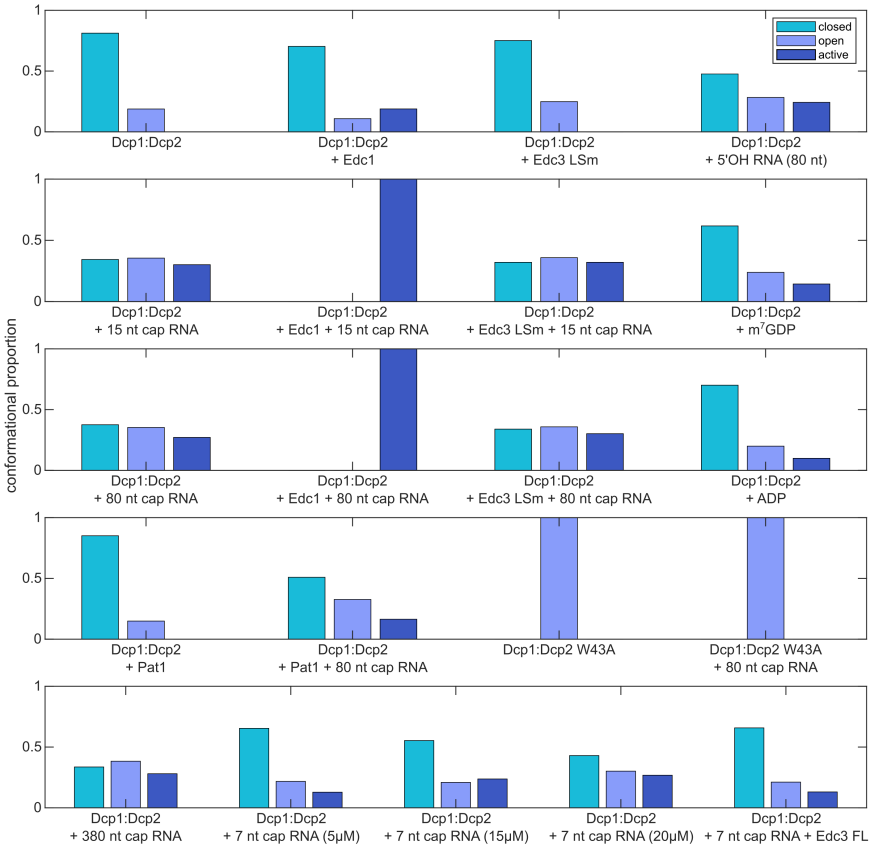

Figure 2.13.: Overview over Dcp1:Dcp2 populations obtained with smFRET measurements using fluorophore labeling positions 119:154. Corresponding values can be found in Table 2.2.

3. Discussion

smFRET experiments are an important method in structural biology to study the conformations and conformational changes of proteins. In this work we showed that smFRET is a suitable method to study the conformational equilibria of the mRNA decapping complex Dcp1:Dcp2 from *S. pombe*. To that end, we theoretically determined ten different combinations of fluorophore labeling positions on Dcp1 and Dcp2 that we expected to yield different FRET efficiencies for the three states the complex can adopt. Interestingly, only two combinations of labeling positions could report on all three states of the protein, so it is not generally correct that any pair of fluorophore labeling positions guarantees reliable measurement results. Thus, in subsequent NMR measurements we could show that for some theoretically predicted suitable labeling pairs, the formation of the active state of the Dcp1:Dcp2 complex is prevented in the presence of the fluorophore labels. More importantly, however, we could confirm that one pair of fluorophore labeling positions is suited to report on the conformations of the decapping complex by performing NMR measurements on the fluorophore labeled complex. Using these validated labeling positions, we could detect the conformations of the mRNA decapping complex in subsequent smFRET experiments and quantitatively confirm previously obtained NMR data of the closed, open and active state of the complex. Next, we extended our smFRET measurements to complexes which are not suitable for NMR studies and so we were able to show that upon addition of capped mRNA to the decapping complex, three peaks can be distinguished in the FRET histogram and we assigned them to the closed, the open and the active conformation. Binding of capped RNA therefore increases the population of the open and of the active conformation such that all conformations are present to similar amounts. This points to an increase in dynamics of Dcp1:Dcp2 in the presence of mRNA substrate and could also explain the strong peak broadening in the corresponding NMR spectra. Moreover, this result is independent of RNA length, as the FRET histograms do not display significant differences for a 7 nt, 15 nt, 80 nt and a 380 nt long capped RNA. We thus conclude that Dcp2 does not act specifically only on capped RNAs of distinct lengths, as it is the case for example for the scavenger decapping enzyme DcpS (Fuchs et al. 2020; Liu 2002). Interestingly, the peak maximum for the active conformation in the presence of capped RNA deviates from the FRET efficiency value of the active state that is formed together with Edc1 and it is shifted to higher FRET efficiencies. A possible explanation could be that under these conditions, a new, yet unknown conformation is formed which is adopted before the fully active state is stabilized. It can however be excluded that this conformation corresponds to the crystal structure of Dcp1:Dcp2:Edc1 from *S. pombe* in the active state that was published by Valkov et al. (PDBiD 5J3T) (Valkov et al. 2016) and that has not been observed in solution, because in that structure, the distance R between the C_β atoms of the fluorophore labeled amino acids would be too large (R = 61 Å; E = 0.27) to result in the FRET

efficiency of the active state we measured in our experiments (E = 0.85 for adding an 80 nt capped RNA) (Figure 3.1).

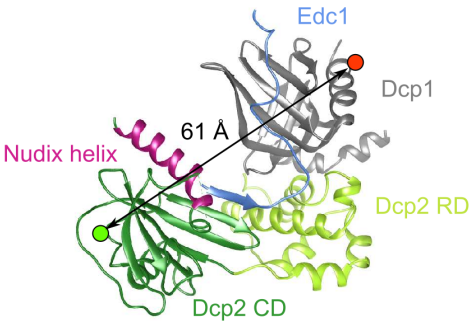

Figure 3.1.: Crystal structure of *S. pombe* Dcp1:Dcp2:Edc1 in the active conformation published by (Valkov et al. 2016) (PDBiD 5J3T). Calculation of the FRET efficiency for fluorophores at positions 119:154 results in E = 0.27.

A more likely explanation for the discrepancy between the FRET efficiencies of the active state in the presence and in the absence of Edc1 is that binding of Edc1 influences the FRET efficiency values by altering the orientation of the fluorophores towards each other or by interfering with their free rotation, which consequently leads to a decrease in energy transfer efficiency between the fluorophores and thus to the lower FRET efficiencies measured in the presence of capped RNA and Edc1. Moreover, binding of Edc1 to the complex at a position between the two fluorophores could lead to an increase in distance between the fluorophores and therefore result in a lower energy transfer efficiency. To support this explanation, crystal structures from Dcp1:Dcp2 from *K. lactis* in the active conformation display a shorter distance between the C_β atoms of the fluorophore labeled amino acids in the absence of Edc1 (PDBiD 5LOP; 36 Å; Figure 3.2 A) (Charenton, Taverniti, et al. 2016) than in the presence of Edc1 (PDBiD 6AM0; 39 Å; Figure 3.2 B) (Mugridge, Tibble, et al. 2018). This points towards a situation in which the presence of Edc1 increases the distance between the fluorophores which decreases the FRET efficiency.

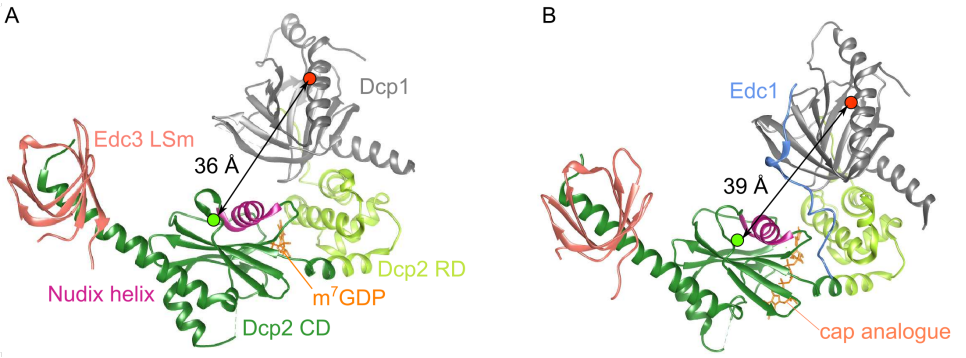

Figure 3.2.: Distances between fluorophore labeling positions in the active conformation of *K. lactis* Dcp1:Dcp2 in the absence (PDBiD 5LOP) and in the presence of Edc1 (PDBiD 6AM0). (A) In the absence of Edc1, the distance between the C_β atoms of the fluorophore labeled amino acids is shorter than (B) in the presence of Edc1.

In addition to studying the influence of capped RNAs of different lengths on the conformations of the Dcp1:Dcp2 decapping complex, we assessed whether different activator proteins and other substrates have an influence on the conformations of Dcp1:Dcp2. It was reported previously that binding of Pat1 and Edc3 enhances the activity of the decapping complex (Lobel, Tibble, and Gross 2019; Paquette et al. 2018). In our studies, however, we did not observe the formation of a stable active conformation of Dcp1:Dcp2 upon binding of Pat1 and Edc3. Furthermore, by comparing the effect of capped RNA and uncapped RNA on the conformation of the decapping complex, we found that the presence of the m^7G cap structure is not

absolutely essential for the formation of the active state, although it has a stabilizing effect on the active conformation. This result is supported by previous evidence from crystal structures, in which the active state of the complex is formed in the presence of cap analogues or m^7GDP (Charenton, Taverniti, et al. 2016; Mugridge, Ziemniak, et al. 2016; Mugridge, Tibble, et al. 2018; Wurm, Holdermann, et al. 2017). Importantly though, we were able to examine Dcp1:Dcp2 in complex with the full length Edc3 protein and a short, capped mRNA. This has not been possible so far in NMR studies as these components together undergo liquid-liquid phase separation at the high concentrations required for NMR measurements. smFRET experiments are performed at picomolar concentrations, so the complex remains soluble and measurements could be performed. However, also here, a shift to the active conformation of the Dcp1:Dcp2 complex could not be observed. We therefore conclude that an activation of the decapping complex by full length Edc3 and RNA (Harigaya et al. 2010; Paquette et al. 2018) does not occur via the stabilization of the active state but it must proceed via a different pathway. This also makes sense on a structural level, as only Edc1 binds to both domains in the active state.

In sum, our studies of the mRNA decapping complex with single molecule FRET methods reflect the high degree of complexity of the various interactions of Dcp2 with substrates and decapping factors and its corresponding conformational rearrangements. We also want to highlight that the choice of fluorophore labeling positions is crucial for a correct interpretation of the FRET efficiencies and should always be cross-validated.

In the future it would be interesting to use smFRET methods to examine the conformations of the Dcp1:Dcp2 complex in its liquid-liquid phase separated state. In the disperse phase, we did not observe a shift to the active state of the complex in the presence of Edc3, but it has been shown recently that the activating effect of Edc3 is much stronger in the phase separated state (Tibble et al. 2021). An examination with smFRET methods would require the mixing of labeled and non-labeled decapping complexes to detect only the fluorescence signal from one complex at a time and to prevent an energy transfer between two different labeled complexes in the much more condensed phase separated state.

Part VI.

Solid state NMR of mRNA decapping enzymes

Results presented in this part were obtained in collaboration with A. Adler and M. Baldus from Utrecht University. A.A. packed the ssNMR rotors and recorded and analysed the NMR spectra. C. Krempl prepared the protein samples including their maturation. R. Sprangers and M. Baldus supervised the project.

1. Introduction

Liquid-liquid phase separation (LLPS) is a process in which two or more miscible liquids demix and separate into distinct phases. In eukaryotic cells, LLPS is a mechanism of biomolecular organization in which proteins and nucleic acids demix, assemble and condense into membrane-less compartments through generating dynamic networks of redundant and weak intermolecular interactions (Li, Banjade, et al. 2012). These protein-rich condensates are dispersed in their environment and display liquid-like properties such as a spherical shape which deforms under shear stress, or the ability to fuse with one another (Brangwynne, Eckmann, et al. 2009). In contrast to cell organelles bound by a membrane, the lack of requiring an enclosing membrane is a particularly interesting property of LLPS droplets as this enables its components to interact with their surrounding environment. In that way, the formation of LLPS condensates helps to maintain the cellular equilibrium by allowing the cell to quickly respond to changing cellular conditions (Banani et al. 2017; Mitrea and Kriwacki 2016). LLPS can occur both in the nucleus (Mao, Zhang, and Spector 2011) and in the cytoplasm (Decker and Parker 2012) of eukaryotic cells and examples include Cajal bodies (Nizami, Deryusheva, and Gall 2010), nucleoli (Brangwynne, Mitchison, and Hyman 2011) and Para speckles (Fox and Lamond 2010) for nuclear condensates, and stress granules (Kedersha et al. 2005), germ granules (Brangwynne, Eckmann, et al. 2009) and processing bodies (P-bodies) (Parker and Sheth 2007; Sheth and Parker 2003) for cytoplasmic condensates. The large number of functionally distinct assemblies in the cell demonstrates their importance for the regulation of cellular processes like mRNA translation, processing, localization, and turnover.

In the past, the molecular details leading to LLPS have been extensively researched and it has been shown that proteins that are involved in this spontaneous self-organization process often contain regions that are intrinsically disordered (IDRs) (Banani et al. 2017; Elbaum-Garfinkle et al. 2015; Fromm, Kamenz, et al. 2014). These IDRs lack a clear tertiary structure and usually contain no or only few hydrophobic amino acids. As a consequence, they can form large networks via charge-charge (Pak et al. 2016), cation-π (Nott et al. 2015), dipole-dipole, and π-π stacking interactions (Frey, Richter, and Görlich 2006; Vernon et al. 2018), as they stimulate interactions between molecules (Brangwynne, Tompa, and Pappu 2015; Gomes and Shorter 2019). Frequently, IDRs also contain short linear motifs which can contact folded protein domains and proteins can interact with RNA via folded RNA recognition motifs (RRMs), which both can lead to phase separation of the involved molecules (Fromm, Kamenz, et al. 2014; Kato et al. 2012). These interactions

are not mutually exclusive but can happen simultaneously, which demonstrates the high redundancy of phase separation processes. LLPS condensates have been shown to rapidly form and dissolve again, depending on the conditions in the cell (Banjade et al. 2015; Fromm, Kamenz, et al. 2014). Additionally, several phase separated proteins can undergo another phase transition and form a more solid, or gel-like, state. This so-called maturation is irreversible and leads for example to the formation of amyloid-like fibrils, which are linked to neurodegenerative disorders, or to the formation of hydrogels, which can still be functional (Hyman, Weber, and Jülicher 2014; Molliex et al. 2015).

In 5' → 3' mRNA decay, the mRNA decapping proteins, including the Dcp1:Dcp2 complex, can undergo LLPS together with mRNA and form mRNA processing bodies (P-bodies) (Dijk 2002; Ingelfinger et al. 2002; Parker and Sheth 2007; Sheth and Parker 2003). The condensation into P-bodies is promoted by protein-protein and protein-RNA interactions as well as by low-complexity protein domains as can be found in the C-terminal IDR of Dcp2 (Fromm, Kamenz, et al. 2014; Schütz, Nöldeke, and Sprangers 2017). *In vitro* the phase separated droplets quickly and irreversibly mature into a gel-like state from which the matured proteins cannot be recovered any more (Damman et al. 2019; Schütz, Nöldeke, and Sprangers 2017). So far, the exact biological function of condensates of the mRNA decapping machinery has not been fully understood, and so it is not clear if these self-organized ribonucleoprotein foci serve to stably store mRNA or if they are a place of active mRNA turnover (Damman et al. 2019; Schütz, Nöldeke, and Sprangers 2017; Tibble et al. 2021).

In solution, enzymes involved in mRNA decapping have been extensively characterized and a lot is known about the conformations of the main decapping enzyme Dcp2 and its interactions with other decapping factors, as well as about the mechanism of Dcp2-mediated decapping of mRNA (Wurm, Holdermann, et al. 2017; Wurm and Sprangers 2019). Dcp2 consists of an intrinsically disordered C-terminus, a catalytic domain (CD) with a NUDIX helix at the active center and an N-terminal regulatory domain (NRD), where it binds the main decapping activator Dcp1 to form the mRNA decapping complex Dcp1:Dcp2. In solution, this complex adopts three distinct conformations which differ from each other in the relative domain orientation of the NRD and CD of Dcp2. In the absence of substrate, the catalytically impaired closed and open states exchange and the closed state is primarily populated. In the presence of substrate and an Edc1 peptide, the complex adopts its active conformation by rotation of the NRD such that a shared active site between the NRD and the CD is formed (Wurm, Holdermann, et al. 2017). Furthermore, helical leucine-rich motifs (HLMs) in the disordered C-terminus of Dcp2 can bind the enhancer of decapping Edc3 via an N-terminal LSm domain and thereby stimulate LLPS (Fromm, Kamenz, et al. 2014; Schütz, Nöldeke, and Sprangers 2017).

The interaction with the scaffolding protein Edc3 is central to the recruitment of Dcp2 into P-bodies in yeast. In addition to the N-terminal LSm domain, Edc3 contains an intrinsically disordered linker region which connects the LSm domain to a well-folded, structured YjeF_N dimerization domain. Edc3 can undergo LLPS and mature into a gel-like state by itself, whereby its IDR and its rigid YjeF_N domain interact to form the condensate while its LSm domain remains flexible (Damman et al. 2019; Schütz, Nöldeke, and Sprangers 2017). By interacting with HLMs in the intrinsically disordered C-terminus of Dcp2 via its LSm domain and

by binding RNA at its IDR, Edc3 involves these factors in the phase separation process, which then quickly leads to the maturation of the newly formed LLPS droplets into a gel-like aggregate of proteins and mRNAs *in vitro*. Edc3 is therefore an important driver of LLPS of the mRNA decapping machinery. Interestingly, it was found that the recruitment of Dcp2 into P-bodies *in vitro* affects its catalytic activity, and so the enzyme displays a reduction in catalytic activity compared to its disperse, non-phase separated state (Tibble et al. 2021).

Despite these important insights, knowledge about the processes leading to the condensation of the decapping proteins on an atomic level and about the conformational states of the involved proteins in the phase separated, and, subsequently, in the mature state, is still sparse. We therefore aim to extend our understanding of the LLPS process of mRNA decapping enzymes in *S. pombe* by studying Edc3 and Dcp2 and their interactions with other mRNA decay factors in the mature state using magic angle spinning solid state NMR (MAS ssNMR; see subsection 2.2.10) (Ader, Frey, et al. 2010; Andronesi et al. 2005; Labokha et al. 2012) and we then combine this information with previous results from solution state NMR (Wurm, Holdermann, et al. 2017). This approach allows us to use residue-specific information about the proteins from solution state NMR to interpret important results from solid state NMR, which has the advantage that both the rigid and the flexible parts of a sample in the mature, gel-like state can be examined (Baldus 2022; Schanda and Ernst 2016). First, we recorded spectra of ^{15}N labeled Edc3 after phase separation and maturation and examined the changes that take place upon RNA and Dcp1:Dcp2 binding. Second, we instead simultaneously labeled the methionine methyl groups of Dcp2 with $^{13}CH_3$ and its nitrogens with ^{15}N to probe the conformational state of the Dcp1:Dcp2 decapping complex after Edc3-induced phase separation and maturation. Furthermore, we added Edc1 and m^7GDP to the Dcp1:Dcp2:Edc3 complex to investigate their influence on the conformations of Dcp1:Dcp2 in the mature state. We speculate that condensation into P-bodies could change the domain orientation and thus the conformation of Dcp2, which is directly connected to its decapping capacity. With that we hope to be able to conclude whether mRNA decapping in condensates is inhibited or enhanced and validate previous evidence of a reduced catalytic activity of Dcp2 in P-bodies *in vitro* (Tibble et al. 2021).

2. Results

2.1. LLPS of Edc3

Edc3 consists of an N-terminal LSm domain and a C-terminal YjeF_N domain which are connected by an internal IDR (Figure 2.1).

In solution, the scaffolding protein dimerizes via its well-folded, structured YjeF_N domain (Sharif, Ozgur, et al. 2013; Tritschler et al. 2009).

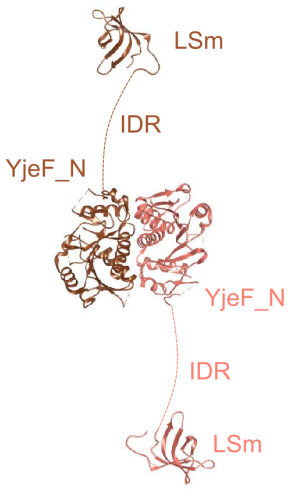

Figure 2.1.: Crystal structure of the human Edc3 LSm domain (PDBiD 2VC8) and the human YjeF_N domain (PDBiD 3D3K). The dimer consists of an N-terminal LSm domain that is connected to the well-folded, structured, C-terminal YjeF_N domain via an intrinsically disordered linker region.

To examine whether this fold is conserved in the mature state, we lyophilized the isolated YjeF_N domain and recorded ^{1}H-detected dipolar ^{15}NH ssNMR spectra (Andronesi et al. 2005) and compared these to spectra of the mature Edc3 full-length (Edc3 FL) protein. An overlay of both spectra shows that they resemble another (Figure 2.2 A, left), so we conclude that the overall fold of the Edc3 protein in the mature state is conserved. This finding is in agreement with previous findings by Damman et al. (Damman et al. 2019). In the ssNMR spectrum of the mature, full length Edc3 some additional peaks can be observed (Figure 2.2 A, left; black boxes) which can be explained by the presence of additional residues in the longer Edc3 construct compared to the isolated YjeF_N domain. The initially surprisingly low number of observable additional signals compared to the much larger number of additional residues in the Edc3 FL construct is most likely due to signal overlap as well as to the flexible nature of the IDR and LSm domain of Edc3 FL, which do therefore not yield resonances in the dipolar ^{15}NH spectrum. Minor chemical shift differences between peaks in the two spectra can also be attributed to the presence of the LSm and IDR domains in the full length protein which slightly change the chemical environment of the YjeF_N domain residues.

To investigate whether the dynamics of Edc3 are altered after LLPS and maturation, we recorded ^{1}H-detected scalar ^{15}NH ssNMR spectra on the lyophilized YjeF_N domain and on the mature Edc3 FL protein. In these scalar-based spectra, only the flexible parts of the proteins are visible (Ahlawat et al. 2022). As expected, the spectrum of Edc3 FL shows several additional signals compared to the YjeF_N spectrum (Figure 2.2 A, right; black ellipses), and these peaks belong mainly to the flexible IDR and partly to the LSm domain of the full length construct. In addition, we observe two prominent, unexpected additional peaks for the YjeF_N domain which disappear for the longer Edc3 FL construct (Figure 2.2 A, right; black boxes). From solution state NMR of the Edc3 YjeF_N domain in the presence of the

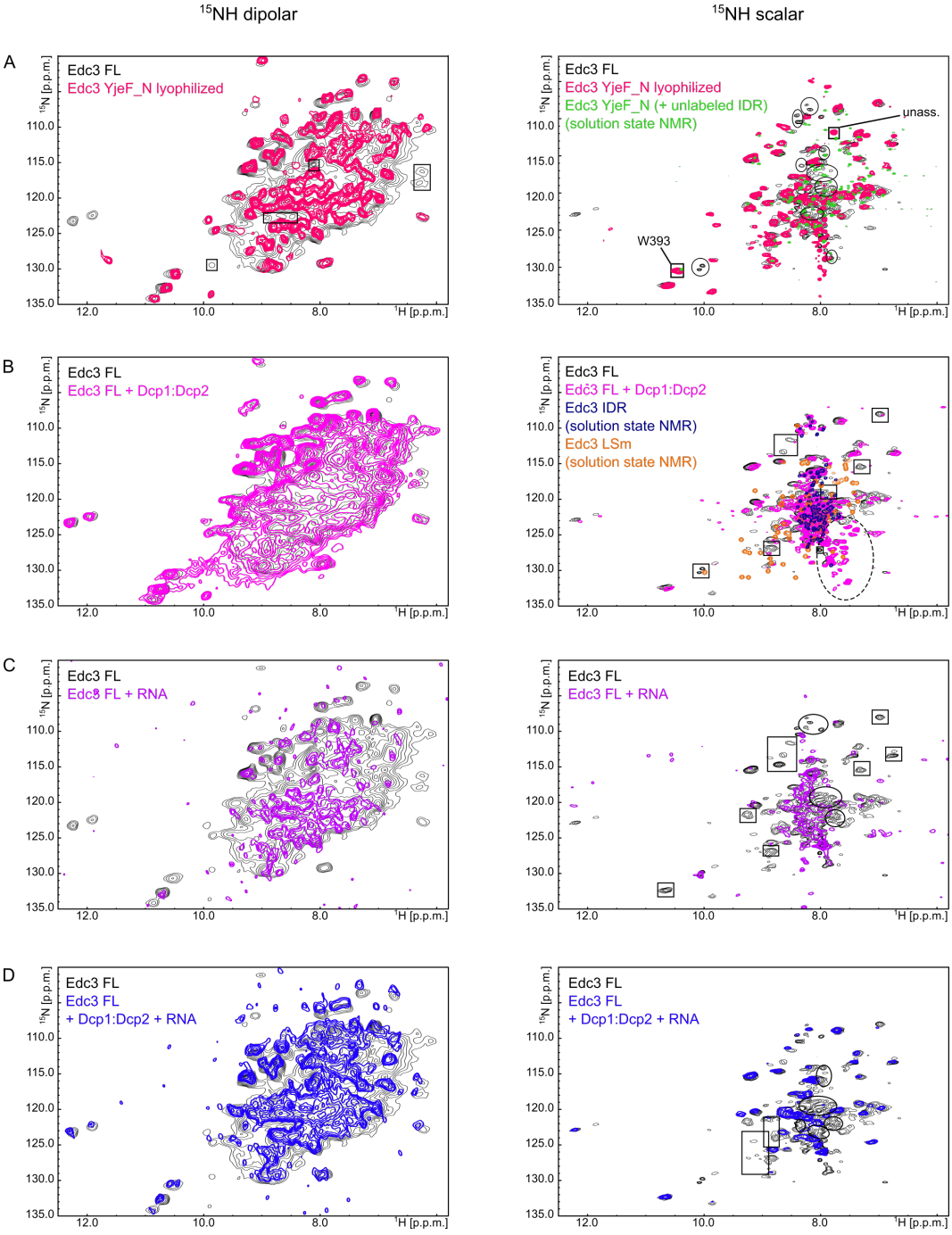

Figure 2.2.: Comparison of ^{15}NH dipolar and scalar spectra of mature Edc3 full length (FL) to mature Edc3 FL bound to different interaction partners. Dipolar (rigid) ^{15}NH spectra are displayed on the left side and scalar-based (flexible) ^{15}NH spectra are shown on the right. In all panels, spectra of Edc3 FL are colored black. In all spectra, Edc3 is ^{15}N labeled and all interaction partners are NMR invisible. (A) Comparison between mature phase Edc3 FL (black) and the lyophilized YjeF_N domain of Edc3 (red). Boxes and squares indicate differences between the spectra. In the panel on the right showing the scalar ^{15}NH spectra, the solution state NMR spectrum of the Edc3 Yjef_N domain in the presence of the Edc3 IDR, taken from (Damman et al. 2019), is shown in green for comparison. (B) Comparison between Edc3 FL in absence (black) and in presence (pink) of the Dcp1:Dcp2 mRNA decapping complex. The panel on the right additionally shows solution state NMR spectra of the Edc3 IDR (from (Schütz, Nöldeke, and Sprangers 2017); dark blue) and of the Edc3 LSm domain (orange). The boxes indicate resonances which disappear in the presence of Dcp1:Dcp2 and the dashed black ellipse shows peaks probably originating from protein degradation. (C) Comparison between Edc3 FL in the absence (black) and in presence of RNA (purple). Boxes and ellipses indicate disappearing resonances which originate from either the YjeF_N domain (squares) or the IDR (ellipses) of Edc3. (D) Comparison between Edc3 FL in the absence (black) and in presence (blue) of Dcp1:Dcp2 and RNA. Boxes and ellipses indicate disappearing resonances which originate from either the LSm domain (squares) or the IDR (ellipses) of Edc3.

unlabeled IDR (Figure 2.2 A, right; green peaks), one of these peaks was assigned to W393 but the second peak remains unassigned. We reason that both peaks belong to N-terminal YjeF_N residues which are flexible in the isolated domain but become rigid or experience significant changes in chemical shift when the IDR and the LSm domain are present at the N-terminal end of the YjeF_N domain. This explanation is supported by previous results from solution state NMR, in which residue W393 experienced a significant chemical shift perturbation upon interaction with the IDR (Damman et al. 2019).

Next, we added the Dcp1:Dcp2 complex to Edc3 FL and recorded dipolar ^{15}NH and scalar ^{15}NH ssNMR spectra as before. An overlay of the dipolar ^{15}NH spectra of Edc3 FL and the Edc3:Dcp1:Dcp2 complex shows that both spectra are nearly identical (Figure 2.2 B, left), so the YjeF_N domain is again conserved and stays rigid upon addition of the decapping complex. The scalar ^{15}NH spectra however show a significant peak loss for Edc3:Dcp1:Dcp2 (Figure 2.2 B, right; black boxes), which indicates binding of Dcp1:Dcp2 to Edc3 that leads to a loss of flexibility. Most changes in chemical shift can be found in residues that likely belong to the folded LSm domain (solution state NMR spectrum shown in orange for comparison in Figure 2.2 B, right) but also to the YjeF_N domain (see Figure 2.2 A, right, red spectrum), since they are clearly distinguishable from signals of the IDR (Figure 2.2 B, right; dark blue peaks) which were obtained from solution NMR (Schütz, Nöldeke, and Sprangers 2017). This result is also in agreement with previous results in solution, where C-terminal Dcp2 residues were found to bind to the LSm domain of Edc3 (Charenton, Taverniti, et al. 2016; Fromm, Truffault, et al. 2012; Fromm, Kamenz, et al. 2014). In addition, some new peaks appear in the scalar ^{15}NH spectrum of Edc3:Dcp1:Dcp2, which, based on their position in the spectrum, most probably stem from degraded protein (Figure 2.2 B, right; dashed ellipse). Overall, binding of Dcp1:Dcp2 to Edc3 leads to significant peak loss in the LSm and in the YjeF_N domain of mature Edc3 and therefore to a rigidification of those Edc3 domains which were found to be flexible in the absence of Dcp1:Dcp2.

Instead of Dcp1:Dcp2, we next added RNA to Edc3 FL and again recorded dipolar and scalar ^{15}NH spectra. Compared to the respective spectra of Edc3 FL without RNA, the peaks in the Edc3:RNA dipolar ^{15}NH spectra are strongly broadened (Figure 2.2 C, left). This could be explained either by increased dynamics of Edc3 in the presence of RNA or by a situation in which the RNA binds to Edc3 in different registers which leads to different chemical shifts of the bound state and thus to the observed line broadening. Alternatively, the poor spectral quality might also be the result of too little protein in the sample resulting in the low signal-to-noise ratio or the recording time of the spectra was too short. In the case of increased dynamics of Edc3 in the presence of RNA we would expect the appearance of additional signals belonging to the YjeF_N domain in the scalar-based spectrum, but again due to low spectral quality, this cannot clearly be observed (Figure 2.2 C, right). Instead, several peaks disappear in the presence of RNA which indicates that RNA binding also leads to a rigidification of the mobile Edc3 domains. Many of the peaks that disappear belong to the IDR of Edc3 (Figure 2.2 C, right; black ellipses), which we could identify from the transfer of the Edc3 IDR assignments from solution-state NMR (see Figure 2.2 B, right; dark blue peaks) (Schütz, Nöldeke, and Sprangers 2017). This result is in agreement with previous results in solution, where the IDR

of Edc3 was found to interact with RNA (Schütz, Nöldeke, and Sprangers 2017). Interestingly, also peaks from the YjeF_N domain disappear (Figure 2.2 C, right; black squares). We conclude that RNA binding rigidifies mobile regions of the YjeF_N domain and in particular the flexible IDR of Edc3. A more detailed analysis is not possible due to the poor spectral resolution.

Finally, we examined changes in Edc3 in the mature state in the presence of both the mRNA decapping complex and mRNA. Again, we recorded dipolar and scalar ^{15}NH spectra and compared them to Edc3 FL. The dipolar spectrum of Edc3 FL in complex with Dcp1:Dcp2 and RNA overlays well with the spectrum of Edc3 FL alone (Figure 2.2 D, left), which points towards a stable, well-folded Edc3 YjeF_N domain in the presence of both interaction partners. The fold of Edc3 with RNA and Dcp1:Dcp2 is thus very similar to the fold of free Edc3 FL. In the scalar-based spectrum, however, many peaks of the IDR (Figure 2.2 D, right; black ellipses) and of the LSm domain (Figure 2.2 D, right; black squares) disappear in the presence of RNA and Dcp1:Dcp2, and only signals of the mobile parts of the YjeF_N domain remain (Figure 2.2 D, right; see also Figure 2.2 A, right). Therefore, the addition of RNA and Dcp1:Dcp2 to Edc3 leads to a rigidification of the flexible LSm domain and of the IDR of Edc3 in the mature state after LLPS.

2.2. LLPS of Dcp2

To obtain further insights into mRNA decapping in condensates, we next labeled the methionine methyl groups and the nitrogens of the main decapping enzyme Dcp2 with $^{13}CH_3$, or ^{15}N, respectively, and recorded ^{1}H-detected dipolar ^{15}NH spectra, to assess the overall fold of the protein, and dipolar $^{13}CH_3$ spectra, to probe the conformation of the decapping complex. In NMR spectra of Dcp1:Dcp2 in solution, the methionine resonances M164 and M221 were found to directly report on the conformation of the Dcp1:Dcp2 complex (Wurm, Holdermann, et al. 2017). Both residues are located at the interface between the N-terminal regulatory domain and the catalytic domain of Dcp2 and for this reason they are very sensitive to changes in chemical environment upon changes in domain orientation of the complex (Figure 2.3 B, C). Thus, these peaks appear at distinct and well distinguishable spectral positions for each conformational state of the complex (Figure 2.3 A).

To examine the fold of the Dcp2 enzyme in the mature state, we compared dipolar ^{15}NH spectra of lyophilized Dcp1:Dcp2 and mature Dcp1:Dcp2:Edc3. Both spectra overlay well, which shows that the fold of Dcp2 is conserved in the mature state (Figure 2.4 A, left). A few peaks however disappear in the mature phase spectrum, which could indicate that slightly more dynamics may be present after Edc3 addition and phase separation compared to the lyophilized sample. It must be noted that the addition of unlabeled Edc3 is necessary for LLPS and subsequent maturation of Dcp2 and it is therefore present in all phase separated samples. The methionine peaks in the dipolar $^{13}CH_3$ spectra of the two samples also overlay well, which shows that the conformation of Dcp1:Dcp2 is the same in both samples (Figure 2.4 A, right). A comparison with solution state NMR spectra of the same complex (see Figure 2.3 A) reveals that the proteins here are in the catalytically inactive, closed state. Interestingly, the lyophilized sample displays an additional small peak as well as a small shoulder next to peak M164, which point towards the presence of a

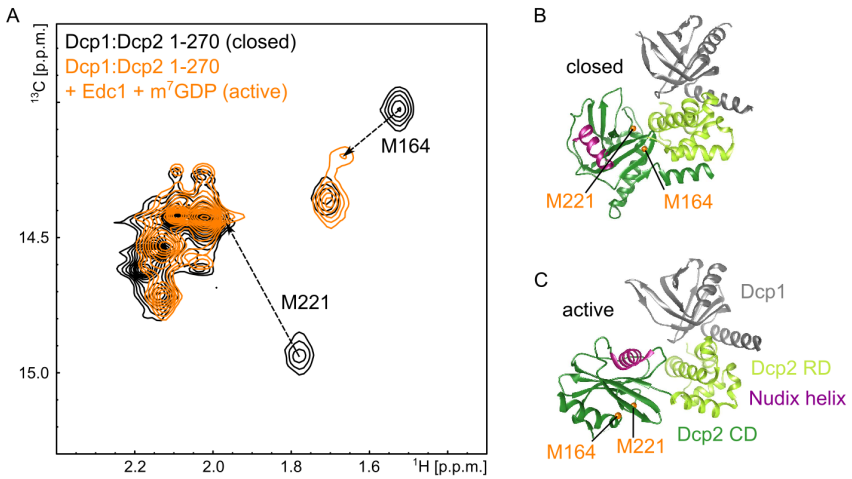

Figure 2.3.: (A) Solution state NMR spectra of Dcp1:Dcp2 in the closed (black) and the active conformation (orange). (B) Crystal structure of the Dcp1:Dcp2 complex in the closed conformation (PDBiD 2qkm, chains A,B). Dcp1 is colored in light blue, the RD of Dcp2 in medium blue and the CD of Dcp2 in dark blue and the Nudix helix, which is involved in catalysis, is colored in pink. Methionine residues 164 and 221 are indicated as orange spheres. (C) Crystal structure of the Dcp1:Dcp2 complex in the active conformation (PDBiD 5n2v).

second conformation. Based on a comparison with solution state NMR spectra, we assign the additional peak to M221 and the shoulder to M164, both for the protein in a more open conformation, as the position of these fits the position of the two peaks for a more open conformation of the complex in solution. Since these peaks are not present in the spectrum of the mature protein, the addition of Edc3 might stabilize the closed conformation of Dcp1:Dcp2.

From previous studies it is known that in solution, the addition of Edc1 to Dcp1:Dcp2 has no influence on the domain orientations of the complex (Wurm, Holdermann, et al. 2017). Dipolar ^{15}NH spectra of mature Dcp1:Dcp2:Edc3:Edc1 however show a strong decrease in observable correlations compared to mature Dcp1:Dcp2:Edc3 (Figure 2.4 B, left), which could be the result of increased dynamics in the sample with Edc1. However, the quality of the spectrum is low, so an increase in dynamics is only a matter of speculation and the loss of signal could also stem from structural inhomogeneity in the phase separated sample that increases upon maturation. In the dipolar $^{13}CH_3$ spectrum, the same peaks as in the mature sample without Edc1 are present and no significant shifts of M221 and M164 can be observed (Figure 2.4 B, right), so the protein does not change its conformation upon Edc1 addition, which is also consistent with data from solution NMR.

The addition of m^{7}GDP to Dcp1:Dcp2 leads to a loss of signal and fewer correlations in the dipolar ^{15}NH spectrum of the mature complex (Figure 2.4 C, left) and the peak positions in the dipolar $^{13}CH_3$ spectrum are the same as without m^{7}GDP (Figure 2.4 C, right). Again, the weak signals in the Dcp1:Dcp2:Edc3:m^{7}GDP spectra point towards an increase in structural inhomogeneity in the mature phase.

Adding both Edc1 and m^{7}GDP to Dcp1:Dcp2:Edc3 leads to an overall signal reduction in the dipolar ^{15}NH spectrum (Figure 2.4 D, left), which may indicate increased dynamics in the sample. More interesting, however, is the appearance of a second peak in the dipolar $^{13}CH_3$ spectrum (Figure 2.4 D, right) at the same position as the second, smaller peak in the lyophilized Dcp1:Dcp2 sample. We assign this resonance to peak M221 in the active state of the decapping complex.

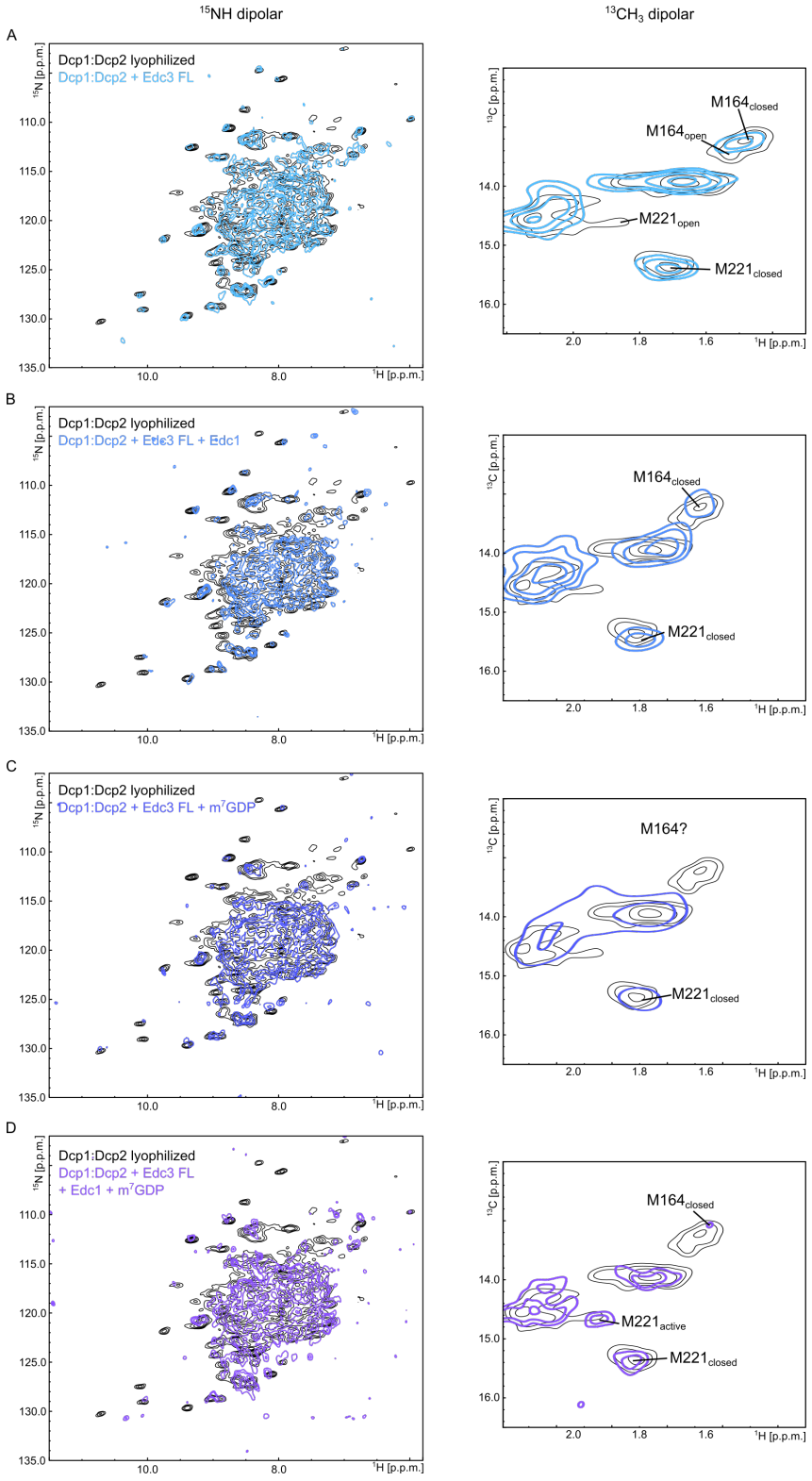

Figure 2.4.: Comparison of ^{15}NH and $^{13}CH_3$ dipolar spectra of lyophilized Dcp1:Dcp2 to mature state Dcp1:Dcp2 with different interaction partners. Dipolar ^{15}NH spectra are shown on the left hand side and dipolar $^{13}CH_3$ spectra are shown on the right. In all panels, spectra of lyophilized Dcp2, in complex with NMR inactive Dcp1, are shown in black and in all spectra, Dcp2 is ^{15}N labeled and the methionines of Dcp2 are $^{13}CH_3$ labeled. All binding partners are NMR invisible. (A) Spectra of lyophilized Dcp1:Dcp2 overlayed with mature phase Dcp1:Dcp2:Edc3. Edc3 is necessary for Dcp1:Dcp2 to undergo liquid-liquid phase separation and maturation. (B) Comparison of lyophilized Dcp1:Dcp2 with mature phase Dcp1:Dcp2:Edc3 in complex with Edc1. (C) Comparison of lyophilized Dcp1:Dcp2 with mature phase Dcp1:Dcp2:Edc3 in complex with m^{7}GDP. (D) Overlay of spectra of lyophilized Dcp1:Dcp2 with spectra of Dcp1:Dcp2:Edc3 in complex with Edc1 and m^{7}GDP.

This is plausible as in solution, the active state is fully adopted in the presence of Edc1 and m^7GDP (Wurm, Holdermann, et al. 2017). Overall, our results suggest that in the mature phase, different conformations of the decapping complex are present at the same time. This can be explained by a model in which the different components contributing to LLPS assemble and mature in a structurally disorganized way. As a consequence, samples used for NMR measurements are inhomogeneous and yield NMR spectra of poor quality, which is in line with our measurement results.

3. Discussion

Liquid-liquid phase separation is a cellular process which has not been fully understood yet and it is currently subject of intensive research (Alberti and Hyman 2021; Jonchhe et al. 2022; Langstein-Skora et al. 2022). The proteins involved in 5' decapping of mRNA, including Edc3 and Dcp2 can, together with mRNA, undergo LLPS and be recruited to P-bodies, after which they mature into a gel-like state (Damman et al. 2019; Fromm, Kamenz, et al. 2014; Schütz, Nöldeke, and Sprangers 2017). Using solid-state NMR we were able to characterize Edc3 and Dcp2 from *S. pombe* in their mature state after LLPS and their recruitment to P-bodies. We could show that solid state NMR, especially in combination with solution state NMR, is a powerful method to characterize complex biomolecular systems as large as 126 kDa (Dcp1:Dcp2:Edc3:Edc1) with up to residue-specific resolution. Thus, by isotopically labeling individual proteins within the complex protein-RNA network and recording their rigid and flexible components, we were able to observe changes in dynamics and conformations of the respective proteins within mRNA P-bodies.

We first analyzed the enhancer of decapping Edc3, which is central for the condensation into P-bodies, after LLPS and maturation and monitored changes in its dynamics in the presence of different interaction partners. We found that interactions with both the Dcp1:Dcp2 complex and with RNA lead to a rigidification of the LSm domain, and the IDR of Edc3, respectively. These results are consistent with previous studies of Edc3 both in solution and in the mature state after phase separation (Damman et al. 2019; Fromm, Truffault, et al. 2012; Fromm, Kamenz, et al. 2014; Schütz, Nöldeke, and Sprangers 2017). Second, we were able to characterize conformational changes of Dcp1:Dcp2 in its mature state, which is only formed in the presence of Edc3. Similar to studies of the decapping complex in solution (Wurm, Holdermann, et al. 2017), we recorded ^{13}C-^{1}H methionine correlation spectra of the complex and found that the complex remains in its closed, catalytically inactive state after LLPS and maturation. Only in the presence of both Edc1 and m^{7}GDP an additional, active conformation could be observed, while the addition of either only Edc1 or only m^{7}GDP did not induce any significant conformational change.

Consistently throughout our expermients, however, the spectra we recorded on the mature protein complexes were of poor quality. This indicates that the gel-like state into which the interaction partners of the mRNA decapping machinery mature is structurally inhomogeneous. As each protein in an unstructured sample experiences a different chemical environment, the chemical shift perturbations of the NMR resonances of each protein are different, which would result in the strong line broadening in the resulting spectra that we observe in our ssNMR measurements of mature Edc3 and Dcp1:Dcp2. Based on these results, we propose a model in which the interaction partners of the mRNA decapping machinery first phase separate and then, likely due to the highly stressful conditions of low salt (< 25 mM NaCl) in the buffer and very high protein concentration, mature into a

structurally inhomogeneous, gel-like state which lacks conformational regulation and from which the individual components cannot be recovered. We thus conclude that the mature state is a state in which the molecular motions and intermolecular contacts that are averaged in solution are frozen out and no longer averaged. To clearly answer if mRNA decapping in P-bodies is inhibited or enhanced, further studies of LLPS of the decapping machinery are needed. However, this work highlights the importance of the interplay of all these interaction partners for LLPS as well as the importance of their dynamics, which are often neglected in structural studies but are critical in physiological systems. Our approach using solid state NMR thus paves the way for future studies of enzyme dynamics and enzymatic states even in large and extended networks of liquid-liquid phase separated condensates.

Part VII.

Conclusion and Outlook

1. Conclusion and Outlook

The field of structural biology is rapidly progressing, not least fueled by impressive advances in the development of AI tools that predict the 3D structures of proteins from their amino acid sequence or that can be used to design novel proteins e.g. for the development of new drugs and vaccines. Studying large biomolecular systems with more traditional techniques such as cryo-EM, X-ray crystallography or NMR spectroscopy remains nonetheless extremely important, especially for validating, complementing, supporting or contradicting data created by AI algorithms. However, the examination of large and complex molecular machines can be challenging. While cryo-EM and X-ray crystallography are for instance ideally suited to obtain static images of protein structures, X-ray crystallography provides little to no information about dynamic processes in the examined system and cryo-EM can only be used to detect large motions and states of proteins but often cannot provide structural data or data on internal motions with atomic resolution. NMR spectroscopy, in contrast, is very well suited to characterize the motions and energy landscapes of proteins and due to advanced isotope labeling techniques, sophisticated pulse sequences and improvements in NMR hardware, information about the structure and the dynamics of complex biomolecules with high molecular weight can be obtained. The greatest power of all these methods, however, lies in their combination and complementarity, as no method is individually capable of providing knowledge about all structural features and motions of a complex and dynamic molecular system but information from multiple different sources and approaches is needed to fully comprehend the system. To enhance our understanding of molecular machines and their functions and to exploit this knowledge to our advantage is therefore only possible when methodologies and approaches from across a variety of scientific fields are combined and shared.

In this thesis the Dcp1:Dcp2 mRNA decapping enzyme was studied in detail using different biophysical methods including solution state NMR at high hydrostatic pressure and on the ^{19}F nucleus, solid state NMR and smFRET, which demonstrates the great value of combining multiple approaches to obtain a comprehensive picture of a biomolecular system. The results presented here add to the existing knowledge about decapping enzymes and address aspects about the enzyme's functions and interactions that have not been investigated in detail before.

To that end, in Part III, information about changes in the molecular volume of the decapping complex when it transitions from the closed to the open state was derived from ^{13}C SQ CPMG NMR experiments at high hydrostatic pressures and additionally, the influence of ATP on this transition was examined. These changes in molecular volume could not be reliably extracted from known crystal structures, which emphasizes the great potential of the methodology we used. Combining methyl labeling and high pressure NMR experiments can therefore provide unique

insights into volumetric properties of large molecular machines.

In Part IV, we explored if the ^{19}F nucleus, which has highly advantageous chemical and physical properties, can be used in NMR spectroscopy to characterize the dynamics of the KIX protein, Dcp1, Dcp2 and DcpS as an alternative to conventional ^{13}C- or ^{15}N- based NMR methods. Although the replacement of a proton with a fluorine atom on the 5-tryptophan did not change the native dynamics of the examined proteins, we found that the ^{19}F nucleus in this position is simultaneously sensitive to both faster motions, like motions of side chains, and slower motions, like motions of the protein backbone, which can result in a strong bias towards one or another and the resulting CPMG RD curves cannot be described by a two-state model any more. Nonetheless, ^{19}F NMR spectroscopy can provide ample insights into protein dynamics and function, as, on the one hand, experiments that are insensitive to tryptophan side chain motions that are fast on the NMR chemical shift timescale are very well suited to extract slow processes like the domain flipping motions in DcpS, and, on the other hand, kinetic and thermodynamic properties that are derived from fluorine relaxation data can be supported by data from complementary techniques, e.g. NMR data that was recorded on methyl groups.

The complementarity of different structural biology methods was also exploited in Part V. Here, we complemented and extended NMR data of the Dcp1:Dcp2 complex by studying interactions of Dcp2 with substrates and decapping factors and its corresponding conformational rearrangements with single molecule FRET experiments, as some of these interactions alter the conformational equilibrium of the complex such that the complex is not suited for NMR measurements any more. Importantly, as the labeling positions of the fluorophores, which are necessary for smFRET experiments, can strongly influence the conformational equilibrium of the complex and thereby prevent a correct interpretation of the FRET efficiencies, we again used NMR experiments on fluorophore labeled complexes to cross-validate our smFRET data. This shows that different methods can simultaneously be used for cross-validation and as mutual complements. Moreover, these results raise the question whether the presence of fluorophore labels can also influence the catalytic activity of the decapping enzyme. To answer this question, activity assays of the Dcp1:Dcp2 complex in the presence and in the absence of fluorophore labels will be compared in the future, and, in addition, it will be examined if the fluorophore tags can also interfere with the RNA body and thereby influence the decapping capacity of the decapping complex in a length-dependent manner.

smFRET experiments provide excellent conditions to study how the conformations of Dcp1:Dcp2 are influenced by Edc3 and RNA in solution, in contrast to solution state NMR experiments, where the required high protein concentrations lead to LLPS of the complex and maturation to a gel-like state. In the mature, gel-like state we were able to examine changes in conformation and dynamics of the decapping factors Edc3 and Dcp2 that took place in the phase transition from the liquid to the solid state by performing solid-state NMR experiments on the mature complex (Part VI). Comparison of solution state NMR data of Dcp1:Dcp2 with the solid-state NMR data of the mature complex allowed us to construct a model in which the involved factors mature into a gel-like state that is structurally stable but lacks conformational regulation and in which some components still retain some degree of flexibility while at the same time these motions are not averaged as it is

the case in solution. These results contribute to our understanding of LLPS and maturation and provide a basis for further studies of large molecular machines in the condensed, phase separated state. In the future, these ssNMR data could be supported by smFRET experiments of Dcp1:Dcp2 in the mature state. As smFRET experiments do not probe an ensemble of molecules, as is the case for ssNMR experiments, the measurements are not averaged, so structural heterogeneities within the sample due to different conformations of Dcp1:Dcp2 can be determined and thereby support or contradict our proposed model of the mature state of Dcp1:Dcp2.

In sum, in this thesis I explored a variety of structural biology methods to study the mRNA decapping machinery with a focus on the Dcp1:Dcp2 decapping complex. In that process, I identified some of the drawbacks of the different methods I used and as a consequence, I combined, validated and extended data on the decapping complex with data obtained from alternative, complementary methods. The new insights I gained in that way add to the existing knowledge about mRNA decapping enzymes and ultimately contribute to a better understanding of how large molecular machines function.

Bibliography

Abiko, Layara Akemi, Anne Grahl, and Stephan Grzesiek (2019). "High Pressure Shifts the β_1-Adrenergic Receptor to the Active Conformation in the Absence of G Protein." In: *Journal of the American Chemical Society* 141.42, pp. 16663–16670. ISSN: 0002-7863, 1520-5126. DOI: 10.1021/jacs.9b06042. URL: https://pubs.acs.org/doi/10.1021/jacs.9b06042.

Acchione, Mauro et al. (2012). "Specific Fluorine Labeling of the HyHEL10 Antibody Affects Antigen Binding and Dynamics." In: *Biochemistry* 51.30, pp. 6017–6027. ISSN: 0006-2960, 1520-4995. DOI: 10.1021/bi300455t. URL: https://pubs.acs.org/doi/10.1021/bi300455t.

Ackermann, Bryce E. and Galia T. Debelouchina (2019). "Heterochromatin Protein HP1α Gelation Dynamics Revealed by Solid-State NMR Spectroscopy." In: *Angewandte Chemie International Edition* 58.19, pp. 6300–6305. ISSN: 1433-7851, 1521-3773. DOI: 10.1002/anie.201901141. URL: https://onlinelibrary.wiley.com/doi/10.1002/anie.201901141.

Ader, Christian, Steffen Frey, et al. (2010). "Amyloid-like interactions within nucleoporin FG hydrogels." In: *Proceedings of the National Academy of Sciences* 107.14, pp. 6281–6285. ISSN: 0027-8424, 1091-6490. DOI: 10.1073/pnas.0910163107. URL: https://pnas.org/doi/full/10.1073/pnas.0910163107.

Ader, Christian, Olaf Pongs, et al. (2010). "Protein dynamics detected in a membrane-embedded potassium channel using two-dimensional solid-state NMR spectroscopy." In: *Biochimica et Biophysica Acta (BBA) - Biomembranes* 1798.2, pp. 286–290. ISSN: 00052736. DOI: 10.1016/j.bbamem.2009.06.023. URL: https://linkinghub.elsevier.com/retrieve/pii/S0005273609002247.

Agrawal, Divya and Christian P. R. Hackenberger (2013). "Site-specific chemical modifications of proteins." In: URL: https://api.semanticscholar.org/CorpusID:97778158.

Ahlawat, Sahil et al. (2022). "Solid-State NMR: Methods for Biological Solids." In: *Chemical Reviews* 122.10, pp. 9643–9737. ISSN: 0009-2665, 1520-6890. DOI: 10.1021/acs.chemrev.1c00852. URL: https://pubs.acs.org/doi/10.1021/acs.chemrev.1c00852.

Ahmmed, Mirja Kaizer et al. (2021). "Phosphorus-31 nuclear magnetic resonance (31P NMR) for quantitative measurements of phospholipids derived from natural products: Effect of analysis conditions." In: *LWT* 142, p. 110991. ISSN: 00236438. DOI: 10.1016/j.lwt.2021.110991. URL: https://linkinghub.elsevier.com/retrieve/pii/S0023643821001444.

Akasaka, Kazuyuki (2003). "Exploring the entire conformational space of proteins by high-pressure NMR." In: *Pure and Applied Chemistry* 75.7, pp. 927–936. ISSN: 1365-3075, 0033-4545. DOI: 10.1351/pac200375070927. URL: https://www.degruyter.com/document/doi/10.1351/pac200375070927/html.

Akasaka, Kazuyuki (2006). "Probing Conformational Fluctuation of Proteins by Pressure Perturbation." In: *Chemical Reviews* 106.5, pp. 1814–1835. ISSN: 0009-2665, 1520-6890. DOI: 10.1021/cr040440z. URL: https://pubs.acs.org/doi/10.1021/cr040440z.

Akasaka, Kazuyuki and Hua Li (2001). "Low-Lying Excited States of Proteins Revealed from Nonlinear Pressure Shifts in ^{1} H and ^{15} N NMR." In: *Biochemistry* 40.30, pp. 8665–8671. ISSN: 0006-2960, 1520-4995. DOI: 10.1021/bi010312u. URL: https://pubs.acs.org/doi/10.1021/bi010312u.

Akasaka, Kazuyuki, Hua Li, et al. (1999). "Pressure response of protein backbone structure. Pressure-induced amide ^{15} N chemical shifts in BPTI." In: *Protein Science* 8.10, pp. 1946–1953. ISSN: 09618368, 1469896X. DOI: 10.1110/ps.8.10.1946. URL: http://doi.wiley.com/10.1110/ps.8.10.1946.

Akasaka, Kazuyuki and Hitoshi Matsuki, eds. (2015). *High Pressure Bioscience: Basic Concepts, Applications and Frontiers*. Vol. 72. Subcellular Biochemistry. Dordrecht: Springer Netherlands. ISBN: 978-94-017-9917-1 978-94-017-9918-8. DOI: 10.1007/978-94-017-9918-8. URL: https://link.springer.com/10.1007/978-94-017-9918-8.

Alberti, Simon and Anthony A. Hyman (2021). "Biomolecular condensates at the nexus of cellular stress, protein aggregation disease and ageing." In: *Nature Reviews Molecular Cell Biology* 22.3, pp. 196–213. ISSN: 1471-0072, 1471-0080. DOI: 10.1038/s41580-020-00326-6. URL: https://www.nature.com/articles/s41580-020-00326-6.

Alderson, T Reid and Lewis E Kay (2020). "Unveiling invisible protein states with NMR spectroscopy." In: *Current Opinion in Structural Biology* 60, pp. 39–49. ISSN: 0959440X. DOI: 10.1016/j.sbi.2019.10.008. URL: https://linkinghub.elsevier.com/retrieve/pii/S0959440X19301186.

Alderson, T. Reid, Cyril Charlier, et al. (2017). "Monitoring Hydrogen Exchange During Protein Folding by Fast Pressure Jump NMR Spectroscopy." In: *Journal of the American Chemical Society* 139.32, pp. 11036–11039. ISSN: 0002-7863, 1520-5126. DOI: 10.1021/jacs.7b06676. URL: https://pubs.acs.org/doi/10.1021/jacs.7b06676.

Alderson, T. Reid and Lewis E. Kay (2021). "NMR spectroscopy captures the essential role of dynamics in regulating biomolecular function." In: *Cell* 184.3, pp. 577–595. ISSN: 0092-8674. DOI: https://doi.org/10.1016/j.cell.2020.12.034. URL: https://www.sciencedirect.com/science/article/pii/S0092867420317566.

Algar, W. Russ et al. (2019). "FRET as a biomolecular research tool — understanding its potential while avoiding pitfalls." In: *Nature Methods* 16.9, pp. 815–829. ISSN: 1548-7091, 1548-7105. DOI: 10.1038/s41592-019-0530-8. URL: https://www.nature.com/articles/s41592-019-0530-8.

Allerhand, Adam and Everett Thiele (1966). "Analysis of Carr—Purcell Spin-Echo NMR Experiments on Multiple-Spin Systems. II. The Effect of Chemical Exchange." In: *The Journal of Chemical Physics* 45.3, pp. 902–916. ISSN: 0021-9606, 1089-7690. DOI: 10.1063/1.1727703. URL: https://pubs.aip.org/aip/jcp/article/45/3/902-916/79629.

Andrew, E. R., A. Bradbury, and R. G. Eades (1958). "Nuclear Magnetic Resonance Spectra from a Crystal rotated at High Speed." In: *Nature* 182.4650, pp. 1659–1659. ISSN: 0028-0836, 1476-4687. DOI: 10.1038/1821659a0. URL: https://www.nature.com/articles/1821659a0.

Andronesi, Ovidiu C. et al. (2005). "Determination of Membrane Protein Structure and Dynamics by Magic-Angle-Spinning Solid-State NMR Spectroscopy." In: *Journal of the American Chemical Society* 127.37, pp. 12965–12974. ISSN: 0002-7863, 1520-5126. DOI: 10.1021/ja0530164. URL: https://pubs.acs.org/doi/10.1021/ja0530164.

Aramini, James M. et al. (2014). "19F NMR Reveals Multiple Conformations at the Dimer Interface of the Nonstructural Protein 1 Effector Domain from Influenza A Virus." In: *Structure* 22.4, pp. 515–525. ISSN: 0969-2126. DOI: https://doi.org/10.1016/j.str.2014.01.010. URL: https://www.sciencedirect.com/science/article/pii/S0969212614000380.

Atkins, P. W. and Ronald Friedman (2011). *Molecular quantum mechanics*. 5th ed. Oxford ; New York: Oxford University Press. 537 pp. ISBN: 978-0-19-954142-3.

Audin, Maxime J. C. et al. (2013). "The Archaeal Exosome: Identification and Quantification of Site-Specific Motions That Correlate with Cap and RNA Binding." In: *Angewandte Chemie International Edition* 52.32, pp. 8312–8316. ISSN: 14337851. DOI: 10.1002/anie.201302811. URL: https://onlinelibrary.wiley.com/doi/10.1002/anie.201302811.

Avis, Johanna M., Graeme L. Conn, and Scott C. Walker (2012). "Cis-Acting Ribozymes for the Production of RNA In Vitro Transcripts with Defined 5' and 3' Ends." In: *Recombinant and In Vitro RNA Synthesis: Methods and Protocols*. Ed. by Graeme L. Conn. Totowa, NJ: Humana Press, pp. 83–98. ISBN: 978-1-62703-113-4. DOI: 10.1007/978-1-62703-113-4_7. URL: https://doi.org/10.1007/978-1-62703-113-4_7.

Axelrod, Daniel (2001). "Total Internal Reflection Fluorescence Microscopy in Cell Biology: Total Internal Reflection Fluorescence." In: *Traffic* 2.11, pp. 764–774. ISSN: 13989219. DOI: 10.1034/j.1600-0854.2001.21104.x. URL: http://doi.wiley.com/10.1034/j.1600-0854.2001.21104.x.

Baldus, Marc (2022). "Biological solid-state NMR: Integrative across different scientific disciplines." In: *Journal of Structural Biology: X* 6, p. 100075. ISSN: 25901524. DOI: 10.1016/j.yjsbx.2022.100075. URL: https://linkinghub.elsevier.com/retrieve/pii/S2590152422000162.

Baldwin, Andrew J and Lewis E Kay (2009). "NMR spectroscopy brings invisible protein states into focus." In: *Nature Chemical Biology* 5.11, pp. 808–814. ISSN: 1552-4450, 1552-4469. DOI: 10.1038/nchembio.238. URL: http://www.nature.com/articles/nchembio.238.

Baldwin, Andrew J. (2014). "An exact solution for R2,eff in CPMG experiments in the case of two site chemical exchange." In: *Journal of Magnetic Resonance* 244, pp. 114–124. ISSN: 10907807. DOI: 10.1016/j.jmr.2014.02.023. URL: https://linkinghub.elsevier.com/retrieve/pii/S1090780714000743.

Banani, Salman F. et al. (2017). "Biomolecular condensates: organizers of cellular biochemistry." In: *Nature Reviews Molecular Cell Biology* 18.5, pp. 285–298. ISSN: 1471-0072, 1471-0080. DOI: 10.1038/nrm.2017.7. URL: http://www.nature.com/articles/nrm.2017.7.

Banerjee, A K (1980). "5'-terminal cap structure in eucaryotic messenger ribonucleic acids." In: *Microbiological Reviews* 44.2, pp. 175–205. ISSN: 0146-0749. DOI: 10.1128/mr.44.2.175-205.1980. URL: https://journals.asm.org/doi/10.1128/mr.44.2.175-205.1980.

Banjade, Sudeep et al. (2015). "Conserved interdomain linker promotes phase separation of the multivalent adaptor protein Nck." In: *Proceedings of the National Academy of Sciences* 112.47. ISSN: 0027-8424, 1091-6490. DOI: 10.1073/pnas.1508778112. URL: https://pnas.org/doi/full/10.1073/pnas.1508778112.

Bann, James G. et al. (2002). "Real-time and equilibrium ¹⁹F-NMR studies reveal the role of domain–domain interactions in the folding of the chaperone PapD." In: *Proceedings of the National Academy of Sciences* 99.2, pp. 709–714. DOI: 10.1073/pnas.022649599. eprint: https://www.pnas.org/doi/pdf/10.1073/pnas.022649599. URL: https://www.pnas.org/doi/abs/10.1073/pnas.022649599.

Bax, Ad, Richard H Griffey, and Bruce L Hawkins (1983). "Correlation of proton and nitrogen-15 chemical shifts by multiple quantum NMR." In: *Journal of Magnetic Resonance (1969)* 55.2, pp. 301–315. ISSN: 00222364. DOI: 10.1016/0022-2364(83)90241-X. URL: https://linkinghub.elsevier.com/retrieve/pii/002223648390241X.

Beach, Heather et al. (2005). "Conservation of μs-ms Enzyme Motions in the Apo- and Substrate-Mimicked State." In: *Journal of the American Chemical Society* 127.25, pp. 9167–9176. ISSN: 0002-7863, 1520-5126. DOI: 10.1021/ja0514949. URL: https://pubs.acs.org/doi/10.1021/ja0514949.

Beck Erlach, Markus et al. (2017). "Pressure dependence of side chain 13C chemical shifts in model peptides Ac-Gly-Gly-Xxx-Ala-NH2." In: *Journal of Biomolecular NMR* 69.2, pp. 53–67. ISSN: 0925-2738, 1573-5001. DOI: 10.1007/s10858-017-0134-5. URL: http://link.springer.com/10.1007/s10858-017-0134-5.

Beelman, Clare A. et al. (1996). "An essential component of the decapping enzyme required for normal rates of mRNA turnover." In: *Nature* 382.6592, pp. 642–646. ISSN: 0028-0836, 1476-4687. DOI: 10.1038/382642a0. URL: http://www.nature.com/articles/382642a0.

Berg, Jeremy M. et al. (2018). *Stryer Biochemie*. Berlin, Heidelberg: Springer Berlin Heidelberg. ISBN: 978-3-662-54619-2 978-3-662-54620-8. DOI: 10.1007/978-3-662-54620-8. URL: http://link.springer.com/10.1007/978-3-662-54620-8.

Bernal, J. D. and D. Crowfoot (1934). "X-Ray Photographs of Crystalline Pepsin." In: *Nature* 133.3369, pp. 794–795. ISSN: 0028-0836, 1476-4687. DOI: 10.1038/133794b0. URL: https://www.nature.com/articles/133794b0.

Bessman, Maurice J., David N. Frick, and Suzanne F. O'Handley (1996). "The MutT Proteins or "Nudix" Hydrolases, a Family of Versatile, Widely Distributed, "Housecleaning" Enzymes." In: *Journal of Biological Chemistry* 271.41, pp. 25059–25062. ISSN: 00219258. DOI: 10.1074/jbc.271.41.25059. URL: https://linkinghub.elsevier.com/retrieve/pii/S0021925819782556.

Bezsonova, Irina et al. (2006). "Hydration and Packing along the Folding Pathway of SH3 Domains by Pressure-Dependent NMR." In: *Biochemistry* 45.15, pp. 4711–4719. ISSN: 0006-2960, 1520-4995. DOI: 10.1021/bi060177r. URL: https://pubs.acs.org/doi/10.1021/bi060177r.

Bhabha, Gira et al. (2011). "A Dynamic Knockout Reveals That Conformational Fluctuations Influence the Chemical Step of Enzyme Catalysis." In: *Science* 332.6026, pp. 234–238. ISSN: 0036-8075, 1095-9203. DOI: 10.1126/science.1198542. URL: https://www.science.org/doi/10.1126/science.1198542.

Bloch, F. (1946). "Nuclear Induction." In: *Physical Review* 70.7, pp. 460–474. ISSN: 0031-899X. DOI: 10.1103/PhysRev.70.460. URL: https://link.aps.org/doi/10.1103/PhysRev.70.460.

Bloch, F., W. W. Hansen, and Martin Packard (1946). "Nuclear Induction." In: *Physical Review* 69.3, pp. 127–127. ISSN: 0031-899X. DOI: 10.1103/PhysRev.69.127. URL: https://link.aps.org/doi/10.1103/PhysRev.69.127.

Blundell, Tom L. and Peter E. Wright (2022). "Structural Biology – Painting the Mechanistic Landscape of Biomolecules." In: *Journal of Molecular Biology* 434.10, p. 167566. ISSN: 0022-2836. DOI: https://doi.org/10.1016/j.jmb.2022.167566. URL: https://www.sciencedirect.com/science/article/pii/S0022283622001401.

Bodenhausen, Geoffrey and David J. Ruben (1980). "Natural abundance nitrogen-15 NMR by enhanced heteronuclear spectroscopy." In: *Chemical Physics Letters* 69.1, pp. 185–189. ISSN: 00092614. DOI: 10.1016/0009-2614(80)80041-8. URL: https://linkinghub.elsevier.com/retrieve/pii/0009261480800418.

Boehr, David D, Ruth Nussinov, and Peter E Wright (2009). "The role of dynamic conformational ensembles in biomolecular recognition." In: *Nature Chemical Biology* 5.11, pp. 789–796. ISSN: 1552-4450, 1552-4469. DOI: 10.1038/nchembio.232. URL: http://www.nature.com/articles/nchembio.232.

Boehr, David D., H. Jane Dyson, and Peter E. Wright (2006). "An NMR Perspective on Enzyme Dynamics." In: *Chemical Reviews* 106.8, pp. 3055–3079. ISSN: 0009-2665, 1520-6890. DOI: 10.1021/cr050312q. URL: https://pubs.acs.org/doi/10.1021/cr050312q.

Boehr, David D., Dan McElheny, et al. (2006). "The Dynamic Energy Landscape of Dihydrofolate Reductase Catalysis." In: *Science* 313.5793, pp. 1638–1642. ISSN: 0036-8075, 1095-9203. DOI: 10.1126/science.1130258. URL: https://www.science.org/doi/10.1126/science.1130258.

Boehr, David D., Dan McElheny, et al. (2010). "Millisecond timescale fluctuations in dihydrofolate reductase are exquisitely sensitive to the bound ligands." In: *Proceedings of the National Academy of Sciences* 107.4, pp. 1373–1378. ISSN: 0027-8424, 1091-6490. DOI: 10.1073/pnas.0914163107. URL: https://pnas.org/doi/full/10.1073/pnas.0914163107.

Boehr, David D. and Peter E. Wright (2008). "How Do Proteins Interact?" In: *Science* 320.5882, pp. 1429–1430. ISSN: 0036-8075, 1095-9203. DOI: 10.1126/science.1158818. URL: https://www.science.org/doi/10.1126/science.1158818.

Boo, Sung Ho and Yoon Ki Kim (2020). "The emerging role of RNA modifications in the regulation of mRNA stability." In: *Experimental & Molecular Medicine* 52.3, pp. 400–408. ISSN: 1226-3613, 2092-6413. DOI: 10.1038/s12276-020-0407-z. URL: https://www.nature.com/articles/s12276-020-0407-z.

Borja, Mark S. et al. (2011). "Dcp1 links coactivators of mRNA decapping to Dcp2 by proline recognition." In: *RNA* 17.2, pp. 278–290. ISSN: 1355-8382, 1469-9001. DOI: 10.1261/rna.2382011. URL: http://rnajournal.cshlp.org/lookup/doi/10.1261/rna.2382011.

Borman, A. M. (2000). "Biochemical characterisation of cap-poly(A) synergy in rabbit reticulocyte lysates: the eIF4G-PABP interaction increases the functional affinity of eIF4E for the capped mRNA 5'-end." In: *Nucleic Acids Research* 28.21, pp. 4068–4075. ISSN: 13624962. DOI: 10.1093/nar/28.21.4068. URL: https://academic.oup.com/nar/article-lookup/doi/10.1093/nar/28.21.4068.

Bossé, Gabriel D. et al. (2013). "The Decapping Scavenger Enzyme DCS-1 Controls MicroRNA Levels in Caenorhabditis elegans." In: *Molecular Cell* 50.2, pp. 281–287. ISSN: 10972765. DOI: 10.1016/j.molcel.2013.02.023. URL: https://linkinghub.elsevier.com/retrieve/pii/S1097276513001792.

Bothe, Jameson R., Zachary W. Stein, and Hashim M. Al-Hashimi (2014). "Evaluating the uncertainty in exchange parameters determined from off-resonance R1ρ relaxation dispersion for systems in fast exchange." In: *Journal of Magnetic Resonance* 244, pp. 18–29. ISSN: 10907807. DOI: 10.1016/j.jmr.2014.04.010. URL: https://linkinghub.elsevier.com/retrieve/pii/S1090780714001177.

Bouvignies, Guillaume et al. (2011). "Solution structure of a minor and transiently formed state of a T4 lysozyme mutant." In: *Nature* 477.7362, pp. 111–114. ISSN: 0028-0836, 1476-4687. DOI: 10.1038/nature10349. URL: https://www.nature.com/articles/nature10349.

Bragg, William Henry (1915). "IX. Bakerian Lecture.— X-rays and crystal structure." In: *Philosophical Transactions of the Royal Society of London. Series A, Containing Papers of a Mathematical or Physical Character* 215.523, pp. 253–274. ISSN: 0264-3952, 2053-9258. DOI: 10.1098/rsta.1915.0009. URL: https://royalsocietypublishing.org/doi/10.1098/rsta.1915.0009.

Bragg, William Lawrence (1929). "The determination of parameters in crystal structures by means of Fourier series." In: *Proceedings of the Royal Society of London. Series A, Containing Papers of a Mathematical and Physical Character* 123.792, pp. 537–559. ISSN: 0950-1207, 2053-9150. DOI: 10.1098/rspa.1929.0083. URL: https://royalsocietypublishing.org/doi/10.1098/rspa.1929.0083.

Brangwynne, Clifford P., Christian R. Eckmann, et al. (2009). "Germline P Granules Are Liquid Droplets That Localize by Controlled Dissolution/Condensation." In: *Science* 324.5935, pp. 1729–1732. ISSN: 0036-8075, 1095-9203. DOI: 10.1126/science.1172046. URL: https://www.science.org/doi/10.1126/science.1172046.

Brangwynne, Clifford P., Timothy J. Mitchison, and Anthony A. Hyman (2011). "Active liquid-like behavior of nucleoli determines their size and shape in *Xenopus laevis* oocytes." In: *Proceedings of the National Academy of Sciences* 108.11, pp. 4334–4339. ISSN: 0027-8424, 1091-6490. DOI: 10.1073/pnas.1017150108. URL: https://pnas.org/doi/full/10.1073/pnas.1017150108.

Brangwynne, Clifford P., Peter Tompa, and Rohit V. Pappu (2015). "Polymer physics of intracellular phase transitions." In: *Nature Physics* 11.11, pp. 899–904. ISSN: 1745-2473, 1745-2481. DOI: 10.1038/nphys3532. URL: https://www.nature.com/articles/nphys3532.

Bridge, Thomas et al. (2023). "Site-specific encoding of photoactivity and photoreactivity into antibody fragments." In: *Nature Chemical Biology*. ISSN: 1552-4450, 1552-4469. DOI: 10.1038/s41589-022-01251-9. URL: https://www.nature.com/articles/s41589-022-01251-9.

Brüschweiler, Sven, Robert Konrat, and Martin Tollinger (2013). "Allosteric Communication in the KIX Domain Proceeds through Dynamic Repacking of the Hydrophobic Core." In: *ACS Chemical Biology* 8.7. PMID: 23651431, pp. 1600–1610. DOI: 10.1021/cb4002188. eprint: https://doi.org/10.1021/cb4002188. URL: https://doi.org/10.1021/cb4002188.

Brüschweiler, Sven, Paul Schanda, et al. (2009). "Direct Observation of the Dynamic Process Underlying Allosteric Signal Transmission." In: *Journal of the American Chemical Society* 131.8, pp. 3063–3068. ISSN: 0002-7863, 1520-5126. DOI: 10.1021/ja809947w. URL: https://pubs.acs.org/doi/10.1021/ja809947w.

Campos-Olivas, Ramón et al. (2002). "Placement of 19F into the center of GB1: effects on structure and stability." In: *FEBS Letters* 517.1-3, pp. 55–60. DOI: https://doi.org/10.1016/S0014-5793(02)02577-2. eprint: https://febs.onlinelibrary.wiley.com/doi/pdf/10.1016/S0014-5793%2802%2902577-2. URL: https://febs.onlinelibrary.wiley.com/doi/abs/10.1016/S0014-5793%2802%2902577-2.

Carr, H. Y. and E. M. Purcell (1954). "Effects of Diffusion on Free Precession in Nuclear Magnetic Resonance Experiments." In: *Physical Review* 94.3, pp. 630–638. ISSN: 0031-899X. DOI: 10.1103/PhysRev.94.630. URL: https://link.aps.org/doi/10.1103/PhysRev.94.630.

Cavanagh, John et al. (2007). "CLASSICAL NMR SPECTROSCOPY." In: *Protein NMR Spectroscopy*. Elsevier, pp. 1–28. ISBN: 978-0-12-164491-8. DOI: 10.1016/B978-012164491-8/50003-8. URL: https://linkinghub.elsevier.com/retrieve/pii/B9780121644918500038.

Ceccon, Alberto, Vitali Tugarinov, and G. Marius Clore (2021). "Quantitative Exchange NMR-Based Analysis of Huntingtin–SH3 Interactions Suggests an Allosteric Mechanism of Inhibition of Huntingtin Aggregation." In: *Journal of the American Chemical Society* 143.25, pp. 9672–9681. ISSN: 0002-7863, 1520-5126. DOI: 10.1021/jacs.1c04786. URL: https://pubs.acs.org/doi/10.1021/jacs.1c04786.

Charenton, Clément, Claudine Gaudon-Plesse, et al. (2017). "A unique surface on Pat1 C-terminal domain directly interacts with Dcp2 decapping enzyme and Xrn1 5'–3' mRNA exonuclease in yeast." In: *Proceedings of the National Academy of Sciences* 114.45. ISSN: 0027-8424, 1091-6490. DOI: 10.1073/pnas.1711680114. URL: https://pnas.org/doi/full/10.1073/pnas.1711680114.

Charenton, Clément, Valerio Taverniti, et al. (2016). "Structure of the active form of Dcp1–Dcp2 decapping enzyme bound to m^7GDP and its Edc3 activator." In: *Nature Structural & Molecular*

Biology 23.11, pp. 982–986. ISSN: 1545-9993, 1545-9985. DOI: 10.1038/nsmb.3300. URL: http://www.nature.com/articles/nsmb.3300.

Charlier, Cyril, T. Reid Alderson, et al. (2018). "Study of protein folding under native conditions by rapidly switching the hydrostatic pressure inside an NMR sample cell." In: *Proceedings of the National Academy of Sciences* 115.18, E4169–E4178. DOI: 10.1073/pnas.1803642115. eprint: https://www.pnas.org/doi/pdf/10.1073/pnas.1803642115. URL: https://www.pnas.org/doi/abs/10.1073/pnas.1803642115.

Charlier, Cyril, Joseph M. Courtney, T. Reid Alderson, et al. (2018). "Monitoring ^{15} N Chemical Shifts During Protein Folding by Pressure-Jump NMR." In: *Journal of the American Chemical Society* 140.26, pp. 8096–8099. ISSN: 0002-7863, 1520-5126. DOI: 10.1021/jacs.8b04833. URL: https://pubs.acs.org/doi/10.1021/jacs.8b04833.

Charlier, Cyril, Joseph M. Courtney, Philip Anfinrud, et al. (2018). "Interrupted Pressure-Jump NMR Experiments Reveal Resonances of On-Pathway Protein Folding Intermediate." In: *The Journal of Physical Chemistry B* 122.49, pp. 11792–11799. ISSN: 1520-6106, 1520-5207. DOI: 10.1021/acs.jpcb.8b08456. URL: https://pubs.acs.org/doi/10.1021/acs.jpcb.8b08456.

Chen, Bo and Robert Tycko (2010). "Structural and dynamical characterization of tubular HIV-1 capsid protein assemblies by solid state nuclear magnetic resonance and electron microscopy: Solid State NMR of HIV-1 Capsid Assemblies." In: *Protein Science* 19.4, pp. 716–730. ISSN: 09618368. DOI: 10.1002/pro.348. URL: https://onlinelibrary.wiley.com/doi/10.1002/pro.348.

Chen, Calvin R and George I Makhatadze (2015). "ProteinVolume: calculating molecular van der Waals and void volumes in proteins." In: *BMC bioinformatics* 16, p. 101. ISSN: 1471-2105. DOI: 10.1186/s12859-015-0531-2. URL: https://europepmc.org/articles/PMC4379742.

Chen, Nan, Martin A. Walsh, et al. (2005). "Crystal Structures of Human DcpS in Ligand-free and m^{7}GDP-bound forms Suggest a Dynamic Mechanism for Scavenger mRNA Decapping." In: *Journal of Molecular Biology* 347.4, pp. 707–718. ISSN: 00222836. DOI: 10.1016/j.jmb.2005.01.062. URL: https://linkinghub.elsevier.com/retrieve/pii/S0022283605001191.

Cheng, Yifan et al. (2015). "A Primer to Single-Particle Cryo-Electron Microscopy." In: *Cell* 161.3, pp. 438–449. ISSN: 00928674. DOI: 10.1016/j.cell.2015.03.050. URL: https://linkinghub.elsevier.com/retrieve/pii/S0092867415003700.

Chrominski, Mikolaj et al. (2020). "Synthesis of Trifluoromethylated Purine Ribonucleotides and Their Evaluation as ^{19} F NMR Probes." In: *The Journal of Organic Chemistry* 85.5, pp. 3440–3453. ISSN: 0022-3263, 1520-6904. DOI: 10.1021/acs.joc.9b03198. URL: https://pubs.acs.org/doi/10.1021/acs.joc.9b03198.

Crowley, Peter B., Ciara Kyne, and William B. Monteith (2012). "Simple and inexpensive incorporation of 19F-Tryptophan for protein NMR spectroscopy." In: *Chemical Communications* 48.86, p. 10681. ISSN: 1359-7345, 1364-548X. DOI: 10.1039/c2cc35347d. URL: http://xlink.rsc.org/?DOI=c2cc35347d.

Cvetkovic, Milos A et al. (2017). "The Rrp4–exosome complex recruits and channels substrate RNA by a unique mechanism." In: *Nature Chemical Biology* 13.5, pp. 522–528. ISSN: 1552-4450, 1552-4469. DOI: 10.1038/nchembio.2328. URL: https://www.nature.com/articles/nchembio.2328.

Dahan, Maxime et al. (1999). "Ratiometric measurement and identification of single diffusing molecules." In: *Chemical Physics* 247.1, pp. 85–106. ISSN: 03010104. DOI: 10.1016/S0301-0104(99)00132-9. URL: https://linkinghub.elsevier.com/retrieve/pii/S0301010499001329.

Dale, R.E., J. Eisinger, and W.E. Blumberg (1979). "The orientational freedom of molecular probes. The orientation factor in intramolecular energy transfer." In: *Biophysical Journal* 26.2, pp. 161–193. ISSN: 00063495. DOI: 10.1016/S0006-3495(79)85243-1. URL: https://linkinghub.elsevier.com/retrieve/pii/S0006349579852431.

Dalvit, Claudio and Anna Vulpetti (2016). "Weak Intermolecular Hydrogen Bonds with Fluorine: Detection and Implications for Enzymatic/Chemical Reactions, Chemical Properties, and Ligand/Protein Fluorine NMR Screening." In: *Chemistry – A European Journal* 22.22, pp. 7592–7601. DOI: https://doi.org/10.1002/chem.201600446. eprint: https://chemistry-europe.onlinelibrary.wiley.com/doi/pdf/10.1002/chem.201600446. URL: https://chemistry-europe.onlinelibrary.wiley.com/doi/abs/10.1002/chem.201600446.

Damman, Reinier et al. (2019). "Atomic-level insight into mRNA processing bodies by combining solid and solution-state NMR spectroscopy." In: *Nature Communications* 10.1, p. 4536. ISSN: 2041-1723. DOI: 10.1038/s41467-019-12402-3. URL: https://www.nature.com/articles/s41467-019-12402-3.

Decker, Carolyn J. and Roy Parker (2012). "P-bodies and stress granules: possible roles in the control of translation and mRNA degradation." In: *Cold Spring Harbor Perspectives in Biology* 4.9, a012286. ISSN: 1943-0264. DOI: 10.1101/cshperspect.a012286.

Delaglio, F et al. (1995). "NMRPipe: a multidimensional spectral processing system based on UNIX pipes." In: *Journal of biomolecular NMR* 6.3, pp. 277–293. ISSN: 0925-2738. DOI: 10.1007/bf00197809. URL: https://doi.org/10.1007/BF00197809.

Deniz, Ashok A, Ted A Laurence, Maxime Dahan, et al. (2001). "Ratiometric Single-Molecule Studies of Freely Diffusing Biomolecules." In: *Annual Review of Physical Chemistry* 52.1, pp. 233–253. ISSN: 0066-426X, 1545-1593. DOI: 10.1146/annurev.physchem.52.1.233. URL: https://www.annualreviews.org/doi/10.1146/annurev.physchem.52.1.233.

Deniz, Ashok A., Maxime Dahan, et al. (1999). "Single-pair fluorescence resonance energy transfer on freely diffusing molecules: Observation of Förster distance dependence and subpopulations." In: *Proceedings of the National Academy of Sciences* 96.7, pp. 3670–3675. ISSN: 0027-8424, 1091-6490. DOI: 10.1073/pnas.96.7.3670. URL: https://pnas.org/doi/full/10.1073/pnas.96.7.3670.

Deniz, Ashok A., Ted A. Laurence, Gangamani S. Beligere, et al. (2000). "Single-molecule protein folding: Diffusion fluorescence resonance energy transfer studies of the denaturation of chymotrypsin inhibitor 2." In: *Proceedings of the National Academy of Sciences* 97.10, pp. 5179–5184. ISSN: 0027-8424, 1091-6490. DOI: 10.1073/pnas.090104997. URL: https://pnas.org/doi/full/10.1073/pnas.090104997.

Deshmukh, Mandar V. et al. (2008). "mRNA Decapping Is Promoted by an RNA-Binding Channel in Dcp2." In: *Molecular Cell* 29.3, pp. 324–336. ISSN: 10972765. DOI: 10.1016/j.molcel.2007.11.027. URL: https://linkinghub.elsevier.com/retrieve/pii/S1097276507008568.

Despic, Vladimir and Samie R. Jaffrey (2023). "mRNA ageing shapes the Cap2 methylome in mammalian mRNA." In: *Nature* 614.7947, pp. 358–366. ISSN: 0028-0836, 1476-4687. DOI: 10.1038/s41586-022-05668-z. URL: https://www.nature.com/articles/s41586-022-05668-z.

Didenko, Tatiana et al. (2013). "Fluorine-19 NMR of integral membrane proteins illustrated with studies of GPCRs." In: *Current Opinion in Structural Biology* 23.5. Protein-carbohydrate interactions / Biophysical methods, pp. 740–747. ISSN: 0959-440X. DOI: https://doi.org/10.1016/j.sbi.2013.07.011. URL: https://www.sciencedirect.com/science/article/pii/S0959440X13001449.

Dijk, E. van (2002). "Human Dcp2: a catalytically active mRNA decapping enzyme located in specific cytoplasmic structures." In: *The EMBO Journal* 21.24, pp. 6915–6924. ISSN: 14602075. DOI: 10.1093/emboj/cdf678. URL: http://emboj.embopress.org/cgi/doi/10.1093/emboj/cdf678.

Doucet, Nicolas, Eric D. Watt, and J. Patrick Loria (2009). "The Flexibility of a Distant Loop Modulates Active Site Motion and Product Release in Ribonuclease A." In: *Biochemistry* 48.30, pp. 7160–7168. ISSN: 0006-2960, 1520-4995. DOI: 10.1021/bi900830g. URL: https://pubs.acs.org/doi/10.1021/bi900830g.

Doucleff, Michaeleen and G. Marius Clore (2008). "Global jumping and domain-specific intersegment transfer between DNA cognate sites of the multidomain transcription factor Oct-1." In: *Proceedings of the National Academy of Sciences* 105.37, pp. 13871–13876. ISSN: 0027-8424, 1091-6490. DOI: 10.1073/pnas.0805050105. URL: https://pnas.org/doi/full/10.1073/pnas.0805050105.

Dreydoppel, Matthias, Paul Becker, et al. (2018). "Equilibrium and Kinetic Unfolding of GB1: Stabilization of the Native State by Pressure." In: *The Journal of Physical Chemistry B* 122.38. PMID: 30185038, pp. 8846–8852. DOI: 10.1021/acs.jpcb.8b06888. eprint: https://doi.org/10.1021/acs.jpcb.8b06888. URL: https://doi.org/10.1021/acs.jpcb.8b06888.

Dreydoppel, Matthias, Britta Dorn, et al. (2021). "Transition-State Compressibility and Activation Volume of Transient Protein Conformational Fluctuations." In: *JACS Au* 1.6. PMID: 34467336, pp. 833–842. DOI: 10.1021/jacsau.1c00062. eprint: https://doi.org/10.1021/jacsau.1c00062. URL: https://doi.org/10.1021/jacsau.1c00062.

Dyson, H.Jane and Peter E. Wright (2005). "Elucidation of the Protein Folding Landscape by NMR." In: *Methods in Enzymology*. Vol. 394. Elsevier, pp. 299–321. ISBN: 978-0-12-182799-1. DOI: 10.1016/S0076-6879(05)94011-1. URL: https://linkinghub.elsevier.com/retrieve/pii/S0076687905940111.

Eckmann, Christian R., Christiane Rammelt, and Elmar Wahle (2011). "Control of poly(A) tail length: Control of poly(A) tail length." In: *Wiley Interdisciplinary Reviews: RNA* 2.3, pp. 348–361. ISSN: 17577004. DOI: 10.1002/wrna.56. URL: https://onlinelibrary.wiley.com/doi/10.1002/wrna.56.

Eisenmesser, Elan Z., Oscar Millet, et al. (2005). "Intrinsic dynamics of an enzyme underlies catalysis." In: *Nature* 438.7064, pp. 117–121. ISSN: 0028-0836, 1476-4687. DOI: 10.1038/nature04105. URL: https://www.nature.com/articles/nature04105.

Eisenmesser, Elan Zohar, Daryl A. Bosco, et al. (2002). "Enzyme Dynamics During Catalysis." In: *Science* 295.5559, pp. 1520–1523. ISSN: 0036-8075, 1095-9203. DOI: 10.1126/science.1066176. URL: https://www.science.org/doi/10.1126/science.1066176.

Elbaum-Garfinkle, Shana et al. (2015). "The disordered P granule protein LAF-1 drives phase separation into droplets with tunable viscosity and dynamics." In: *Proceedings of the National Academy of Sciences* 112.23, pp. 7189–7194. ISSN: 0027-8424, 1091-6490. DOI: 10.1073/pnas.1504822112. URL: https://pnas.org/doi/full/10.1073/pnas.1504822112.

Falzone, Christopher J., Peter E. Wright, and Stephen J. Benkovic (1994). "Dynamics of a flexible loop in dihydrofolate reductase from Escherichia coli and its implication for catalysis." In: *Biochemistry* 33.2, pp. 439–442. ISSN: 0006-2960, 1520-4995. DOI: 10.1021/bi00168a007. URL: https://pubs.acs.org/doi/abs/10.1021/bi00168a007.

Farber, Patrick J. and Anthony Mittermaier (2015). "Relaxation dispersion NMR spectroscopy for the study of protein allostery." In: *Biophysical Reviews* 7.2, pp. 191–200. ISSN: 1867-2450, 1867-2469. DOI: 10.1007/s12551-015-0166-6. URL: http://link.springer.com/10.1007/s12551-015-0166-6.

Farrow, Neil A. et al. (1994). "A heteronuclear correlation experiment for simultaneous determination of 15N longitudinal decay and chemical exchange rates of systems in slow equilibrium." In: *Journal of Biomolecular NMR* 4.5, pp. 727–734. ISSN: 0925-2738, 1573-5001. DOI: 10.1007/BF00404280. URL: http://link.springer.com/10.1007/BF00404280.

Fischer, Niels et al. (2015). "Structure of the E. coli ribosome-EF-Tu complex at <3 Å resolution by Cs-corrected cryo-EM." In: *Nature* 520.7548, pp. 567–570. ISSN: 1476-4687. DOI: 10.1038/nature14275.

Fitzpatrick, Anthony W. P. et al. (2017). "Cryo-EM structures of tau filaments from Alzheimer's disease." In: *Nature* 547.7662, pp. 185–190. ISSN: 0028-0836, 1476-4687. DOI: 10.1038/nature23002. URL: https://www.nature.com/articles/nature23002.

Floor, Stephen N., Mark S. Borja, and John D. Gross (2012). "Interdomain dynamics and coactivation of the mRNA decapping enzyme Dcp2 are mediated by a gatekeeper tryptophan." In: *Proceedings of the National Academy of Sciences* 109.8, pp. 2872–2877. ISSN: 0027-8424, 1091-6490. DOI: 10.1073/pnas.1113620109. URL: https://pnas.org/doi/full/10.1073/pnas.1113620109.

Forster, Th. (1946). "Energiewanderung und Fluoreszenz." In: *Die Naturwissenschaften* 33.6, pp. 166–175. ISSN: 0028-1042, 1432-1904. DOI: 10.1007/BF00585226. URL: http://link.springer.com/10.1007/BF00585226.

Förster, Th. and Th. Forster (1960). "Transfer Mechanisms of Electronic Excitation Energy." In: *Radiation Research Supplement* 2, p. 326. ISSN: 04858611. DOI: 10.2307/3583604. URL: https://www.jstor.org/stable/3583604?origin=crossref.

Fox, A. H. and A. I. Lamond (2010). "Paraspeckles." In: *Cold Spring Harbor Perspectives in Biology* 2.7, a000687–a000687. ISSN: 1943-0264. DOI: 10.1101/cshperspect.a000687. URL: http://cshperspectives.cshlp.org/lookup/doi/10.1101/cshperspect.a000687.

Fraser, James S. et al. (2009). "Hidden alternative structures of proline isomerase essential for catalysis." In: *Nature* 462.7273, pp. 669–673. ISSN: 0028-0836, 1476-4687. DOI: 10.1038/nature08615. URL: http://www.nature.com/articles/nature08615.

Frauenfelder, Hans, Stephen G. Sligar, and Peter G. Wolynes (1991). "The Energy Landscapes and Motions of Proteins." In: *Science* 254.5038, pp. 1598–1603. ISSN: 0036-8075, 1095-9203. DOI: 10.1126/science.1749933. URL: https://www.science.org/doi/10.1126/science.1749933.

Frei, J. Niclas et al. (2020). "Conformational plasticity of ligand-bound and ternary GPCR complexes studied by 19F NMR of the β1-adrenergic receptor." In: *Nature Communications* 11.1, p. 669. ISSN: 2041-1723. DOI: 10.1038/s41467-020-14526-3. URL: https://www.nature.com/articles/s41467-020-14526-3.

Frey, Steffen, Ralf P. Richter, and Dirk Görlich (2006). "FG-Rich Repeats of Nuclear Pore Proteins Form a Three-Dimensional Meshwork with Hydrogel-Like Properties." In: *Science* 314.5800, pp. 815–817. ISSN: 0036-8075, 1095-9203. DOI: 10.1126/science.1132516. URL: https://www.science.org/doi/10.1126/science.1132516.

Fromm, Simon A, Vincent Truffault, et al. (2012). "The structural basis of Edc3- and Scd6-mediated activation of the Dcp1:Dcp2 mRNA decapping complex: Structure of the Edc3-Dcp2 complex." In: *The EMBO Journal* 31.2, pp. 279–290. ISSN: 02614189. DOI: 10.1038/emboj.2011.408. URL: http://emboj.embopress.org/cgi/doi/10.1038/emboj.2011.408.

Fromm, Simon A., Julia Kamenz, et al. (2014). "In Vitro Reconstitution of a Cellular Phase-Transition Process that Involves the mRNA Decapping Machinery." In: *Angewandte Chemie International*

Edition 53.28, pp. 7354–7359. ISSN: 1433-7851, 1521-3773. DOI: 10.1002/anie.201402885. URL: https://onlinelibrary.wiley.com/doi/10.1002/anie.201402885.

Fuchs, Anna-Lisa et al. (2020). "Molecular basis of the selective processing of short mRNA substrates by the DcpS mRNA decapping enzyme." In: *Proceedings of the National Academy of Sciences* 117.32, pp. 19237–19244. ISSN: 0027-8424, 1091-6490. DOI: 10.1073/pnas.2009362117. URL: https://pnas.org/doi/full/10.1073/pnas.2009362117.

Furter, Rolf (1998). "Expansion of the genetic code: Site-directed p-fluoro-phenylalanine incorporation in Escherichia coli." In: *Protein Science* 7.2, pp. 419–426. DOI: https://doi.org/10.1002/pro.5560070223. eprint: https://onlinelibrary.wiley.com/doi/pdf/10.1002/pro.5560070223. URL: https://onlinelibrary.wiley.com/doi/abs/10.1002/pro.5560070223.

Furukawa, Ayako et al. (2016). "Quantitative analysis of protein–ligand interactions by NMR." In: *Progress in Nuclear Magnetic Resonance Spectroscopy* 96, pp. 47–57. ISSN: 00796565. DOI: 10.1016/j.pnmrs.2016.02.002. URL: https://linkinghub.elsevier.com/retrieve/pii/S007965651600008X.

Gagné, Donald et al. (2020). *Use of High Pressure NMR Spectroscopy to Rapidly Identify Proteins with Internal Ligand-Binding Voids*. preprint. Biophysics. DOI: 10.1101/2020.08.25.267195. URL: http://biorxiv.org/lookup/doi/10.1101/2020.08.25.267195.

Gardner, Kevin H. and Lewis E. Kay (1997). "Production and Incorporation of ^{15} N, ^{13} C, ^{2} H (^{1} H-δ1 Methyl) Isoleucine into Proteins for Multidimensional NMR Studies." In: *Journal of the American Chemical Society* 119.32, pp. 7599–7600. ISSN: 0002-7863, 1520-5126. DOI: 10.1021/ja9706514. URL: https://pubs.acs.org/doi/10.1021/ja9706514.

Garneau, Nicole L., Jeffrey Wilusz, and Carol J. Wilusz (2007). "The highways and byways of mRNA decay." In: *Nature Reviews Molecular Cell Biology* 8.2, pp. 113–126. ISSN: 1471-0072, 1471-0080. DOI: 10.1038/nrm2104. URL: http://www.nature.com/articles/nrm2104.

Gelis, Ioannis et al. (2007). "Structural Basis for Signal-Sequence Recognition by the Translocase Motor SecA as Determined by NMR." In: *Cell* 131.4, pp. 756–769. ISSN: 00928674. DOI: 10.1016/j.cell.2007.09.039. URL: https://linkinghub.elsevier.com/retrieve/pii/S009286740701269X.

Ghassemi, Nader et al. (2022). "Solid-State NMR Investigations of Extracellular Matrixes and Cell Walls of Algae, Bacteria, Fungi, and Plants." In: *Chemical Reviews* 122.10, pp. 10036–10086. ISSN: 0009-2665, 1520-6890. DOI: 10.1021/acs.chemrev.1c00669. URL: https://pubs.acs.org/doi/10.1021/acs.chemrev.1c00669.

Ghosh, Ujjayini et al. (2021). "Structural differences in amyloid-β fibrils from brains of nondemented elderly individuals and Alzheimer's disease patients." In: *Proceedings of the National Academy of Sciences* 118.45, e2111863118. ISSN: 0027-8424, 1091-6490. DOI: 10.1073/pnas.2111863118. URL: https://pnas.org/doi/full/10.1073/pnas.2111863118.

Glowacz, Katarzyna A. (2021). "Untersuchung der Konformationsgleichgewichte des Dcp1:Dcp2-Decapping Komplexes mittels Einzelmolekül FRET." Master's thesis. University of Regensburg, Center for Biochemistry.

Gomes, Edward and James Shorter (2019). "The molecular language of membraneless organelles." In: *Journal of Biological Chemistry* 294.18, pp. 7115–7127. ISSN: 00219258. DOI: 10.1074/jbc.TM118.001192. URL: https://linkinghub.elsevier.com/retrieve/pii/S0021925820367910.

Goto, Natalie K and Lewis E Kay (2000). "New developments in isotope labeling strategies for protein solution NMR spectroscopy." In: *Current Opinion in Structural Biology* 10.5, pp. 585–592. ISSN:

0959440X. DOI: 10.1016/S0959-440X(00)00135-4. URL: https://linkinghub.elsevier.com/retrieve/pii/S0959440X00001354.

Gronenborn, Angela M. (2022). "Small, but powerful and attractive: 19F in biomolecular NMR." In: *Structure* 30.1, pp. 6–14. ISSN: 09692126. DOI: 10.1016/j.str.2021.09.009. URL: https://linkinghub.elsevier.com/retrieve/pii/S0969212621003373.

Gross, Michael and Rainer Jaenicke (1994). "Proteins under pressure. The influence of high hydrostatic pressure on structure, function and assembly of proteins and protein complexes." In: *European Journal of Biochemistry* 221.2, pp. 617–630. ISSN: 0014-2956, 1432-1033. DOI: 10.1111/j.1432-1033.1994.tb18774.x. URL: https://onlinelibrary.wiley.com/doi/10.1111/j.1432-1033.1994.tb18774.x.

Grzesiek, Stephan et al. (1993). "Carbon-13 line narrowing by deuterium decoupling in deuterium/carbon-13/nitrogen-15 enriched proteins. Application to triple resonance 4D J connectivity of sequential amides." In: *Journal of the American Chemical Society* 115.10, pp. 4369–4370. ISSN: 0002-7863, 1520-5126. DOI: 10.1021/ja00063a068. URL: https://pubs.acs.org/doi/abs/10.1021/ja00063a068.

Gu, Meigang et al. (2004). "Insights into the Structure, Mechanism, and Regulation of Scavenger mRNA Decapping Activity." In: *Molecular Cell* 14.1, pp. 67–80. ISSN: 10972765. DOI: 10.1016/S1097-2765(04)00180-7. URL: https://linkinghub.elsevier.com/retrieve/pii/S1097276504001807.

Gueron, M., J. L. Leroy, and R. H. Griffey (1983). "Proton nuclear magnetic relaxation of nitrogen-15-labeled nucleic acids via dipolar coupling and chemical shift anisotropy." In: *Journal of the American Chemical Society* 105.25, pp. 7262–7266. ISSN: 0002-7863, 1520-5126. DOI: 10.1021/ja00363a009. URL: https://pubs.acs.org/doi/abs/10.1021/ja00363a009.

Gust, Alexander et al. (2014). "A Starting Point for Fluorescence-Based Single-Molecule Measurements in Biomolecular Research." In: *Molecules* 19.10, pp. 15824–15865. ISSN: 1420-3049. DOI: 10.3390/molecules191015824. URL: http://www.mdpi.com/1420-3049/19/10/15824.

Ha, Taekjip et al. (1999). "Single-molecule fluorescence spectroscopy of enzyme conformational dynamics and cleavage mechanism." In: *Proceedings of the National Academy of Sciences* 96.3, pp. 893–898. ISSN: 0027-8424, 1091-6490. DOI: 10.1073/pnas.96.3.893. URL: https://pnas.org/doi/full/10.1073/pnas.96.3.893.

Han, Gye Won et al. (2005). "Crystal structure of an Apo mRNA decapping enzyme (DcpS) from Mouse at 1.83 Å resolution." In: *Proteins: Structure, Function, and Bioinformatics* 60.4, pp. 797–802. ISSN: 08873585. DOI: 10.1002/prot.20467. URL: https://onlinelibrary.wiley.com/doi/10.1002/prot.20467.

Hansen, D. Flemming, Pramodh Vallurupalli, and Lewis E. Kay (2008). "An Improved ^{15} N Relaxation Dispersion Experiment for the Measurement of Millisecond Time-Scale Dynamics in Proteins." In: *The Journal of Physical Chemistry B* 112.19, pp. 5898–5904. ISSN: 1520-6106, 1520-5207. DOI: 10.1021/jp074793o. URL: https://pubs.acs.org/doi/10.1021/jp074793o.

Harigaya, Yuriko et al. (2010). "Identification and Analysis of the Interaction between Edc3 and Dcp2 in Saccharomyces cerevisiae." In: *Molecular and Cellular Biology* 30.6. PMID: 20086104, pp. 1446–1456. DOI: 10.1128/MCB.01305-09. eprint: https://doi.org/10.1128/MCB.01305-09. URL: https://doi.org/10.1128/MCB.01305-09.

Hartmann, S. R. and E. L. Hahn (1962). "Nuclear Double Resonance in the Rotating Frame." In: *Physical Review* 128.5, pp. 2042–2053. ISSN: 0031-899X. DOI: 10.1103/PhysRev.128.2042. URL: https://link.aps.org/doi/10.1103/PhysRev.128.2042.

He, Feng and Allan Jacobson (2015). "Control of mRNA decapping by positive and negative regulatory elements in the Dcp2 C-terminal domain." In: *RNA* 21.9, pp. 1633–1647. ISSN: 1355-8382, 1469-9001. DOI: 10.1261/rna.052449.115. URL: http://rnajournal.cshlp.org/lookup/doi/10.1261/rna.052449.115.

Heise, Henrike et al. (2005). "Molecular-level secondary structure, polymorphism, and dynamics of full-length α-synuclein fibrils studied by solid-state NMR." In: *Proceedings of the National Academy of Sciences* 102.44, pp. 15871–15876. ISSN: 0027-8424, 1091-6490. DOI: 10.1073/pnas.0506109102. URL: https://pnas.org/doi/full/10.1073/pnas.0506109102.

Hellenkamp, Björn et al. (2018). "Precision and accuracy of single-molecule FRET measurements—a multi-laboratory benchmark study." In: *Nature Methods* 15.9, pp. 669–676. ISSN: 1548-7091, 1548-7105. DOI: 10.1038/s41592-018-0085-0. URL: https://www.nature.com/articles/s41592-018-0085-0.

Hendrix, Jelle and Don C. Lamb (2013). "Pulsed Interleaved Excitation." In: *Methods in Enzymology*. Vol. 518. Elsevier, pp. 205–243. ISBN: 978-0-12-388422-0. DOI: 10.1016/B978-0-12-388422-0.00009-1. URL: https://linkinghub.elsevier.com/retrieve/pii/B9780123884220000091.

Hennig, Janosch and Michael Sattler (2014). "The dynamic duo: Combining NMR and small angle scattering in structural biology: Combining NMR and SAS." In: *Protein Science* 23.6, pp. 669–682. ISSN: 09618368. DOI: 10.1002/pro.2467. URL: https://onlinelibrary.wiley.com/doi/10.1002/pro.2467.

Hennig, Mirko, Lincoln G. Scott, et al. (2007). "Synthesis of 5-Fluoropyrimidine Nucleotides as Sensitive NMR Probes of RNA Structure." In: *Journal of the American Chemical Society* 129.48, pp. 14911–14921. ISSN: 0002-7863, 1520-5126. DOI: 10.1021/ja073825i. URL: https://pubs.acs.org/doi/10.1021/ja073825i.

Henzler-Wildman, Katherine and Dorothee Kern (2007). "Dynamic personalities of proteins." In: *Nature* 450.7172, pp. 964–972. ISSN: 0028-0836, 1476-4687. DOI: 10.1038/nature06522. URL: https://www.nature.com/articles/nature06522.

Ho, Bosco and Franz Gruswitz (2008). "HOLLOW: generating accurate representations of channel and interior surfaces in molecular structures." English. In: *BMC Structural Biology* 8, pp. 1–6. ISSN: 1472-6807. DOI: 10.1186/1472-6807-8-49.

Hoang, Joshua and R. Scott Prosser (2014). "Conformational Selection and Functional Dynamics of Calmodulin: A ^{19} F Nuclear Magnetic Resonance Study." In: *Biochemistry* 53.36, pp. 5727–5736. ISSN: 0006-2960, 1520-4995. DOI: 10.1021/bi500679c. URL: https://pubs.acs.org/doi/10.1021/bi500679c.

Hoffmann, Falk, Frans A. A. Mulder, and Lars V. Schäfer (2022). "How Much Entropy Is Contained in NMR Relaxation Parameters?" In: *The Journal of Physical Chemistry B* 126.1. PMID: 34936366, pp. 54–68. DOI: 10.1021/acs.jpcb.1c07786. eprint: https://doi.org/10.1021/acs.jpcb.1c07786. URL: https://doi.org/10.1021/acs.jpcb.1c07786.

Hollingsworth, Scott A. and Ron O. Dror (2018). "Molecular Dynamics Simulation for All." In: *Neuron* 99.6, pp. 1129–1143. ISSN: 08966273. DOI: 10.1016/j.neuron.2018.08.011. URL: https://linkinghub.elsevier.com/retrieve/pii/S0896627318306846.

Hull, William E. and Brian D. Sykes (1974). "Fluorotyrosine alkaline phosphatase. Fluorine-19 nuclear magnetic resonance relaxation times and molecular motion of the individual fluorotyrosines." In: *Biochemistry* 13.17. PMID: 4602295, pp. 3431–3437. DOI: 10.1021/bi00714a002. eprint: https://doi.org/10.1021/bi00714a002. URL: https://doi.org/10.1021/bi00714a002.

Hyman, Anthony A., Christoph A. Weber, and Frank Jülicher (2014). "Liquid-Liquid Phase Separation in Biology." In: *Annual Review of Cell and Developmental Biology* 30.1, pp. 39–58. ISSN: 1081-0706, 1530-8995. DOI: 10.1146/annurev-cellbio-100913-013325. URL: https://www.annualreviews.org/doi/10.1146/annurev-cellbio-100913-013325.

Iadanza, Matthew G. et al. (2018). "A new era for understanding amyloid structures and disease." In: *Nature Reviews Molecular Cell Biology* 19.12, pp. 755–773. ISSN: 1471-0072, 1471-0080. DOI: 10.1038/s41580-018-0060-8. URL: https://www.nature.com/articles/s41580-018-0060-8.

Ingelfinger, Dierk et al. (2002). "The human LSm1-7 proteins colocalize with the mRNA-degrading enzymes Dcp1/2 and Xrnl in distinct cytoplasmic foci." In: *RNA (New York, N.Y.)* 8.12, pp. 1489–1501. ISSN: 1355-8382.

Ishima, Rieko and Dennis A. Torchia (1999). "Estimating the time scale of chemical exchange of proteins from measurements of transverse relaxation rates in solution." In: *Journal of Biomolecular NMR* 14.4, pp. 369–372. ISSN: 09252738. DOI: 10.1023/A:1008324025406. URL: http://link.springer.com/10.1023/A:1008324025406.

Jackson, Jennifer C., Jared T. Hammill, and Ryan A. Mehl (2007). "Site-Specific Incorporation of a 19F-Amino Acid into Proteins as an NMR Probe for Characterizing Protein Structure and Reactivity." In: *Journal of the American Chemical Society* 129.5. PMID: 17263397, pp. 1160–1166. DOI: 10.1021/ja064661t. eprint: https://doi.org/10.1021/ja064661t. URL: https://doi.org/10.1021/ja064661t.

Jalkanen, Aimee L., Stephen J. Coleman, and Jeffrey Wilusz (2014). "Determinants and implications of mRNA poly(A) tail size – Does this protein make my tail look big?" In: *Seminars in Cell & Developmental Biology* 34, pp. 24–32. ISSN: 10849521. DOI: 10.1016/j.semcdb.2014.05.018. URL: https://linkinghub.elsevier.com/retrieve/pii/S1084952114001736.

Januszyk, Kurt and Christopher D Lima (2014). "The eukaryotic RNA exosome." In: *Current Opinion in Structural Biology* 24, pp. 132–140. ISSN: 0959440X. DOI: 10.1016/j.sbi.2014.01.011. URL: https://linkinghub.elsevier.com/retrieve/pii/S0959440X14000128.

Jeener, J. et al. (1979). "Investigation of exchange processes by two-dimensional NMR spectroscopy." In: *The Journal of Chemical Physics* 71.11, pp. 4546–4553. ISSN: 0021-9606, 1089-7690. DOI: 10.1063/1.438208. URL: https://pubs.aip.org/aip/jcp/article/71/11/4546-4553/785197.

Jiang, Yajun and Charalampos G. Kalodimos (2017). "NMR Studies of Large Proteins." In: *Journal of Molecular Biology* 429.17, pp. 2667–2676. ISSN: 00222836. DOI: 10.1016/j.jmb.2017.07.007. URL: https://linkinghub.elsevier.com/retrieve/pii/S0022283617303431.

Jonas, Stefanie and Elisa Izaurralde (2013). "The role of disordered protein regions in the assembly of decapping complexes and RNP granules." In: *Genes & Development* 27.24, pp. 2628–2641. ISSN: 0890-9369, 1549-5477. DOI: 10.1101/gad.227843.113. URL: http://genesdev.cshlp.org/lookup/doi/10.1101/gad.227843.113.

Jonchhe, Sagun et al. (2022). "Small Molecules Modulate Liquid-to-Solid Transitions in Phase-Separated Tau Condensates." In: *Angewandte Chemie International Edition* 61.23. ISSN: 1433-7851, 1521-3773. DOI: 10.1002/anie.202113156. URL: https://onlinelibrary.wiley.com/doi/10.1002/anie.202113156.

Jumper, John et al. (2021). "Highly accurate protein structure prediction with AlphaFold." In: *Nature* 596.7873, pp. 583–589. ISSN: 0028-0836, 1476-4687. DOI: 10.1038/s41586-021-03819-2. URL: https://www.nature.com/articles/s41586-021-03819-2.

Kalbitzer, Hans Robert et al. (2013). "Intrinsic Allosteric Inhibition of Signaling Proteins by Targeting Rare Interaction States Detected by High-Pressure NMR Spectroscopy." In: *Angewandte Chemie International Edition* 52.52, pp. 14242–14246. ISSN: 14337851. DOI: 10.1002/anie.201305741. URL: https://onlinelibrary.wiley.com/doi/10.1002/anie.201305741.

Kalinowski, H-O. (1986). "^{3} H-NMR: Handbook of Tritium NMR Spectroscopy and Applications. Von E. A. Evans, D. C. Warrell, J. A. Elvidge und J. R. Jones. John Wiley & Sons, Chichester - New York - Brisbane - Toronto - Singapore 1985. 249 S., 54 Tab., geb. $37,-. ISBN 0-471-90583-6." In: *Nachrichten aus Chemie, Technik und Laboratorium* 34.1, pp. 37–38. ISSN: 03415163. DOI: 10.1002/nadc.19860340113. URL: https://onlinelibrary.wiley.com/doi/10.1002/nadc.19860340113.

Kaplan, Mohammed et al. (2016). "EGFR Dynamics Change during Activation in Native Membranes as Revealed by NMR." In: *Cell* 167.5, 1241–1251.e11. ISSN: 00928674. DOI: 10.1016/j.cell.2016.10.038. URL: https://linkinghub.elsevier.com/retrieve/pii/S0092867416314593.

Kasinath, Vignesh, Kim A. Sharp, and A. Joshua Wand (2013). "Microscopic Insights into the NMR Relaxation-Based Protein Conformational Entropy Meter." In: *Journal of the American Chemical Society* 135.40. PMID: 24007504, pp. 15092–15100. DOI: 10.1021/ja405200u. eprint: https://doi.org/10.1021/ja405200u. URL: https://doi.org/10.1021/ja405200u.

Kato, Masato et al. (2012). "Cell-free Formation of RNA Granules: Low Complexity Sequence Domains Form Dynamic Fibers within Hydrogels." In: *Cell* 149.4, pp. 753–767. ISSN: 00928674. DOI: 10.1016/j.cell.2012.04.017. URL: https://linkinghub.elsevier.com/retrieve/pii/S0092867412005144.

Kedersha, Nancy et al. (2005). "Stress granules and processing bodies are dynamically linked sites of mRNP remodeling." In: *Journal of Cell Biology* 169.6, pp. 871–884. ISSN: 1540-8140, 0021-9525. DOI: 10.1083/jcb.200502088. URL: https://rupress.org/jcb/article/169/6/871/51749/Stress-granules-and-processing-bodies-are.

Keeler, J. (2013). *Understanding NMR Spectroscopy*. Wiley. ISBN: 9781118723340. URL: https://books.google.de/books?id=HzGXJSASsCsC.

Kempf, James G. and J. Patrick Loria (2002). "Protein Dynamics from Solution NMR." In: *Cell Biochemistry and Biophysics* 37.3, pp. 187–212. ISSN: 1085-9195, 1085-9195. DOI: 10.1385/CBB:37:3:187. URL: http://link.springer.com/10.1385/CBB:37:3:187.

Kendrew, J. C. et al. (1958). "A Three-Dimensional Model of the Myoglobin Molecule Obtained by X-Ray Analysis." In: *Nature* 181.4610, pp. 662–666. ISSN: 0028-0836, 1476-4687. DOI: 10.1038/181662a0. URL: https://www.nature.com/articles/181662a0.

Kerfah, Rime et al. (2015). "Methyl-specific isotopic labeling: a molecular tool box for solution NMR studies of large proteins." In: *Current Opinion in Structural Biology* 32, pp. 113–122. ISSN: 0959440X. DOI: 10.1016/j.sbi.2015.03.009. URL: https://linkinghub.elsevier.com/retrieve/pii/S0959440X15000366.

Key, Jason et al. (2009). "Principles of Ligand Binding within a Completely Buried Cavity in HIF2α PAS-B." In: *Journal of the American Chemical Society* 131.48, pp. 17647–17654. ISSN: 0002-7863, 1520-5126. DOI: 10.1021/ja9073062. URL: https://pubs.acs.org/doi/10.1021/ja9073062.

Khan, Farid et al. (2006). "19F NMR Studies of the Native and Denatured States of Green Fluorescent Protein." In: *Journal of the American Chemical Society* 128.33. PMID: 16910667, pp. 10729–10737. DOI: 10.1021/ja060618u. eprint: https://doi.org/10.1021/ja060618u. URL: https://doi.org/10.1021/ja060618u.

Kim, Eunkyung, Sanghwa Lee, et al. (2013). "A single-molecule dissection of ligand binding to a protein with intrinsic dynamics." In: *Nature Chemical Biology* 9.5, pp. 313–318. ISSN: 1552-4450, 1552-4469. DOI: 10.1038/nchembio.1213. URL: https://www.nature.com/articles/nchembio.1213.

Kim, Tae Hun, Ka Young Chung, et al. (2013). "The Role of Ligands on the Equilibria Between Functional States of a G Protein-Coupled Receptor." In: *Journal of the American Chemical Society* 135.25, pp. 9465–9474. ISSN: 0002-7863, 1520-5126. DOI: 10.1021/ja404305k. URL: https://pubs.acs.org/doi/10.1021/ja404305k.

Kim, Younggyu, Sam O. Ho, et al. (2008). "Efficient Site-Specific Labeling of Proteins via Cysteines." In: *Bioconjugate Chemistry* 19.3. PMID: 18275130, pp. 786–791. DOI: 10.1021/bc7002499. eprint: https://doi.org/10.1021/bc7002499. URL: https://doi.org/10.1021/bc7002499.

Kitahara, Ryo and Kazuyuki Akasaka (2003). "Close identity of a pressure-stabilized intermediate with a kinetic intermediate in protein folding." In: *Proceedings of the National Academy of Sciences* 100.6, pp. 3167–3172. ISSN: 0027-8424, 1091-6490. DOI: 10.1073/pnas.0630309100. URL: https://pnas.org/doi/full/10.1073/pnas.0630309100.

Kitahara, Ryo, Hiroaki Yamada, et al. (2002). "High Pressure NMR Reveals that Apomyoglobin is an Equilibrium Mixture from the Native to the Unfolded." In: *Journal of Molecular Biology* 320.2, pp. 311–319. ISSN: 00222836. DOI: 10.1016/S0022-2836(02)00449-7. URL: https://linkinghub.elsevier.com/retrieve/pii/S0022283602004497.

Kitevski-LeBlanc, Julianne L. and R. Scott Prosser (2012). "Current applications of 19F NMR to studies of protein structure and dynamics." In: *Progress in Nuclear Magnetic Resonance Spectroscopy* 62, pp. 1–33. ISSN: 00796565. DOI: 10.1016/j.pnmrs.2011.06.003. URL: https://linkinghub.elsevier.com/retrieve/pii/S0079656511000549.

Kleckner, Ian R. and Mark P. Foster (2011). "An introduction to NMR-based approaches for measuring protein dynamics." In: *Biochimica et Biophysica Acta (BBA) - Proteins and Proteomics* 1814.8, pp. 942–968. ISSN: 15709639. DOI: 10.1016/j.bbapap.2010.10.012. URL: https://linkinghub.elsevier.com/retrieve/pii/S1570963910002864.

Kloiber, Karin et al. (2011). "Longitudinal exchange: an alternative strategy towards quantification of dynamics parameters in ZZ exchange spectroscopy." In: *Journal of Biomolecular NMR* 51.1, pp. 123–129. ISSN: 0925-2738, 1573-5001. DOI: 10.1007/s10858-011-9547-8. URL: http://link.springer.com/10.1007/s10858-011-9547-8.

Köhn, Maja and Rolf Breinbauer (2004). "The Staudinger Ligation—A Gift to Chemical Biology." In: *Angewandte Chemie International Edition* 43.24, pp. 3106–3116. DOI: https://doi.org/10.1002/anie.200401744. eprint: https://onlinelibrary.wiley.com/doi/pdf/10.1002/anie.200401744. URL: https://onlinelibrary.wiley.com/doi/abs/10.1002/anie.200401744.

Korzhnev, Dmitry M., Irina Bezsonova, et al. (2006). "Probing the Transition State Ensemble of a Protein Folding Reaction by Pressure-Dependent NMR Relaxation Dispersion." In: *Journal of the American Chemical Society* 128.15, pp. 5262–5269. ISSN: 0002-7863, 1520-5126. DOI: 10.1021/ja0601540. URL: https://pubs.acs.org/doi/10.1021/ja0601540.

Korzhnev, Dmitry M. and Lewis E. Kay (2008). "Probing Invisible, Low-Populated States of Protein Molecules by Relaxation Dispersion NMR Spectroscopy: An Application to Protein Folding." In: *Accounts of Chemical Research* 41.3, pp. 442–451. ISSN: 0001-4842, 1520-4898. DOI: 10.1021/ar700189y. URL: https://pubs.acs.org/doi/10.1021/ar700189y.

Korzhnev, Dmitry M., Philipp Neudecker, et al. (2005). "Multiple-Site Exchange in Proteins Studied with a Suite of Six NMR Relaxation Dispersion Experiments: An Application to the Folding of a Fyn

SH3 Domain Mutant." In: *Journal of the American Chemical Society* 127.44, pp. 15602–15611. ISSN: 0002-7863, 1520-5126. DOI: 10.1021/ja054550e. URL: https://pubs.acs.org/doi/10.1021/ja054550e.

Korzhnev, Dmitry M., Vladislav Yu. Orekhov, et al. (2003). "Off-resonance R1ρ relaxation outside of the fast exchange limit: An experimental study of a cavity mutant of T4 lysozyme." In: *Journal of Biomolecular NMR* 26.1, pp. 39–48. ISSN: 09252738. DOI: 10.1023/A:1023039902737. URL: http://link.springer.com/10.1023/A:1023039902737.

Korzhnev, Dmitry M., Xavier Salvatella, et al. (2004). "Low-populated folding intermediates of Fyn SH3 characterized by relaxation dispersion NMR." In: *Nature* 430.6999, pp. 586–590. ISSN: 0028-0836, 1476-4687. DOI: 10.1038/nature02655. URL: http://www.nature.com/articles/nature02655.

Kovrigin, Evgenii L. and J. Patrick Loria (2006). "Enzyme Dynamics along the Reaction Coordinate: Critical Role of a Conserved Residue." In: *Biochemistry* 45.8, pp. 2636–2647. ISSN: 0006-2960, 1520-4995. DOI: 10.1021/bi0525066. URL: https://pubs.acs.org/doi/10.1021/bi0525066.

Kremer, Werner et al. (2011). "Pulsed Pressure Perturbations, an Extra Dimension in NMR Spectroscopy of Proteins." In: *Journal of the American Chemical Society* 133.34, pp. 13646–13651. ISSN: 0002-7863, 1520-5126. DOI: 10.1021/ja2050698. URL: https://pubs.acs.org/doi/10.1021/ja2050698.

Krempl, Christina and Remco Sprangers (2023). "Assessing the applicability of 19F labeled tryptophan residues to quantify protein dynamics." In: *Journal of Biomolecular NMR* 77.1, pp. 55–67. ISSN: 1573-5001. DOI: 10.1007/s10858-022-00411-2. URL: https://doi.org/10.1007/s10858-022-00411-2.

Krempl, Christina, Jan Philip Wurm, et al. (2023). "Insights into the Structure of Invisible Conformations of Large Methyl Group Labeled Molecular Machines from High Pressure NMR." In: *Journal of Molecular Biology* 435.11, p. 167922. ISSN: 00222836. DOI: 10.1016/j.jmb.2022.167922. URL: https://linkinghub.elsevier.com/retrieve/pii/S0022283622005496.

Krivdin, Leonid B. (2023). "Tritium NMR: A compilation of data and a practical guide." In: *Magnetic Resonance in Chemistry* 61.4, pp. 195–247. ISSN: 0749-1581, 1097-458X. DOI: 10.1002/mrc.5329. URL: https://onlinelibrary.wiley.com/doi/10.1002/mrc.5329.

Kuloğlu, E. Sonay et al. (2002). "Structural Rearrangement of Human Lymphotactin, a C Chemokine, under Physiological Solution Conditions." In: *Journal of Biological Chemistry* 277.20, pp. 17863–17870. ISSN: 00219258. DOI: 10.1074/jbc.M200402200. URL: https://linkinghub.elsevier.com/retrieve/pii/S002192582085282X.

Kurosaki, Tatsuaki, Maximilian W. Popp, and Lynne E. Maquat (2019). "Quality and quantity control of gene expression by nonsense-mediated mRNA decay." In: *Nature Reviews Molecular Cell Biology* 20.7, pp. 406–420. ISSN: 1471-0072, 1471-0080. DOI: 10.1038/s41580-019-0126-2. URL: http://www.nature.com/articles/s41580-019-0126-2.

Łabno, Anna, Rafał Tomecki, and Andrzej Dziembowski (2016). "Cytoplasmic RNA decay pathways - Enzymes and mechanisms." In: *Biochimica et Biophysica Acta (BBA) - Molecular Cell Research* 1863.12, pp. 3125–3147. ISSN: 01674889. DOI: 10.1016/j.bbamcr.2016.09.023. URL: https://linkinghub.elsevier.com/retrieve/pii/S0167488916302531.

Labokha, Aksana A et al. (2012). "Systematic analysis of barrier-forming FG hydrogels from Xenopus nuclear pore complexes." In: *The EMBO Journal* 32.2, pp. 204–218. ISSN: 0261-4189, 1460-2075. DOI: 10.1038/emboj.2012.302. URL: http://emboj.embopress.org/cgi/doi/10.1038/emboj.2012.302.

Laidler, Keith J. and M. Christine King (1983). "Development of transition-state theory." In: *The Journal of Physical Chemistry* 87.15, pp. 2657–2664. ISSN: 0022-3654, 1541-5740. DOI: 10.1021/j100238a002. URL: https://pubs.acs.org/doi/abs/10.1021/j100238a002.

Langstein-Skora, Iris et al. (2022). *Sequence- and chemical specificity define the functional landscape of intrinsically disordered regions*. preprint. Biophysics. DOI: 10.1101/2022.02.10.480018. URL: http://biorxiv.org/lookup/doi/10.1101/2022.02.10.480018.

Laskowski, Roman A., Fabian Gerick, and Janet M. Thornton (2009). "The structural basis of allosteric regulation in proteins." In: *FEBS Letters* 583.11, pp. 1692–1698. ISSN: 00145793. DOI: 10.1016/j.febslet.2009.03.019. URL: http://doi.wiley.com/10.1016/j.febslet.2009.03.019.

Lau, E. Y. and J. T. Gerig (2000). "Origins of Fluorine NMR Chemical Shifts in Fluorine-Containing Proteins." In: *Journal of the American Chemical Society* 122.18, pp. 4408–4417. ISSN: 0002-7863, 1520-5126. DOI: 10.1021/ja992107w. URL: https://pubs.acs.org/doi/10.1021/ja992107w.

Lee, Nam Ki, Achillefs N. Kapanidis, et al. (2005). "Accurate FRET Measurements within Single Diffusing Biomolecules Using Alternating-Laser Excitation." In: *Biophysical Journal* 88.4, pp. 2939–2953. ISSN: 00063495. DOI: 10.1529/biophysj.104.054114. URL: https://linkinghub.elsevier.com/retrieve/pii/S0006349505733464.

Lee, Woonghee, Mehdi Rahimi, et al. (2021). "POKY: a software suite for multidimensional NMR and 3D structure calculation of biomolecules." In: *Bioinformatics (Oxford, England)* 37.18, pp. 3041–3042. ISSN: 1367-4803. DOI: 10.1093/bioinformatics/btab180. URL: https://europepmc.org/articles/PMC8479676.

Lee, Woonghee, Marco Tonelli, and John L. Markley (2014). "NMRFAM-SPARKY: enhanced software for biomolecular NMR spectroscopy." In: *Bioinformatics* 31.8, pp. 1325–1327. ISSN: 1367-4803. DOI: 10.1093/bioinformatics/btu830. eprint: https://academic.oup.com/bioinformatics/article-pdf/31/8/1325/50306354/bioinformatics_31_8_1325.pdf. URL: https://doi.org/10.1093/bioinformatics/btu830.

LeMaster, David M. (1987). "Chiral β and random fractional deuteration for the determination of protein sidechain conformation by NMR." In: *FEBS Letters* 223.1, pp. 191–196. ISSN: 00145793. DOI: 10.1016/0014-5793(87)80534-3. URL: http://doi.wiley.com/10.1016/0014-5793%2887%2980534-3.

Lento, Cristina and Derek J. Wilson (2022). "Subsecond Time-Resolved Mass Spectrometry in Dynamic Structural Biology." In: *Chemical Reviews* 122.8, pp. 7624–7646. ISSN: 0009-2665, 1520-6890. DOI: 10.1021/acs.chemrev.1c00222. URL: https://pubs.acs.org/doi/10.1021/acs.chemrev.1c00222.

Lerner, Eitan, Anders Barth, et al. (2021). "FRET-based dynamic structural biology: Challenges, perspectives and an appeal for open-science practices." In: *eLife* 10, e60416. ISSN: 2050-084X. DOI: 10.7554/eLife.60416. URL: https://elifesciences.org/articles/60416.

Lerner, Eitan, Thorben Cordes, et al. (2018). "Toward dynamic structural biology: Two decades of single-molecule Förster resonance energy transfer." In: *Science* 359.6373, eaan1133. ISSN: 0036-8075, 1095-9203. DOI: 10.1126/science.aan1133. URL: https://www.science.org/doi/10.1126/science.aan1133.

Lett, Martin Joseph et al. (2023). *Single-cycle SARS-CoV-2 vaccine elicits high protection and sterilizing immunity in hamsters*. preprint. Molecular Biology. DOI: 10.1101/2023.05.17.541127. URL: http://biorxiv.org/lookup/doi/10.1101/2023.05.17.541127.

Li, Chuan, Luisa P. Mori, et al. (2023). "The chaperone protein p32 stabilizes HIV-1 Tat and strengthens the p-TEFb/RNAPII/TAR complex promoting HIV transcription elongation." In: *Proceedings of the National Academy of Sciences* 120.1, e2217476120. ISSN: 0027-8424, 1091-6490. DOI: 10.1073/pnas.2217476120. URL: https://pnas.org/doi/10.1073/pnas.2217476120.

Li, Pilong, Sudeep Banjade, et al. (2012). "Phase transitions in the assembly of multivalent signalling proteins." In: *Nature* 483.7389, pp. 336–340. ISSN: 0028-0836, 1476-4687. DOI: 10.1038/nature10879. URL: http://www.nature.com/articles/nature10879.

Li, You and Megerditch Kiledjian (2010). "Regulation of mRNA decapping." In: *WIREs RNA* 1.2, pp. 253–265. DOI: https://doi.org/10.1002/wrna.15. eprint: https://wires.onlinelibrary.wiley.com/doi/pdf/10.1002/wrna.15. URL: https://wires.onlinelibrary.wiley.com/doi/abs/10.1002/wrna.15.

Liebau, Jobst et al. (2020). "Unveiling the activation dynamics of a fold-switch bacterial glycosyltransferase by 19F NMR." In: *Journal of Biological Chemistry* 295.29, pp. 9868–9878. ISSN: 00219258. DOI: 10.1074/jbc.RA120.014162. URL: https://linkinghub.elsevier.com/retrieve/pii/S0021925817489290.

Lima, Christopher D., Michael G. Klein, and Wayne A. Hendrickson (1997). "Structure-Based Analysis of Catalysis and Substrate Definition in the HIT Protein Family." In: *Science* 278.5336, pp. 286–290. ISSN: 0036-8075, 1095-9203. DOI: 10.1126/science.278.5336.286. URL: https://www.science.org/doi/10.1126/science.278.5336.286.

Liu, H. (2002). "The scavenger mRNA decapping enzyme DcpS is a member of the HIT family of pyrophosphatases." In: *The EMBO Journal* 21.17, pp. 4699–4708. ISSN: 14602075. DOI: 10.1093/emboj/cdf448. URL: http://emboj.embopress.org/cgi/doi/10.1093/emboj/cdf448.

Liu, Hudan and Megerditch Kiledjian (2005). "Scavenger Decapping Activity Facilitates 5' to 3' mRNA Decay." In: *Molecular and Cellular Biology* 25.22, pp. 9764–9772. ISSN: 0270-7306, 1098-5549. DOI: 10.1128/MCB.25.22.9764-9772.2005. URL: https://journals.asm.org/doi/10.1128/MCB.25.22.9764-9772.2005.

Liu, Jeffrey J., Reto Horst, et al. (2012). "Biased Signaling Pathways in β_2 -Adrenergic Receptor Characterized by ^{19} F-NMR." In: *Science* 335.6072, pp. 1106–1110. ISSN: 0036-8075, 1095-9203. DOI: 10.1126/science.1215802. URL: https://www.science.org/doi/10.1126/science.1215802.

Liu, Quansheng, Jaclyn C. Greimann, and Christopher D. Lima (2006). "Reconstitution, Activities, and Structure of the Eukaryotic RNA Exosome." In: *Cell* 127.6, pp. 1223–1237. ISSN: 00928674. DOI: 10.1016/j.cell.2006.10.037. URL: https://linkinghub.elsevier.com/retrieve/pii/S0092867406014279.

Liu, Shin-Wu, Xinfu Jiao, et al. (2004). "Functional analysis of mRNA scavenger decapping enzymes." In: *RNA* 10.9, pp. 1412–1422. ISSN: 1355-8382, 1469-9001. DOI: 10.1261/rna.7660804. URL: http://rnajournal.cshlp.org/lookup/doi/10.1261/rna.7660804.

Liu, Shin-Wu, Vaishnavi Rajagopal, et al. (2008). "Mechanistic and Kinetic Analysis of the DcpS Scavenger Decapping Enzyme." In: *Journal of Biological Chemistry* 283.24, pp. 16427–16436. ISSN: 00219258. DOI: 10.1074/jbc.M800341200. URL: https://linkinghub.elsevier.com/retrieve/pii/S002192582071447X.

Lobel, Joseph H., Ryan W. Tibble, and John D. Gross (2019). "Pat1 activates late steps in mRNA decay by multiple mechanisms." In: *Proceedings of the National Academy of Sciences* 116.47, pp. 23512–23517. ISSN: 0027-8424, 1091-6490. DOI: 10.1073/pnas.1905455116. URL: https://pnas.org/doi/full/10.1073/pnas.1905455116.

Loria, J. Patrick, Rebecca B. Berlow, and Eric D. Watt (2008). "Characterization of Enzyme Motions by Solution NMR Relaxation Dispersion." In: *Accounts of Chemical Research* 41.2, pp. 214–221. ISSN: 0001-4842, 1520-4898. DOI: 10.1021/ar700132n. URL: https://pubs.acs.org/doi/10.1021/ar700132n.

Lu, Manman et al. (2019). "19F NMR relaxation studies of fluorosubstituted tryptophans." In: *Journal of Biomolecular NMR* 73.8, pp. 401–409. ISSN: 0925-2738, 1573-5001. DOI: 10.1007/s10858-019-00268-y. URL: http://link.springer.com/10.1007/s10858-019-00268-y.

Luck, Linda A. et al. (1996). "19F NMR relaxation studies on 5-fluorotryptophan- and tetradeutero-5-fluorotryptophan-labeled E. coli glucose/galactose receptor." In: *Journal of Biomolecular NMR* 7, pp. 261–272.

Lundström, Patrik et al. (2007). "A single-quantum methyl 13C-relaxation dispersion experiment with improved sensitivity." In: *Journal of Biomolecular NMR* 38, pp. 79–88.

Luo, Yang, Zhenkun Na, and Sarah A. Slavoff (2018). "P-Bodies: Composition, Properties, and Functions." In: *Biochemistry* 57.17, pp. 2424–2431. ISSN: 0006-2960, 1520-4995. DOI: 10.1021/acs.biochem.7b01162. URL: https://pubs.acs.org/doi/10.1021/acs.biochem.7b01162.

Luz, Z. and S. Meiboom (1963). "Nuclear Magnetic Resonance Study of the Protolysis of Trimethylammonium Ion in Aqueous Solution—Order of the Reaction with Respect to Solvent." In: *The Journal of Chemical Physics* 39.2, pp. 366–370. ISSN: 0021-9606, 1089-7690. DOI: 10.1063/1.1734254. URL: https://pubs.aip.org/aip/jcp/article/39/2/366-370/207334.

Lykke-Andersen, Søren and Torben Heick Jensen (2015). "Nonsense-mediated mRNA decay: an intricate machinery that shapes transcriptomes." In: *Nature Reviews Molecular Cell Biology* 16.11, pp. 665–677. ISSN: 1471-0072, 1471-0080. DOI: 10.1038/nrm4063. URL: http://www.nature.com/articles/nrm4063.

Maeno, Akihiro et al. (2015). "Cavity as a Source of Conformational Fluctuation and High-Energy State: High-Pressure NMR Study of a Cavity-Enlarged Mutant of T4Lysozyme." In: *Biophysical Journal* 108.1, pp. 133–145. ISSN: 00063495. DOI: 10.1016/j.bpj.2014.11.012. URL: https://linkinghub.elsevier.com/retrieve/pii/S0006349514011965.

Makino, Debora Lika, Marc Baumgärtner, and Elena Conti (2013). "Crystal structure of an RNA-bound 11-subunit eukaryotic exosome complex." In: *Nature* 495.7439, pp. 70–75. ISSN: 0028-0836, 1476-4687. DOI: 10.1038/nature11870. URL: http://www.nature.com/articles/nature11870.

Makino, Debora Lika and Elena Conti (2013). "Structure determination of an 11-subunit exosome in complex with RNA by molecular replacement." In: *Acta Crystallographica Section D Biological Crystallography* 69.11, pp. 2226–2235. ISSN: 0907-4449. DOI: 10.1107/S0907444913011438. URL: https://scripts.iucr.org/cgi-bin/paper?S0907444913011438.

Malys, N. (2004). "The 'scavenger' m^7GpppX pyrophosphatase activity of Dcs1 modulates nutrient-induced responses in yeast." In: *Nucleic Acids Research* 32.12, pp. 3590–3600. ISSN: 1362-4962. DOI: 10.1093/nar/gkh687. URL: https://academic.oup.com/nar/article-lookup/doi/10.1093/nar/gkh687.

Malys, Naglis and John E.G. McCarthy (2006). "Dcs2, a Novel Stress-induced Modulator of m^7GpppX Pyrophosphatase Activity that Locates to P Bodies." In: *Journal of Molecular Biology* 363.2, pp. 370–382. ISSN: 00222836. DOI: 10.1016/j.jmb.2006.08.015. URL: https://linkinghub.elsevier.com/retrieve/pii/S0022283606010266.

Manglik, Aashish et al. (2015). "Structural Insights into the Dynamic Process of β2-Adrenergic Receptor Signaling." In: *Cell* 161.5, pp. 1101–1111. ISSN: 0092-8674. DOI: https://doi.org/10.1016/j.cell.2015.04.043. URL: https://www.sciencedirect.com/science/article/pii/S0092867415004997.

Mangus, David A, Matthew C Evans, and Allan Jacobson (2003). "[No title found]." In: *Genome Biology* 4.7, p. 223. ISSN: 14656906. DOI: 10.1186/gb-2003-4-7-223. URL: http://genomebiology.biomedcentral.com/articles/10.1186/gb-2003-4-7-223.

Mao, Yuntao S., Bin Zhang, and David L. Spector (2011). "Biogenesis and function of nuclear bodies." In: *Trends in genetics: TIG* 27.8, pp. 295–306. ISSN: 0168-9525. DOI: 10.1016/j.tig.2011.05.006.

Marchanka, Alexander and Teresa Carlomagno (2019). "Solid-State NMR Spectroscopy of RNA." In: *Methods in Enzymology*. Vol. 615. Elsevier, pp. 333–371. ISBN: 978-0-12-816762-5. DOI: 10.1016/bs.mie.2018.08.029. URL: https://linkinghub.elsevier.com/retrieve/pii/S0076687918303276.

Markus, M.A. et al. (1994). "Effect of Deuteration on the Amide Proton Relaxation Rates in Proteins. Heteronuclear NMR Experiments on Villin 14T." In: *Journal of Magnetic Resonance, Series B* 105.2, pp. 192–195. ISSN: 10641866. DOI: 10.1006/jmrb.1994.1122. URL: https://linkinghub.elsevier.com/retrieve/pii/S1064186684711228.

Mazal, Hisham and Gilad Haran (2019). "Single-molecule FRET methods to study the dynamics of proteins at work." In: *Current Opinion in Biomedical Engineering* 12, pp. 8–17. ISSN: 24684511. DOI: 10.1016/j.cobme.2019.08.007. URL: https://linkinghub.elsevier.com/retrieve/pii/S2468451119300261.

McLennan, A. G. (2006). "The Nudix hydrolase superfamily." In: *Cellular and Molecular Life Sciences CMLS* 63.2, pp. 123–143. ISSN: 1420-682X, 1420-9071. DOI: 10.1007/s00018-005-5386-7. URL: https://link.springer.com/10.1007/s00018-005-5386-7.

McLennan, Alexander G. (2013). "Substrate ambiguity among the nudix hydrolases: biologically significant, evolutionary remnant, or both?" In: *Cellular and Molecular Life Sciences* 70.3, pp. 373–385. ISSN: 1420-682X, 1420-9071. DOI: 10.1007/s00018-012-1210-3. URL: http://link.springer.com/10.1007/s00018-012-1210-3.

Medintz, Igor and Niko Hildebrandt, eds. (2013). *FRET – Förster Resonance Energy Transfer*. 1st ed. Wiley. ISBN: 978-3-527-32816-1 978-3-527-65602-8. DOI: 10.1002/9783527656028. URL: https://onlinelibrary.wiley.com/doi/book/10.1002/9783527656028.

Meiboom, S. and D. Gill (1958). "Modified Spin-Echo Method for Measuring Nuclear Relaxation Times." In: *Review of Scientific Instruments* 29.8, pp. 688–691. ISSN: 0034-6748, 1089-7623. DOI: 10.1063/1.1716296. URL: https://pubs.aip.org/aip/rsi/article/29/8/688-691/299672.

Meziane, Oussama et al. (2015). "The human decapping scavenger enzyme DcpS modulates microRNA turnover." In: *Scientific Reports* 5.1, p. 16688. ISSN: 2045-2322. DOI: 10.1038/srep16688. URL: http://www.nature.com/articles/srep16688.

Michalet, X. et al. (2013). "Development of new photon-counting detectors for single-molecule fluorescence microscopy." In: *Philosophical Transactions of the Royal Society B: Biological Sciences* 368.1611, p. 20120035. ISSN: 0962-8436, 1471-2970. DOI: 10.1098/rstb.2012.0035. URL: https://royalsocietypublishing.org/doi/10.1098/rstb.2012.0035.

Millet, Oscar et al. (2000). "The Static Magnetic Field Dependence of Chemical Exchange Linebroadening Defines the NMR Chemical Shift Time Scale." In: *Journal of the American Chemical*

Society 122.12, pp. 2867–2877. ISSN: 0002-7863, 1520-5126. DOI: 10.1021/ja993511y. URL: https://pubs.acs.org/doi/10.1021/ja993511y.

Minks, Caroline et al. (1999). "Atomic Mutations at the Single Tryptophan Residue of Human Recombinant Annexin V: Effects on Structure, Stability, and Activity." In: *Biochemistry* 38.33, pp. 10649–10659. ISSN: 0006-2960, 1520-4995. DOI: 10.1021/bi990580g. URL: https://pubs.acs.org/doi/10.1021/bi990580g.

Mitchell, Philip et al. (1997). "The Exosome: A Conserved Eukaryotic RNA Processing Complex Containing Multiple 3'→5' Exoribonucleases." In: *Cell* 91.4, pp. 457–466. ISSN: 00928674. DOI: 10.1016/S0092-8674(00)80432-8. URL: https://linkinghub.elsevier.com/retrieve/pii/S0092867400804328.

Mitrea, Diana M. and Richard W. Kriwacki (2016). "Phase separation in biology; functional organization of a higher order." In: *Cell Communication and Signaling* 14.1, p. 1. ISSN: 1478-811X. DOI: 10.1186/s12964-015-0125-7. URL: https://biosignaling.biomedcentral.com/articles/10.1186/s12964-015-0125-7.

Mittermaier, Anthony K. and Lewis E. Kay (2009). "Observing biological dynamics at atomic resolution using NMR." In: *Trends in Biochemical Sciences* 34.12, pp. 601–611. ISSN: 09680004. DOI: 10.1016/j.tibs.2009.07.004. URL: https://linkinghub.elsevier.com/retrieve/pii/S0968000409001649.

"Modern Aspects of ^{31} P NMR Spectroscopy" (2019). In: Iaroshenko, Viktor. *Organophosphorus Chemistry*. Weinheim, Germany: Wiley-VCH Verlag GmbH & Co. KGaA, pp. 457–498. ISBN: 978-3-527-67224-0 978-3-527-33572-5. DOI: 10.1002/9783527672240.ch9. URL: https://onlinelibrary.wiley.com/doi/10.1002/9783527672240.ch9.

Moerner, W. E. and David P. Fromm (2003). "Methods of single-molecule fluorescence spectroscopy and microscopy." In: *Review of Scientific Instruments* 74.8, pp. 3597–3619. ISSN: 0034-6748, 1089-7623. DOI: 10.1063/1.1589587. URL: https://pubs.aip.org/aip/rsi/article/74/8/3597-3619/347480.

Molliex, Amandine et al. (2015). "Phase Separation by Low Complexity Domains Promotes Stress Granule Assembly and Drives Pathological Fibrillization." In: *Cell* 163.1, pp. 123–133. ISSN: 00928674. DOI: 10.1016/j.cell.2015.09.015. URL: https://linkinghub.elsevier.com/retrieve/pii/S0092867415011769.

Montelione, Gaetano T. and Gerhard Wagner (1989). "2D Chemical exchange NMR spectroscopy by proton-detected heteronuclear correlation." In: *Journal of the American Chemical Society* 111.8, pp. 3096–3098. ISSN: 0002-7863, 1520-5126. DOI: 10.1021/ja00190a072. URL: https://pubs.acs.org/doi/abs/10.1021/ja00190a072.

Montemayor, Eric J. et al. (2020). "Molecular basis for the distinct cellular functions of the Lsm1–7 and Lsm2–8 complexes." In: *RNA* 26.10, pp. 1400–1413. ISSN: 1355-8382, 1469-9001. DOI: 10.1261/rna.075879.120. URL: http://rnajournal.cshlp.org/lookup/doi/10.1261/rna.075879.120.

Mueller, Luciano (1979). "Sensitivity enhanced detection of weak nuclei using heteronuclear multiple quantum coherence." In: *Journal of the American Chemical Society* 101.16, pp. 4481–4484. ISSN: 0002-7863, 1520-5126. DOI: 10.1021/ja00510a007. URL: https://pubs.acs.org/doi/abs/10.1021/ja00510a007.

Mugridge, Jeffrey S, Marcin Ziemniak, et al. (2016). "Structural basis of mRNA-cap recognition by Dcp1–Dcp2." In: *Nature Structural & Molecular Biology* 23.11, pp. 987–994. ISSN: 1545-9993, 1545-9985. DOI: 10.1038/nsmb.3301. URL: http://www.nature.com/articles/nsmb.3301.

Mugridge, Jeffrey S., Jeff Coller, and John D. Gross (2018). "Structural and molecular mechanisms for the control of eukaryotic 5' – 3' mRNA decay." In: *Nature Structural & Molecular Biology* 25.12, pp. 1077–1085. ISSN: 1545-9993, 1545-9985. DOI: 10.1038/s41594-018-0164-z. URL: http://www.nature.com/articles/s41594-018-0164-z.

Mugridge, Jeffrey S., Ryan W. Tibble, et al. (2018). "Structure of the activated Edc1-Dcp1-Dcp2-Edc3 mRNA decapping complex with substrate analog poised for catalysis." In: *Nature Communications* 9.1, p. 1152. ISSN: 2041-1723. DOI: 10.1038/s41467-018-03536-x. URL: https://www.nature.com/articles/s41467-018-03536-x.

Muhlrad, Denise, Carolyn J. Decker, and Roy Parker (1995). "Turnover Mechanisms of the Stable Yeast *PGK1* mRNA." In: *Molecular and Cellular Biology* 15.4, pp. 2145–2156. ISSN: 1098-5549. DOI: 10.1128/MCB.15.4.2145. URL: https://www.tandfonline.com/doi/full/10.1128/MCB.15.4.2145.

Müller, Barbara K. et al. (2005). "Pulsed Interleaved Excitation." In: *Biophysical Journal* 89.5, pp. 3508–3522. ISSN: 00063495. DOI: 10.1529/biophysj.105.064766. URL: https://linkinghub.elsevier.com/retrieve/pii/S000634950572991X.

Murray, Dylan T. et al. (2017). "Structure of FUS Protein Fibrils and Its Relevance to Self-Assembly and Phase Separation of Low-Complexity Domains." In: *Cell* 171.3, 615–627.e16. ISSN: 00928674. DOI: 10.1016/j.cell.2017.08.048. URL: https://linkinghub.elsevier.com/retrieve/pii/S0092867417310073.

Neu, Ancilla et al. (2015). "An excess of catalytically required motions inhibits the scavenger decapping enzyme." In: *Nature Chemical Biology* 11.9, pp. 697–704. ISSN: 1552-4450, 1552-4469. DOI: 10.1038/nchembio.1866. URL: http://www.nature.com/articles/nchembio.1866.

Neudecker, Philipp, Patrik Lundström, and Lewis E. Kay (2009). "Relaxation Dispersion NMR Spectroscopy as a Tool for Detailed Studies of Protein Folding." In: *Biophysical Journal* 96.6, pp. 2045–2054. ISSN: 00063495. DOI: 10.1016/j.bpj.2008.12.3907. URL: https://linkinghub.elsevier.com/retrieve/pii/S0006349509003312.

Ng, Calista K.L. et al. (2015). "Loss of the scavenger mRNA decapping enzyme DCPS causes syndromic intellectual disability with neuromuscular defects." In: *Human Molecular Genetics* 24.11, pp. 3163–3171. ISSN: 1460-2083, 0964-6906. DOI: 10.1093/hmg/ddv067. URL: https://academic.oup.com/hmg/article-lookup/doi/10.1093/hmg/ddv067.

Nie, Shuming, Daniel T. Chiu, and Richard N. Zare (1994). "Probing Individual Molecules with Confocal Fluorescence Microscopy." In: *Science* 266.5187, pp. 1018–1021. ISSN: 0036-8075, 1095-9203. DOI: 10.1126/science.7973650. URL: https://www.science.org/doi/10.1126/science.7973650.

Nikolaev, Yaroslav and Konstantin Pervushin (2007). "NMR Spin State Exchange Spectroscopy Reveals Equilibrium of Two Distinct Conformations of Leucine Zipper GCN4 in Solution." In: *Journal of the American Chemical Society* 129.20, pp. 6461–6469. ISSN: 0002-7863, 1520-5126. DOI: 10.1021/ja0685295. URL: https://pubs.acs.org/doi/10.1021/ja0685295.

Nishiyama, Yusuke et al. (2023). "Ultrafast Magic Angle Spinning Solid-State NMR Spectroscopy: Advances in Methodology and Applications." In: *Chemical Reviews* 123.3, pp. 918–988. ISSN: 0009-2665, 1520-6890. DOI: 10.1021/acs.chemrev.2c00197. URL: https://pubs.acs.org/doi/10.1021/acs.chemrev.2c00197.

Nizami, Z., S. Deryusheva, and J. G. Gall (2010). "The Cajal Body and Histone Locus Body." In: *Cold Spring Harbor Perspectives in Biology* 2.7, a000653–a000653. ISSN: 1943-0264. DOI: 10.1101/cshperspect.a000653. URL: http://cshperspectives.cshlp.org/lookup/doi/10.1101/cshperspect.a000653.

Noren, Christopher J. et al. (1989). "A General Method for Site-specific Incorporation of Unnatural Amino Acids into Proteins." In: *Science* 244.4901, pp. 182–188. DOI: 10.1126/science.2649980. eprint: https://www.science.org/doi/pdf/10.1126/science.2649980. URL: https://www.science.org/doi/abs/10.1126/science.2649980.

Nott, Timothy J. et al. (2015). "Phase Transition of a Disordered Nuage Protein Generates Environmentally Responsive Membraneless Organelles." In: *Molecular Cell* 57.5, pp. 936–947. ISSN: 10972765. DOI: 10.1016/j.molcel.2015.01.013. URL: https://linkinghub.elsevier.com/retrieve/pii/S1097276515000143.

Nuss, D L and Y Furuichi (1977). "Characterization of the $m^7G(5')pppN$-pyrophosphatase activity from HeLa cells." In: *Journal of Biological Chemistry* 252.9, pp. 2815–2821. ISSN: 00219258. DOI: 10.1016/S0021-9258(17)40435-2. URL: https://linkinghub.elsevier.com/retrieve/pii/S0021925817404352.

O'Connor, Desmond V. and David Phillips (1984). *Time-Correlated Single Photon Counting*. Elsevier. ISBN: 978-0-12-524140-3. DOI: 10.1016/B978-0-12-524140-3.X5001-1. URL: https://linkinghub.elsevier.com/retrieve/pii/B9780125241403X50011.

Ogunjimi, Abiodun A. et al. (2010). "The Ubiquitin Binding Region of the Smurf HECT Domain Facilitates Polyubiquitylation and Binding of Ubiquitylated Substrates." In: *Journal of Biological Chemistry* 285.9, pp. 6308–6315. ISSN: 00219258. DOI: 10.1074/jbc.M109.044537. URL: https://linkinghub.elsevier.com/retrieve/pii/S002192581937797X.

Ohki, Shin-ya and Masatsune Kainosho (2008). "Stable isotope labeling methods for protein NMR spectroscopy." In: *Progress in Nuclear Magnetic Resonance Spectroscopy* 53.4, pp. 208–226. ISSN: 00796565. DOI: 10.1016/j.pnmrs.2008.01.003. URL: https://linkinghub.elsevier.com/retrieve/pii/S0079656508000034.

Ollerenshaw, Jason E., Vitali Tugarinov, and Lewis E. Kay (2003). "Methyl TROSY: explanation and experimental verification." In: *Magnetic Resonance in Chemistry* 41.10, pp. 843–852. ISSN: 0749-1581, 1097-458X. DOI: 10.1002/mrc.1256. URL: https://onlinelibrary.wiley.com/doi/10.1002/mrc.1256.

Overbeck, Jan H., Werner Kremer, and Remco Sprangers (2020). "A suite of 19F based relaxation dispersion experiments to assess biomolecular motions." In: *Journal of Biomolecular NMR* 74.12, pp. 753–766. ISSN: 0925-2738, 1573-5001. DOI: 10.1007/s10858-020-00348-4. URL: https://link.springer.com/10.1007/s10858-020-00348-4.

Overbeck, Jan H., David Stelzig, et al. (2022). "Observation of conformational changes that underlie the catalytic cycle of Xrn2." In: *Nature Chemical Biology* 18.10, pp. 1152–1160. ISSN: 1552-4450, 1552-4469. DOI: 10.1038/s41589-022-01111-6. URL: https://www.nature.com/articles/s41589-022-01111-6.

Oyen, David et al. (2017). "Defining the Structural Basis for Allosteric Product Release from *E. coli* Dihydrofolate Reductase Using NMR Relaxation Dispersion." In: *Journal of the American Chemical Society* 139.32, pp. 11233–11240. ISSN: 0002-7863, 1520-5126. DOI: 10.1021/jacs.7b05958. URL: https://pubs.acs.org/doi/10.1021/jacs.7b05958.

Pak, Chi W. et al. (2016). "Sequence Determinants of Intracellular Phase Separation by Complex Coacervation of a Disordered Protein." In: *Molecular Cell* 63.1, pp. 72–85. ISSN: 10972765. DOI: 10.1016/j.molcel.2016.05.042. URL: https://linkinghub.elsevier.com/retrieve/pii/S1097276516302283.

Palmer, Arthur G. (2015). "Enzyme Dynamics from NMR Spectroscopy." In: *Accounts of Chemical Research* 48.2, pp. 457–465. ISSN: 0001-4842, 1520-4898. DOI: 10.1021/ar500340a. URL: https://pubs.acs.org/doi/10.1021/ar500340a.

Palmer, Arthur G. and Hans Koss (2019). "Chemical Exchange." In: *Methods in Enzymology*. Vol. 615. Elsevier, pp. 177–236. ISBN: 978-0-12-816762-5. DOI: 10.1016/bs.mie.2018.09.028. URL: https://linkinghub.elsevier.com/retrieve/pii/S0076687918303914.

Palmer, Arthur G., Christopher D. Kroenke, and J. Patrick Loria (2001). "Nuclear Magnetic Resonance Methods for Quantifying Microsecond-to-Millisecond Motions in Biological Macromolecules." In: *Methods in Enzymology*. Vol. 339. Elsevier, pp. 204–238. ISBN: 978-0-12-182240-8. DOI: 10.1016/S0076-6879(01)39315-1. URL: https://linkinghub.elsevier.com/retrieve/pii/S0076687901393151.

Palmer, Arthur G. and Francesca Massi (2006). "Characterization of the Dynamics of Biomacromolecules Using Rotating-Frame Spin Relaxation NMR Spectroscopy." In: *Chemical Reviews* 106.5, pp. 1700–1719. ISSN: 0009-2665, 1520-6890. DOI: 10.1021/cr0404287. URL: https://pubs.acs.org/doi/10.1021/cr0404287.

Palmer, Arthur G. III (2004). "NMR Characterization of the Dynamics of Biomacromolecules." In: *Chemical Reviews* 104.8. PMID: 15303831, pp. 3623–3640. DOI: 10.1021/cr030413t. eprint: https://doi.org/10.1021/cr030413t. URL: https://doi.org/10.1021/cr030413t.

Pan, Benxun et al. (2022). "GPCR large-amplitude dynamics by ^{19} F-NMR of aprepitant bound to the neurokinin 1 receptor." In: *Proceedings of the National Academy of Sciences* 119.15, e2122682119. ISSN: 0027-8424, 1091-6490. DOI: 10.1073/pnas.2122682119. URL: https://pnas.org/doi/full/10.1073/pnas.2122682119.

Paquette, David R et al. (2018). "Control of mRNA decapping by autoinhibition." In: *Nucleic Acids Research* 46.12, pp. 6318–6329. ISSN: 0305-1048, 1362-4962. DOI: 10.1093/nar/gky233. URL: https://academic.oup.com/nar/article/46/12/6318/4956184.

Paravastu, Anant K. et al. (2009). "Seeded growth of β-amyloid fibrils from Alzheimer's brain-derived fibrils produces a distinct fibril structure." In: *Proceedings of the National Academy of Sciences* 106.18, pp. 7443–7448. ISSN: 0027-8424, 1091-6490. DOI: 10.1073/pnas.0812033106. URL: https://pnas.org/doi/full/10.1073/pnas.0812033106.

Parker, Roy (2012). "RNA Degradation in *Saccharomyces cerevisae*." In: *Genetics* 191.3, pp. 671–702. ISSN: 1943-2631. DOI: 10.1534/genetics.111.137265. URL: https://academic.oup.com/genetics/article/191/3/671/5934987.

Parker, Roy and Ujwal Sheth (2007). "P Bodies and the Control of mRNA Translation and Degradation." In: *Molecular Cell* 25.5, pp. 635–646. ISSN: 10972765. DOI: 10.1016/j.molcel.2007.02.011. URL: https://linkinghub.elsevier.com/retrieve/pii/S1097276507001116.

Parker, Roy and Haiwei Song (2004). "The enzymes and control of eukaryotic mRNA turnover." In: *Nature Structural & Molecular Biology* 11.2, pp. 121–127. ISSN: 1545-9993, 1545-9985. DOI: 10.1038/nsmb724. URL: http://www.nature.com/articles/nsmb724.

Pervushin, Konstantin et al. (1997). "Attenuated T_2 relaxation by mutual cancellation of dipole–dipole coupling and chemical shift anisotropy indicates an avenue to NMR structures of very large biological macromolecules in solution." In: *Proceedings of the National Academy of Sciences* 94.23, pp. 12366–12371. ISSN: 0027-8424, 1091-6490. DOI: 10.1073/pnas.94.23.12366. URL: https://pnas.org/doi/full/10.1073/pnas.94.23.12366.

Pervushin, Konstantin et al. (1998). "Transverse Relaxation-Optimized Spectroscopy (TROSY) for NMR Studies of Aromatic Spin Systems in ^{13} C-Labeled Proteins." In: *Journal of the American Chemical Society* 120.25, pp. 6394–6400. ISSN: 0002-7863, 1520-5126. DOI: 10.1021/ja980742g. URL: https://pubs.acs.org/doi/10.1021/ja980742g.

Pettersen, Eric F. et al. (2004). "UCSF Chimera—A visualization system for exploratory research and analysis." In: *Journal of Computational Chemistry* 25.13, pp. 1605–1612. DOI: https://doi.org/10.1002/jcc.20084. eprint: https://onlinelibrary.wiley.com/doi/pdf/10.1002/jcc.20084. URL: https://onlinelibrary.wiley.com/doi/abs/10.1002/jcc.20084.

Piccirillo, Christopher, Richie Khanna, and Megerditch Kiledjian (2003). "Functional characterization of the mammalian mRNA decapping enzyme hDcp2." In: *RNA (New York, N.Y.)* 9.9, pp. 1138–1147. ISSN: 1355-8382. DOI: 10.1261/rna.5690503. URL: https://europepmc.org/articles/PMC1370477.

Pines, A., M.G. Gibby, and J.S. Waugh (1972). "Proton-enhanced nuclear induction spectroscopy 13C chemical shielding anisotropy in some organic solids." In: *Chemical Physics Letters* 15.3, pp. 373–376. ISSN: 00092614. DOI: 10.1016/0009-2614(72)80191-X. URL: https://linkinghub.elsevier.com/retrieve/pii/000926147280191X.

Polyhach, Yevhen, Enrica Bordignon, and Gunnar Jeschke (2011). "Rotamer libraries of spin labelled cysteines for protein studies." In: *Phys. Chem. Chem. Phys.* 13.6, pp. 2356–2366. ISSN: 1463-9076, 1463-9084. DOI: 10.1039/C0CP01865A. URL: http://xlink.rsc.org/?DOI=C0CP01865A.

Privalov, Peter L. and Stanley J. Gill (1988). "Stability of Protein Structure and Hydrophobic Interaction." In: *Advances in Protein Chemistry*. Vol. 39. Elsevier, pp. 191–234. ISBN: 978-0-12-034239-6. DOI: 10.1016/S0065-3233(08)60377-0. URL: https://linkinghub.elsevier.com/retrieve/pii/S0065323308603770.

Puffer, Barbara et al. (2009). " 5-Fluoro pyrimidines: labels to probe DNA and RNA secondary structures by 1D 19 F NMR spectroscopy." In: *Nucleic Acids Research* 37.22, pp. 7728–7740. ISSN: 0305-1048. DOI: 10.1093/nar/gkp862. eprint: https://academic.oup.com/nar/article-pdf/37/22/7728/16757538/gkp862.pdf. URL: https://doi.org/10.1093/nar/gkp862.

Puhl, Ana C. et al. (2019). "New targets for HIV drug discovery." In: *Drug Discovery Today* 24.5, pp. 1139–1147. ISSN: 13596446. DOI: 10.1016/j.drudis.2019.03.013. URL: https://linkinghub.elsevier.com/retrieve/pii/S1359644618305270.

Purcell, E. M., H. C. Torrey, and R. V. Pound (1946). "Resonance Absorption by Nuclear Magnetic Moments in a Solid." In: *Physical Review* 69.1, pp. 37–38. ISSN: 0031-899X. DOI: 10.1103/PhysRev.69.37. URL: https://link.aps.org/doi/10.1103/PhysRev.69.37.

Reif, Bernd et al. (2021). "Solid-state NMR spectroscopy." In: *Nature Reviews Methods Primers* 1.1, p. 2. ISSN: 2662-8449. DOI: 10.1038/s43586-020-00002-1. URL: https://www.nature.com/articles/s43586-020-00002-1.

Religa, Tomasz L., Amy M. Ruschak, et al. (2011). "Site-Directed Methyl Group Labeling as an NMR Probe of Structure and Dynamics in Supramolecular Protein Systems: Applications to the Proteasome and to the ClpP Protease." In: *Journal of the American Chemical Society* 133.23, pp. 9063–9068. ISSN: 0002-7863, 1520-5126. DOI: 10.1021/ja202259a. URL: https://pubs.acs.org/doi/10.1021/ja202259a.

Religa, Tomasz L., Remco Sprangers, and Lewis E. Kay (2010). "Dynamic Regulation of Archaeal Proteasome Gate Opening As Studied by TROSY NMR." In: *Science* 328.5974, pp. 98–102. ISSN: 0036-8075, 1095-9203. DOI: 10.1126/science.1184991. URL: https://www.science.org/doi/10.1126/science.1184991.

Roche, Julien et al. (2013). "Effect of Internal Cavities on Folding Rates and Routes Revealed by Real-Time Pressure-Jump NMR Spectroscopy." In: *Journal of the American Chemical Society* 135.39, pp. 14610–14618. ISSN: 0002-7863, 1520-5126. DOI: 10.1021/ja406682e. URL: https://pubs.acs.org/doi/10.1021/ja406682e.

Rosenzweig, Rina et al. (2013). "Unraveling the Mechanism of Protein Disaggregation Through a ClpB-DnaK Interaction." In: *Science* 339.6123, pp. 1080–1083. DOI: 10.1126/science.1233066. eprint: https://www.science.org/doi/pdf/10.1126/science.1233066. URL: https://www.science.org/doi/abs/10.1126/science.1233066.

Ruben, Eliza A. et al. (2020). "19F NMR reveals the conformational properties of free thrombin and its zymogen precursor prethrombin-2." In: *Journal of Biological Chemistry* 295.24, pp. 8227–8235. ISSN: 0021-9258. DOI: https://doi.org/10.1074/jbc.RA120.013419. URL: https://www.sciencedirect.com/science/article/pii/S0021925817494129.

Sahu, Debashish, G. Marius Clore, and Junji Iwahara (2007). "TROSY-Based *z* -Exchange Spectroscopy: Application to the Determination of the Activation Energy for Intermolecular Protein Translocation between Specific Sites on Different DNA Molecules." In: *Journal of the American Chemical Society* 129.43, pp. 13232–13237. ISSN: 0002-7863, 1520-5126. DOI: 10.1021/ja074604f. URL: https://pubs.acs.org/doi/10.1021/ja074604f.

Salzmann, Michael et al. (1998). "TROSY in triple-resonance experiments: New perspectives for sequential NMR assignment of large proteins." In: *Proceedings of the National Academy of Sciences* 95.23, pp. 13585–13590. ISSN: 0027-8424, 1091-6490. DOI: 10.1073/pnas.95.23.13585. URL: https://pnas.org/doi/full/10.1073/pnas.95.23.13585.

Samoson, Ago (2019). "H-MAS." In: *Journal of Magnetic Resonance* 306, pp. 167–172. ISSN: 10907807. DOI: 10.1016/j.jmr.2019.07.010. URL: https://linkinghub.elsevier.com/retrieve/pii/S1090780719301375.

Sarkar, Paramita et al. (2007). "Proline cis-trans Isomerization Controls Autoinhibition of a Signaling Protein." In: *Molecular Cell* 25.3, pp. 413–426. ISSN: 10972765. DOI: 10.1016/j.molcel.2007.01.004. URL: https://linkinghub.elsevier.com/retrieve/pii/S1097276507000081.

Sarker, Muzaddid et al. (2016). "Tracking Transitions in Spider Wrapping Silk Conformation and Dynamics by 19F Nuclear Magnetic Resonance Spectroscopy." In: *Biochemistry* 55.21. PMID: 27153372, pp. 3048–3059. DOI: 10.1021/acs.biochem.6b00429. eprint: https://doi.org/10.1021/acs.biochem.6b00429. URL: https://doi.org/10.1021/acs.biochem.6b00429.

Sattler, Michael and Stephen W Fesik (1996). "Use of deuterium labeling in NMR: overcoming a sizeable problem." In: *Structure* 4.11, pp. 1245–1249. ISSN: 09692126. DOI: 10.1016/S0969-2126(96)00133-5. URL: https://linkinghub.elsevier.com/retrieve/pii/S0969212696001335.

Saxon, Eliana and Carolyn R. Bertozzi (2000). "Cell Surface Engineering by a Modified Staudinger Reaction." In: *Science* 287.5460, pp. 2007–2010. ISSN: 00368075, 10959203. URL: http://www.jstor.org/stable/3074893.

Schäfer, Ingmar B. et al. (2019). "Molecular Basis for poly(A) RNP Architecture and Recognition by the Pan2-Pan3 Deadenylase." In: *Cell* 177.6, 1619–1631.e21. ISSN: 00928674. DOI: 10.1016/j.cell.2019.04.013. URL: https://linkinghub.elsevier.com/retrieve/pii/S009286741930399X.

Schanda, Paul and Bernhard Brutscher (2006). "Hadamard frequency-encoded SOFAST-HMQC for ultrafast two-dimensional protein NMR." In: *Journal of Magnetic Resonance* 178.2, pp. 334–339. ISSN: 1090-7807. DOI: https://doi.org/10.1016/j.jmr.2005.10.007. URL: https://www.sciencedirect.com/science/article/pii/S1090780705003459.

Schanda, Paul, Bernhard Brutscher, et al. (2008). "Folding of the KIX Domain: Characterization of the Equilibrium Analog of a Folding Intermediate using 15N/13C Relaxation Dispersion and Fast 1H/2H Amide Exchange NMR Spectroscopy." In: *Journal of Molecular Biology* 380.4, pp. 726–741. ISSN: 00222836. DOI: 10.1016/j.jmb.2008.05.040. URL: https://linkinghub.elsevier.com/retrieve/pii/S0022283608006062.

Schanda, Paul and Matthias Ernst (2016). "Studying dynamics by magic-angle spinning solid-state NMR spectroscopy: Principles and applications to biomolecules." In: *Progress in Nuclear Magnetic Resonance Spectroscopy* 96, pp. 1–46. ISSN: 00796565. DOI: 10.1016/j.pnmrs.2016.02.001. URL: https://linkinghub.elsevier.com/retrieve/pii/S0079656516000078.

Schneider, Claudia and David Tollervey (2013). "Threading the barrel of the RNA exosome." In: *Trends in Biochemical Sciences* 38.10, pp. 485–493. ISSN: 09680004. DOI: 10.1016/j.tibs.2013.06.013. URL: https://linkinghub.elsevier.com/retrieve/pii/S0968000413001059.

Schoenberg, Daniel R. and Lynne E. Maquat (2012). "Regulation of cytoplasmic mRNA decay." In: *Nature Reviews Genetics* 13.4, pp. 246–259. ISSN: 1471-0056, 1471-0064. DOI: 10.1038/nrg3160. URL: http://www.nature.com/articles/nrg3160.

Schrimpf, Waldemar et al. (2018). "PAM: A Framework for Integrated Analysis of Imaging, Single-Molecule, and Ensemble Fluorescence Data." In: *Biophysical Journal* 114.7, pp. 1518–1528. ISSN: 00063495. DOI: 10.1016/j.bpj.2018.02.035. URL: https://linkinghub.elsevier.com/retrieve/pii/S0006349518302959.

Schuler, Benjamin (2006). "Application of Single Molecule Förster Resonance Energy Transfer to Protein Folding." In: Yawen, Bai and Nussinov Ruth. *Protein Folding Protocols*. Vol. 350. New Jersey: Humana Press, pp. 115–138. ISBN: 978-1-59745-189-5. DOI: 10.1385/1-59745-189-4:115. URL: http://link.springer.com/10.1385/1-59745-189-4:115.

Schuler, Benjamin and William A Eaton (2008). "Protein folding studied by single-molecule FRET." In: *Current Opinion in Structural Biology* 18.1, pp. 16–26. ISSN: 0959440X. DOI: 10.1016/j.sbi.2007.12.003. URL: https://linkinghub.elsevier.com/retrieve/pii/S0959440X07002035.

Schulz, Sarah et al. (2016). "TFE and Spt4/5 open and close the RNA polymerase clamp during the transcription cycle." In: *Proceedings of the National Academy of Sciences* 113.13. ISSN: 0027-8424, 1091-6490. DOI: 10.1073/pnas.1515817113. URL: https://pnas.org/doi/full/10.1073/pnas.1515817113.

Schütz, Stefan, Erik R. Nöldeke, and Remco Sprangers (2017). "A synergistic network of interactions promotes the formation of in vitro processing bodies and protects mRNA against decapping." In: *Nucleic Acids Research* 45.11, pp. 6911–6922. ISSN: 0305-1048, 1362-4962. DOI: 10.1093/nar/gkx353. URL: https://academic.oup.com/nar/article-lookup/doi/10.1093/nar/gkx353.

Schütz, Stefan and Remco Sprangers (2020). "Methyl TROSY spectroscopy: A versatile NMR approach to study challenging biological systems." In: *Progress in Nuclear Magnetic Resonance Spectroscopy* 116, pp. 56–84. ISSN: 00796565. DOI: 10.1016/j.pnmrs.2019.09.004. URL: https://linkinghub.elsevier.com/retrieve/pii/S0079656519300470.

Scott, Andrew M., Jedd D. Wolchok, and Lloyd J. Old (2012). "Antibody therapy of cancer." In: *Nature Reviews Cancer* 12.4, pp. 278–287. ISSN: 1474-175X, 1474-1768. DOI: 10.1038/nrc3236. URL: https://www.nature.com/articles/nrc3236.

Séraphin, Bertrand (1992). "The HIT protein family: a new family of proteins present in prokaryotes, yeast and mammals." In: *DNA Sequence* 3.3, pp. 177–179. ISSN: 1042-5179. DOI: 10.3109/10425179209034013. URL: http://www.tandfonline.com/doi/full/10.3109/10425179209034013.

Sharif, Humayun and Elena Conti (2013). "Architecture of the Lsm1-7-Pat1 Complex: A Conserved Assembly in Eukaryotic mRNA Turnover." In: *Cell Reports* 5.2, pp. 283–291. ISSN: 22111247. DOI: 10.1016/j.celrep.2013.10.004. URL: https://linkinghub.elsevier.com/retrieve/pii/S2211124713005731.

Sharif, Humayun, Sevim Ozgur, et al. (2013). "Structural analysis of the yeast Dhh1–Pat1 complex reveals how Dhh1 engages Pat1, Edc3 and RNA in mutually exclusive interactions." In: *Nucleic Acids Research* 41.17, pp. 8377–8390. ISSN: 1362-4962, 0305-1048. DOI: 10.1093/nar/gkt600. URL: https://academic.oup.com/nar/article-lookup/doi/10.1093/nar/gkt600.

Shatkin, A (1976). "Capping of eucaryotic mRNAs." In: *Cell* 9.4, pp. 645–653. ISSN: 00928674. DOI: 10.1016/0092-8674(76)90128-8. URL: https://linkinghub.elsevier.com/retrieve/pii/0092867476901288.

She, Meipei, Carolyn J Decker, Nan Chen, et al. (2006). "Crystal structure and functional analysis of Dcp2p from Schizosaccharomyces pombe." In: *Nature Structural & Molecular Biology* 13.1, pp. 63–70. ISSN: 1545-9993, 1545-9985. DOI: 10.1038/nsmb1033. URL: http://www.nature.com/articles/nsmb1033.

She, Meipei, Carolyn J Decker, Kumar Sundramurthy, et al. (2004). "Crystal structure of Dcp1p and its functional implications in mRNA decapping." In: *Nature Structural & Molecular Biology* 11.3, pp. 249–256. ISSN: 1545-9993, 1545-9985. DOI: 10.1038/nsmb730. URL: http://www.nature.com/articles/nsmb730.

She, Meipei, Carolyn J. Decker, Dmitri I. Svergun, et al. (2008). "Structural Basis of Dcp2 Recognition and Activation by Dcp1." In: *Molecular Cell* 29.3, pp. 337–349. ISSN: 10972765. DOI: 10.1016/j.molcel.2008.01.002. URL: https://linkinghub.elsevier.com/retrieve/pii/S1097276508000105.

Shen, Vincent et al. (2008). "DcpS scavenger decapping enzyme can modulate pre-mRNA splicing." In: *RNA* 14.6, pp. 1132–1142. ISSN: 1355-8382, 1469-9001. DOI: 10.1261/rna.1008208. URL: http://rnajournal.cshlp.org/lookup/doi/10.1261/rna.1008208.

Sheth, Ujwal and Roy Parker (2003). "Decapping and Decay of Messenger RNA Occur in Cytoplasmic Processing Bodies." In: *Science* 300.5620, pp. 805–808. ISSN: 0036-8075, 1095-9203. DOI: 10.1126/science.1082320. URL: https://www.science.org/doi/10.1126/science.1082320.

Shi, Pan et al. (2011). "Site-specific 19F NMR chemical shift and side chain relaxation analysis of a membrane protein labeled with an unnatural amino acid." In: *Protein Science* 20.1, pp. 224–228. DOI: https://doi.org/10.1002/pro.545. eprint: https://onlinelibrary.wiley.com/doi/pdf/10.1002/pro.545. URL: https://onlinelibrary.wiley.com/doi/abs/10.1002/pro.545.

Singh, Jasbir et al. (2008). "DcpS as a Therapeutic Target for Spinal Muscular Atrophy." In: *ACS Chemical Biology* 3.11, pp. 711–722. ISSN: 1554-8929, 1554-8937. DOI: 10.1021/cb800120t. URL: https://pubs.acs.org/doi/10.1021/cb800120t.

Sinturel, Flore et al. (2012). "Activation of 5'-3' exoribonuclease Xrn1 by cofactor Dcs1 is essential for mitochondrial function in yeast." In: *Proceedings of the National Academy of Sciences* 109.21, pp. 8264–8269. ISSN: 0027-8424, 1091-6490. DOI: 10.1073/pnas.1120090109. URL: https://pnas.org/doi/full/10.1073/pnas.1120090109.

Sochor, Florian et al. (2016). "19F-labeling of the adenine H2-site to study large RNAs by NMR spectroscopy." In: *Journal of Biomolecular NMR* 64, pp. 63–74.

Sonenberg, Nahum and Alan G. Hinnebusch (2009). "Regulation of Translation Initiation in Eukaryotes: Mechanisms and Biological Targets." In: *Cell* 136.4, pp. 731–745. ISSN: 00928674. DOI: 10.1016/j.cell.2009.01.042. URL: https://linkinghub.elsevier.com/retrieve/pii/S0092867409000907.

Song, Man-Gen, Sophie Bail, and Megerditch Kiledjian (2013). "Multiple Nudix family proteins possess mRNA decapping activity." In: *RNA* 19.3, pp. 390–399. ISSN: 1355-8382, 1469-9001. DOI: 10.1261/rna.037309.112. URL: http://rnajournal.cshlp.org/lookup/doi/10.1261/rna.037309.112.

Sprangers, Remco (2021). "High-pressure NMR measurements provide insights into the different structural states that proteins can adopt." In: *Biophysical Journal* 120.5, pp. 749–751. ISSN: 00063495. DOI: 10.1016/j.bpj.2021.01.014. URL: https://linkinghub.elsevier.com/retrieve/pii/S0006349521000515.

Sprangers, Remco, Anna Gribun, et al. (2005). "Quantitative NMR spectroscopy of supramolecular complexes: Dynamic side pores in ClpP are important for product release." In: *Proceedings of the National Academy of Sciences* 102.46, pp. 16678–16683. ISSN: 0027-8424, 1091-6490. DOI: 10.1073/pnas.0507370102. URL: https://pnas.org/doi/full/10.1073/pnas.0507370102.

Sprangers, Remco and Lewis E. Kay (2007). "Quantitative dynamics and binding studies of the 20S proteasome by NMR." In: *Nature* 445.7128, pp. 618–622. ISSN: 0028-0836, 1476-4687. DOI: 10.1038/nature05512. URL: https://www.nature.com/articles/nature05512.

Stafford, Kate A. et al. (2015). "Conformational Preferences Underlying Reduced Activity of a Thermophilic Ribonuclease H." In: *Journal of Molecular Biology* 427.4, pp. 853–866. ISSN: 00222836. DOI: 10.1016/j.jmb.2014.11.023. URL: https://linkinghub.elsevier.com/retrieve/pii/S0022283614006500.

Steiger, Michelle et al. (2003). "Analysis of recombinant yeast decapping enzyme." In: *RNA* 9.2, pp. 231–238. ISSN: 1355-8382, 1469-9001. DOI: 10.1261/rna.2151403. URL: http://rnajournal.cshlp.org/lookup/doi/10.1261/rna.2151403.

Stiller, John B. et al. (2019). "Probing the transition state in enzyme catalysis by high-pressure NMR dynamics." In: *Nature Catalysis* 2.8, pp. 726–734. ISSN: 2520-1158. DOI: 10.1038/s41929-019-0307-6. URL: https://www.nature.com/articles/s41929-019-0307-6.

Stoecklin, Georg and Nancy Kedersha (2013). "Relationship of GW/P-Bodies with Stress Granules." In: *Ten Years of Progress in GW/P Body Research*. Ed. by Edward K. L. Chan and Marvin J. Fritzler. Vol. 768. Series Title: Advances in Experimental Medicine and Biology. New York, NY: Springer New York, pp. 197–211. ISBN: 978-1-4614-5106-8 978-1-4614-5107-5. DOI: 10.1007/978-1-4614-5107-5_12. URL: http://link.springer.com/10.1007/978-1-4614-5107-5_12.

Sugase, Kenji, H. Jane Dyson, and Peter E. Wright (2007). "Mechanism of coupled folding and binding of an intrinsically disordered protein." In: *Nature* 447.7147, pp. 1021–1025. ISSN: 0028-0836, 1476-4687. DOI: 10.1038/nature05858. URL: https://www.nature.com/articles/nature05858.

Takeuchi, Koh, Haribabu Arthanari, and Gerhard Wagner (2016). "Perspective: revisiting the field dependence of TROSY sensitivity." In: *Journal of Biomolecular NMR* 66.4, pp. 221–225. ISSN: 0925-2738, 1573-5001. DOI: 10.1007/s10858-016-0075-4. URL: http://link.springer.com/10.1007/s10858-016-0075-4.

Teixeira, Daniela and Roy Parker (2007). "Analysis of P-Body Assembly in *Saccharomyces cerevisiae*." In: *Molecular Biology of the Cell* 18.6. Ed. by Thomas Fox, pp. 2274–2287. ISSN: 1059-1524, 1939-4586. DOI: 10.1091/mbc.e07-03-0199. URL: https://www.molbiolcell.org/doi/10.1091/mbc.e07-03-0199.

Tharun, Sundaresan and Roy Parker (2001). "Targeting an mRNA for Decapping." In: *Molecular Cell* 8.5, pp. 1075–1083. ISSN: 10972765. DOI: 10.1016/S1097-2765(01)00395-1. URL: https://linkinghub.elsevier.com/retrieve/pii/S1097276501003951.

Theillet, François-Xavier et al. (2012). "Site-Specific Mapping and Time-Resolved Monitoring of Lysine Methylation by High-Resolution NMR Spectroscopy." In: *Journal of the American Chemical Society* 134.18, pp. 7616–7619. ISSN: 0002-7863, 1520-5126. DOI: 10.1021/ja301895f. URL: https://pubs.acs.org/doi/10.1021/ja301895f.

Tibble, Ryan W. et al. (2020). *Biomolecular condensates amplify mRNA decapping by coupling protein interactions with conformational changes in Dcp1/Dcp2*. preprint. Biochemistry. DOI: 10.1101/2020.07.09.195057. URL: http://biorxiv.org/lookup/doi/10.1101/2020.07.09.195057.

Tibble, Ryan W. et al. (2021). "Biomolecular condensates amplify mRNA decapping by biasing enzyme conformation." In: *Nature Chemical Biology* 17.5, pp. 615–623. ISSN: 1552-4450, 1552-4469. DOI: 10.1038/s41589-021-00774-x. URL: http://www.nature.com/articles/s41589-021-00774-x.

Topisirovic, Ivan et al. (2011). "Cap and cap-binding proteins in the control of gene expression: Cap and cap-binding proteins in the control of gene expression." In: *Wiley Interdisciplinary Reviews: RNA* 2.2, pp. 277–298. ISSN: 17577004. DOI: 10.1002/wrna.52. URL: https://onlinelibrary.wiley.com/doi/10.1002/wrna.52.

Trinkaus, Victoria A. et al. (2021). "In situ architecture of neuronal α-Synuclein inclusions." In: *Nature Communications* 12.1, p. 2110. ISSN: 2041-1723. DOI: 10.1038/s41467-021-22108-0. URL: https://www.nature.com/articles/s41467-021-22108-0.

Tritschler, Felix et al. (2009). "Structural Basis for the Mutually Exclusive Anchoring of P Body Components EDC3 and Tral to the DEAD Box Protein DDX6/Me31B." In: *Molecular Cell* 33.5, pp. 661–668. ISSN: 10972765. DOI: 10.1016/j.molcel.2009.02.014. URL: https://linkinghub.elsevier.com/retrieve/pii/S1097276509001300.

Tucker, Morgan et al. (2002). "Ccr4p is the catalytic subunit of a Ccr4p/Pop2p/Notp mRNA deadenylase complex in *Saccharomyces cerevisiae*." In: *The EMBO Journal* 21.6, pp. 1427–1436. ISSN: 02614189. DOI: 10.1093/emboj/21.6.1427. URL: http://emboj.embopress.org/cgi/doi/10.1093/emboj/21.6.1427.

Tugarinov, Vitali, Peter M. Hwang, et al. (2003). "Cross-Correlated Relaxation Enhanced ^{1}H - ^{13}C NMR Spectroscopy of Methyl Groups in Very High Molecular Weight Proteins and Protein Complexes." In: *Journal of the American Chemical Society* 125.34, pp. 10420–10428. ISSN: 0002-7863, 1520-5126. DOI: 10.1021/ja030153x. URL: https://pubs.acs.org/doi/10.1021/ja030153x.

Tugarinov, Vitali, Voula Kanelis, and Lewis E Kay (2006). "Isotope labeling strategies for the study of high-molecular-weight proteins by solution NMR spectroscopy." In: *Nature Protocols* 1.2, pp. 749–754. ISSN: 1754-2189, 1750-2799. DOI: 10.1038/nprot.2006.101. URL: https://www.nature.com/articles/nprot.2006.101.

Tugarinov, Vitali, David S. Libich, et al. (2015). "The Energetics of a Three-State Protein Folding System Probed by High-Pressure Relaxation Dispersion NMR Spectroscopy." In: *Angewandte Chemie International Edition* 54.38, pp. 11157–11161. ISSN: 14337851. DOI: 10.1002/anie.201505416. URL: https://onlinelibrary.wiley.com/doi/10.1002/anie.201505416.

Tunyasuvunakool, Kathryn et al. (2021). "Highly accurate protein structure prediction for the human proteome." In: *Nature* 596.7873, pp. 590–596. ISSN: 0028-0836, 1476-4687. DOI: 10.1038/s41586-021-03828-1. URL: https://www.nature.com/articles/s41586-021-03828-1.

Tyagi, Swati and Edward A Lemke (2012). "Genetically Encoded Click Chemistry for Single-Molecule FRET of Proteins." In: vol. 113, pp. 169–187. DOI: 10.1016/B978-0-12-407239-8.00009-4.

Tycko, Robert (2006). "Molecular structure of amyloid fibrils: insights from solid-state NMR." In: *Quarterly Reviews of Biophysics* 39.1, pp. 1–55. ISSN: 0033-5835, 1469-8994. DOI: 10.1017/S0033583506004173. URL: https://www.cambridge.org/core/product/identifier/S0033583506004173/type/journal_article.

Tycko, Robert (2011). "Solid-State NMR Studies of Amyloid Fibril Structure." In: *Annual Review of Physical Chemistry* 62.1, pp. 279–299. ISSN: 0066-426X, 1545-1593. DOI: 10.1146/annurev-physchem-032210-103539. URL: https://www.annualreviews.org/doi/10.1146/annurev-physchem-032210-103539.

Valkov, Eugene et al. (2016). "Structure of the Dcp2–Dcp1 mRNA-decapping complex in the activated conformation." In: *Nature Structural & Molecular Biology* 23.6, pp. 574–579. ISSN: 1545-9993, 1545-9985. DOI: 10.1038/nsmb.3232. URL: http://www.nature.com/articles/nsmb.3232.

Vallurupalli, Pramodh and Lewis E. Kay (2006). "Complementarity of ensemble and single-molecule measures of protein motion: A relaxation dispersion NMR study of an enzyme complex." In: *Proceedings of the National Academy of Sciences* 103.32, pp. 11910–11915. ISSN: 0027-8424, 1091-6490. DOI: 10.1073/pnas.0602310103. URL: https://pnas.org/doi/full/10.1073/pnas.0602310103.

Vallurupalli, Pramodh, Ashok Sekhar, et al. (2017). "Probing conformational dynamics in biomolecules via chemical exchange saturation transfer: a primer." In: *Journal of Biomolecular NMR* 67.4, pp. 243–271. ISSN: 0925-2738, 1573-5001. DOI: 10.1007/s10858-017-0099-4. URL: http://link.springer.com/10.1007/s10858-017-0099-4.

Venters, Ronald A., Bennett T. Farmer II, et al. (1996). "Characterizing the Use of Perdeuteration in NMR Studies of Large Proteins:13C,15N and1H Assignments of Human Carbonic Anhydrase II." In: *Journal of Molecular Biology* 264.5, pp. 1101–1116. ISSN: 00222836. DOI: 10.1006/jmbi.1996.0699. URL: https://linkinghub.elsevier.com/retrieve/pii/S0022283696906993.

Venters, Ronald A., Chih-Chin Huang, et al. (1995). "High-level 2H/13C/15N labeling of proteins for NMR studies." In: *Journal of Biomolecular NMR* 5.4, pp. 339–344. ISSN: 0925-2738, 1573-5001. DOI: 10.1007/BF00182275. URL: http://link.springer.com/10.1007/BF00182275.

Vernon, Robert McCoy et al. (2018). "Pi-Pi contacts are an overlooked protein feature relevant to phase separation." In: *eLife* 7, e31486. ISSN: 2050-084X. DOI: 10.7554/eLife.31486. URL: https://elifesciences.org/articles/31486.

Voith von Voithenberg, Lena and Don C. Lamb (2018). "Single Pair Förster Resonance Energy Transfer: A Versatile Tool To Investigate Protein Conformational Dynamics." In: *BioEssays* 40.3, p. 1700078. ISSN: 02659247. DOI: 10.1002/bies.201700078. URL: https://onlinelibrary.wiley.com/doi/10.1002/bies.201700078.

Wand, A. Joshua and Kim A. Sharp (2018). "Measuring Entropy in Molecular Recognition by Proteins." In: *Annual Review of Biophysics* 47.1. PMID: 29345988, pp. 41–61. DOI: 10.1146/annurev-biophys-060414-034042. eprint: https://doi.org/10.1146/annurev-biophys-060414-034042. URL: https://doi.org/10.1146/annurev-biophys-060414-034042.

Wang, Feng, Christopher B. Marshall, et al. (2012). "Structures of KIX domain of CBP in complex with two FOXO3a transactivation domains reveal promiscuity and plasticity in coactivator recruitment." In: *Proceedings of the National Academy of Sciences* 109.16, pp. 6078–6083. DOI: 10.1073/pnas.1119073109. eprint: https://www.pnas.org/doi/pdf/10.1073/pnas.1119073109. URL: https://www.pnas.org/doi/abs/10.1073/pnas.1119073109.

Wang, Lei and Peter G. Schultz (2005). "Expanding the Genetic Code." In: *Angewandte Chemie International Edition* 44.1, pp. 34–66. DOI: https://doi.org/10.1002/anie.200460627. eprint: https://onlinelibrary.wiley.com/doi/pdf/10.1002/anie.200460627. URL: https://onlinelibrary.wiley.com/doi/abs/10.1002/anie.200460627.

Wang, Tuo, Pyae Phyo, and Mei Hong (2016). "Multidimensional solid-state NMR spectroscopy of plant cell walls." In: *Solid State Nuclear Magnetic Resonance* 78, pp. 56–63. ISSN: 09262040. DOI: 10.1016/j.ssnmr.2016.08.001. URL: https://linkinghub.elsevier.com/retrieve/pii/S0926204016300595.

Wang, Zuoren, Xinfu Jiao, et al. (2002). "The hDcp2 protein is a mammalian mRNA decapping enzyme." In: *Proceedings of the National Academy of Sciences* 99.20, pp. 12663–12668. ISSN: 0027-8424, 1091-6490. DOI: 10.1073/pnas.192445599. URL: https://pnas.org/doi/full/10.1073/pnas.192445599.

Wang, Zuoren and Megerditch Kiledjian (2001). "Functional Link between the Mammalian Exosome and mRNA Decapping." In: *Cell* 107.6, pp. 751–762. ISSN: 00928674. DOI: 10.1016/S0092-8674(01)00592-X. URL: https://linkinghub.elsevier.com/retrieve/pii/S009286740100592X.

Watson, J. D. and F. H. C. Crick (1953). "Molecular Structure of Nucleic Acids: A Structure for Deoxyribose Nucleic Acid." In: *Nature* 171.4356, pp. 737–738. ISSN: 0028-0836, 1476-4687. DOI: 10.1038/171737a0. URL: https://www.nature.com/articles/171737a0.

Weingarth, Markus, Geoffrey Bodenhausen, and Piotr Tekely (2009). "Low-power decoupling at high spinning frequencies in high static fields." In: *Journal of Magnetic Resonance* 199.2, pp. 238–241. ISSN: 1090-7807. DOI: https://doi.org/10.1016/j.jmr.2009.04.015. URL: https://www.sciencedirect.com/science/article/pii/S1090780709001232.

Welte, Hannah et al. (2020). "What does fluorine do to a protein? Thermodynamic, and highly-resolved structural insights into fluorine-labelled variants of the cold shock protein." In: *Scientific Reports* 10. DOI: 10.1038/s41598-020-59446-w.

Wentinck, Koen, Christos Gogou, and Dimphna H. Meijer (2022). "Putting on molecular weight: Enabling cryo-EM structure determination of sub-100-kDa proteins." In: *Current Research in Structural Biology* 4, pp. 332–337. ISSN: 2665928X. DOI: 10.1016/j.crstbi.2022.09.005. URL: https://linkinghub.elsevier.com/retrieve/pii/S2665928X22000290.

Williamson, Michael P., Timothy F. Havel, and Kurt Wüthrich (1985). "Solution conformation of proteinase inhibitor IIA from bull seminal plasma by 1H nuclear magnetic resonance and distance geometry." In: *Journal of Molecular Biology* 182.2, pp. 295–315. ISSN: 00222836. DOI: 10.1016/0022-2836(85)90347-X. URL: https://linkinghub.elsevier.com/retrieve/pii/002228368590347X.

Willkomm, Sarah et al. (2022). "Single-molecule FRET uncovers hidden conformations and dynamics of human Argonaute 2." In: *Nature Communications* 13.1, p. 3825. ISSN: 2041-1723. DOI: 10.1038/s41467-022-31480-4. URL: https://www.nature.com/articles/s41467-022-31480-4.

Wilusz, Carol J., Michael Wormington, and Stuart W. Peltz (2001). "The cap-to-tail guide to mRNA turnover." In: *Nature Reviews Molecular Cell Biology* 2.4, pp. 237–246. ISSN: 1471-0072, 1471-0080. DOI: 10.1038/35067025. URL: http://www.nature.com/articles/35067025.

Wojtczak, Blazej A. et al. (2018). "5'-Phosphorothiolate Dinucleotide Cap Analogues: Reagents for Messenger RNA Modification and Potent Small-Molecular Inhibitors of Decapping Enzymes." In: *Journal of the American Chemical Society* 140.18, pp. 5987–5999. ISSN: 0002-7863, 1520-5126. DOI: 10.1021/jacs.8b02597. URL: https://pubs.acs.org/doi/10.1021/jacs.8b02597.

Wu, Donghui et al. (2014). "Lsm2 and Lsm3 bridge the interaction of the Lsm1-7 complex with Pat1 for decapping activation." In: *Cell Research* 24.2, pp. 233–246. ISSN: 1001-0602, 1748-7838. DOI: 10.1038/cr.2013.152. URL: http://www.nature.com/articles/cr2013152.

Wurm, Jan Philip, Iris Holdermann, et al. (2017). "Changes in conformational equilibria regulate the activity of the Dcp2 decapping enzyme." In: *Proceedings of the National Academy of Sciences* 114.23, pp. 6034–6039. ISSN: 0027-8424, 1091-6490. DOI: 10.1073/pnas.1704496114. URL: https://pnas.org/doi/full/10.1073/pnas.1704496114.

Wurm, Jan Philip, Jan Overbeck, and Remco Sprangers (2016). "The *S. pombe* mRNA decapping complex recruits cofactors and an Edc1-like activator through a single dynamic surface." In: *RNA* 22.9, pp. 1360–1372. ISSN: 1355-8382, 1469-9001. DOI: 10.1261/rna.057315.116. URL: http://rnajournal.cshlp.org/lookup/doi/10.1261/rna.057315.116.

Wurm, Jan Philip and Remco Sprangers (2019). "Dcp2: an mRNA decapping enzyme that adopts many different shapes and forms." In: *Current Opinion in Structural Biology* 59, pp. 115–123. ISSN: 0959440X. DOI: 10.1016/j.sbi.2019.07.009. URL: https://linkinghub.elsevier.com/retrieve/pii/S0959440X19300442.

Wurm, Jan Philip, Sihyun Sung, et al. (2021). "Molecular basis for the allosteric activation mechanism of the heterodimeric imidazole glycerol phosphate synthase complex." In: *Nature Communications* 12.1, p. 2748. ISSN: 2041-1723. DOI: 10.1038/s41467-021-22968-6. URL: https://www.nature.com/articles/s41467-021-22968-6.

Xiao, Gaoyi, James F Parsons, et al. (1998). "Conformational changes in the crystal structure of rat glutathione transferase M1-1 with global substitution of 3-fluorotyrosine for tyrosine." In: *Journal of Molecular Biology* 281.2, pp. 323–339. ISSN: 00222836. DOI: 10.1006/jmbi.1998.1935. URL: https://linkinghub.elsevier.com/retrieve/pii/S0022283698919350.

Xiao, Peng, David Bolton, et al. (2019). "Solid-state NMR spectroscopy based atomistic view of a membrane protein unfolding pathway." In: *Nature Communications* 10.1, p. 3867. ISSN: 2041-1723. DOI: 10.1038/s41467-019-11849-8. URL: https://www.nature.com/articles/s41467-019-11849-8.

Xie, Tao et al. (2020). "Conformational states dynamically populated by a kinase determine its function." In: *Science* 370.6513, eabc2754. ISSN: 0036-8075, 1095-9203. DOI: 10.1126/science.abc2754. URL: https://www.science.org/doi/10.1126/science.abc2754.

Xu, Nianhua, Chyi-Ying A. Chen, and Ann-Bin Shyu (1997). "Modulation of the Fate of Cytoplasmic mRNA by AU-Rich Elements: Key Sequence Features Controlling mRNA Deadenylation and Decay." In: *Molecular and Cellular Biology* 17.8, pp. 4611–4621. ISSN: 1098-5549. DOI: 10.1128/MCB.17.8.4611. URL: https://www.tandfonline.com/doi/full/10.1128/MCB.17.8.4611.

Xu, Xingjian, Donald Gagné, et al. (2021). "Volume and compressibility differences between protein conformations revealed by high-pressure NMR." In: *Biophysical Journal* 120.5, pp. 924–935. ISSN: 00063495. DOI: 10.1016/j.bpj.2020.12.034. URL: https://linkinghub.elsevier.com/retrieve/pii/S0006349521000783.

Xue, Mengjun et al. (2019). "How internal cavities destabilize a protein." In: *Proceedings of the National Academy of Sciences* 116.42, pp. 21031–21036. DOI: 10.1073/pnas.1911181116. eprint: https://www.pnas.org/doi/pdf/10.1073/pnas.1911181116. URL: https://www.pnas.org/doi/abs/10.1073/pnas.1911181116.

Yang, Daiwen and Lewis E. Kay (1999). "[No title found]." In: *Journal of Biomolecular NMR* 13.1, pp. 3–10. ISSN: 09252738. DOI: 10.1023/A:1008329230975. URL: http://link.springer.com/10.1023/A:1008329230975.

Yang, Edward, Erik van Nimwegen, et al. (2003). "Decay Rates of Human mRNAs: Correlation With Functional Characteristics and Sequence Attributes." In: *Genome Research* 13.8, pp. 1863–1872.

ISSN: 1088-9051. DOI: 10.1101/gr.1272403. URL: http://genome.cshlp.org/lookup/doi/10.1101/gr.1272403.

Yang, Haitao and Zihe Rao (2021). "Structural biology of SARS-CoV-2 and implications for therapeutic development." In: *Nature Reviews Microbiology* 19.11, pp. 685–700. ISSN: 1740-1526, 1740-1534. DOI: 10.1038/s41579-021-00630-8. URL: https://www.nature.com/articles/s41579-021-00630-8.

Ycas, Peter D. et al. (2020). "2-Fluorotyrosine is a valuable but understudied amino acid for protein-observed 19F NMR." In: *Journal of Biomolecular NMR* 74.1. DOI: 10.1007/s10858-019-00290-0. URL: https://par.nsf.gov/biblio/10174597.

Ye, Gang, Bin Liu, and Fang Li (2022). "Cryo-EM structure of a SARS-CoV-2 omicron spike protein ectodomain." In: *Nature Communications* 13.1, p. 1214. ISSN: 2041-1723. DOI: 10.1038/s41467-022-28882-9. URL: https://www.nature.com/articles/s41467-022-28882-9.

Ye, Libin, Sacha Thierry Larda, et al. (2015). "A comparison of chemical shift sensitivity of trifluoromethyl tags: optimizing resolution in 19F NMR studies of proteins." In: *Journal of Biomolecular NMR* 62.1, pp. 97–103. ISSN: 0925-2738, 1573-5001. DOI: 10.1007/s10858-015-9922-y. URL: http://link.springer.com/10.1007/s10858-015-9922-y.

Ye, Yue Qi, Michal Malon, et al. (2014). "Rapid measurement of multidimensional 1H solid-state NMR spectra at ultra-fast MAS frequencies." In: *Journal of Magnetic Resonance* 239, pp. 75–80. ISSN: 10907807. DOI: 10.1016/j.jmr.2013.12.010. URL: https://linkinghub.elsevier.com/retrieve/pii/S1090780713003297.

Zhang, Yi et al. (2016). "High Pressure ZZ-Exchange NMR Reveals Key Features of Protein Folding Transition States." In: *Journal of the American Chemical Society* 138.46. PMID: 27781428, pp. 15260–15266. DOI: 10.1021/jacs.6b09887. eprint: https://doi.org/10.1021/jacs.6b09887. URL: https://doi.org/10.1021/jacs.6b09887.

Zhao, Jiawei, Matthias Elgeti, et al. (2023). *Conformational dynamics of the μ-opioid receptor determine ligand intrinsic efficacy*. preprint. Biochemistry. DOI: 10.1101/2023.04.28.538657. URL: http://biorxiv.org/lookup/doi/10.1101/2023.04.28.538657.

Zhao, Jing, Linda Hyman, and Claire Moore (1999). "Formation of mRNA 3' Ends in Eukaryotes: Mechanism, Regulation, and Interrelationships with Other Steps in mRNA Synthesis." In: *Microbiology and Molecular Biology Reviews* 63.2, pp. 405–445. ISSN: 1092-2172, 1098-5557. DOI: 10.1128/MMBR.63.2.405-445.1999. URL: https://journals.asm.org/doi/10.1128/MMBR.63.2.405-445.1999.

Zhou, Mi et al. (2015). "DcpS is a transcript-specific modulator of RNA in mammalian cells." In: *RNA* 21.7, pp. 1306–1312. ISSN: 1355-8382, 1469-9001. DOI: 10.1261/rna.051573.115. URL: http://rnajournal.cshlp.org/lookup/doi/10.1261/rna.051573.115.

Zinder, John C., Elizabeth V. Wasmuth, and Christopher D. Lima (2016). "Nuclear RNA Exosome at 3.1 Å Reveals Substrate Specificities, RNA Paths, and Allosteric Inhibition of Rrp44/Dis3." In: *Molecular Cell* 64.4, pp. 734–745. ISSN: 10972765. DOI: 10.1016/j.molcel.2016.09.038. URL: https://linkinghub.elsevier.com/retrieve/pii/S1097276516305901.